Torsion in Helically Reinforced Prestressed Concrete Poles

by

Michael Eduard Kuebler

A thesis
presented to the University of Waterloo
in fulfillment of the
thesis requirement for the degree of
Master of Applied Science
in
Civil Engineering

Waterloo, Ontario, Canada, 2008

AUTHOR'S DECLARATION

I hereby declare that I am the sole author of this thesis. This is a true copy of the thesis, including any required final revisions, as accepted by my examiners.

I understand that my thesis may be made electronically available to the public.

Abstract

Reinforced concrete poles are commonly used as street lighting and electrical transmission poles. Typical concrete lighting poles experience very little load due to torsion. The governing design loads are typically bending moments as a result of wind on the arms, fixtures, and the pole itself. The Canadian pole standard, CSA A14-07 relates the helical reinforcing to the torsion capacity of concrete poles. This issue and the spacing of the helical reinforcing elements are investigated.

Based on the ultimate transverse loading classification system in the Canadian standard, the code provides a table with empirically derived minimum helical reinforcing amounts that vary depending on: 1) the pole class and 2) distance from the tip of the pole. Research into the minimum helical reinforcing requirements in the Canadian code has determined that the values were chosen empirically based on manufacturer's testing. The CSA standard recommends two methods for the placement of the helical reinforcing: either all the required helical reinforcing is wound in one direction or an overlapping system is used where half of the required reinforcing is wound in each direction. From a production standpoint, the process of placing and tying this helical steel is time consuming and an improved method of reinforcement is desirable. Whether the double helix method of placement produces stronger poles in torsion than the single helix method is unknown. The objectives of the research are to analyze the Canadian code (CSA A14-07) requirements for minimum helical reinforcement and determine if the Canadian requirements are adequate. The helical reinforcement spacing requirements and the effect of spacing and direction of the helical reinforcing on the torsional capacity of a pole is also analyzed. Double helix and single helix reinforcement methods are compared to determine if there is a difference between the two methods of reinforcement.

The Canadian pole standard (CSA A14-07) is analyzed and compared to the American and German standards. It was determined that the complex Canadian code provides more conservative spacing requirements than the American and German codes however the spacing requirements are based on empirical results alone. The rationale behind the Canadian code requirements is unknown.

A testing program was developed to analyze the spacing requirements in the CSA A14-07 code. Fourteen specimens were produced with different helical reinforcing amounts: no reinforcement, single and double helical spaced CSA A14-07 designed reinforcement, and single helical specimens with twice the designed spacing values. Two specimens were produced based on the single helical

reinforcement spacing. One specimen was produced with helical reinforcement wound in the clockwise direction and another with helical reinforcement in the counter clockwise direction. All specimens were tested under a counter clockwise torsional load. The clockwise specimens demonstrated the response of prestressed concrete poles with effective helical reinforcement whereas the counter clockwise reinforced specimens represented theoretically ineffective reinforcement. Two tip sizes were produced and tested: 165 mm and 210 mm.

A sudden, brittle failure was noted for all specimens tested. The helical reinforcement provided no post-cracking ductility. It was determined that the spacing and direction of the helical reinforcement had little effect on the torsional capacity of the pole. Variable and scattered test results were observed. Predictions of the cracking torque based on the ACI 318-05, CSA A23.3-04 and Eurocode 2 all proved to be unconservative. Strut and tie modelling of the prestressing transfer zone suggested that the spacing of the helical steel be 40 mm for the 165 mm specimens and 53 mm for the 210 mm specimens. Based on the results of the strut and tie modelling, it is likely that the variability and scatter in the test results is due to pre-cracking of the specimens. All the 165 mm specimens and the large spaced 210 mm specimens were inadequately reinforced in the transfer zone. The degree of pre-cracking in the specimen likely causes the torsional capacity of the pole to vary.

The strut and tie model results suggest that the requirements of the Canadian code can be simplified and rationalized. Similar to the American spacing requirements of 25 mm in the prestressing transfer zone, a spacing of 30 mm to 50 mm is recommended dependent on the pole tip size. Proper concrete mixes, adequate concrete strengths, prestressing levels, and wall thickness should be emphasized in the torsional CSA A14-07 design requirements since all have a large impact on the torsional capacity of prestressed concrete poles.

Recommendations and future work are suggested to conclusively determine if direction and spacing have an effect on torsional capacity or to determine the factors causing the scatter in the results. The performance of prestressed concrete poles reinforced using the suggestions presented should also be further investigated. Improving the ability to predict the cracking torque based on the codes or reducing the scatter in the test results should also be studied.

Acknowledgements

The author would like to thank Mr. Ken Bowman, Mr. Terry Ridgway, and Mr. Doug Hirst for their suggestions and technical assistance during the testing program.

Special thanks to Mr. Ron Ragwen, Mr. Uli Kuebler, and Sky Cast Inc. whose support during the experimental testing made this research possible. Thanks also to Mr. Nick Lawler for his assistance during testing.

The author would also like to thank his parents and friends for their support during the past two years. A final thank you is extended to his supervisor, Professor Dr. Maria Anna Polak, P. Eng., whose guidance and suggestions have been invaluable during this research.

Table of Contents

List of Tables

List of Figures

Chapter 1
Introduction

1.1 Background

1.1.1 Brief History of Prestressed Concrete Poles

Concrete poles have been used since the invention of reinforced concrete. In their paper titled "Spun Prestressed Concrete Poles – Past, Present, and Future", Fouad, Sherman and Werner (1992) present a summary of the past 150 years of concrete poles. According to Fouad et al. the first concrete poles were used in Germany in 1856 for supporting telegraph lines. In 1867, Joseph Monier of France produced the first iron-reinforced concrete poles. The concrete poles had increased strength and durability but usage was limited due to the heavier weight when compared to wood and steel. The first spun cast concrete poles were first produced in 1907, by a German firm Otto Schlosser in Meissen, northwest of Dresden. The result of the spinning process was a lighter pole due to the hollow section. Since concrete poles were considered maintenance-free, by 1932, 250,000 poles were in use in Europe, 150,000 in Germany only. Fouad et al. indicate that several poles built in the first quarter of the 20th century are still in use today. For example, a 19 m high pole in Newmarkt, Germany was built in 1924 with a 280 mm tip diameter, 50 MPa concrete, 18 to 20 mm diameter longitudinal steel and 5 mm circumferential spiral wire at a spacing of 80 to 100 mm.

Eugene Freyssinet developed the first prestressed concrete poles during the 1930's and produced poles that could withstand higher loads without cracking and exhibited elastic characteristics. World War II and the shortage of steel after the war increased the use of prestressed concrete poles since less steel was required for production compared to conventional reinforced concrete poles. By the 1950's the first spun cast prestressed concrete poles were in production in Europe. The poles had improved strength, durability, and were lighter when compared with other products. The result was that transportation and erection was simplified. On the North American continent, reinforced concrete poles were not used until the 1930's. Prestressed poles were not used until the middle of the 1950's in the United States and became more common when the Virginia Electric Power Company (VEPCO) and Bayshore Concrete Products started to produce efficient European designs of tapered spun prestressed concrete poles (Fouad et al., 1992).

Fouad et al. also presented the advantages of concrete poles over steel and wood poles. Steel poles normally cost more and require longer delivery times. Large wood poles on the other hand are becoming scarce and expensive due to heavy forest cutting, fire, drought and disease. Fouad et al. (1992) stated that "4 to 6 million wood poles become defective each year mainly due to rot and attack by insects and woodpeckers." In contrast, properly built prestressed concrete poles offer a somewhat elastic, corrosion resistant, maintenance-free, and long lasting aesthetic product. Fouad et al. (1992) suggest that while concrete poles are initially more expensive than wood poles, a life-cycle cost analysis provides economic advantages due to the longer life span and reduced maintenance costs associated with concrete poles.

A wide range of spun concrete poles can be produced, ranging from 6 m long, 200 mm base diameter poles to 100 m long, 2 m base diameter poles (Fouad et al., 1992). Concrete poles can be used in a variety of applications, including street lighting, electrical distribution, rail electrification, communication towers, supports for wind turbines and several pole sections can be joined together to produce 100 m long post-tensioned towers for communication equipment (Fouad et al., 1992). The use of concrete poles has spread throughout Europe and North America and has become a popular alternative to wood and steel poles.

1.1.2 Typical Concrete Poles Failures

The governing design loads are typically due to wind on the pole, arms, and fixtures. These loads primarily produce bending moments, but also shear forces, and torsional moments. While failures caused by overloads of moment, shear, and torsion are possible, very few have been documented and no photos could be found. A few of the documented cases of concrete pole failures found by the author are presented.

During the course of the thesis research two or three poles failed in the City of Kitchener in June of 2007. A storm caused high winds in the area and caused several trees and branches to fall all over town. On Glasgow Street, falling branches landed on electrical lines causing the prestressed concrete poles to fall over. While no known investigation was completed and very little information was available to the author, it appeared from the pieces found that segregation of the concrete had occurred during production. It is the author's opinion that perhaps the sudden forces on the electrical lines caused the inner cement paste to crack and spall causing the prestressing strands to break into

the hollow middle section of the pole. The loss of the strands could cause the pole to lose all resistance and stability leading to the premature failure of the pole.

Vehicle impacts typically cause shear failure of concrete poles between the bumper level and the ground (Dilger and Ghali, 1986). A typical shear failure caused by vehicle impact is shown in Figure 1.1. The crack caused by vehicle impact originates at the bumper level and proceeds diagonally towards the ground level. As described by Dilger and Ghali (1986), disintegration of the surrounding concrete occurs and may cause the pole to ultimately fall over. The use of tight spirals can minimize the damaged area of the pole, while longitudinal reinforcement will provide the pole stability in the case of complete concrete section loss.

Figure 1.1: Shear failure caused by vehicle impact (Sky Cast, 2008)

Damage and failure caused by vehicle impact is not always limited to the bumper level and surrounding area. Improper embedment and vehicle impact forces can also cause failure to occur below the ground. Inertia forces on the upper portion of the pole due to the vehicle impact can alternatively cause the pole to snap higher up (Dilger and Ghali, 1986). Figure 1.2 shows an architectural pole failure due to a vehicle impact. The failure of this pole occurred in two places. On impact, cracking occurred below the ground where openings in the pole were made for electrical

wiring. Poles are typically reinforced with crash cages at points where vehicle collisions are possible. Crash cages are made from conventional longitudinal steel reinforcement and tied together with helical steel cages. Due to the sudden load on the pole and inertia forces (whiplash effect caused by the collision), the upper portion of the pole shown in Figure 1.2 broke where the crash cage longitudinal steel was terminated.

a)

b)

Figure 1.2 a) and b): Pole failure caused by vehicle impact and inertia effects (Sky Cast Inc., 2007)

Another failure typically found in concrete poles and linked to segregation of the concrete and poor concrete mixtures is shown in Figure 1.3. Segregation of the concrete during production of the concrete poles creates several durability problems. Segregation creates a layer of fines and cement paste along the inner surface of the wall. Differential shrinkage between the fine layer along the inside of the pole and coarser layer on the outside of the pole can cause longitudinal cracks to develop in the weaker cement paste layer (Dilger et al, 1996). Water infiltration then causes rusting of the steel reinforcement leading to corrosion issues and increase cracking and spalling of the concrete.


a)

b)

Figure 1.3 a) and b): Longitudinal cracking, corrosion and spalling caused by differential shrinkage and segregation of concrete mix

1.2 Justification and Scope of Research

This research primarily deals with torsional behaviour of typical spun cast concrete lighting poles and the helical reinforcement used as transverse reinforcement. The Canadian pole standard, CSA A14-07 (2007) gives the minimum helical reinforcing percentages required for each concrete pole class. The helical reinforcing percentages are complex and the rationale behind the helical reinforcement percentages is unknown since they vary directly with the wall thickness, distance from the tip of the pole, and the pole's bending capacity. Research into the minimum helical reinforcing requirements in the Canadian code has determined that the values were chosen with some testing and established empirically. The Canadian code also suggests that the reinforcement influences the torsional capacity of the pole, whereas factors such as wall thickness and concrete strength are not presented as prominently. CSA A14-07 (2007) allows two methods for the placement of the helical reinforcing: 1) as a tight single helix along the length of the pole, or 2) as an overlapping double helix consisting of two single helical wires wound in opposite directions. Confusion has occurred in the industry due to the two allowable methods for helical reinforcement placement. Purchasers and manufacturers have questioned whether the double helix method of placement produces stronger poles in torsion than the single helix method.

A deeper understanding of the reason for helical reinforcement placement in prestressed concrete poles is needed for the simplification and rationalization of the CSA A14-07 minimum helical reinforcing requirements. The purpose of the helical reinforcing steel, how much is required, and whether the direction and/or spacing of the steel influences the torsional capacity of the concrete pole must be determined to properly understand the helical reinforcing problem.

The research scope is limited to lighting and hydro poles where torsional loads are relatively small and bending or shear typically govern the design. Where torsional loads are large and govern the design, poles must be designed accordingly. Poles governed by large torsional loads are not part of this research.

1.3 Objectives

The objectives of this research are to:

- Analyze the Canadian code (CSA A14-07) requirements for minimum helical reinforcement and determine whether the requirements are adequate and,
- Determine the role of the helical steel reinforcement in sustaining torsional loads.

The research objectives are completed by: researching the development of the spacing requirements for helical reinforcement in prestressed concrete poles, comparing the Canadian requirements against pole codes from other countries, establishing whether spacing and direction (winding) of the helical reinforcing has an effect on the torsional capacity of a pole, determining the difference between the double helix and single helix reinforcement methods allowed by the Canadian code, and by analyzing, through full scale testing, the mode of failure, post-cracking behaviour, and reason for inclusion of helical reinforcement in prestressed concrete poles to determine the main factors that influence the torsional capacity of prestressed concrete poles.

1.4 Contributions

The thesis summarizes current manufacturing and design practices for prestressed concrete poles. The thesis gives a summary of concrete pole codes and literature and also provides a comparison between the Canadian requirements for the design of prestressed concrete poles and the American and German requirements.

A pole analysis program created as part of the research simplifies the design and analysis of prestressed concrete poles and provides clear graphical output to the designer. Rational and simple requirements are also presented for the design of helical reinforcing steel and the purpose for helical steel in prestressed concrete poles is clarified.

1.5 Organization of Thesis

The remaining portion of the thesis is separated into six chapters. First a literature review (Chapter 2) of concrete pole research, governing pole and concrete codes, and models for torsional response of concrete members are presented. The cracking torque equations are derived and variations found in the literature discussed. The mechanics and governing equations for the post-cracking torsion models are also presented.

A MatLab program created for the flexural, shear, and torsional analysis of prestressed concrete poles is presented in Chapter 3. Two other programs created to model the post-cracking torsional behaviour of concrete poles are also discussed. Flowcharts and the program logic are presented and validation/comparison of the output to existing data is given.

Chapter 4 summarizes the experimental testing program conducted and design of the specimens. The design of the experimental specimens including the concrete mix/strength, prestressing strand, helical reinforcement is discussed and the general spun cast production sequence is presented and explained. The experimental test setup and instrumentation, and the testing procedure used are given in Chapter 5. The experimental results and observations are summarized for each specimen in Chapter 6. Pictures of the failure for each specimen and general remarks on each test are presented.

Chapter 7 contains an analysis of the experimental results. The chapter includes discussion on the influence of helical reinforcing direction and spacing as well as concrete quality. A comparison of the predicted cracking torques and torsional model behaviours to the experimental results is presented and discussed. Factors important to the cracking torque of prestressed concrete poles are analyzed. Comparison of the experimental data to a database of torsional pole testing results is also presented. Finally an investigation into the applied loads on lighting poles and minimum transverse reinforcement requirements in the prestressing transfer zone and the remaining portion of the pole is discussed. The conclusions and recommendations are presented in Chapter 8. Appendices are also attached which contain material reports and more detailed analysis and testing information.

Chapter 2
Literature Review

2.1 Literature on Concrete Poles

Publications and papers related to concrete poles and prestressed concrete poles generally fall into the following categories: analysis techniques (typically bending capacity), concrete mixtures (durability and performance), construction techniques, and impact/bending testing. Only a few papers discussed helical reinforcing and the reasoning for placing it. None mentioned how spacing requirements were developed for concrete poles while only one paper dealt with the combined bending and torsional capacity of prestressed concrete poles. The following sections summarize the findings of the papers dealing with concrete poles.

2.1.1 Field Behaviour of Prestressed Concrete Poles

Fouad et al. (1994) studied the performance of spun prestressed concrete poles during Hurricane Andrew in Dade County, Florida. Hurricane Andrew was a category 4 hurricane with wind speeds in the range of 211 to 249 km/h (131 to 155 mph). Fouad et al. inspected poles in Dade Country and found they were in good structural condition even though cracking and near ultimate strength loads had been applied. The poles were able to dissipate energy and survive the storm due to an inherent ductility achieved through partial prestressing and a round cross section. The cracks formed due to the hurricane appeared to fully close, indicating no yielding of prestressing steel and that the elasticity was maintained. Full-scale bending tests were performed on six poles subjected to the hurricane winds and it was determined that the storm did not cause a reduction in the strength of the poles. In fact, the poles failed at loads 8 and 32 percent greater than the theoretical ultimate design capacity. Fouad et al. suggested that the improved performance could be attributed to the high compaction forces applied to the concrete in the spinning process. The result is a much denser concrete with reduced water-cement ratio and improved material properties. Fouad et al. indicated that a modulus of elasticity 28 percent larger than cast concrete can be achieved through spinning of the concrete. It was noted that the failure rate for all concrete poles (both prestressed and static cast) during Hurricane Andrew was 8 percent as compared to 80 percent for wood poles in the same area. The 8 percent of

concrete pole failures were all statically-cast square poles while no failures of spun-cast round poles were reported.

The behaviour and design of static cast prestressed concrete poles were studied by Rosson et al. (1996). Two full-scale poles were tested as prototypes to test the design methodology suggested in the paper. Two poles were tested in bending, one constructed with helical steel (No. 9 gauge/2.9 mm diameter spaced at 152 mm) and the other without. The mix used consisted of 318 kg of cement, 159 kg of Class C fly ash, 500 kg of masonry sand, 750 kg of 13 mm limestone, 136 kg of water, and 5.3 L of Rheobuild. The corresponding water-cement ratio was 0.43 and slump was measured as 203 mm.

During testing, the cracks due to bending were closed after release of the load showing that corrosion of steel due to cracked concrete is prevented due to prestressing. The pole without spiral reinforcement failed at a higher load than the one with spiral reinforcement. The pole with spiral reinforcement failed in compression at the ground line and failure was confined due to the spiral reinforcement. The second pole tested without spiral reinforcement failed due to a combination of unconfined longitudinal cracking between prestressing strands and crushing at the ground line.

The shear strength provided by the concrete was deemed adequate to resist the design shear forces and therefore shear reinforcement provided by the helical steel was not required. Rosson et al. suggested however, that spiral reinforcement be placed for the entire length of the pole due to longitudinal cracking in overload situations. Spiral reinforcement was found to confine the failure of the concrete and prevent longitudinal cracking. Rosson et al. (1996) suggested that high shear forces below the ground line can develop between active and passive soil pressures which can also cause longitudinal cracking between strands.

2.1.2 FRP and Prestressed Concrete Poles

Terrasi and Lees (2003) investigated the bending and torsional behaviour of five full-scale CFRP prestressed concrete lighting prototype poles. The use of CFRP instead of steel prestressing strands allowed for a non-corrodible, lightweight, and high strength pole to be produced. CFRP poles were initially investigated to produce high power transmission pylons in Switzerland (Terrasi et al, 2002). The weight reduction is due to the smaller cover (15-20 mm) required for CFRP tendons. Steel prestressing strands in contrast require covers of 40-50 mm for protection against aggressive environmental effects and corrosion. Terrasi and Lees (2003) determined that a CFRP reinforced

lighting pole could be constructed and a weight reduction of 30% could be achieved. They also found that the total material, production, and installations costs were equivalent to that of a steel-prestressed concrete pole.

Terrasi and Lees (2003) tested the poles at low levels of pure torsion and to failure in combined torsion and bending. Three different types of FRP shear reinforcement were also investigated using geogrids typically used for slope stabilization and spirally wound CFRP tapes. High strength concrete with cube compressive strength over 90 MPa was used, containing silica fume and 0-6 mm aggregates. The poles tested were 120 mm at the tip with a taper of 10 mm/m to the butt of the pole. Pure torsion tests were undertaken to verify the load clamping system to be used and investigate the torsional behaviour of the poles. Specimens were not tested until failure and a maximum torsion load of 280 N-m was applied to the specimens. The torsion moment and twist angle relationship was determined to be linear over the applied torsion loading range.

It was concluded that the poles "showed sufficient bending rotation capacity to make up for the lack of plasticity of the brittle CFRP prestressing tendons" (Terrasi and Lees, 2003). FRP shear reinforcement was found to have no effect on the behaviour of the specimens in the bending/torsional testing, however an ultimate load increase and post-peak carrying capacity was noted for the PVA fiber geogrid. The fuse box (or hand hole) location was varied during testing to determine whether missing portions of the pole near the ground line would cause a reduction in moment capacity. It was found that the ultimate capacity was the same whether the fuse box was on the compressive or tensile flange, and that the capacity increased if the opening was located on the neutral axis. The bending/torsional capacities of the pole specimens varied from 10.6 kN-m to 14.2 kN-m.

Kaufmann et al. (2004) also investigated the use of short fiber reinforced cement or mortar for use in spun cast structures. They found that heavy and costly conventional steel could be replaced by lightweight polymer and carbon fibres. Spun cast lighting pylons were constructed based on mixtures investigated in the paper. Flow properties and mixture consistency were investigated and optimized for spun cast applications.

Research using FRP sheets for retrofitting four concrete lighting poles was conducted by Chahrour and Soudki (2006). The use of FRP laminates was investigated to develop an efficient and reliable method of retrofitting concrete lighting poles in field situations. Glass and carbon FRP sheets were investigated and flexural testing was conducted after the deteriorated portions of the poles were repaired. Chahrour and Soudki (2006) concluded that the use of glass and carbon FRP sheets

impregnated with epoxy and placed as confinement to the poles or in both directions (transversely and longitudinally) were efficient methods for repairing and restoring the flexural capacity of the concrete poles. The bidirectional FRP system gave better flexural responses for load capacity, stiffness, deflection, and ductility than the unidirectional FRP repaired and undamaged poles.

2.1.3 Helical Reinforcement in Concrete Poles

Dilger and Ghali (1986) studied the response of spun cast concrete poles (prestressed and static cast) to vehicle impact loads to determine the safety aspects of using such poles for lighting and power transmission. Previous studies by the Department of Highways, Ontario, Canada, entitled "Impact Testing of Lighting Poles and Sign Supports, 1967-1968" (Smith, 1970) tested three conventionally reinforced, spun concrete poles at high vehicle speeds. The first two poles were 15.25 m long while the third was only 8 m long. Vehicle speeds for each test were 85 km/h, 78 km/h, and 69 km/h respectively. It was found in all three tests that the pole fell onto the vehicle, causing severe damage to the cars. The upper 3 m of the poles appeared to break due to the inertia effects of the impact forces. The report recommended that concrete poles be used only where protective barriers and rails could prevent vehicle impact.

Dilger and Ghali (1986) analyzed the previous findings and investigated how prestressed concrete poles would behave when hit by a vehicle compared to normally reinforced concrete poles. It was speculated that prestressed concrete poles would lead to a brittle failure due to the high prestressing forces. The poles tested by Dilger and Ghali were lighter and shorter prestressed concrete poles (12 m long) typically used in lighting situations. From the 11 tests it was found that closely spaced spiral reinforcement increased the shear resistance significantly at the base of the pole where impact with the vehicle occurred. Prestressed concrete poles also exhibited higher shear strengths than mild steel reinforced concrete poles. Wall thickness was determined to be significant for the shear resistance of the concrete pole and the bedding type was also significant for impact resistance. Dilger and Ghali concluded that thick walls and closely spaced spirals increase the impact resistance of concrete poles, while thin walls with nominal spiral reinforcement lead to low impact resistance. Tested poles all failed due to shearing between the bumper level and the ground and fell away from the vehicle contradicting the results of the Department of Highways, Ontario tests. Dilger and Ghali contributed the difference in the way the poles fell to the smaller pole lengths and wall thicknesses which resulted in smaller inertia forces during vehicle impact. The authors also discussed whether "strong" or "weak" poles should be designed. For higher impact vehicle speeds, they suggested that poles be

designed to break upon impact to save lives of the passengers. An excess of spiral reinforcement could lead to stronger and more dangerous poles for high speed vehicle impacts.

Fouad et al. (1992) suggested that closely spaced spirals (4 to 5 mm in diameter) wrapped around the strands provide the needed reinforcement to resist temperature stresses, transfer forces at the pole ends and contribute to the torsional and shear strength of the member.

2.1.4 Concrete Mixes for Spun-cast Concrete Poles

Dilger, Ghali and Rao (1996), Dilger and Rao (1997), and Wang, Dilger, and Kuebler (2001) determined that special mix designs were required for spun cast concrete poles. It was found that normal concrete mixes would have serious segregation problems due to the spinning process, and the dry or coarse mixes would not consolidate properly. Drying shrinkage, freeze thaw, chloride penetration, mix proportions and mixing time, spinning speeds and duration were all investigated. The spinning process seemed to be the cause of differential shrinkage due to the segregation of fines from the coarse aggregate. Differential shrinkage between the inner and outer layers was linked to the longitudinal cracking of concrete poles causing deterioration, reduction in strength, and reduced life expectancy (Figure 2.1 and Figure 2.2). Longitudinal cracking was noted as a typical problem with poles in service. To eliminate segregation and therefore significantly improve the strength and durability of concrete poles, special mix designs were suggested. Slag and silica fume were also included in the study and found to improve the results for spun concrete. A mix suggested for use in production by Wang, Dilger, and Kuebler (2001) had the following components: 1255 kg/m^3 coarse aggregate, 650 kg/m^3 sand, 341 kg/m^3 cement, 34 kg/m^3 silica fume, 9.5 L of superplasticizer, 1.15 L of air entraining agent (5.3% air), and 115 kg/m^3 water.

2.1.5 Published Guides and Specifications for Prestressed Concrete Pole Design

2.1.5.1 Guide Specification for Prestressed Concrete Poles

The PCI Guide Specifications for Prestressed Concrete Poles (PCI Committee on Prestressed Concrete Poles, 1982) indicate that cold drawn steel (Section 2.01-E) should be used as helical reinforcement for the entire length of the pole and the ratio of steel to concrete taken as not less than 0.1 percent (Section 3.03-A). The spiral pitch should not be greater than 102 mm (4 in.) or the radius of the pole, whichever is less.

Figure 2.1: Spalling, corrosion, and longitudinal cracking of concrete pole due to segregation and differential shrinkage

Figure 2.2: Longitudinal cracking caused by differential shrinkage

No formulae or design recommendations are given for torsional strengths, however Section 3.01 states that the design should be performed using published ultimate strength methods accepted by the industry as good engineering practices.

2.1.5.2 Guide for Design of Prestressed Concrete Poles

The Guide for Design of Prestressed Concrete Poles published by PCI (PCI Committee on Prestressed Concrete Poles, 1983) adds additional information to the specifications published by PCI. Section 10.1 explains that the helical reinforcement is used to help resist radial stresses under the wedging effect. The wedging effect is caused by the prestressing forces and the tensile stresses developed in the transfer lengths (approximately 50 times the strand diameter), which produce radial pressure against the surrounding concrete. The helical reinforcement prevents and minimizes longitudinal cracks in the pole which can develop due to this radial pressure.

The guide suggests that the helical reinforcement be No. 6 gauge wire with a yield strength of 483 MPa. Helical reinforcement is suggested at 0.1 percent of the concrete wall area in a 3 m (10 ft) increment (Clause 10.4). Minimum pitch of spirals is given as 25.4 mm, governed by the 19 mm aggregate size, and no maximum pitch is specified. No information is given on the torsional design of the concrete pole.

2.1.5.3 Guide for the Design and Use of Concrete Poles

The Guide for the Design and Use of Concrete Poles published by ASCE (ASCE Concrete Pole Task Committee, 1987) states that the helical reinforcement is used to control longitudinal cracking and improve shear and torsion strength (Clause 2.4.3). The guide indicates that the cold drawn steel (Clause 3.3.3) helical reinforcement is required throughout full length of the pole and since theories are not well developed, common practice suggests that the volume of helical steel be not less than 0.1 percent. Spacing of the helical reinforcement is not to be greater than 102 mm (4 in) or the radius of pole, whichever is less. The guide notes that prestressing loads near ends of pole and shear or torsion loads may require additional helical steel. It also states that helical spacing greater than 102 mm (4 in) may be allowed if the manufacturer presents evidence of satisfactory performance and end-user agrees.

No information is given in the guide with regards to torsional capacity of poles. Clause 2.2.5 of the guide indicates that “good theory for design of poles to resist torsional loads does not exist” and that extensive research is required to develop mathematical models for the combined loading situations in poles. It also suggests that design of the poles for torsion is limited to the testing of specimens (Clause 2.2.5).

2.1.5.4 Guide for the Design of Prestressed Concrete Poles (ASCE/PCI Joint Report)

The Guide for the Design of Prestressed Concrete Poles (ASCE-PCI Committee Report, 1997) was developed as a joint publication to summarize the previous three documents published by PCI and ASCE. The spiral reinforcement is explained in Section 3.3 to be required for resisting radial stresses caused by wedging effect of strand at release, and to minimize cracking due to torsion, shear, and shrinkage. As previously mentioned, longitudinal cracking can be produced due to the radial pressures at transfer locations. The guide indicates that the helical steel is to be in the range of No. 5 to 11 gauge wire (4.6 mm to 2.3 mm in diameter), depending on pole use and size. Poles with high

shear forces may require additional helical steel. The minimum area of spiral steel is given as 0.1 percent of the concrete wall area in a unit length increment. Additional reinforcement is required at tip and butt to resist stresses caused by prestressing. The guide indicates that the minimum pitch (spacing) of the helical reinforcement is to be 4/3 of the maximum aggregate size (19 mm), and not less than 25.4 mm (1 in). The maximum pitch is not to exceed 102 mm (4 in), unless shown through testing that performance is not impaired.

The ASCE/PCI (ASCE-PCI Committee Report, 1997) guide for pole design gives the following equations for the design of circular and square poles due to torsion. The design of concrete poles for torsion governed by $T_n \le \phi T_c$, where $\phi = 0.85$ and T_n is the applied load.

The torsional capacity for a cross section is given by:

$$T_c = \frac{J}{r_o}\sqrt{F_t^{\,2} + F_t f_{pc}} \tag{2-1}$$

for a circular cross section, where J is the polar moment of inertia and r_o is the outside radius of the section.

$$T_c = 6\sqrt{f_c'}\sqrt{1+\frac{10 f_{pc}}{f_c'}}\sum \eta x^2 y \tag{2-2}$$

for a square section, where $\eta = \dfrac{0.35}{0.75+\dfrac{b}{d}}$.

The tensile strength of concrete, F_t, is taken as $4\sqrt{f_c'}$ (f'_c in psi) and f_{pc} is the prestressing compression in the concrete. The formula is the same as the formula given in AASHTO LTS-4-M (2001). The ACI-318-05 (ACI Committee 318, 2005) formula also gives the same results however, is presented differently.

2.2 AASHTO and Canadian Highway Bridge Design Code Requirements for Concrete Poles

2.2.1 AASHTO Standard Specifications for Structural Supports for Highway Signs, Luminaries, and Traffic Signals

The Standard Specifications for Structural Supports for Highway Signs, Luminaries and Traffic Signals prepared by the AASHTO subcommittee on Bridges and Structures provides equations for calculating the bending and torsional strengths of hollow prestressed concrete poles (AASHTO LTS-4-M, 2001; Section 7). The torsional strength formulae presented are identical to those given in the ASCE-PCI joint publication (ASCE-PCI Committee Report, 1997), and ACI-318-05 (ACI Committee 318, 2005). The spacing requirements for helical reinforcement is also identical to the ASCE-PCI joint publication, and are suggested as a maximum spacing of 100 mm (4 in) throughout the length of the pole, except at the transfer ends where the maximum is set as 25 mm (1 in).

The previous version of the AASHTO standard (AASHTO LTS-3 (1994), 1994) gives requirements for helical reinforcement in prestressed concrete poles in Section 6. A minimum spiral reinforcement of 11 gauge wire (approximately 3 mm) spaced at 102 mm (4 in) spacing is recommended along the full length of the pole (Section 6: Clause 1.6.3). The helical reinforcement should therefore not be spaced larger than 102 mm.

2.2.2 Canadian Highway Bridge Design Code

The Canadian Highway Bridge Design Code (CAN/CSA-S6-06, 2006) has a clause specifically for highway accessory supports (Clause 12.5). Any concrete highway accessory support must be designed according to Section 8 of the Canadian Highway Bridge Design Code (CHBDC), which is similar to CSA A23.3-04 (2004). Loads on the supports should be calculated using the methods in Annex A3.2, which are also similar to the AASHTO formulae.

2.3 Design of Concrete Poles

The governing design loads are typically due to wind on the pole, arms, and fixtures. These loads primarily produce bending moments, but also shear forces, and torsional moments. In some cases, where guy wires are used, axially loads may be large enough to cause the pole to be treated as a compression member. Typical concrete lighting poles experience very little load due to shear and

torsion, and generally both loading conditions do not control the design. Where poles are used in a shear or torsion situation however, a code based design must be performed and adequate reinforcing must be included.

Generally the design of prestressed concrete poles is governed by the flexural capacity. Typically the flexural loads on the pole due to the wind are larger than the shear and torsional loads applied due to the slenderness and height of the pole. For the design of poles for bending and shear the standard beam approach can be used. The shear resistance provided by the concrete alone is usually adequate since the applied shear loads are generally low. The contribution of the transverse reinforcement to the shear resistance is typically ignored in design. Torsionally, the contribution of the transverse reinforcement is often ignored as well and the cracking torque is used as the limiting value.

The governing codes and standards however, give requirements which govern the design of the helical reinforcement in concrete pole. The standards governing the design and helical reinforcement for concrete poles in Canada, Germany, and the United States are presented and compared in the following sections.

2.3.1 CSA A14 (Canadian Standard)

In Canada, concrete poles are built according to CSA Standard A14 “Concrete Poles” (CSA A14-07, 2007). The current version of the code is CSA A14-07 with previous versions being published in 2000 (CSA A14-00, 2000) and 1979 (CSA A14-M1979, 1979). CSA A14-07 (2007) states that concrete poles are different than other members used in building design and therefore the equations used for predicting torsional strength in building design are not suitable (Annex B). The standard provides no formulae for the design of the poles, but indicates that empirical design methods may be required to determine torsional strength (Clause 4.3.4.2) and also references AASHTO LTS-4-M (2001) as a source for design formulae.

The code indicates indirectly that helical reinforcing steel amount and direction contributes to the torsional strength of the concrete pole. CSA A14-07 presents tables with the minimum amounts of helical reinforcing for a certain class of pole (Table 2-1 and Table 2-2) and minimum torsional capacities based on these minimum helical reinforcing amounts (Table 2-3). Table 2-3 also presents the tip diameter of each pole class, however it does not indicate the wall thickness, concrete strength, and other factors important to the torsional response of the pole.

Table 2-1: Minimum Ultimate Transverse Capacity (CSA A14-07 Table 1)

Class	Minimum tip load pole is required to resist, kN (lb)
AA*	2.0 (450)
AL	2.7 (600)
A	2.7 (600)
BL	4.0 (900)
B	4.0 (900)
CL	5.3 (1 200)
C	5.3 (1 200)
D	6.7 (1 500)
E	8.5 (1 900)
F	10.7 (2 400)
G	13.3 (3 000)
H	16.5 (3 700)
J	20.0 (4 500)
K	24.0 (5 400)
L	28.5 (6 400)
M	33.4 (7 500)
N	38.7 (8 700)
O	44.5 (10 000)

**The maximum length for Class AA poles is 10.00 m.*
Note: *The purchaser should take into account the wind loading on the pole in determining the classification required for a specific application.*

Table 2-2: Minimum Amounts of Helical Reinforcing (CSA A14-07 Table 2)

Class	Location	% of volume
AA	Tip	0.10
	1.5 m (59 in) from tip	0.06
AL, BL, and CL	Tip	0.20
	1.5 m (59 in) from tip	0.08
A to F	Tip	0.35
	1.5 m (59 in) from tip	0.20
	4.5 m (177 in) from tip	0.15
G to O	Tip	0.45
	1.5 m (59 in) from tip	0.30
	4.5 m (177 in) from tip	0.20

Table 2-3: Minimum Torsional Capacities (CSA A14-07 Table 3)

Class	Pole tip diameter, mm (in)	Torsional capacity, kN•m (lb•ft)	
		Non-pre-stressed	Pre-stressed
AA, AL, and BL	—	—	—
A and B	120 (4.75)	0.75 (550)	1.50 (1 100)
CL	140 (5.50)	1.25 (925)	2.50 (1 850)
C, D, E, and F	160 (6.50)	1.87 (1 375)	3.75 (2 750)
G, H, and J	200 (8.00)	3.50 (2 580)	7.00 (5 160)
K, L, and M	240 (9.50)	5.62 (4 150)	11.25 (8 300)
N and O	280 (11.00)	8.25 (6 080)	16.50 (12 160)

The tables provided in CSA A14-07 (2007) are empirical and based on limited testing results. The source and basis of the tables could not be further explained.

According the Canadian standard, poles are assigned a class rating based on the ultimate transverse load held during testing at 0.6 m from the tip of the pole (Table 2-1). The tip load also represents the shear capacity of the pole. As the class letter goes from AA to O, the pole capacities increase, and as a result, the pole tip diameter increases as well. The pitch of the helical reinforcing is calculated based on an assumed wall thickness of 45 mm (Clause 4.2.4) and the minimum helical reinforcing

amounts found in Table 2-2. The minimum torsional capacities expected from poles reinforced with the minimum helical reinforcing values are indicated in Table 2-3. CSA A14-07 (2007) states that poles of class AA, AL, and BL should not be used in torsion applications and therefore no minimum torsional capacities are listed Table 2-3 (Clause 4.2.6). Clause 4.2.5 recommends two methods for the placement of the helical reinforcing: either all the required helical reinforcing is wound in one direction or an overlapping system is used where half of the required reinforcing is wound in each direction.

When needed, the Canadian code states that poles can be designed for torsional strengths in excess of Table 2-3. It indicates that the pole designs should be based on empirical methods (Clause 4.3.4.2) and that the poles should have helical reinforcement wound in both directions with a maximum pitch of 1/5 of the pole diameter measured anywhere along the length (Clause 4.3.4.3).

In addition to the helical steel required for torsion, the minimum amount of helical reinforcing was added originally to prevent splitting of the pole due to the transfer of prestressing forces and other environmental effects (CSA A14-M1979, 1979). According to the CSA A14-M1979 (1979), additional spiral reinforcement requirements were included to prevent splitting at the butt of the pole. The standard also states that the splitting of the butt may be related to the cycles of freeze and thaw and concrete poles manufacturers in Southern Ontario determined that including additional spiral reinforcement to the reinforcement required for torsional strength solved the problem of splitting at the butt of the pole (preface of CSA A14-M1979, 1979). Studies conducted by Dilger et al. (1996; 1997) and Wang et al. (2001), on the other hand, indicate that the addition of helical steel to prevent splitting at the butt of the pole was incorrect. The addition of more steel to prevent splitting would only cause further problems. With more helical steel in the pole, there would be more of a possibility for corrosion and eventual spalling of the concrete. Special consideration to the concrete mixes and elimination of concrete segregation would be better than the addition of helical steel.

The requirements added by the CSA A14-M1979 standard are stated in Clause 4.4, helical reinforcement. Clause 4.4.1 states that helical reinforcement is included for torsional strength and to reinforce areas of the pole that contain openings. A helical steel reinforcement ratio of 0.1 percent of the concrete wall area was recommended (Clause 4.4.4). The old standard suggested using 3 mm wire at pitches varying from 100 mm at the tip to 300 mm at the butt along the full length of the pole to control cracking. The interior 13 mm of wall thickness was also neglected in the calculation of the helical reinforcement amount for spun concrete poles according to the 1979 code. The reduction in

wall thickness for the calculation is likely due to the segregation and cement paste layer in spun poles using improper concrete mixes. The current standard (CSA A14-07) suggests that the calculation of helical steel be based on an assumed wall thickness of 45 mm. This provision likely was included for this same reason.

For vehicular impact, the old standard indicates the failure mode should be ductile. To ensure ductility, the standard suggests the use of mild steel in the pole and that 1/3 of the flexural strength of the pole is achieved with the mild steel (Clause 6.1.3). In the torsional testing section of the old standard it is suggested that single helically reinforced poles be tested so the helix is unwound upon testing (Clause 7.5.4; unwinding of the helical steel is referred to as the counter clockwise (CCW) direction from this point on). Clause 7.5.4 is no longer stated in the new standard.

2.3.2 DIN EN 12843: Precast concrete products – Masts and poles and DIN EN 40-4: Lighting Columns (German Standards)

The production of spun cast prestressed concrete poles in Germany is governed by DIN EN 12843 (2004) for masts and poles and DIN EN 40-4 (2006) for lighting columns. Both standards have the same requirements when it comes to torsional reinforcement. The minimum amount of helical reinforcing is recommended as 0.05% of the longitudinal concrete cross section for poles with a base diameter of <= 400 mm (DIN EN 12843, 2004; Clause 4.3.8.2). The percentage increases to 0.15% for poles with a base diameter >= 800 mm. It should also be noted that for non-spun cast (or static cast) prestressed concrete poles, DIN EN 12843 suggests that no transverse reinforcement is required when verified by tests and justified by experience.

DIN 4228 (Feb 1989) was the previous version of the German code for precast concrete poles (DIN 4228, 1989). In the previous code requirements for helical steel spacing were proportional to the diameter of the helical wire (Table 2-4). The spacing of the helical steel decreased as the diameter of the helical wire was reduced. The design is also governed by Eurocode 2 (EN 1992-1-1:2004, 2004) and EN 13369:2004, Common Rules for Precast Concrete Products.

Table 2-4: DIN 4228 (1989): Helical steel spacing requirements

Helical Steel Diameter (mm)	Spacing of Helical Steel (mm)
5	60
4	40
3	30

2.3.3 ASTM Standard: Standard Specification for Spun Cast Prestressed Concrete Poles (U.S.A Standard)

The ASTM C 1089-06 Standard Specification for Spun Cast Prestressed Concrete Poles (ASTM C 1089-06, 2006) gives guidelines for the placement of the helical reinforcing which are based on reports published by ASCE and PCI. A maximum spacing of the helical reinforcing is given as 102 mm (4 in), except for 305 mm (1 ft) from the pole's tip and butt where the maximum is to be 25 mm (1 in) (Clause 6.1.2). For design of prestressed concrete poles the standard references the ASCE-PCI Committee Report on the Design of Prestressed Concrete Poles (ASCE-PCI Committee Report, 1997). The previous version of the standard, ASTM C 1089-97 (1997), has the same helical reinforcing guidelines as the 2006 standard.

2.3.4 Comparison of Helical Reinforcement Code Spacing Requirements

The formula used for the calculation of the helical reinforcement spacing is the same regardless of the code used. The derivation of the formula for helical reinforcement in concrete poles can be found in the ASCE-PCI Committee report: 'Guide for the Design of Prestressed Concrete Poles'. The derivation begins with the helical reinforcement ratio, A_c/A_s and the percentage of helically reinforcement, ρ. If the expressions for the area of concrete and the area of steel provided (based on the helical reinforcing spacing) are substituted in, the formula for helical reinforcing spacing can be derived as shown in Figure 2.3.

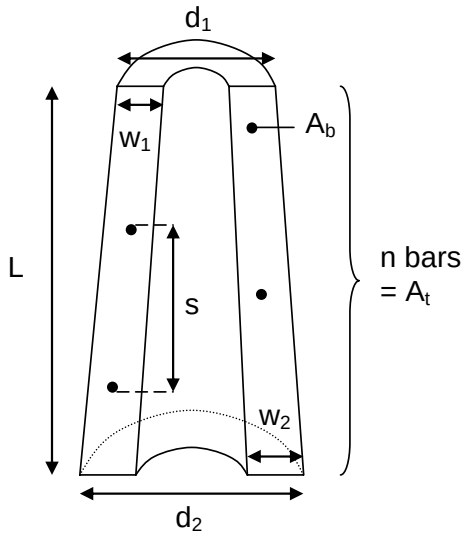

$$\rho = \frac{A_t}{A_c} \quad \begin{cases} \frac{s}{2} = \frac{L}{n} & A_c = 2\left[\frac{1}{2}(w_1 + w_2)L\right] \\ & \text{assume } w = w_1 \approx w_2 \\ A_t = nA_b & A_c = 2wL \end{cases}$$

$$\boxed{s = \frac{A_b}{\rho \cdot w}}$$

Figure 2.3: Derivation of helical reinforcement spacing formula for hollow tapered concrete poles

The formula is simplified with the assumption that the wall thickness remains approximately the same throughout the considered length. The following simplified design formula for the spacing of helical reinforcement ignoring tapered changes to the wall thickness can be used:

$$s = \frac{A_s}{\rho \cdot w} \tag{2-3}$$

where s is the spacing of the helical reinforcing, A_s the area of one helix, ρ is the given reinforcing percentage (from codes), and w is the assumed wall thickness of the pole.

The simplified equation indicates that the helical reinforcing spacing is dependent on the wall thickness of the pole. It suggests that, as the wall thickness is increased, and a larger volume of concrete is created, the spacing of the helical reinforcing is decreased, given that the helical reinforcing steel area is kept constant. The Canadian standard proposes tighter spacing requirements for larger capacity poles as well, suggesting that the helical reinforcing is linked to the capacity of the pole. Comparing the American, German, and Canadian concrete pole standards to each other reveals that the Canadian standard is more complex and gives tighter spacing requirements (Figure 2.4 and Table 2-5). Each code suggests a decrease in helical reinforcement spacing is required as the wall thickness of the pole increases. The American maximum spacing limit of 102 mm governs all designs unless large wall thicknesses are used (> 80 mm). The variation in spacing limits between codes suggests that the reasoning for including the helical reinforcing is not fully understood.

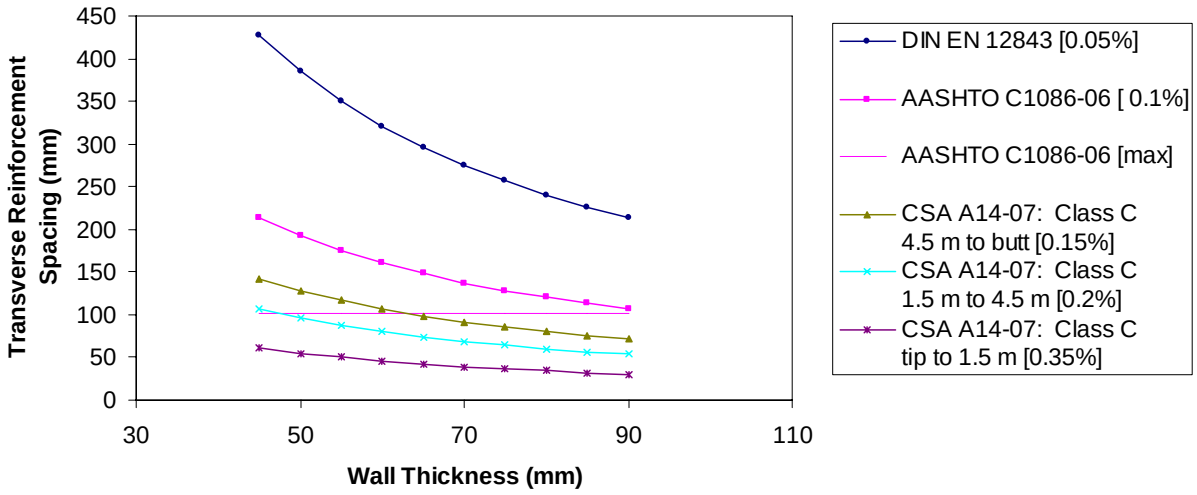

Figure 2.4: Helical spacing versus wall thickness for CSA A14-07, ASTM C 1089-06 and DIN EN 12843

Table 2-5: Helical reinforcement spacing code comparison

Code	Minimum Transverse Reinforcement Ratio (%)	Comments		Transverse Spacing (mm)							
		Standard Tip Diameter (mm)		120	140	150	160	200	210	240	280
		Wall Thickness (mm)**		45	50	55	60	65	70	75	80
DIN EN 12843	0.05%			428	385	350	321	296	275	257	241
ASTM C 1089-06#	0.10%	ASTM refers to the PCI Guide for the Design of Prestressed Concrete Poles & AASHTO LTS-4-M. Max. spacing (102 mm) governs.		102	102	102	102	102	102	102	102
				(214)	(192)	(175)	(160)	(148)	(137)	(128)	(120)
CSA A14-07*	0.10%	Class AA***	(1)	214	192	175	160	148	137	128	120
	0.06%		(2)	356	321	292	267	247	229	214	200
	0.20%	Class AL***, BL***, and CL	(1)	107	96	87	80	74	69	64	60
	0.08%		(2)	267	241	219	200	185	172	160	150
	0.35%	Class A to F	(1)	61	55	50	46	42	39	37	34
	0.20%		(2)	107	96	87	80	74	69	64	60
	0.15%		(3)	143	128	117	107	99	92	86	80
	0.45%	Class G to O	(1)					33	31	29	27
	0.30%		(2)					49	46	43	40
	0.20%		(3)					74	69	64	60

Notes:

Formula for calculating spacing (mm):

$s = As / (\rho * w)$

As = cross sectional area of transverse bar (mm^2)
w = wall thickness of concrete pole (mm)
ρ = transverse reinforcement ratio

Assumptions used for table:

As = 9.62 mm2 (3.5 mm diameter), and w

(1) = tip to 1.5 m from tip
(2) = 1.5 m to 4.5 m from tip
(3) = 4.5 m from tip to pole butt
* CSA A14-07 allows single helix at spacing given in table or double helix of steel at double the spacing
** assumed wall thickness, wall thickness depends on applied loads and reinforcement
*** not for torsional use (CSA)
#ASTM max. spacing - 102 mm (4 in.) min. spacing - 25.4 mm (1 in.), 25.4 mm for 300 mm at tip and butt of pole; values in brackets represent spacing calculated with 0.1%.

Min. Tip Diameters for CSA:

Class AA, AL, BL	-
Class A and B	120 mm
Class CL	140 mm
Class C, D, E, and F	160 mm
Class G, H, and J	200 mm
Class K, L, and M	240 mm
Class N and O	280 mm

2.4 Torque Resistance Formulae

2.4.1 Cracking Torque Resistance

Several variations on the cracking torque formulae have been suggested in the literature and codes. All are derived from Bredt's "thin-tube" theory. MacGregor and Ghoneim (1995) explained the derivation of the code formulae in a code background paper. Bredt's "thin-tube" theory (Figure 2.5) relates the shear stresses due to torsion in a thin-walled tube as:

$$\tau = \frac{T}{2A_o t} \tag{2-4}$$

where T is the applied torque, A_o is the area enclosed by the shear flow path, and t is the thickness of the member.

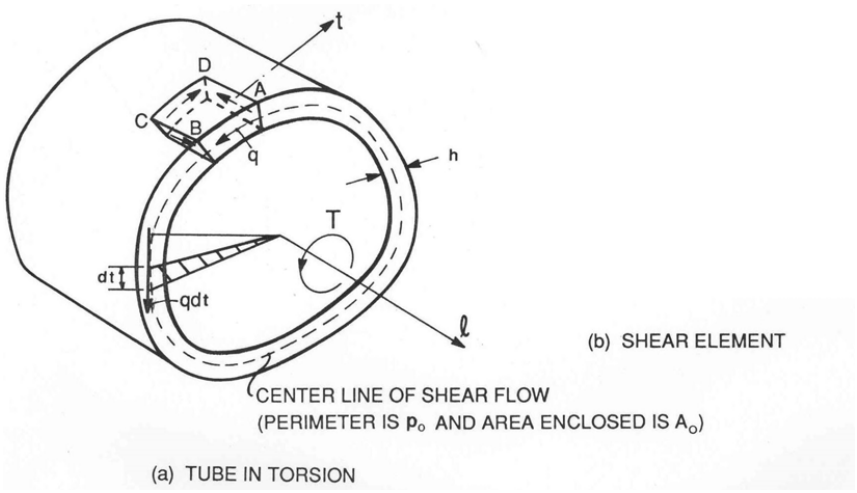

Figure 2.5: Bredt's "thin-tube" theory (ACI Committee 445, 2006)

The shear stress is set equal to the tensile strength of concrete in biaxial tension-compression (σ_1, taken as $4\sqrt{f_c'}$ in the codes). For the case of the American and Canadian Code (ACI-318-05 and CSA A23.3-04) the thickness, t is approximated as $0.75A_{cp}/p_{cp}$ and A_o is taken as $2/3A_{cp}$ where p_{cp} is the perimeter of the concrete and A_{cp} is the area enclosed by this perimeter.

Hsu (1984) explains that prestressing will increase the cracking strength of a concrete member subjected to torsion. Hsu states, "the prestress creates a compressive stress that, in combination with the shear stress created by the torsional moment or shear force, results in a shear-compression biaxial state of stress" (Hsu, 1984, pg. 171). This biaxial stress state causes the increase in torsional cracking strength. For prestressed concrete the effect of the prestress on the principal tensile stress is derived using Mohr's circle and is added as the factor $\sqrt{1+\frac{f_{pc}}{4\sqrt{f_c'}}}$ (Figure 2.6). Adding the prestressing factor to the equation for cracking torque of plain concrete gives the general equation for the cracking torque of a section.

$$T_{cr} = \sigma_1 \left(\frac{A_{cp}^2}{p_{cp}} \right) \sqrt{1+\frac{f_{pc}}{4\sqrt{f_c'}}} \tag{2-5}$$

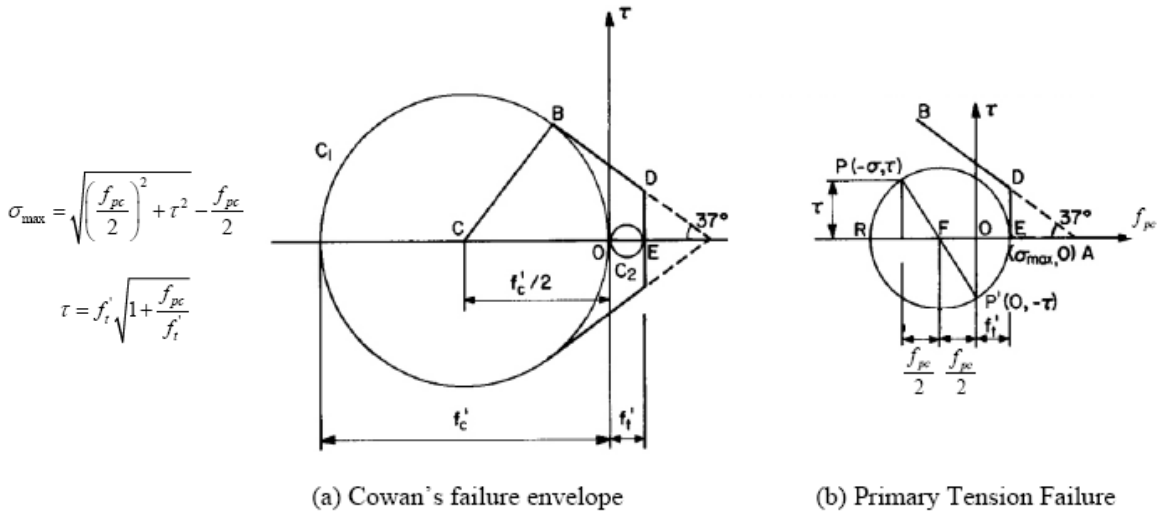

Figure 2.6: Derivation of prestressing factor (ACI Committee 445, 2006)

The American pole standard refers to the AASHTO LTS-4-M (2001) and ASCE-PCI Guide for The Design of Prestressed Concrete Poles (ASCE-PCI Committee Report, 1997) torque formulae. The formulae suggested are identical to the ACI-318-05 (2005) cracking torque formula (Clause R11.6.1) as presented below:

$$T_{cr}^{ACI} = \phi 0.33\sqrt{f'_c}\,\frac{A_{cp}^{\ 2}}{p_{cp}}\sqrt{1+\frac{f_{pc}}{0.33\sqrt{f'_c}}} \quad (f'_c \text{ in MPa}) \tag{2-6}$$

$$T_{cr}^{ACI} = \phi 4\sqrt{f'_c}\left(\frac{A_{cp}^2}{p_{cp}}\right)\sqrt{1+\frac{f_{pc}}{4\sqrt{f'_c}}} \quad (f'_c \text{ in psi}) \tag{2-7}$$

where ϕ is a safety factor for shear and torsion taken as 0.75, f'_c is the concrete compression strength in MPa or psi, A_{cp} is the area of the section including any holes, p_{cp} is the perimeter of the cross section, and f_{cp} is the average compression stress in the concrete due to prestressing in MPa.

For hollow sections, ACI-318-05 (2005) suggests that A_g (the gross section area) be used instead of A_{cp}. The changes were made in the 2002 code based on the 1999 cracking torque formula. A more detailed explanation is given in Clause R11.6.1 in ACI-318-05.

The formula given in CSA A23.3-04 (2004) Canadian concrete standard is practically identical except modified to work with the safety factors given in the Canadian code. In fact, the 0.38 factor is derived from the 0.33 factor from ACI and multiplied by the 0.75 ACI safety factor and divided by the 0.65 CSA concrete material safety factor.

$$T_{cr}^{CSA} = \left(\frac{A_c^{\ 2}}{p_c} \right) 0.38\lambda\phi_c \sqrt{f'_c} \sqrt{1 + \frac{\phi_p f_{cp}}{0.38\lambda\phi_c \sqrt{f'_c}}} \quad (f'_c \text{ in MPa}) \tag{2-8}$$

where λ is a factor for low density concrete (taken as 1 for normal concrete), ϕ_c is a material safety factor taken as 0.65 or 0.7 for precast concrete (Clause 16.1.3), f'_c is the concrete compression strength in MPa, A_c is the area of the section including any holes, p_c is the perimeter of the cross section, ϕ_p is a material safety factor for prestressing steel taken as 0.9, and f_{pc} is the average compression stress in the concrete due to prestressing in MPa. For hollow sections A_c is replaced by $1.5A_g$ if the wall thickness is less than $0.75A_c/p_c$.

The torsional formulae from the CHBDC (CAN/CSA-S6-06, 2006) are similar to those in the CSA A23.3-04 (2004). Torsion is considered significant in the design of a member if the factored torsional load is greater than a quarter of the cracking torque (CHBDC, Clause 8.9.1.1). The cracking torque formula is identical to the formula from CSA A23.3-04 (2004) but uses a factor 0.32 (0.8 multiplied by 0.4 from the f_{cr} term) instead of 0.38 for the biaxial tension compression strength of concrete (CHBDC, Clause 8.9.1.1).

$$T_{cr} = 0.80\phi_c f_{cr} \frac{A_{cp}^{\ 2}}{p_{cp}} \sqrt{1 + \frac{f_{ce}}{0.80\phi_c f_{cr}}} \tag{2-9}$$

where $f_{cr} = 0.4\sqrt{f'_c}$ for normal concrete, and f_{ce} is the stress in the concrete due to prestressing and $\phi_c = 0.75$.

In the German (DIN EN 12843) pole standard, Eurocode 2 (EC 2-1-1:2004, 2004) is referenced to calculate the torsional capacities of poles. EC2 is identical to the German concrete standard, DIN 1045 (2001). Similar to the cracking torque formulae presented for ACI and CSA, EC2 suggests the following formula (taken from Clause 6.3.2, and adding the prestressing effects included by Mohr's circle and the equation for the tensile strength of concrete):

$$T_{cr}^{EC2} = 2A_k t_{ef,i} f_{ctd} \sqrt{1 + \frac{\sigma_{cp}}{f_{ctd}}} \tag{2-10}$$

where $f_{ctd} = \alpha_{ct} \frac{f_{ctk,0.05}}{\gamma_c}$, $f_{ctk,0.05} = 0.7 f_{ctm}$, $f_{ctm} = \begin{cases} 0.30 f_{ck}^{(2/3)} & \text{for } f_{ck} \le 50 \text{ MPa concrete} \\ 2.12 \ln\left(1 + \frac{f_{cm}}{10}\right) & \text{for } f_{ck} > 50 \text{ MPa concrete} \end{cases}$

and $f_{cm} = f_{ck} + 8(MPa)$. A_k is the area enclosed by the centerline of the shear flow thickness including hollow area, $t_{ef,i}$ is the effective wall thickness taken as A/u but not less than twice the distance between the edge and centre of the longitudinal reinforcement (hollow sections use real thickness as an upper limit), A is the total area of the cross section including hollow areas, u is the circumference of the cross section, σ_{cp} is the compressive stress in the concrete due to prestressing, and f_{ctd} is the design tensile strength of the concrete. α_{ct} is a factor for long term effects normally taken as 1, γ_c is the partial safety factor for concrete (1.5 for persistent or transient loads, 1.2 for accidental or 1.0 for unfactored), and $f_{ctk,0.05}$ is the 5% fractal of the characteristic tensile strength of concrete. The mean characteristic tensile strength is represented as f_{ctm} and the characteristic concrete compressive strength (equivalent to f_c') is f_{ck}. f_{cm} is the mean characteristic compressive strength.

The formulae used in the ASCE-PCI Guide (ASCE-PCI Committee Report, 1997) and AASHTO LTS-4-M (2001) are the same as the formulae given in the ACI-318-05 (2005). The previous AASHTO LTS-3 (1994) standard recommended the use of equations modified from the American Concrete Institute standard at that time for nominal moment strength provided by concrete (discussed in AASHTO 1994 – 1986 Commentary). It included an axial stress factor, F_N. Axial stresses, due to prestressing, increase the torsional capacity. An upper limit of 2 for F_N was assumed as a reasonable limit due to the limited research data available for the torsional capacity of prestressed concrete without stirrups. For ultimate strength design torsional strengths are given by the following equation for hollow poles with a inner diameter not more than one-half the pole diameter or width:

$$T_u^{AASHTO,94} = 0.066 \sqrt{f_c'} d_p^{\,3} F_N F_V F_S \tag{2-11}$$

where f_c' in MPa

F_N = axial stress factor = $(1 + 0.29 F_P / A_c)$ where A_c is area of concrete in m^2

F_P = total prestress force after losses in MN

F_S = shape factor = 1.0 for square section, 0.67 for octagonal sections, and 0.58 for circular

F_V = shear reduction factor = $\dfrac{1}{\sqrt{1+\left(\dfrac{0.4 d_p V_p}{T}\right)^2}}$

The cracking torque formulae found in the literature all take the same form as described by MacGregor and Ghoneim (1995), the only difference being the value assumed for the tensile strength of concrete in biaxial tension-compression.

Hsu and Mo (1985) presented a formula for torsional cracking strength based on Bredt's "thin-tube" theory. Using a concrete tensile strength of $2.5\sqrt{f_c^{'}}$ while setting the area A_o to the area of the concrete section, A_c, and using the actual wall thickness of the member Hsu and Mo suggested the following formula:

$$T_{cr}^{HM} = 2A_c t(2.5\sqrt{f_c^{`}})\sqrt{1+\frac{10\sigma}{f_c^{`}}} \quad (f^{`}_c \text{ in psi}) \tag{2-12}$$

where σ = the uniform prestress. The tensile strength is taken as $2.5\sqrt{f_c^{'}}$ and $\dfrac{f_c^{`}}{10}$ ($f^{`}_c$ is in psi) within the prestressing factor. Hsu (1968) showed that an effective cracking torque could be calculated based on the total percentage of torsion reinforcement, both longitudinal and transverse.

$$T_{cr}^{HMeff} = (1+4\rho_{tot})T_{cr}^{HM} \tag{2-13}$$

where T_{cr}^{HM} is as presented above by Hsu and Mo (1985) and $\rho_{tot} = \rho_l + \rho_t$. The longitudinal and transverse reinforcement ratios can be expressed as $\rho_l = \dfrac{A_l}{A_c}$ and $\rho_t = \dfrac{A_t u}{A_c s}$ respectively where: A_l is the area of longitudinal steel, A_c is the area of the concrete section, A_t is the area of one leg of the transverse reinforcement, s is the stirrup spacing, and u is the perimeter of the centre line of the stirrups.

Rahal and Collins (1996) suggested a formula similar to the CSA equation (CSA A23.3-04, 2004), but used $5\sqrt{f_c'}$ instead for the tensile strength of the concrete. The resulting equation for cracking torque is:

$$T_{cr}^{RC} = 5\sqrt{f_c'}\left(\frac{A_c^2}{p_c}\right)\sqrt{1+\frac{f_{pc}}{5\sqrt{f_c'}}} \quad (f'_c \text{ in psi}) \tag{2-14}$$

Similar to Rahal and Collins, Ghoneim and MacGregor (1993) suggested the following formula for cracking torque:

$$T_{cr}^{GM} = 0.46\sqrt{f_c'}\left(\frac{A_c^2}{p_c}\right)\sqrt{1+\frac{f_{pc}}{0.46\sqrt{f_c'}}} \quad (f'_c \text{ in MPa}) \tag{2-15}$$

It should be noted that the T_{cr} equation suggested by Ghoneim and MacGregor (1993) and Rahal and Collins (1996) are for beams subjected to pure torsion whereas the formulae provided by the codes are for combined stresses (Koutchoukai and Belarbi, 2001). The result is that the equations presented by all authors are 40% larger than the code values (Koutchoukai and Belarbi, 2001).

2.4.2 Ultimate Torsional Resistance

The 'State of the Art Report: Design for Torsion in Concrete Structures' by ACI Committee 445 (2006) presents the development of Rausch's space truss model for torsion which is the basis for all codes equations (ACI, CSA, EC2). Presented in the three paragraphs below is a summary of the development from the ACI Committee report.

Ritter (1899) and Mörsch (1902) developed the first theories for shear using a plane truss model consisting of struts and ties. The reinforced concrete member was constructed using compressive carrying struts (concrete) and tension carrying ties (steel). The concept of the struts and ties gave a simple approach to solving shear problems. Rausch extended the 2-D plane truss model developed by Ritter and Mörsch and added the lever arm area idea proposed by Bredt in his "thin-tube" theory.

The space truss model developed by Rausch, in 1927 gave the first theory for torsion. Rausch's space truss model resisted the applied torsional moment by diagonal concrete compressive struts and steel tension ties in the longitudinal and transverse direction (Figure 2.7). Rausch also assumed that the struts were at an angle of 45 degrees and the ties were connected by hinges at the joints. The

forces in the struts, *D*, the forces in the longitudinal bars, *X*, and the forces in the hoop bars, *Q*, are related to one another by equilibrium of the joints in the longitudinal, lateral, and radial directions ($X = Q = \frac{D}{\sqrt{2}}$). The shear flow *q* can be expressed as *Q/s* where *s* is the distance between each successive node in the *Q* and *X* directions.

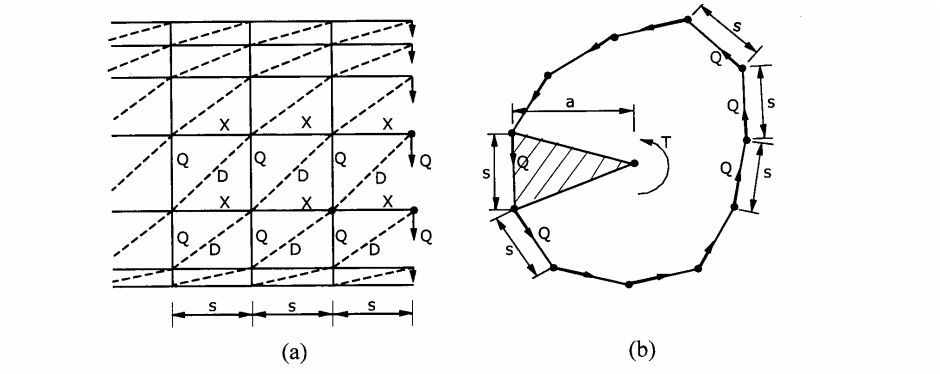

Figure 2.7: Rausch's space truss model (ACI Committee 445, 2006)

Rausch assumed failure to occur when the transverse steel (A_t) at a spacing of s_t reached the yield stress (f_{ty}). Therefore $q = Q/s = A_t f_{ty} / s_t$ and using Bredt's lever arm idea the ultimate torque is:

$$T_n = \frac{2 A_o A_t f_{ty}}{s_t} \tag{2-16}$$

where A_o is the area enclosed by the shear flow path, A_t is the area, f_{ty} is the yield stress, and s_t is the spacing of transverse reinforcement.

When the code equations are compared to Rausch's original equation many similarities can be observed. The only difference is the addition of safety factors and the angle (θ), which represents the angle of inclination of the diagonal compressive stresses to the longitudinal axis of the member.

ACI-318-05 (Clause 11.6.3.6): $T_n = \phi 2 A_o A_t f_{yt} \cot\theta / s \quad \phi = 0.75$ (2-17)

CSA A23-3-04 (Clause 11.3.10.3): $T_r = 2 A_o A_t \phi_s f_y \cot\theta / s \quad \phi_s = 0.85$ (2-18)

Eurocode 2 (Clause 6.3.2): $T_{Rd2} = 2 A_k A_{sw} (f_{sw} / \gamma_c) \cot\theta / s \quad \gamma_c = 1.15$ (2-19)

where A_o, *and* A_k are the areas bounded by the shear flow perimeter, A_t *and* A_{sw} are the areas of transverse (torsional) reinforcement, f_y, f_{yt}, *and* f_{sw} are the yield stress of the transverse reinforcement,

and s is the spacing of the transverse reinforcement. θ is the angle of inclination of the diagonal compressive stresses and ϕ, ϕ_s, *and* γ_c are the code specific safety factors.

The CHBDC and CSA A23.3-04 provide the same formula for calculating the ultimate torsional resistance of a section, except a higher material resistance is used for the prestressing and reinforcing steel (0.95 and 0.90 respectively).

In addition each code has additional clauses for checking the adequate amount of longitudinal reinforcing and cross section/concrete strut crushing strengths. The lowest value is taken then as the ultimate torsional resistance. In the case of concrete poles the cross section is usually strong enough for crushing and the governing factor is the transverse/helical reinforcement.

2.5 Minimum Transverse Reinforcing Spacing

Transverse reinforcement for torsion in all codes is determined by setting $T_r > T_f$ and adding the amount to the transverse reinforcement required for shear. T_r is calculated using the formulae given in section 2.4.2. In the case of CSA A23.3-04 (2004) and ACI-318-05 (2005), if T_f is less than $0.25T_{cr}$ then torsional transverse reinforcement is not required.

The minimum transverse reinforcement requirements for torsion are based on the minimum shear reinforcing requirements and are empirically based. ACI gives the following minimum requirement for shear and torsion transverse reinforcement (Clause 11.6.5.4):

$$A_v + \frac{A_t}{2} = 0.75\sqrt{f_c'}\left(\frac{b_w s}{f_{yt}}\right) \text{ (Imperial units) but not less than } (50b_w s)/f_{yt} \qquad (2\text{-}20)$$

$$A_v + \frac{A_t}{2} = 0.0625\sqrt{f_c'}\left(\frac{b_w s}{f_{yt}}\right) \text{ (SI units: 0.0625 = 1/16) but not less than } (0.33b_w s)/f_{yt} \qquad (2\text{-}21)$$

where A_v is the area of shear reinforcement (in^2, mm^2), A_t is the area of torsional reinforcement (in^2, mm^2), f'_c is the concrete compressive strength (psi, MPa), b_w is the width of the web (in, mm), s is the spacing of the transverse reinforcement (in, mm), and f_{yt} is the yield stress of the transverse reinforcement (psi, MPa).

Clause 11.5.6.3 indicates that the minimum shear reinforcement, $A_{v,min}$ is equal to the right hand side of the equations above. For prestressed members it is suggested that the minimum shear reinforcement be the smaller of Clause 11.5.6.3 and 11.5.6.4 (shown below):

$$A_{v,\min} = \frac{A_{ps} f_{pu} s}{80 f_{yd}} \sqrt{\frac{d}{b_w}} \text{ (Imperial units)} \quad (2\text{-}22)$$

where $A_{v,min}$ is the minimum area of shear reinforcement (in^2), A_{ps} is the area of prestressing reinforcement (in^2), f_{pu} is the prestressing ultimate stress (psi), b_w is the width of the web (in), s is the spacing of the transverse reinforcement (in), d is the distance from the compressive flange to the reinforcing steel (in), and f_{yd} is the yield stress of the transverse reinforcement (psi).

The maximum spacing for transverse reinforcement according to ACI-318-05 is as follows (Clause 11.5.5.1):

$d/2$ for non-prestressed members

$0.75h$ for prestressed members or 24 inches whichever smaller

where d is the distance from the compressive flange to the reinforcing steel, and h is the height of the section.

ACI-318-05 Clause 11.5.5.2 gives another spacing requirement that at least one transverse reinforcement steel bar must intercept a 45 degree inclined line to the member axis drawn through the midpoint of the member extending to the flexural tension steel. In addition if the shear force in the steel exceeds $4\sqrt{f_c'} b_w d$ ($0.33\sqrt{f_c'} b_w d$) then the requirements of Clause 11.5.5.1 and 11.5.5.2 must be decreased by half (Clause 11.5.5.3). Clause 11.6.6 also limits the maximum spacing for transverse torsional reinforcement as $p_h/8$ (where p_h is the perimeter at the level of the transverse reinforcement) or 12 inches whichever smaller.

CSA A23.3-04 presents similar requirements to those of ACI-318-05 for minimum shear reinforcement and maximum spacing. According to CSA Clause 11.3.8.1 torsional reinforcement can be placed using spirals and the maximum spiral spacing is governed as follows:

If $V_f < (0.125\phi_c f_c' b_w d_v + V_p)$ or $T_f \le 0.25 T_{cr}$ then

s_{max} is 600 mm or $0.7d_v$ (where d_v is the effective depth).

If $V_f > (0.10\phi_c f_c' b_w d_v + V_p)$ or $T_f > 0.25 T_{cr}$ then Clause 11.3.8.3 reduces the requirements by half to:

s_{max} is 300 mm or $0.35d_v$ (where d_v is the effective depth).

where f'_c is the compressive strength in MPa, b_w is the effective web width (mm), d_v is the effective shear depth (mm), V_p is the shear force due to prestressing (kN), T_f is the factored torsional moment, T_{cr} is the cracking torque and s_{max} is the maximum spacing of the transverse reinforcement (mm).

CSA A23.3-04 Clause 11.3.8.2 indicates one line of effective shear reinforcement must intercept a line drawn at 35 degrees from the member axis. The minimum amount of transverse reinforcement is given by Clause 11.2.8.2 and is calculated as follows:

$$A_{v,\min} = 0.06\sqrt{f_c'}\left(\frac{b_w s}{f_y}\right) \tag{2-23}$$

where b_w is the effective web width (mm) with the effective depth of the section (d_v) (mm), s is the spacing the reinforcing (mm), and f_y is the reinforcement yield stress (MPa). For a solid circular section b_w is taken as the diameter (Clause 11.2.10.3).

The requirements are also very similar to those given in the CHBDC (CAN/CSA-S6-06, 2006). According to CHBDC Clause 8.1.4.5.2 torsional reinforcement can be placed using spirals and the maximum spiral spacing is governed as follows:

If $V_f < (0.10\phi_c f_c' b_w d_v + V_p)$ or $T_f \le 0.25T_{cr}$ then

s_{max} is 600 mm or $0.75d_v$ (where d_v is the effective depth).

If $V_f > (0.10\phi_c f_c' b_w d_v + V_p)$ or $T_f > 0.25T_{cr}$ then

s_{max} is 300 mm or $0.33d_v$ (where d_v is the effective depth).

The minimum amount of transverse reinforcement is given by CHBDC Clause 8.9.1.3 and is calculated using:

$$A_{v,\min} = 0.15 f_{cr}\left(\frac{b_w s}{f_y}\right) \tag{2-24}$$

where b_w is the effective web width with the effective depth of the section (d_v), s is the spacing the reinforcing, and f_y is the reinforcement yield stress. For a solid circular section b_w is taken as the diameter. If the 0.4 factor is included from the f_{cr} variable the formula given by Clause 8.9.1.3 gives the 0.06 coefficient used in CSA A23-3-04 (2004).

EC-2 suggests the minimum shear reinforcement be taken as (Clause 9.2.2 (5) and (6)):

$$A_{v,\min} = 0.08\sqrt{f_{ck}}\left(\frac{b_w s}{f_{yk}}\right) \tag{2-25}$$

where f_{ck} is the characteristic compressive strength (MPa), b_w is the effective web width (mm), s is the spacing of the transverse reinforcement (mm), and f_{yk} is the characteristic yield stress of the transverse reinforcement (MPa).

Maximum spacing of the transverse reinforcement, $s_{t,max}$ is taken as 0.75d or 600 mm whichever is less. For torsion Clause 9.2.3 (2) indicates that the minimum requirements for shear are generally sufficient for minimum torsional reinforcement required.

The minimum requirements for torsion could alternatively be derived by setting $T_r >= \lambda T_{cr}$ (Ali and White, 1999 and Koutchoukali and Belarbi, 2001). The cracking torque is multiplied by a factor, taken as 1.2 (Koutchoukali and Belarbi, 2001) or 1.5-1.7 (Ali and White, 1999), to include reserve strength after cracking. Koutchoukali and Belarbi presented the following equation for the transverse reinforcement requirements derived using the cracking torque equation given by Ghoneim and MacGregor (1993):

$$\left(\frac{A_t}{s}\right)_{\min} = 0.28\frac{\sqrt{f_c'}A_c^{\,2}}{f_{yt}A_o p_c} \tag{2-26}$$

where A_t is the transverse reinforcement area (mm^2), s is the spacing (mm), f'_c is the compressive stress in the concrete (MPa), A_c is the area of the concrete (mm^2), f_{yt} is the yield stress of the transverse reinforcement (MPa), A_O is the area enclosed by the shear flow path (mm^2), and p_c is the perimeter of the concrete section (mm).

Similarly Ali and White (1999) derived an equation for minimum transverse reinforcement from the ACI cracking torque formula relating to the longitudinal reinforcement and not the concrete strength.

$$\left(\frac{A_t}{s}\right)_{\min} = \frac{A_l}{p_h \frac{f_{yv}}{f_{yl}}\cot^2(\theta)} \tag{2-27}$$

where A_t is the transverse reinforcement area (mm^2), s is the spacing (mm), A_l is the area of the longitudinal reinforcement (mm^2), f_{yv} is the yield stress of the transverse reinforcement (MPa), f_{yl} is

the yield stress of the longitudinal reinforcement (MPa), θ is the angle of inclination of the diagonal compressive stresses, and p_h is the perimeter of area enclosed by the transverse reinforcement (mm).

If the λ factor is not used in the derivation and the CSA cracking torque formula is used the following expression can be derived:

$$\left(\frac{A_t}{s}\right)_{\min} = \frac{0.38\sqrt{f_c'}t}{f_y \cot(\theta)} \tag{2-28}$$

where A_t is the transverse reinforcement area (mm^2), s is the spacing (mm), f_c' is the compressive strength (MPa), t is the thickness of the shear flow zone (mm), f_y is the yield stress of the transverse reinforcement (MPa), and θ is the angle of inclination of the diagonal compressive stresses.

2.6 Torsion Models

2.6.1 Mechanics of Torsion in Reinforced Concrete Members

The modelling of torsion generally must satisfy three principles: Equilibrium, Compatibility, and Constitutive Relationships. For torsion we must add equations relating to the shape, and twisting of the cross section to the equations used for shear. As summarized by Hsu (1988) in the following table, there are a total of 16 equations and 19 variables required to model torsion behaviour for reinforced concrete members.

Table 2-6: Summary of Variables and Equations for Torsion (Hsu, 1988)

	Variables			Equations		
Category	Stress or force	Strain, deformation, or geometry	Material	Equilibrium	Compatibility	Material
For shear	σ_1	ϵ_1	ζ	Eq. (1)	Eq. (4)	†Eq. (7*)
	σ_2	ϵ_2		(2)	(5)	(8)
	τ_{12}	γ_{12}		(3)	(6)	*(9*)
	σ_d	ϵ_d				(10)
	*σ_r 0	ϵ_r				(11)
	f_1	α				
	f_2					
Additional for torsion	T	θ	k_1	(23)	(24)	(28)
		ψ			(25)	†(29)
		t_d			(26)	
		ϵ_{as}			(27)	
Total for torsion		7 + 10 + 2 = 19			4 + 7 + 5 = 16	

*When tensile strength of concrete is neglected, $\sigma_r = 0$ and Eq. (9) become irrelevant.
**Eq. (7) used in shear is replaced by Eq. (29) applicable to torsion.

2.6.1.1 Equilibrium Conditions

To derive equations for equilibrium in a torsion member, a coordinate system must be established. Typically the *r* and *d* directions are used to define the coordinates of principal stress in the diagonal concrete struts (Figure 2.8). The *l* and *t* directions are used to represent the coordinate system of the reinforced concrete member. For a typical horizontal and vertical reinforced member, the *l* and *t* directions are in the same directions as the longitudinal steel and transverse steel respectively.

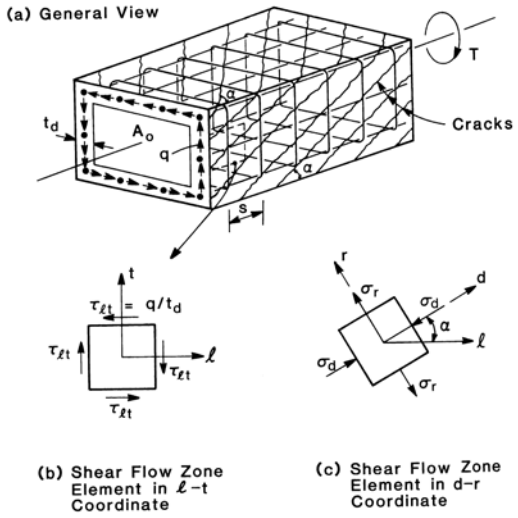

Figure 2.8: Coordinate systems and variable definition (ACI Committee 445, 2006)

The equations for Mohr's circular stress condition relate the stress in the concrete in the *r* and *d* directions to the stresses in the reinforced concrete section in the *l* and *t* directions. The stresses in the conventional steel and prestressing strands must be added to maintain equilibrium of the section. The equations presented included prestressing stresses.

$$\sigma_l = \sigma_d \cos^2 \alpha + \sigma_r \sin^2 \alpha + \rho_l f_l + \rho_{lp} f_{lp} \tag{2-29}$$

$$\sigma_t = \sigma_d \sin^2 \alpha + \sigma_r \cos^2 \alpha + \rho_t f_t + \rho_{tp} f_{tp} \tag{2-30}$$

$$\tau_{lt} = (-\sigma_d + \sigma_r) \sin \alpha \cos \alpha \tag{2-31}$$

where: all ρ are taken with respect to the thickness of the shear flow zone t_d

Typically, for torsional analysis the tensile strength of concrete is neglected ($\sigma_r = 0$). Also for pure torsion applications two variables are already known, $\sigma_l = \sigma_t = 0$.

A fourth equilibrium equation is required relating the shear stress acting on the cross section to the applied T and the shear flow zone of the member. Bredt's equilibrium condition gives the equilibrium of the cross section as a whole.

$$\tau_{lt} = \frac{T}{2A_o t_d} \tag{2-32}$$

where: T is the applied torque, A_o is the area enclosed by the shear flow path, and t_d is the thickness of the shear flow zone

2.6.1.2 Compatibility Conditions

The compatibility conditions relate the strains in the r and d directions to the strains in the l and t directions. The deformations caused by the shear stress must satisfy the following equations:

$$\varepsilon_l = \varepsilon_d \cos^2\alpha + \varepsilon_r \sin^2\alpha \tag{2-33}$$

$$\varepsilon_t = \varepsilon_d \sin^2\alpha + \varepsilon_r \cos^2\alpha \tag{2-34}$$

$$\frac{\gamma_{lt}}{2} = (-\varepsilon_d + \varepsilon_r)\sin\alpha\cos\alpha \tag{2-35}$$

The twisting angle of a member, θ in torsion can be related to the shear strain, γ_{lt} in the wall of a tube using the warping deformation compatibility condition:

$$\theta = \frac{p_o}{2A_o}\gamma_{lt} \tag{2-36}$$

where: p_o is the perimeter of the shear flow path, and A_o is the area enclosed by the path

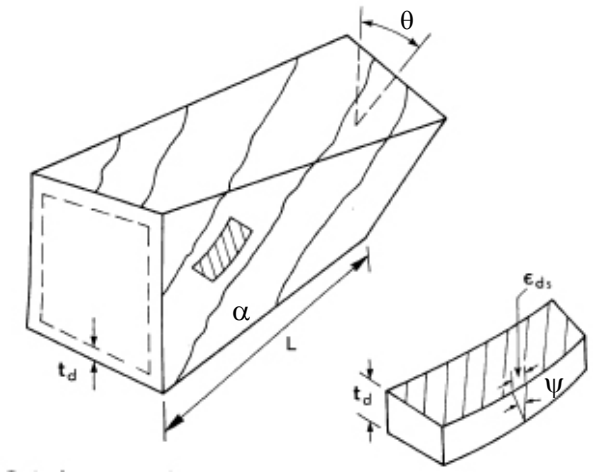

Figure 2.9: Warping of member wall section (Collins and Mitchell, 1974)

The diagonal compression struts are under compression due to shear but also bending due to the warping of the member wall (Figure 2.9). The equation for relating the curvature of the concrete strut, ψ to the angle of twist, θ by the angle of inclination of the diagonal compression strut, α is:

$$\psi = \theta \sin 2\alpha \tag{2-37}$$

Due to the bending of the compression strut, there are two additional compatibility equations needed to relate the strain distribution in the strut to the shear flow thickness, t_d. Using Bernoulli's plane section hypothesis from bending theory, the maximum strain at the surface of the compression strut, ε_{ds} is related to the curvature of the strut as follows (Figure 2.10):

$$t_d = \frac{\varepsilon_{ds}}{\psi} \tag{2-38}$$

The average strain in the *d* direction is simply:

$$\varepsilon_d = \frac{\varepsilon_{ds}}{2} \tag{2-39}$$

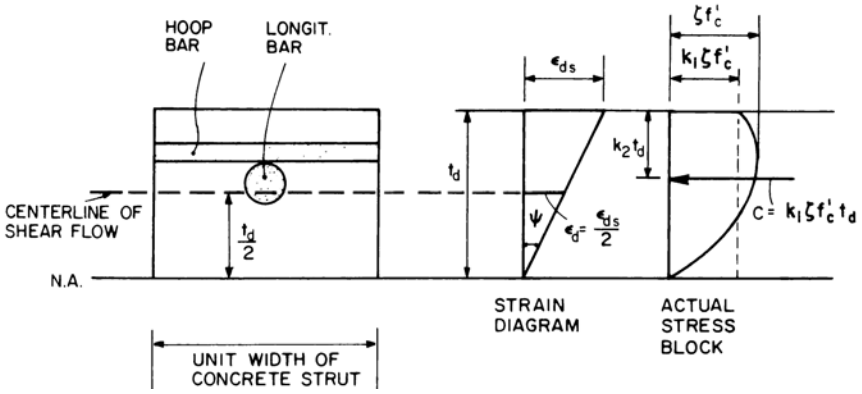

Figure 2.10: Strain and Stress Distribution in Concrete Struts (ACI Committee 445, 2006)

2.6.1.3 Material Laws (Constitutive Conditions)

For the concrete, the non-softened (in the case of the Compression Field Theory - Spalled Model) or softened stress-strain (Softened Truss Model) compressive curve is used and the tensile strength of concrete is neglected (Figure 2.11).

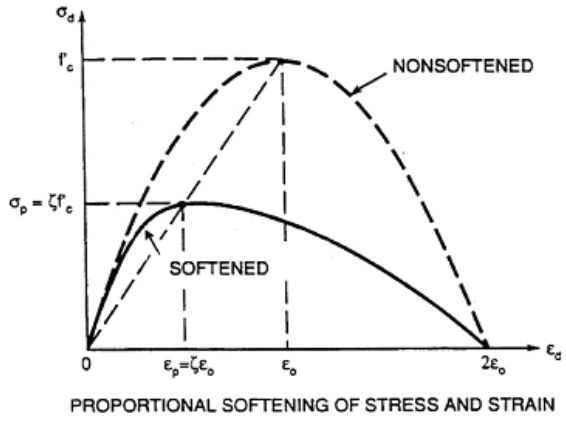

Figure 2.11: Softened stress-strain curve for concrete (Pang and Hsu, 1996)

In the case of the Compression Field Theory (Spalled Model), the non-softened curve for concrete is used and the concrete stress is calculated using compression block theory. The stress in the concrete is then $\sigma_d = \alpha f_c^{`}$ and the depth of the compression block is calculated using $a = \beta t_d$.

For the Softened Truss Model the stress in the concrete strut is calculated using the softening coefficient and the coefficient k_1 which considers the bending and axial compression in the strut. The stress in concrete is calculated as:

$$\sigma_d = k_1 \varsigma f_c^{'} \tag{2-40}$$

where k_1 is the ratio of the average stress to peak stress in the stress block, ς is the softening coefficient

$$k_1 = \frac{\varepsilon_{ds}}{\zeta \varepsilon_o}\left(1 - \frac{1}{3}\frac{\varepsilon_{ds}}{\zeta \varepsilon_o}\right) \quad \text{where} \quad \frac{\varepsilon_{ds}}{\zeta \varepsilon_o} \le 1 \tag{2-41}$$

$$k_1 = \left[1 - \frac{\zeta^2}{(2-\zeta)^2}\right]\left(1 - \frac{1}{3}\frac{\zeta \varepsilon_o}{\varepsilon_{ds}}\right) + \frac{\zeta^2}{(2-\zeta)^2}\frac{\varepsilon_{ds}}{\zeta \varepsilon_o}\left(1 - \frac{1}{3}\frac{\varepsilon_{ds}}{\zeta \varepsilon_o}\right) \quad \text{where} \quad \frac{\varepsilon_{ds}}{\zeta \varepsilon_o} > 1 \tag{2-42}$$

$$\zeta = \frac{5.8}{\sqrt{f_c^{'}(MPa)}}\frac{0.9}{\sqrt{1 + 400\varepsilon_r}} \le 0.9 \tag{2-43}$$

For both theories a simple elastic-perfectly plastic stress strain relationship is assumed for the conventional steel reinforcement. The elastic portion of the prestressing curve is considered a linear relationship and the plastic portion is approximated by Ramberg-Osgood curve (Hsu, 1991).

Conventional Steel:

$$\varepsilon_t \ge \varepsilon_{ty} \quad f_t = f_{ty} \tag{2-44}$$

$$\varepsilon_t < \varepsilon_{ty} \quad f_t = E_s \varepsilon_t \tag{2-45}$$

$$\varepsilon_l \ge \varepsilon_{ly} \quad f_l = f_{ly} \tag{2-46}$$

$$\varepsilon_l < \varepsilon_{ly} \quad f_l = E_s \varepsilon_l \tag{2-47}$$

Prestressing Steel:

$$f_p = E_{ps}(\varepsilon_{dec} + \varepsilon_s) \quad f_p \le 0.7 f_{pu} \tag{2-48}$$

$$f_p = \frac{E^{'}_{ps}(\varepsilon_{dec} + \varepsilon_s)}{\left[1 + \left(\left(E^{'}_{ps}(\varepsilon_{dec} + \varepsilon_s)\right)/ f_{pu}\right)^m\right]^{1/m}} \quad f_p > 0.7 f_{pu} \tag{2-49}$$

2.6.2 Analytical Models for Torsion

There are two primary models used for torsional analysis of a section: the Compression Field Theory and the Softened Truss Model. The two theories are both based on Rausch's truss model and are considered compatibility compression field theories based on the variable-angle truss model (Hsu, 1984). The assumptions of the variable-angle truss model are listed below as given in Hsu (1984):

1. The truss model is constructed using the diagonal concrete struts inclined at an angle, α, and the longitudinal and transverse bars.

2. The diagonal concrete struts carry the principal compressive stress. The shear resistances of the concrete struts and the compression chord are not considered.

3. Longitudinal and transverse bars carry only axial tension (no dowel resistance).

4. The tensile strength of concrete is neglected.

5. For a solid section subjected to torsion, the concrete core does not contribute to the torsional resistance.

2.6.2.1 Compression Field Theory "Spalled Model"

The Compression Field Theory was proposed first by Mitchell and Collins (1974). The theory was derived in a similar way to the "tension field theory" by Wagner (1929) and assumes that after cracking the concrete carries no tension and shear and torsion are carried by fields of diagonal compression.

In addition Mitchell and Collins (1974) also suggested, based on experimental evidence that the outer concrete would spall at high loads. Mitchell and Collins (1974) suggested that compression in concrete will push off the corners of the concrete while tension in the transverse steel will try to hold the concrete (Figure 2.12). As a result, large tensile stresses are developed. Since concrete is weak in tension, the concrete cover spalls off. The process is explained further by Rahal and Collins (1996). The field of compressive stresses changes direction at the corner of a section and tensile stresses are developed perpendicular to the compressive trajectories. Concrete cracks when the tensile stresses reach the tensile strength of the concrete. Bond deterioration effects and less concrete area available to resist the tensile forces causes the concrete to crack along the stirrups. The concrete cover spalls and reduces the area of concrete (A_o) available to resist the applied torsion.

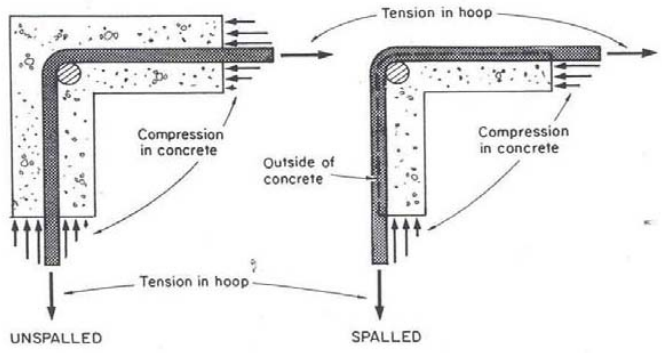

Figure 2.12: Spalling of Concrete Cover (ACI Committee 445, 2006)

The spalling assumption was verified using an ideal concrete beam with steel angles on all sides reducing the cover to zero and making concrete spalling impossible. For this test the diagonal compression field theory was able to predict the observed behaviour well (Mitchell and Collins, 1974). The Compression Field Theory therefore takes the effective outer edge of the shear flow zone as transverse reinforcement centreline (Figure 2.13).

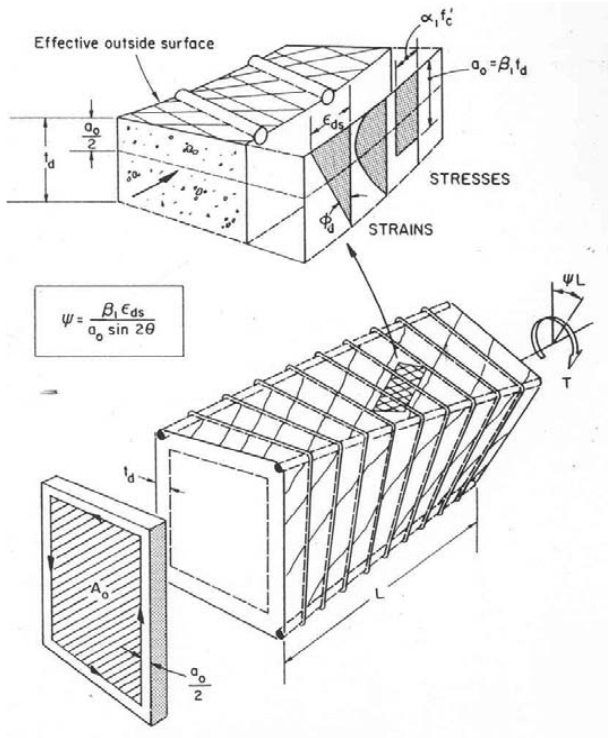

Figure 2.13: Compression Field Theory Shear Flow (ACI Committee 445, 2006)

The area enclosed by the shear flow path and perimeter of the shear flow path are taken as follows:

$$A_o = A_{oh} - \frac{a_o}{2} p_h \tag{2-50}$$

$$p_o = p_h - 4a_o \tag{2-51}$$

where $a_o = \beta_l t_d$ (stress block factors), A_{oh} is the area measured to the middle of the outer closed stirrups, and p_h is the outer perimeter of the cross section.

A typical solution for a pure torsion case would take the following form (from ACI Committee 445, 2006):

1. A value of strain is selected in the *d* direction.
2. The value of the equivalent depth of compression is then estimated.
3. Using the estimated depth of compression and the geometry the values A_o and p_o can be calculated.
4. Tensile stresses in the longitudinal and transverse steel as well as the diagonal compressive stresses can then be calculated from the truss equilibrium equations.
5. Strains in the *l*, *t* and *d* directions can be calculated and the values can be used to check the estimated value of the compression depth.
6. Convergence the compression depth gives the torque resistance and twist of the member.

The full torque-twist curve is found by selecting varying values of strain in the *d* direction up to 0.0035.

2.6.2.2 Softened Truss Model

The Softened Truss Model was proposed by Hsu (1988) and is similar to the theory developed by Collins and Mitchell. The Softened Truss Model used the same equilibrium and compatibility equations but included the softening effects of the compressive strength of concrete. The Softened Truss Model assumes that the concrete outside of the transverse reinforcement participates in resisting the applied torsion and therefore no spalling of the concrete occurs (Figure 2.14).

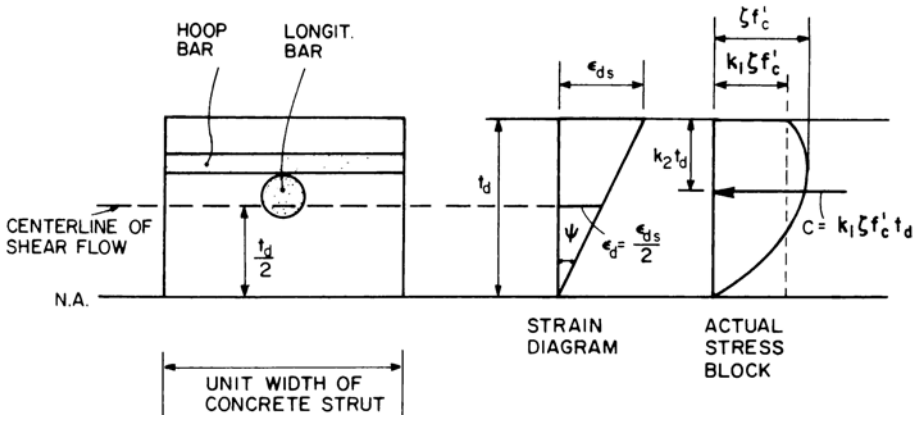

Figure 2.14: Softened Truss Model Stress Distribution (ACI Committee 445, 2006)

Since the spalling of the concrete is not consider and the shear flow thickness is measured from the outer concrete surface, the area enclosed by the shear flow path and perimeter of the shear flow path (A_o and p_o) are found using the following equations:

$$A_o = A_c - \frac{t_d}{2} p_c + \xi t_d^{\,2} \tag{2-52}$$

$$p_o = p_c - 4\xi t_d \tag{2-53}$$

where: A_c is the member cross section, p_c is the member perimeter, t_d is the shear flow zone thickness, and ξ is a shape factor (1 for rectangular, 0.25 for circular).

To determine the torque-twist curve of a member using the Softened Truss Model, the rotating-angled softened truss model approach is used (Hsu, 1988):

1. First a value of strain in the *d* direction is taken and a trial value of strain in the *r* direction is assumed.
2. The softening coefficient, k_1 coefficient, and stress in the *d* direction can then be calculated.
3. A trial value of the shear flow thickness is assumed and used to calculate the A_o and p_o.
4. The angle of inclination can be calculated using the strains in the *l* direction.
5. The shear flow thickness is calculated using the angle of inclination.

6. The strain in the *r* direction is calculated and yielding in the *t* direction is checked. If the strain in *r* does not match the initial guess, a new value of strain in *r* is selected until convergence occurs.

7. Once the strain has converged, the torque and twist values can be calculated.

The full torque-twist curve is found by selecting varying values of strain in the *d* direction up to 0.0035.

Another approach taken by Hsu and Zhang (1997) is the Fixed-Angled Softened Truss Model. Instead of calculating the angle of inclination, it is a known variable and calculated from the applied stresses in the *l* and *t* directions and the shear stress in the *lt* directions. Hsu and Zhang (1997) were able to consistently achieve very good results with the Fixed-Angled Softened Truss Model which is based on a macroscopic "smeared-crack" model.

2.6.2.3 Differences between the Compression Field Theory and Softened Truss Model

There are few differences between the two theories presented in the previous section. The Compression Field Theory (CFT) assumes spalling of the concrete cover and uses a non-softened stress-strain curve for the concrete. The Softened Truss Model (STM) does not consider concrete cover spalling and uses the softened stress-strain curve.

The use of the non-softened concrete stress-strain curve was found to yield very unconservative torsional strengths according to Hsu (1984) and therefore the softened curve should be used. However the conservative assumption of cover spalling and the unconservative assumption a non-softened stress-strain curve used in the CFT appeared to balance one another (ACI Committee 445, 2006). McMullen and El-Degwy (1985) tested thirteen rectangular beams and compared the results to both the CFT and STM models. McMullen and El-Degwy concluded that the STM gave the most realistic predictions of the torsion strain curves but gave different failure modes than the experimental results. The CFT however gave the best prediction of the failure result. Spalling was found to occur either at or after the maximum torque and therefore McMullen and El-Degwy suggested that the full cross section be used in analysis. Rahal and Collins (1996) indicate that the magnitude of the compressive force changing direction at the corner is the critical parameter in spalling. The potential for spalling increases with an increase in cover and applied load level, since compressive forces will be larger while the tensile strength of concrete and spacing of reinforcement are other factors (Rahal and Collins, 1996). Rahal (2000) explains that while it is conservative to assume that the cover spalls

off, experimental evidence indicates that spalling will occur when cover is larger. However when the cover is small the concrete cover portion contributes in resisting the applied torque. It is suggested therefore by Rahal and Collins (1996) that spalling should be considered in sections where the concrete cover exceeds 30 percent of the ratio of the area of concrete to the perimeter of the concrete (A_c/p_c) and the parameters A_{oh} and p_h be used instead of A_c and p_c. The conservative assumption that the concrete cover spalls off near ultimate conditions is used in the ACI, CSA, and Eurocode 2 codes. Current revisions to the base model have been done for each theory. Modified Compression Field theory was incorporated into the CFT model which included the effects of a softened concrete compression curve. The Softened Truss Model was modified to the previously mentioned Fixed-Angled STM model, improving the model's prediction of test results. However the issue still remains to what extent spalling occurs and researchers are also trying to better understand the softened curve of concrete and the shear flow zone.

While there are differences between the two models, there are many advantages of using one of these models over other models, such as skew-bending theories. Hsu (1984) explains that the variable-angle truss models provide a clear concept for shear and torsion after cracking and therefore provide a good basis for design codes. The models also provide a unified theory for shear and torsion which includes the interaction between torsion, shear, bending, and axial loads, and the effects of prestressing. The theories can also predict the entire load response history after cracking reasonably well whereas with skew-bending theories only the ultimate failure load can be determined.

Chapter 3
Analytical Models for Concrete Pole Design

3.1 General Pole Design

The design of bending and shear in concrete poles is based on the standard beam approach used for all concrete members. The design for bending moments in concrete poles involves the hollow circular geometry. As the neutral axis changes location (due to loading), the concrete compression area must be re-calculated based on the circular geometry (Figure 3.1). The area of the circular segment must be calculated knowing the angle, θ, to the chord segment and the radius of the pole. When the neutral axis is larger than the wall thickness, a donut shaped area must be calculated. The area of the hollow inner circular segment must be subtracted from the outer concrete area. Several papers address the design of concrete poles and outlined solutions using computer programs (Rosson et al., 1996; Bolander et al., 1988; and the ASCE-PCI Committee Report, 1997).

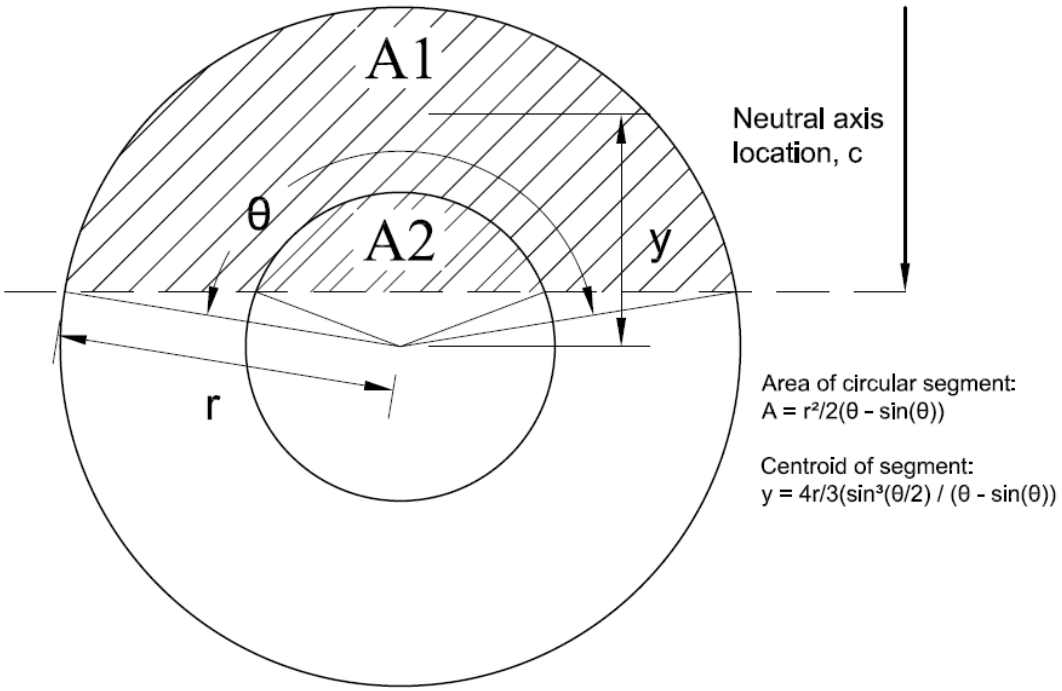

Figure 3.1: Calculation of pole concrete compression area

To aid in the analysis of the concrete pole specimens, a MatLab program was created to calculate the bending resistance of prestressed concrete poles. The program was based on the papers by Rosson et al. (1996), Bolander et al. (1988), and the ASCE-PCI Committee Report on concrete pole design (1997). The pole design experience of The Walter Fedy Partnership, a consulting company in Kitchener, Ontario was also used as a starting point for the program. Using the design formulae and values outlined in ACI-318-05 and CSA A23.3-04, the program can calculate the cracking moments and ultimate moments from both codes. The program was then further developed to include shear and torsional resistances and the ability to analyze the moment resistance about the longitudinal axis at any reinforcement angle, κ (Figure 3.2). It was determined that the rotated geometry presented in Figure 3.2 a) represents the critical moment design geometry for round poles (geometry Figure 3.2 b) has slightly higher moment resistances).

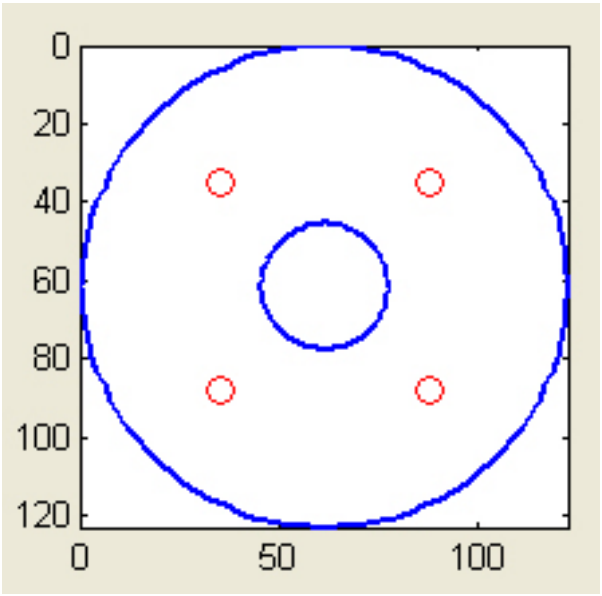

a)

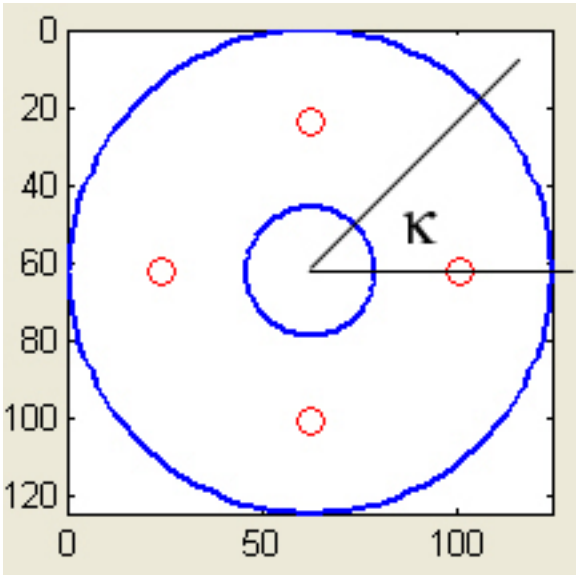

b)

Figure 3.2: Rotated geometry of prestressing strands

3.2 Pole Capacity Calculation Program

A summary and flowchart (Figure 3.3) of the pole capacity calculation program is provided to demonstrate how the program calculates the capacity of the concrete pole. The program's results were validated by comparison with a prestressed pole design completed by The Walter Fedy Partnership.

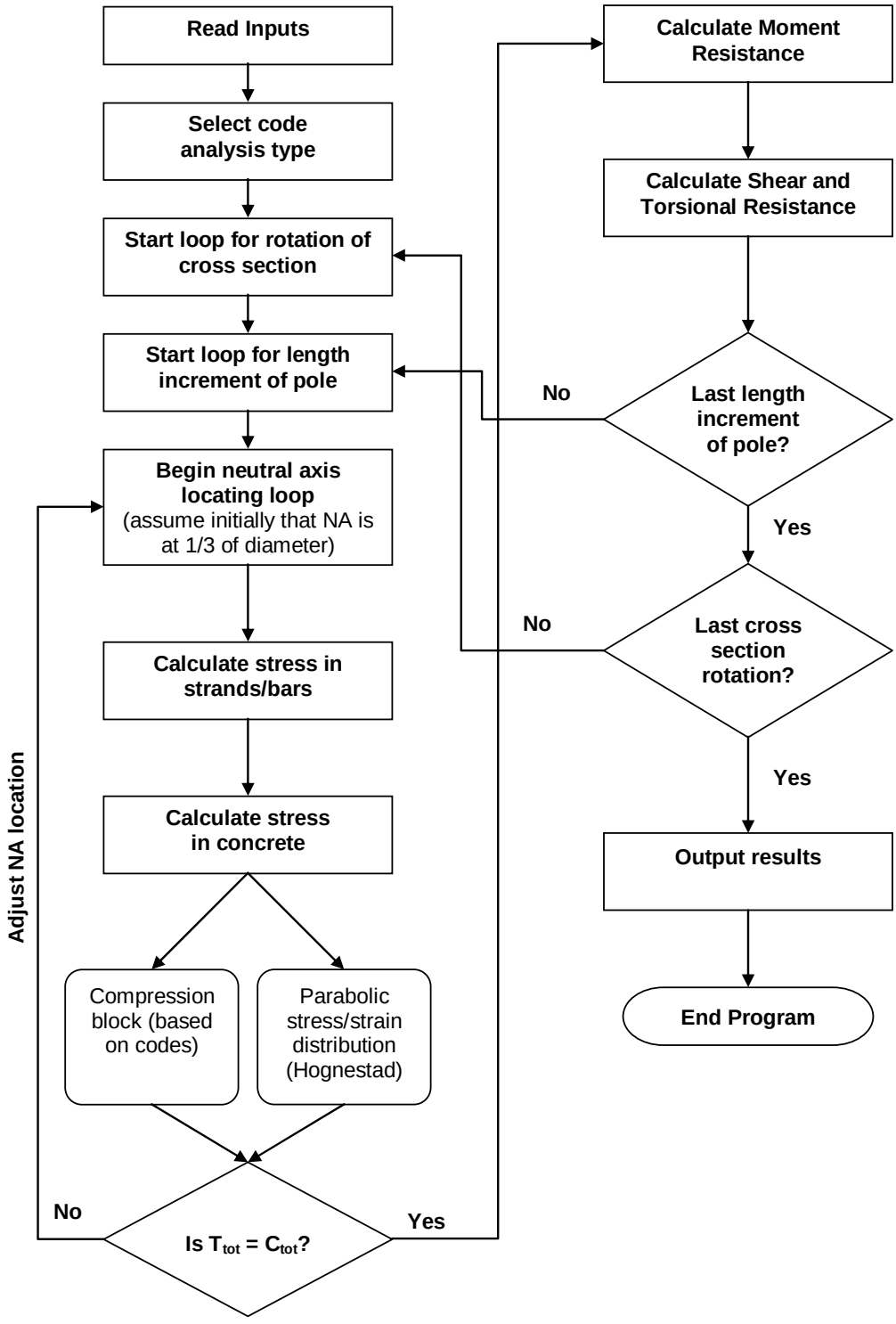

Figure 3.3: Flowchart of Pole Capacity Calculation Program

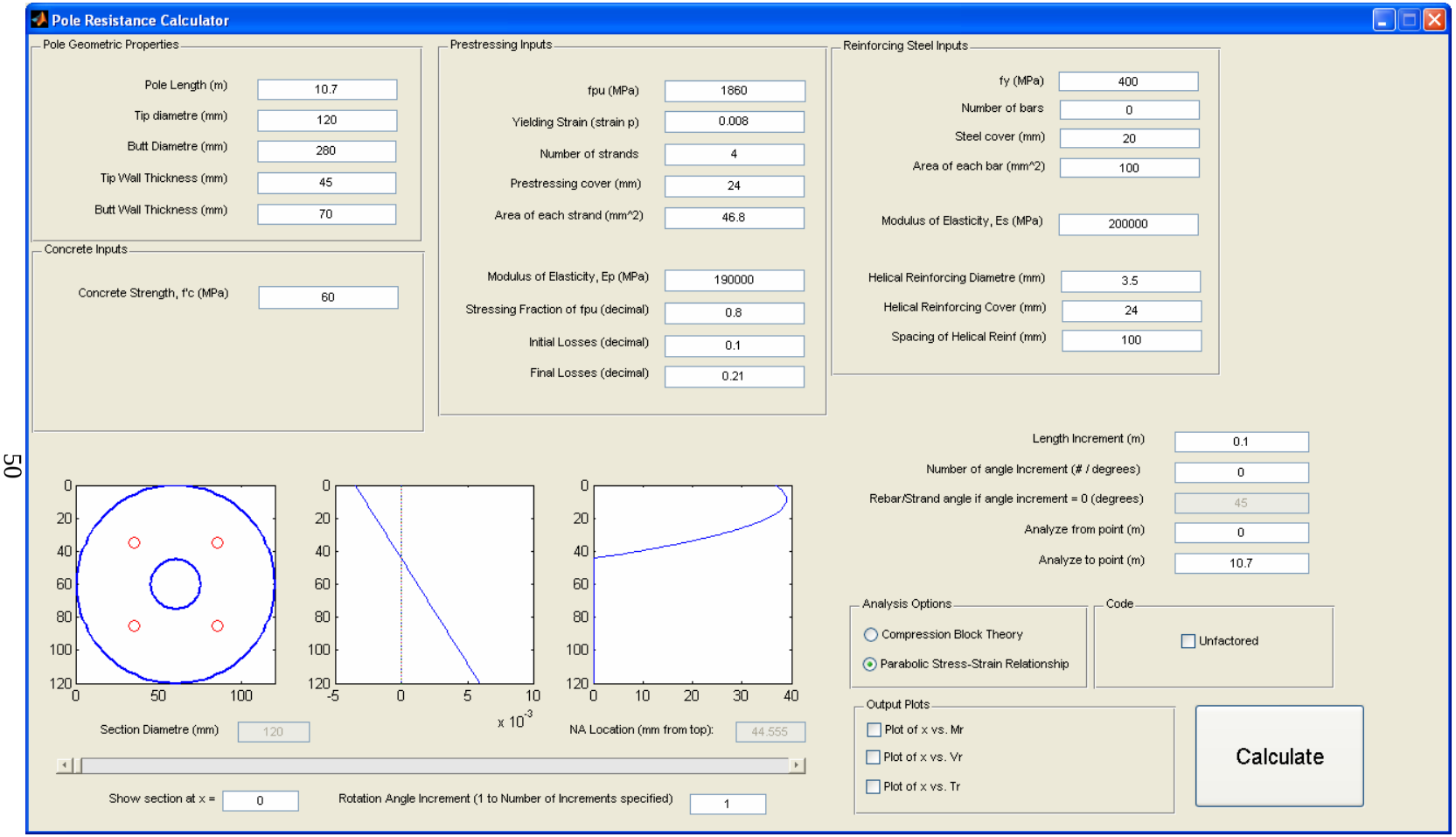

Figure 3.4: Screenshot of Pole Capacity Calculation Program

The analysis begins by reading the inputs from the graphical user interface (Figure 3.4). The user can specify the geometric properties of the pole, the concrete/prestressing/reinforcing steel properties and helical reinforcing amount and spacing. The analysis can be run using the compression block theory as outlined in the ACI and CSA concrete codes or using Hognestad's parabola for the concrete stress-strain relationship. The user can also specify the analysis length increments, whether to analyze a rotated cross section, and if unfactored or factored results are required. Plots of the moment, shear, and torsion capacities along the length of the pole can also be selected to be outputted.

The calculations begin by setting the factors of safety and constants (modulus of elasticity/rupture, and ultimate concrete strain) according to either the ACI or CSA standards. At this stage, the intervals for the length and cross section rotation analysis are also set. The cross section rotation loop and the length increment loops are started and the capacity analysis process is initiated for one increment and rotation.

First the location of each prestressing strand and steel reinforcement bar is calculated and the distance, *d*, from the top of the section is stored. The neutral axis is calculated by trial and error. A loop is initiated to find the neutral axis location (the initial first step is to assume a neutral axis of 1/3 the diameter from the compression side. Using the ultimate compressive strain value of concrete as the initial point at the top of the section and drawing a line through the assumed neutral axis provides a strain diagram for the calculation of stress in the concrete and steel. The stresses in the strands and reinforcing bars are calculated based on this strain diagram and checked for yielding. The concrete stresses are calculated using either the compression block theory or Hognestad's parabolic stress-strain relationship (presented below).

$$f_2 = f_c^{'}\left(\frac{2\varepsilon}{\varepsilon_o} - \left(\frac{\varepsilon}{\varepsilon_o}\right)^2\right) \tag{3-1}$$

where ε is the strain in the concrete, $f_c^{'}$ is the concrete compressive strength, and $\varepsilon_o = 0.002$.

For the compression block theory the area of the concrete circular segments in the compression zone are calculated and multiplied by the stress block to get the resulting compressive force. The centroid of the circular segment and lever arm from the neutral axis is also determined to locate the location of the resultant compression force on the cross section. Using the parabolic stress-strain

relationship requires the layer analysis method to determine stresses in the concrete (Figure 3.5). The outer sections of the circular segments (where the circular segment is still less than the wall thickness) are divided into 10 layers. The middle portion of the pole (where the inner hollow circular is located) is divided into 12 layers. The area of each layer and the centroid are then calculated. The associated average stress point for the layer is found by drawing a line from the centroid of the layer to the parabolic stress-strain curve. Once the average stress value is found it is multiplied by the area of the layer and the compression force for the layer is determined. The strands and steel in the compression zone are also included in the analysis. The tensile forces in the steel below the neutral axis are calculated as in the standard beam approach. The tensile and compressive forces are then added as T_{tot} and C_{tot} respectively. The process of calculating the compressive and tensile forces is repeated until the T_{tot} and C_{tot} values are equal. If the values are not equal, the NA location is adjusted based on the difference between the values and the process is repeated. When the values are equal, the neutral axis location is determined. Knowing the location of the neutral axis and the tensile and compressive forces in the section allows the moment of resistance to be calculated.

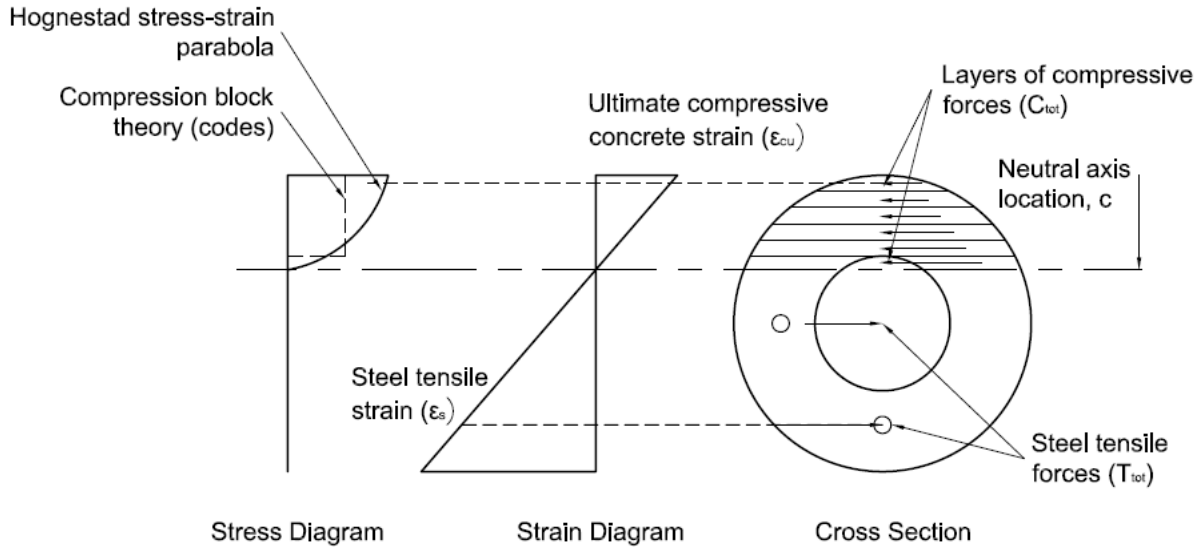

Figure 3.5: Diagram of layered parabolic stress-strain analysis

Once the moment resistance is known, the concrete strength at prestressing transfer is determined and the cracking moment is calculated. A sub-program then determines the torsional and shear capacities of the section using standard methods from the concrete codes. The CSA general method (based on the Compression Field Theory) is used for the shear and torsion capacities and requires the

use of a loop to iterate for the strain at midpoint of the section. The ACI method does not require the loop. The sub-program returns the shear and torsional resistance values separated into the steel and concrete contributions. Following the calculations for shear and torsion, the entire process of calculating the moment capacity is repeated until the entire length of the pole has been analyzed. If rotations of the cross section are selected by the user, the process is repeated again for the entire length of the pole using the modified cross section layout. When all the iterations have been completed the program outputs the capacity results in graphical and text format for moment, shear, and torsion (Figure 3.6, Figure 3.7, and Figure 3.8).

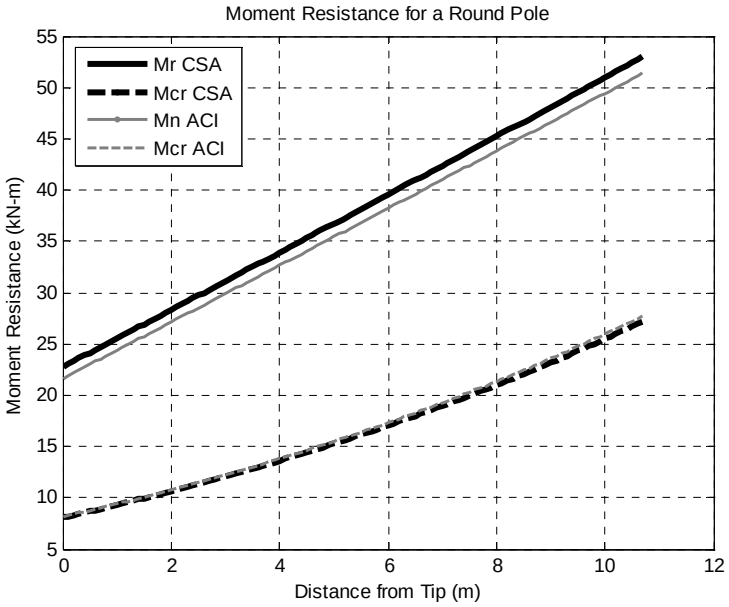

Figure 3.6: Moment resistance output from pole program

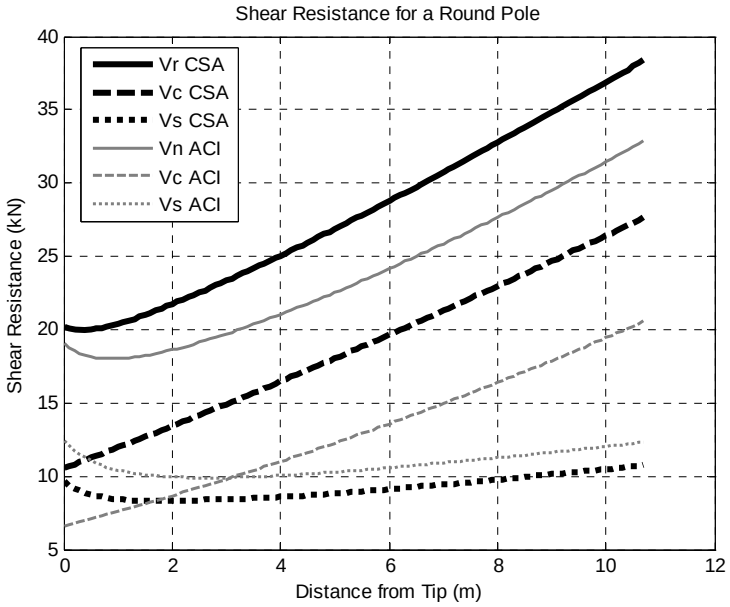

Figure 3.7: Shear resistance output from pole program

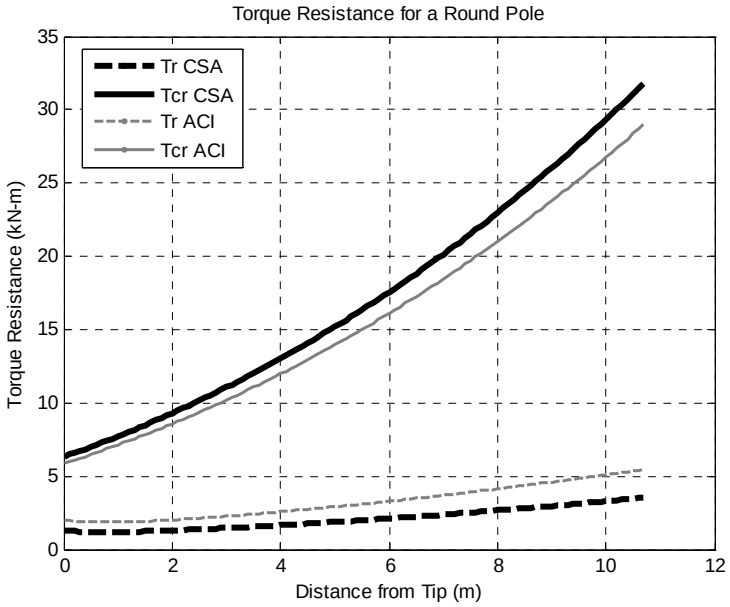

Figure 3.8: Torsional resistance output from pole program

3.3 Torsional Response Program using Analytical Models for Torsion

A separate program was developed to predict the post-cracking behaviour of concrete members subjected to pure torsional loads. Two torsion analysis procedures were adopted based on the analytical models presented in section 2.6.2 and papers on the Diagonal Compression Field Theory (Mitchell and Collins, 1974; Collins and Mitchell, 1980) and the Softened Truss Model Theory (Hsu, 1988; Hsu and Mo, 1985 (a, b, and c); Hsu, 1988; Hsu, 1991 (a, and b)). Prestressing contributions were added to the torsion programs based on a paper by McMullen and El-Degwy (1985). The paper by McMullen and El-Degwy also provided some test results to validate the program output. In addition, a draft copy of the ACI Committee 445 State of the Art report on Torsion in Structural Concrete was referenced (ACI Committee 445, 2008) and 'Torsion in Reinforced Concrete' by Hsu (1984). The programs were adjusted to predict the response of prestressed concrete poles and used to analyze the experimental results (Section 7.3). The two torsion models were programmed in MatLab and are summarized in the following paragraphs and flowcharts.

The Compression Field Theory (CFT) and Softened Truss Model (STM) were programmed in steps similar to those described in section 2.6.2. The process begins with selecting a value for the strain in the diagonal strut (compressive direction). For each model the complete load history can be determined by using the strain steps from 0 to 0.0035. The STM model (Figure 3.9) assumes a value for the strain in the *r* direction (principal tensile direction, perpendicular to the compressive strut). The softened concrete stress is the calculated and a shear flow zone thickness, t_d is assumed. The stress and strains in the steel are calculated based on these assumptions and strain in the *r* direction and shear flow zone thickness are checked. If the shear flow zone thickness and strain in the *r* direction are close to the assumed values, the loops are terminated and the twist, torque and other values are calculated.

The difference between the STM and CFT models is that the strain in the *r* direction is not needed and that the spalled concrete cross section dimensions are used for the CFT model. Since softening of concrete is not considered in the CFT model, the principal tensile strain is not needed and stress block coefficients are used instead, which are based on the strain in the diagonal compressive direction and the strain at the top of the stress-strain curve, ε_o. The CFT procedure is simplified to two loops, since the strain in the *r* direction is not needed (Figure 3.10).

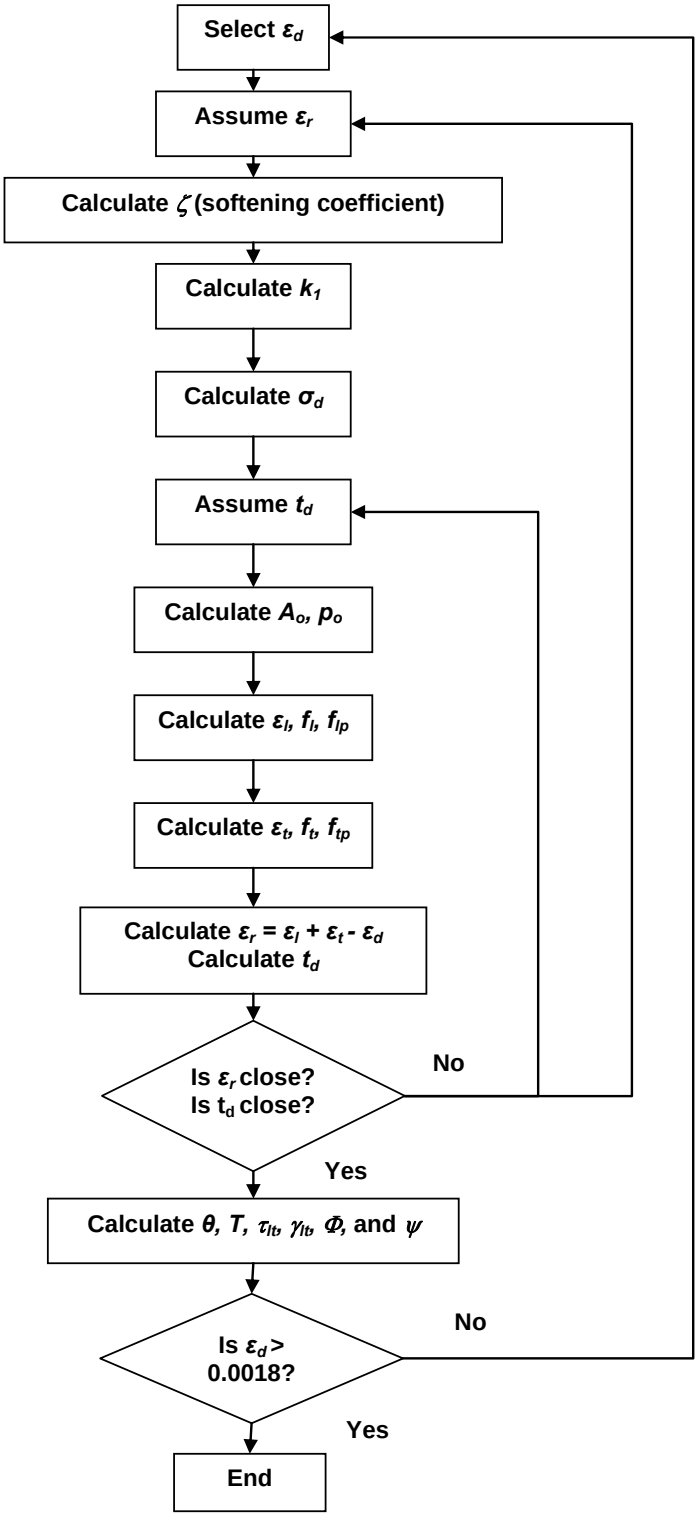

Figure 3.9: Flowchart of the Softened Truss Model Program

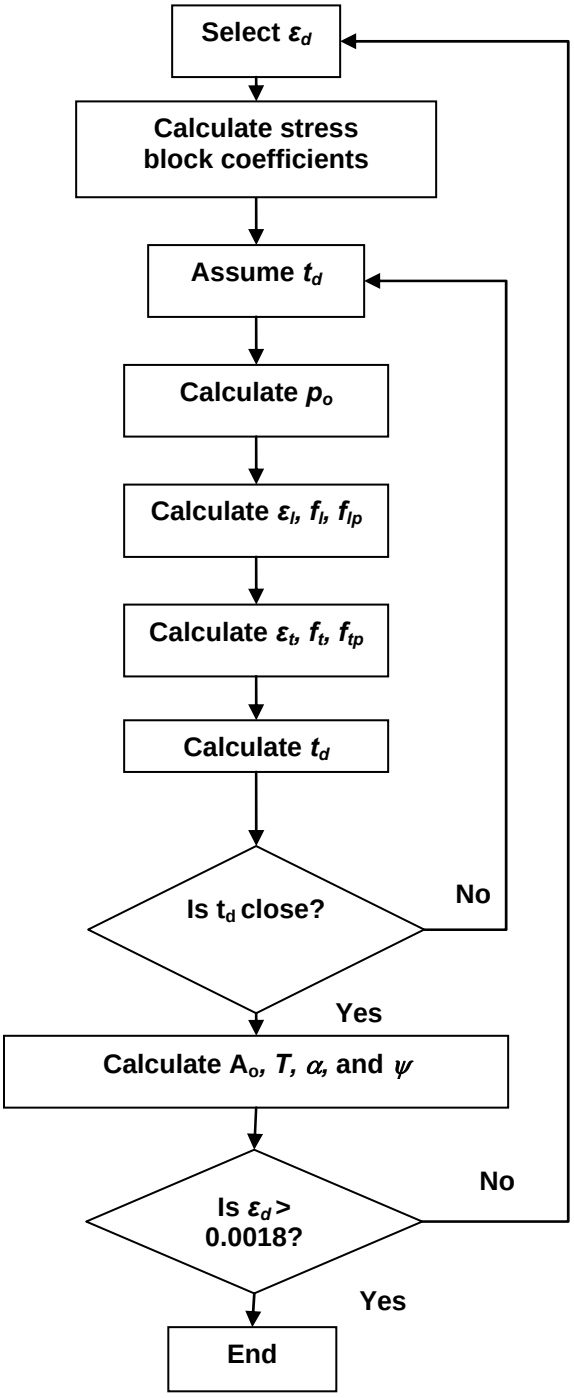

Figure 3.10: Flowchart of the Compression Field Theory (spalled model) program

3.3.1 Validation of the Torsional Response Program Output

In order to use to the torsional response programs, the output of selected members was compared to existing model results. Three comparisons are presented; two from McMullen and El-Degwy (1985) and one from Hsu (1991b). The program is capable of reproducing accurately.

The first comparison is a box section softened truss model example from Hsu (1991b). The specimen details are summarized in Figure 3.11. The comparison is presented in Figure 3.12. The second comparison (Figure 3.13) with the test results includes specimen PB1 from McMullen and El-Degwy (1985). The details of PB1 specimen are as follows: 178 mm wide, 356 mm deep rectangular beam (146 and 324 mm to the transverse reinforcement centre), concrete strength of 45.8 MPa, 4 - ¼" longitudinal prestressing strands (yield stress of 1638 MPa) stressed to a final stress (including losses) of 1099 MPa, modulus of elasticity taken as 188,900 MPa, 4 – No. 3 longitudinal reinforcing bars (yield stress of 435 MPa), and transverse reinforcement provided by No. 2 bars (yield stress of 310 MPa) spaced at 65 mm. The third comparison is also for a specimen described by McMullen and El-Degwy (1985) and called specimen PB4 (Figure 3.14). Details of the specimen are: 178 mm wide, 356 mm deep rectangular beam (143 and 321 mm to the transverse reinforcement centre), concrete strength of 45.5 MPa, 4 – 7/16" longitudinal prestressing strands (yield stress of 1709 MPa) stressed to a final stress (including losses) of 1150 MPa, modulus of elasticity taken as 192,400 MPa, 4 – No. 6 longitudinal reinforcing bars (yield stress of 419 MPa), and transverse reinforcement provided by No. 3 bars (yield stress of 435 MPa) spaced at 60 mm.

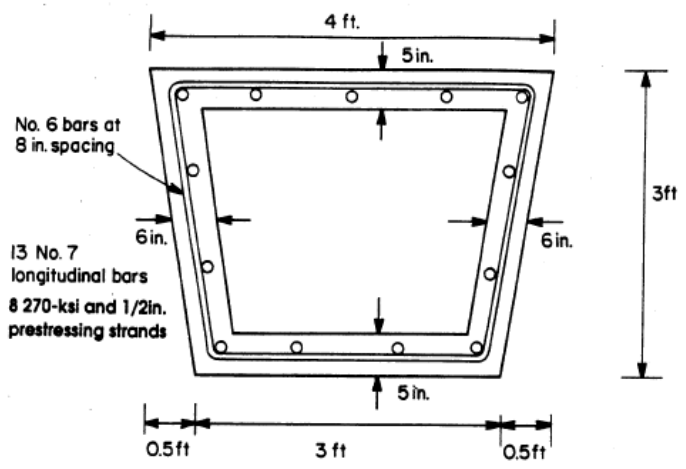

Figure 3.11: Box section example details (Hsu, 1991b)

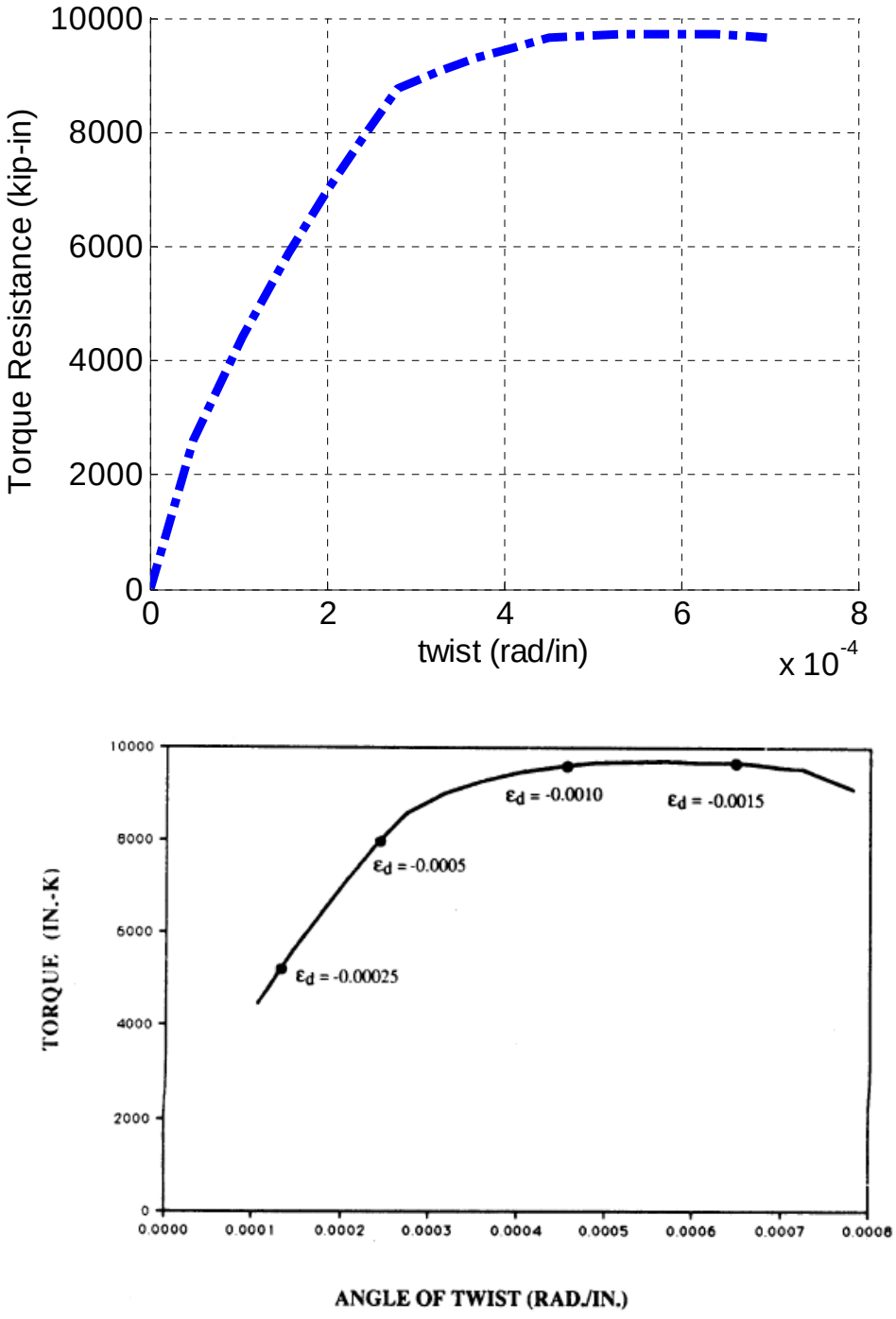

Figure 3.12: Comparison of Softened Truss Model example (Hsu, 1991) and Torsional Response program output

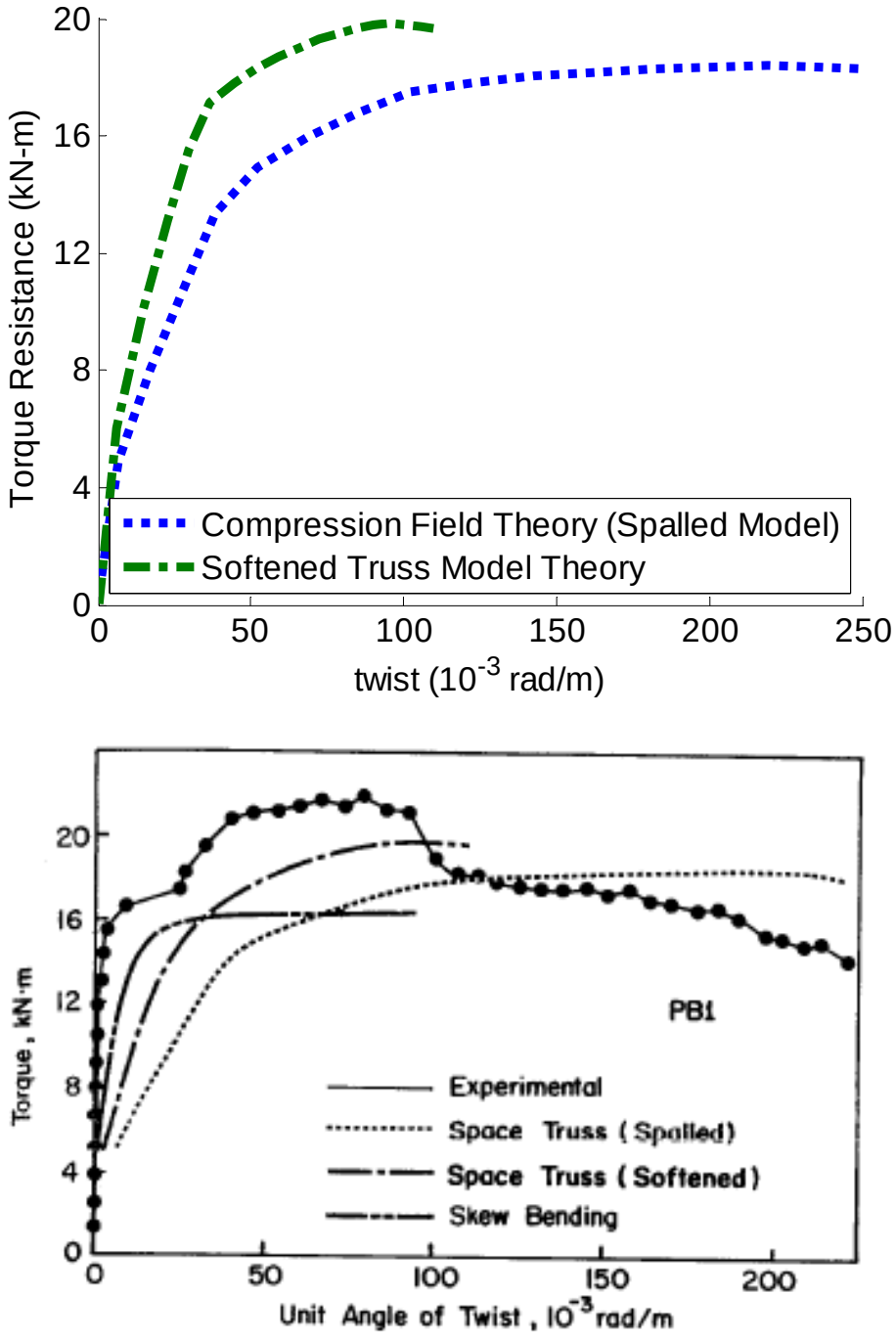

Figure 3.13: Comparison of McMullen and El-Degwy (1985) specimen PB1 results and Torsional Response program output

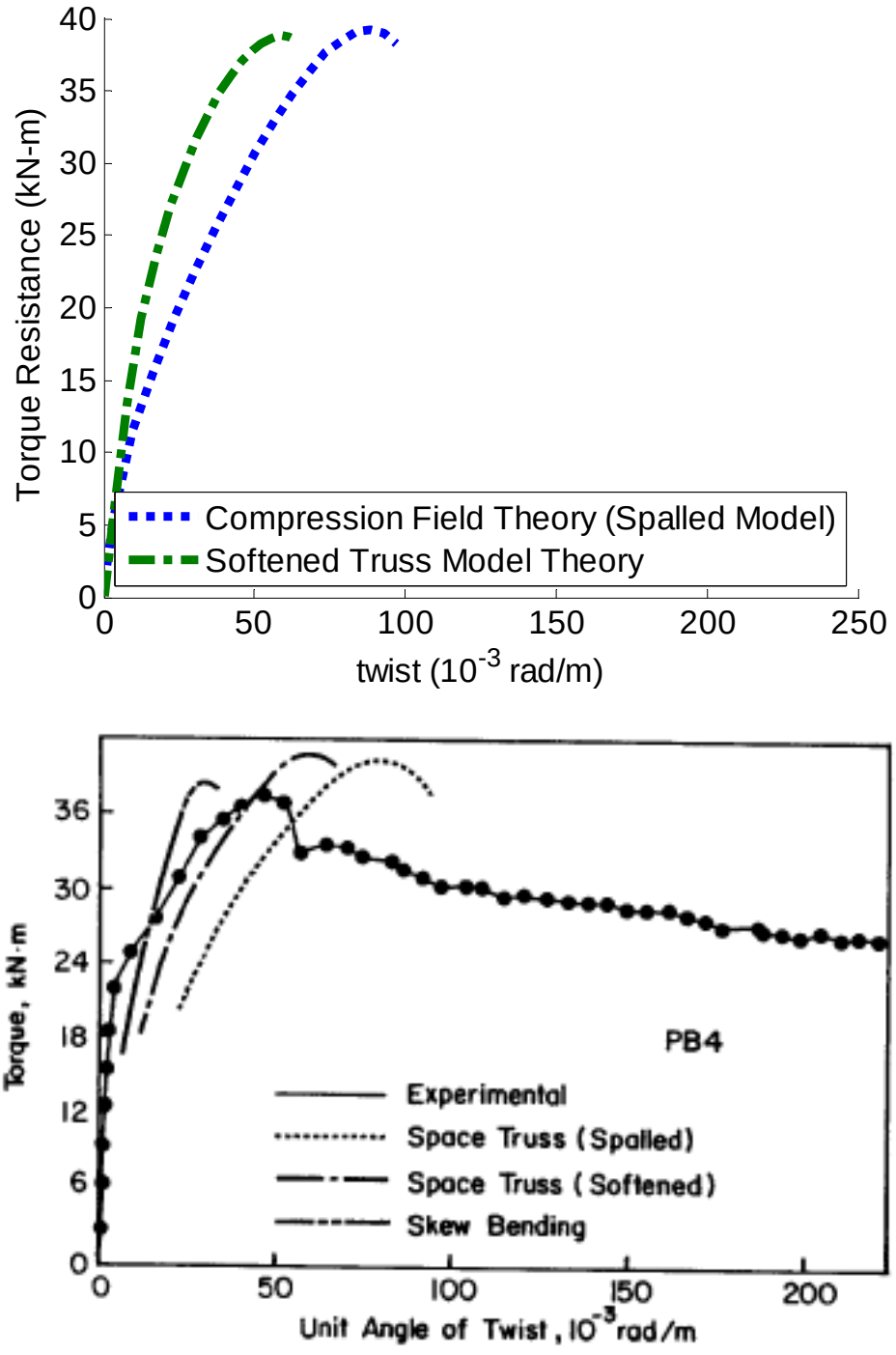

Figure 3.14: Comparison of McMullen and El-Degwy (1985) specimen PB4 results and Torsional Response program output

Chapter 4
Design of Test Program

4.1 General

A testing program was developed to determine the effect that helical reinforcement direction and spacing (also referred to as pitch) have on the torsional response of prestressed concrete poles. A total of 14 poles were produced with varying tip diameters, helical reinforcement directions, spacing, and with single or double helical reinforcement. The specimens were produced by Sky Cast Inc. in Guelph. Testing was also performed using the testing bed at Sky Cast Inc. with instrumentation from the University of Waterloo, Civil and Environmental Engineering Department.

4.2 Experimental Program

The experimental program consisted of 14 Class C poles with differences in the direction of helical steel and with varying spacing requirements. Two sizes of poles were produced, 165 mm tip diameters and 210 mm tip diameters. For each size, three specimens were produced according to CSA A14-07 (2007) standard. One specimen used a double helix (Figure 4.1 c)) to provide the necessary percentage of helical reinforcement. The double helix consisted of two helixes, one wound in each direction to form an overlapping system. The spacing of each half helix was governed by the percentage of reinforcement required in the CSA code. The other two specimens, had a single helix wound at half the spacing of the double helix halves. To achieve the same percentage of helical reinforcement as the double helix using a single helix, the spacing of the reinforcement must be reduced by half. The difference between the two specimens was that one had helical reinforcement wound in the clockwise direction while the other was wound in the counter clockwise direction (Figure 4.1). The poles in which the torsional load creates compressive principal stresses along the direction of spirals is denoted as the counter clockwise direction (-CCW). The pole with the opposite direction (with tensile torsional stresses along the spirals) is denoted as the clockwise direction (-CW). Theoretically the counter clockwise reinforcement should be ineffective in resisting torque.

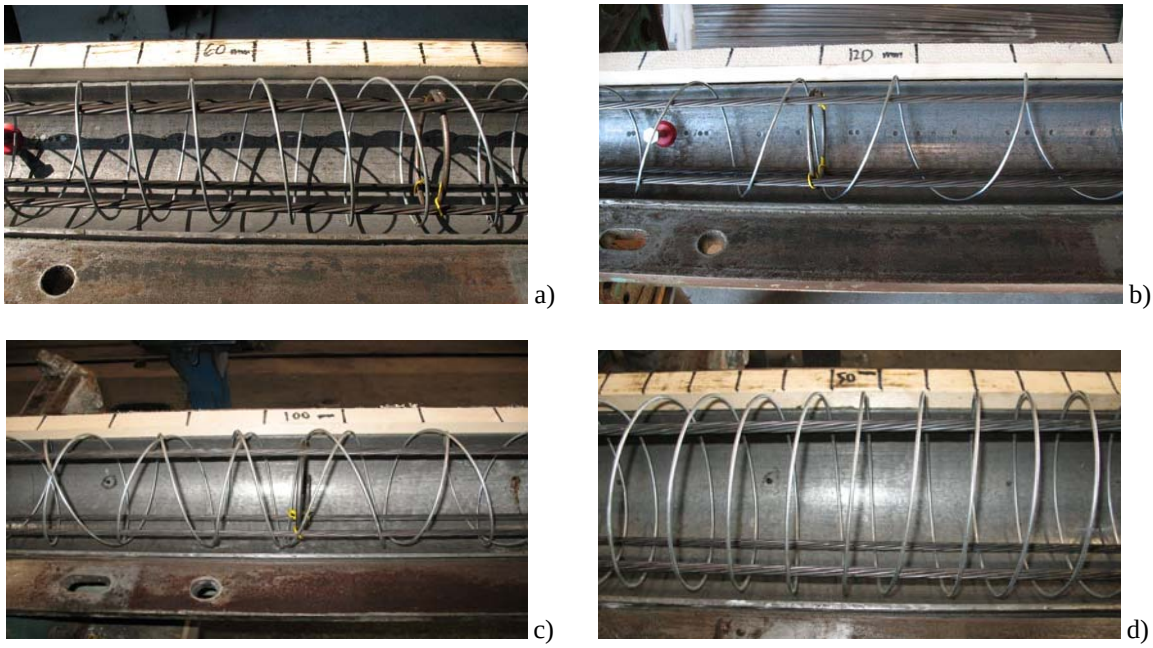

Figure 4.1: Example helical reinforcing layouts a) 165-CW-N, b) 165-CCW-L c) 210-D d) 210-CCW-N

The remaining three poles for each pole size were produced against the CSA standard. One pole contained no helical steel at all while the other two poles had a single helix spaced at twice the CSA standards. One specimen was produced with the helix in the clockwise direction while the other was placed in the counter clockwise direction.

These poles were produced for two reasons: 1) to observe the effect of increasing the spacing of the helical steel on the torsional response of the pole, 2) to compare the response of the single helix with the double helix specimen. Since the torsional loads would be applied in the counter clockwise direction, theoretical only one half of the steel (one helix) in the double helical specimen would be engaged and be effective in resisting the applied load. The theory would suggest that a specimen with half the helical steel (CW-L) of a double helical specimen would perform the same as the double helical specimen (-D).

The poles without any helical reinforcement were produced to compare against the poles with helical steel wound in the counter clockwise direction. According to the theory for the poles loaded in the counter clockwise direction, the helical steel in the single helix should be ineffective in resisting the applied load. These poles should therefore behave similar to the poles without helical reinforcement. The experimental program has been summarized in Table 4-1 and Table 4-2.

Table 4-1: Summary of experimental program

165 mm tip 210 mm tip Specimens (Class C)	Comments
-C **-C-2**	No helical reinforcement. Two controls were produced.
-CW-N	Single helix of reinforcement. Wound in the clockwise direction. Applied torque causes the helix to tighten and wind up (steel is theoretically effective). Spacing according to CSA A14-07 requirements.
-CCW-N	Single helix of reinforcement. Wound in the counter clockwise direction. Applied torque causes the helix to unwind (steel is theoretically ineffective). Spacing according to CSA A14-07 requirements.
-D	Double helix of reinforcement. One helix wound in each direction to form overlapping system. Each half spaced at twice the spacing of the CSA A14-07 requirements. Theoretically only one half should be effective in resisting applied torque.
-CW-L	Single helix of reinforcement. Wound in the clockwise direction. Applied torque causes the helix to tighten and wind up (steel is theoretically effective). Spacing at twice the CSA A14-07 requirements (equivalent to half the reinforcing placed in the –D specimen).
-CCW-L	Single helix of reinforcement. Wound in the counter clockwise direction. Applied torque causes the helix to unwind (steel is theoretically ineffective). Spacing at twice the CSA A14-07 requirements (equivalent to half the reinforcing placed in the –D specimen).

Table 4-2: Specimen description

Pole ID	**Description** (first spacing number for first 1.5 m from tip, second for remaining)
165-C	Un-reinforced
165-C-2	Un-reinforced
165-D	Double helix, 60mm and 100mm spacing (half helix spaced at 120mm and 200mm)
165-CW-L	Single helix, clockwise helix direction, spacing of 120 mm and 200 mm.
165-CCW-L	Single helix, counter clockwise helix direction, spacing of 120 mm and 200 mm.
165-CW-N	Single helix, clockwise helix direction, spacing of 60 mm and 100 mm.
165-CCW-N	Single helix, counter clockwise helix direction, spacing of 60 mm and 100 mm.
210-C	Un-reinforced
210-C-2	Un-reinforced
210-D	Double helix, 50mm and 85mm spacing (half helix spaced at 100mm and 170mm)
210-CW-L	Single helix, clockwise helix direction, spacing of 100 mm and 170 mm.
210-CCW-L	Single helix, counter clockwise helix direction, spacing of 100 mm and 170 mm.
210-CW-N	Single helix, clockwise helix direction, spacing of 50 mm and 85 mm.
210-CCW-N	Single helix, counter clockwise helix direction, spacing of 50 mm and 85 mm.

4.3 General Specimen Dimensions

The experimental test specimens were designed based on an existing Class B pole from Sky Cast Inc. To analyze how tip diameter and wall thickness change the torsional response of a prestressed concrete pole, two tip diameters and wall thicknesses were chosen. According to CSA A14-07 classification system, the 165 mm and 210 mm tip diameter poles are Class C poles (Table 4-3). The poles were designed to be 10.7 m long lighting poles, however only a 3 m test length was required to perform torsional testing as per CSA A14-07 Clause 7.4.4.2, and therefore the poles were produced with a length of 5.75 m. The taper for both poles from the tip to the butt of the pole was 15 mm/m. Design wall thicknesses for the 165 mm tip poles were 45 mm and 65 mm for the tip and pole end respectively. For the 210 mm tip poles the tip wall thickness was designed as 55 mm and the pole end wall thickness as 75 mm. The wall thickness at 5.75 m was calculated as 55 mm and 65 mm respectively for the 165 mm and 210 mm tip poles. Wall thicknesses were based on the existing Sky Cast Inc. pole designs and checked to ensure crushing of the concrete would not occur once the prestressing transfer force was applied. Two poles (1 – 165 mm tip and 1 – 210 mm tip) were poured per day in a double mould layout. Each set of poles were reinforced using the same helical reinforcing layout (-D, -CW-L. –CCW-N, etc…). Detailed design drawings for each specimen type are included in Figure 4.2 to Figure 4.13. The second control specimens (C-2) were produced using the same specifications as the first control specimens. The drawings show the prestressing strand layout and helical steel reinforcement spacing patterns. Concrete fill volumes are also noted on the drawings in an effort to achieve consistent wall thicknesses between specimens (see section 4.3 for more information on specimen preparation).

Table 4-3: Specimen design dimensions and classification

	Experimental Specimens	
Pole Class	Class C	
Tip diameter (mm)	165	210
Butt diameter (mm)	325	370
Taper (mm/m)	15	15
Length (m)	10.7	10.7
Tip wall thickness (mm)	45	55
Pole end (@ 10.7 m) wall thickness (mm)	65	75

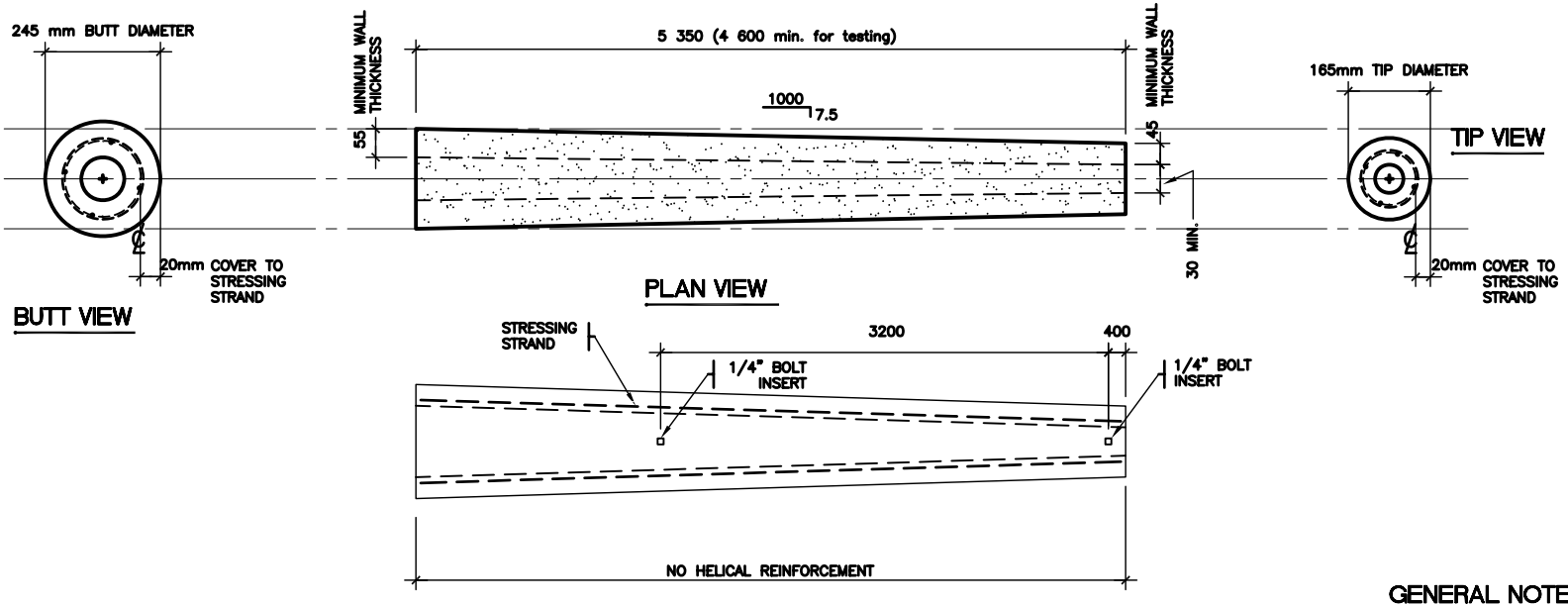

REINFORCING PLAN

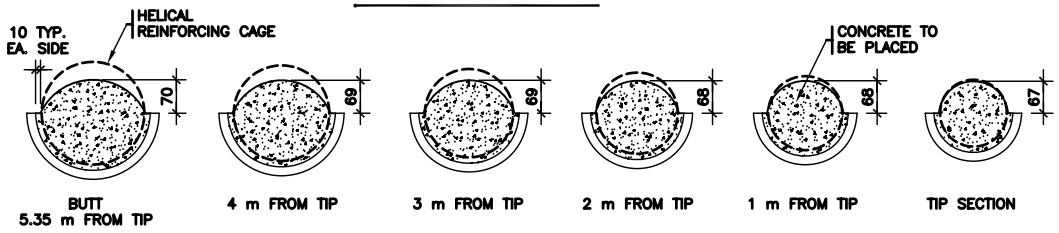

CONCRETE FILL SECTIONS

GENERAL NOTES

1. PRESTRESSING STRANDS TO BE LOW RELAXATION STEEL
2. PRESTRESSING STRANDS TO BE TENSIONED TO 80% OF ULTIMATE STRAND STRENGTH.
3. REINFORCING AND PRESTRESSING STRANDS TO HAVE 20mm CLEAR COVER.
4. CLAMP LENGTH IS 1830mm (72") OR 10% OF POLE LENGTH (WHICHEVER IS GREATER)
5. CAPACITIES BASED ON PRESTRESS LOSSES OF 10% AT TRANSFER AND 21% LONG TERM. MOMENTS TAKEN AT TOP OF CLAMP LENGTH, TORQUE TAKEN AT 600mm FROM TIP.
6. SPIRAL REINFORCING TO BE COLD DRAWN STEEL WIRE CONFORMING TO A.S.T.M. A641 OR C.S.A. G30.3 WITH CLASS 'A' GALVANIZED COATING AS PER A.S.T.M. A641

DESIGN DATA

REINFORCING					LOAD RESISTANCE DATA			CONCRETE	
PRESTRESS STRAND NUMBER & DIAMETER (mm)	STRAND GRADE (MPa)	REINFORCING BARS NUMBER & SIZE	REBAR GRADE (MPa)	BAR LENGTH (m)	CRACKING MOMENT @3.6m Mcr (kNm)	UNFACTORED MOMENT CAPACITY@3.6m Mr (kNm)	CRACKING TORQUE @0.6m Tcr (kNm)	REQUIRED COMPRESSIVE STRENGTH at TRANSFER (MPa)	28 DAY COMPRESSIVE STRENGTH (MPa)
4 – 9mm / (3/8")	1860				13.0	32.8	7.1	25	60

SCALE	N.T.S.
DATE	JUN. 24/07
JOB No.	00–00–00
CAD FILE	
SHEET No.	165-1

PROJECT NAME
UNIVERSITY OF WATERLOO
TORSIONAL TEST SPECIMENS

DRAWING TITLE
FIGURE 4.2: 165 CONTROL SPECIMEN (165-C)

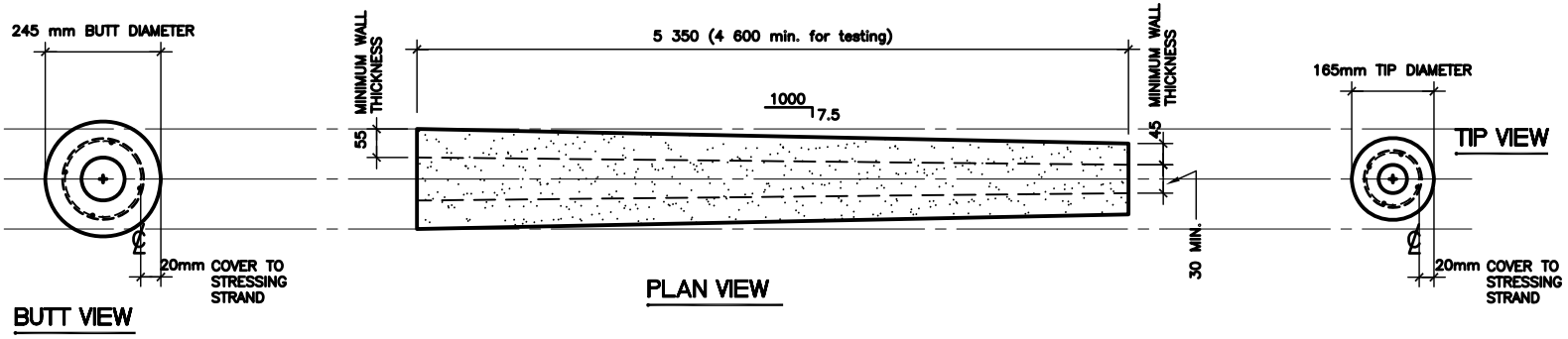

BUTT VIEW

PLAN VIEW

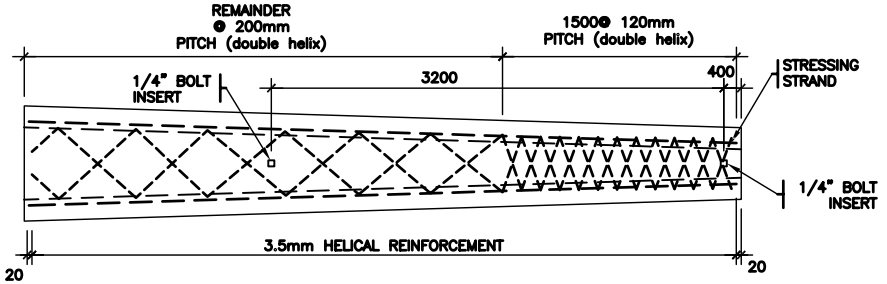

REINFORCING PLAN

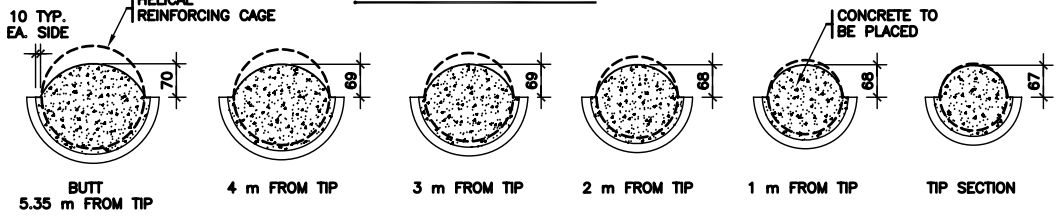

CONCRETE FILL SECTIONS

GENERAL NOTES

1. PRESTRESSING STRANDS TO BE LOW RELAXATION STEEL
2. PRESTRESSING STRANDS TO BE TENSIONED TO 80% OF ULTIMATE STRAND STRENGTH.
3. REINFORCING AND PRESTRESSING STRANDS TO HAVE 20mm CLEAR COVER.
4. CLAMP LENGTH IS 1830mm (72") OR 10% OF POLE LENGTH (WHICHEVER IS GREATER)
5. CAPACITIES BASED ON PRESTRESS LOSSES OF 10% AT TRANSFER AND 21% LONG TERM. MOMENTS TAKEN AT TOP OF CLAMP LENGTH, TORQUE TAKEN AT 600mm FROM TIP.
6. SPIRAL REINFORCING TO BE COLD DRAWN STEEL WIRE CONFORMING TO A.S.T.M. A641 OR C.S.A. G30.3 WITH CLASS 'A' GALVANIZED COATING AS PER A.S.T.M. A641

DESIGN DATA

REINFORCING					LOAD RESISTANCE DATA			CONCRETE	
PRESTRESS STRAND NUMBER & DIAMETER (mm)	STRAND GRADE (MPa)	REINFORCING BARS NUMBER & SIZE	REBAR GRADE (MPa)	BAR LENGTH (m)	CRACKING MOMENT @3.6m Mcr (kNm)	UNFACTORED MOMENT CAPACITY@3.6m Mr (kNm)	CRACKING TORQUE @0.6m Tcr (kNm)	REQUIRED COMPRESSIVE STRENGTH at TRANSFER (MPa)	28 DAY COMPRESSIVE STRENGTH (MPa)
4 – 9mm / (3/8")	1860				13.0	32.8	7.1	25	60

PROJECT NAME
UNIVERSITY OF WATERLOO
TORSIONAL TEST SPECIMENS

DRAWING TITLE
FIGURE 4.3: 165 DOUBLE HELIX SPECIMEN (165-D)

SCALE	N.T.S.
DATE	JUN. 24/07
JOB No.	00–00–00
CAD FILE	
SHEET No.	165-2

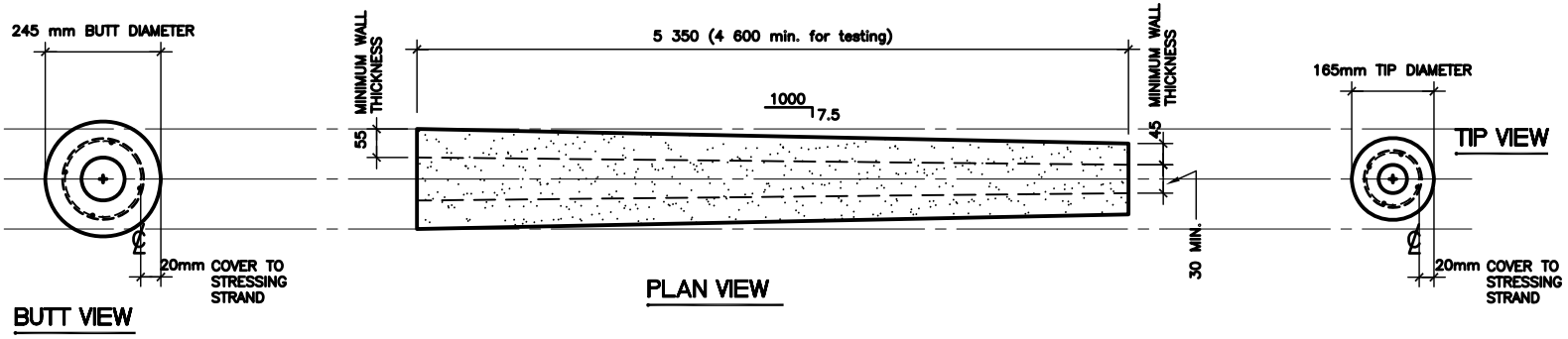

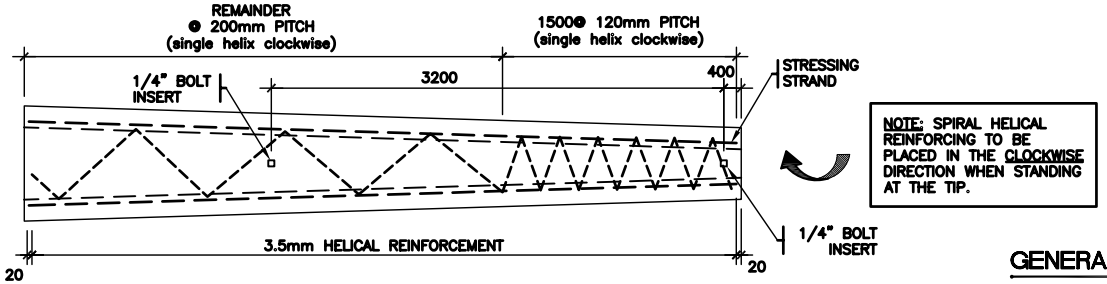

NOTE: SPIRAL HELICAL REINFORCING TO BE PLACED IN THE CLOCKWISE DIRECTION WHEN STANDING AT THE TIP.

REINFORCING PLAN

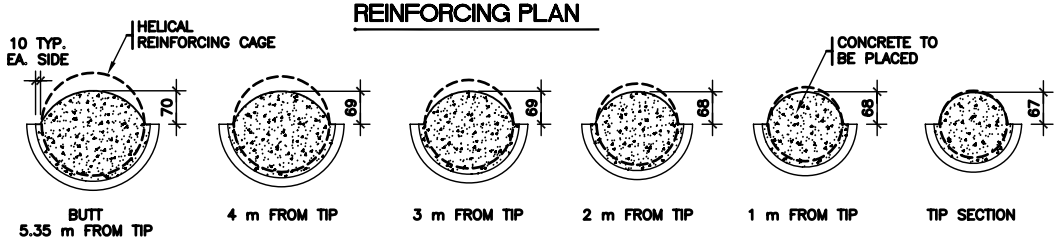

CONCRETE FILL SECTIONS

GENERAL NOTES

1. PRESTRESSING STRANDS TO BE LOW RELAXATION STEEL
2. PRESTRESSING STRANDS TO BE TENSIONED TO 80% OF ULTIMATE STRAND STRENGTH.
3. REINFORCING AND PRESTRESSING STRANDS TO HAVE 20mm CLEAR COVER.
4. CLAMP LENGTH IS 1830mm (72") OR 10% OF POLE LENGTH (WHICHEVER IS GREATER)
5. CAPACITIES BASED ON PRESTRESS LOSSES OF 10% AT TRANSFER AND 21% LONG TERM. MOMENTS TAKEN AT TOP OF CLAMP LENGTH, TORQUE TAKEN AT 600mm FROM TIP.
6. SPIRAL REINFORCING TO BE COLD DRAWN STEEL WIRE CONFORMING TO A.S.T.M. A641 OR C.S.A. G30.3 WITH CLASS 'A' GALVANIZED COATING AS PER A.S.T.M. A641

DESIGN DATA

REINFORCING					LOAD RESISTANCE DATA			CONCRETE	
PRESTRESS STRAND NUMBER & DIAMETER (mm)	STRAND GRADE (MPa)	REINFORCING BARS NUMBER & SIZE	REBAR GRADE (MPa)	BAR LENGTH (m)	CRACKING MOMENT @3.6m Mcr (kNm)	UNFACTORED MOMENT CAPACITY@3.6m Mr (kNm)	CRACKING TORQUE @0.6m Tcr (kNm)	REQUIRED COMPRESSIVE STRENGTH at TRANSFER (MPa)	28 DAY COMPRESSIVE STRENGTH (MPa)
4 – 9mm / (3/8")	1860				13.0	32.8	7.1	25	60

PROJECT NAME	UNIVERSITY OF WATERLOO TORSIONAL TEST SPECIMENS
DRAWING TITLE	FIGURE 4.4: 165 SINGLE CW HELIX LARGE SPACED SPECIMEN (165-CW-L)
SCALE	N.T.S.
DATE	JUN. 24/07
JOB No.	00–00–00
CAD FILE	
SHEET No.	165-3

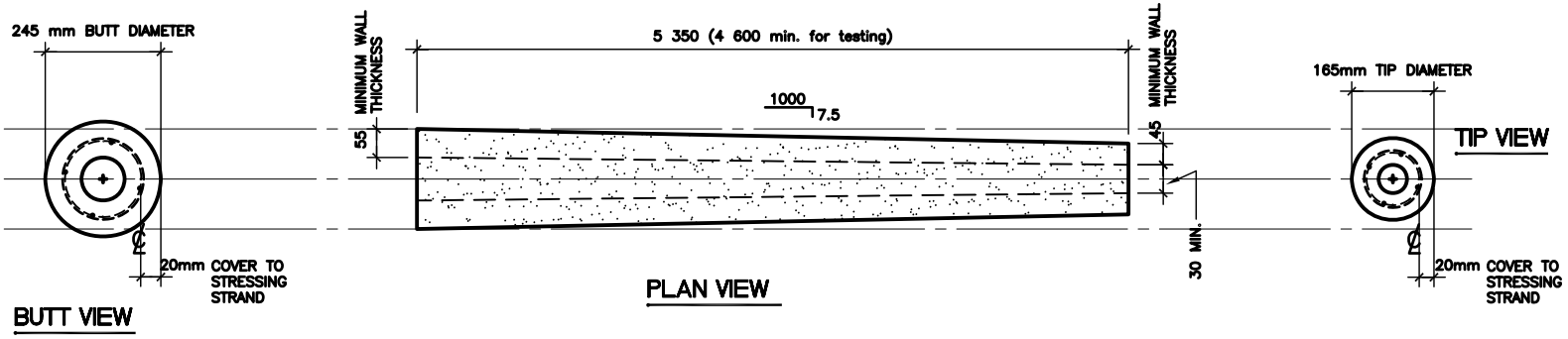

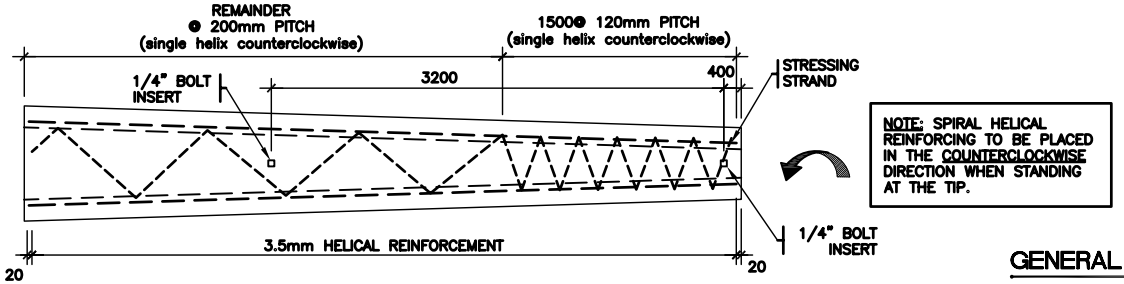

REINFORCING PLAN

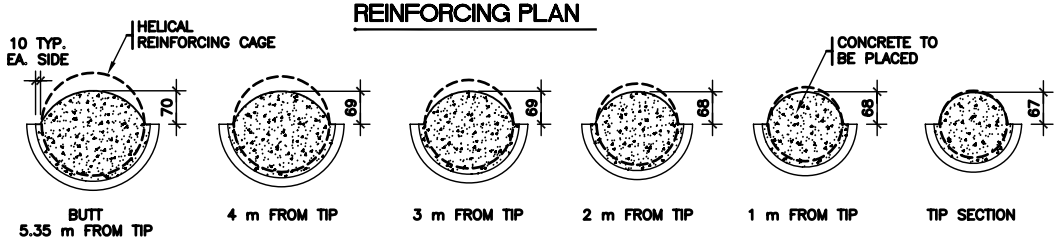

CONCRETE FILL SECTIONS

GENERAL NOTES

1. PRESTRESSING STRANDS TO BE LOW RELAXATION STEEL
2. PRESTRESSING STRANDS TO BE TENSIONED TO 80% OF ULTIMATE STRAND STRENGTH.
3. REINFORCING AND PRESTRESSING STRANDS TO HAVE 20mm CLEAR COVER.
4. CLAMP LENGTH IS 1830mm (72") OR 10% OF POLE LENGTH (WHICHEVER IS GREATER)
5. CAPACITIES BASED ON PRESTRESS LOSSES OF 10% AT TRANSFER AND 21% LONG TERM. MOMENTS TAKEN AT TOP OF CLAMP LENGTH, TORQUE TAKEN AT 600mm FROM TIP.
6. SPIRAL REINFORCING TO BE COLD DRAWN STEEL WIRE CONFORMING TO A.S.T.M. A641 OR C.S.A. G30.3 WITH CLASS 'A' GALVANIZED COATING AS PER A.S.T.M. A641

DESIGN DATA

REINFORCING					LOAD RESISTANCE DATA			CONCRETE	
PRESTRESS STRAND NUMBER & DIAMETER (mm)	STRAND GRADE (MPa)	REINFORCING BARS NUMBER & SIZE	REBAR GRADE (MPa)	BAR LENGTH (m)	CRACKING MOMENT @3.6m Mcr (kNm)	UNFACTORED MOMENT CAPACITY@3.6m Mr (kNm)	CRACKING TORQUE @0.6m Tcr (kNm)	REQUIRED COMPRESSIVE STRENGTH at TRANSFER (MPa)	28 DAY COMPRESSIVE STRENGTH (MPa)
4 – 9mm / (3/8")	1860				13.0	32.8	7.1	25	60

PROJECT NAME
UNIVERSITY OF WATERLOO
TORSIONAL TEST SPECIMENS

DRAWING TITLE
FIGURE 4.5: 165 SINGLE CCW HELIX LARGE SPACED SPECIMEN (165-CCW-L)

SCALE	N.T.S.
DATE	JUN. 24/07
JOB No.	00–00–00
CAD FILE	
SHEET No.	165-4

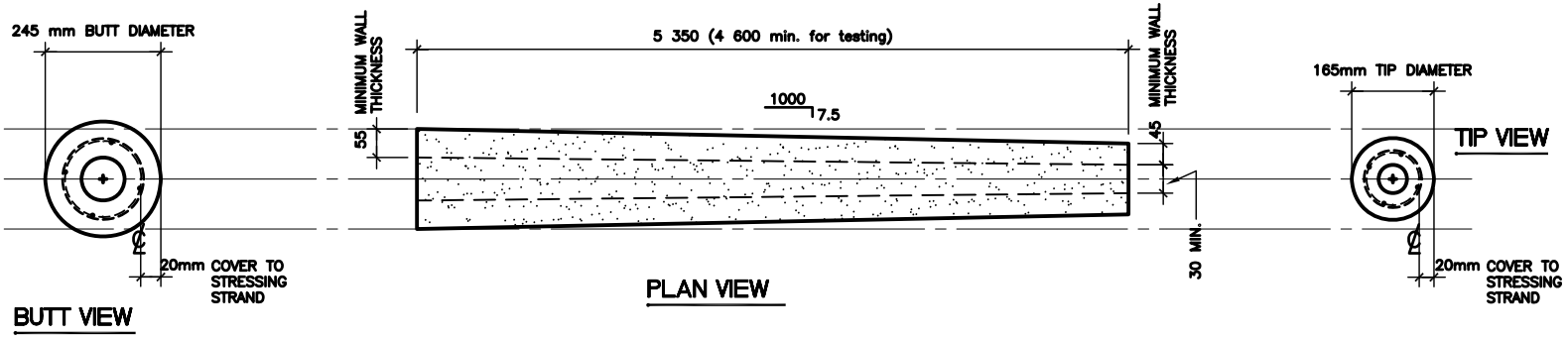

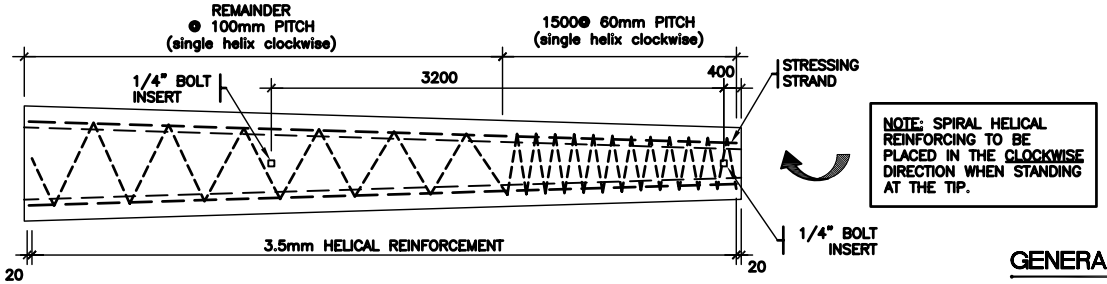

REINFORCING PLAN

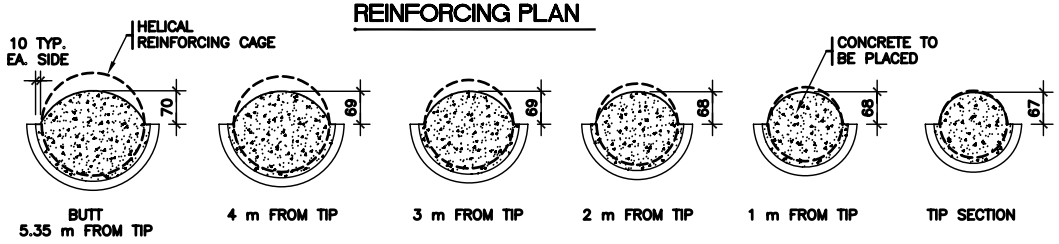

CONCRETE FILL SECTIONS

GENERAL NOTES

1. PRESTRESSING STRANDS TO BE LOW RELAXATION STEEL
2. PRESTRESSING STRANDS TO BE TENSIONED TO 80% OF ULTIMATE STRAND STRENGTH.
3. REINFORCING AND PRESTRESSING STRANDS TO HAVE 20mm CLEAR COVER.
4. CLAMP LENGTH IS 1830mm (72") OR 10% OF POLE LENGTH (WHICHEVER IS GREATER)
5. CAPACITIES BASED ON PRESTRESS LOSSES OF 10% AT TRANSFER AND 21% LONG TERM. MOMENTS TAKEN AT TOP OF CLAMP LENGTH, TORQUE TAKEN AT 600mm FROM TIP.
6. SPIRAL REINFORCING TO BE COLD DRAWN STEEL WIRE CONFORMING TO A.S.T.M. A641 OR C.S.A. G30.3 WITH CLASS 'A' GALVANIZED COATING AS PER A.S.T.M. A641

DESIGN DATA

REINFORCING					LOAD RESISTANCE DATA			CONCRETE	
PRESTRESS STRAND NUMBER & DIAMETER (mm)	STRAND GRADE (MPa)	REINFORCING BARS NUMBER & SIZE	REBAR GRADE (MPa)	BAR LENGTH (m)	CRACKING MOMENT @3.6m Mcr (kNm)	UNFACTORED MOMENT CAPACITY@3.6m Mr (kNm)	CRACKING TORQUE @0.6m Tcr (kNm)	REQUIRED COMPRESSIVE STRENGTH at TRANSFER (MPa)	28 DAY COMPRESSIVE STRENGTH (MPa)
4 – 9mm / (3/8")	1860				13.0	32.8	7.1	25	60

PROJECT NAME
UNIVERSITY OF WATERLOO
TORSIONAL TEST SPECIMENS

DRAWING TITLE
FIGURE 4.6: 165 SINGLE CW HELIX NORMAL SPACED SPECIMEN (165-CW-N)

SCALE	N.T.S.
DATE	JUN. 24/07
JOB No.	00–00–00
CAD FILE	
SHEET No.	165-5

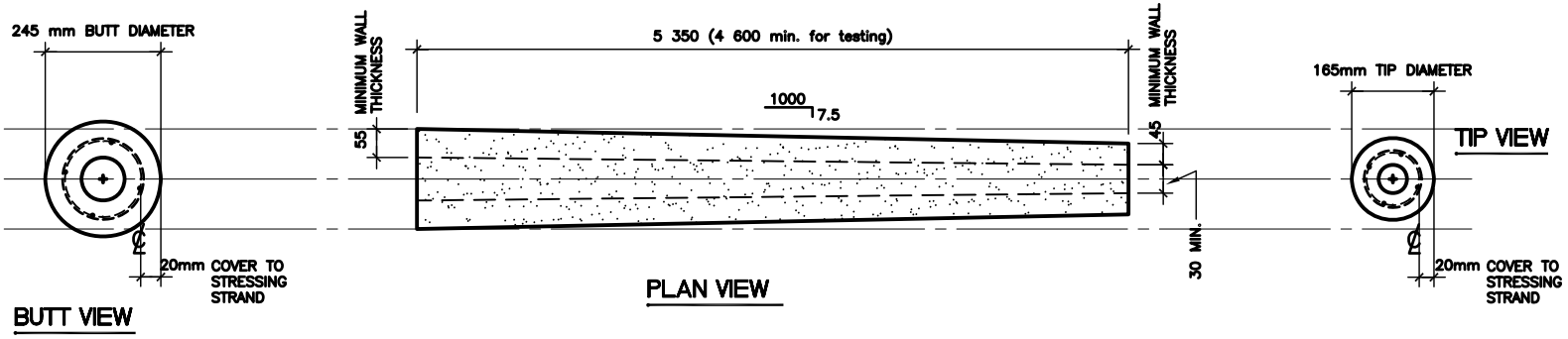

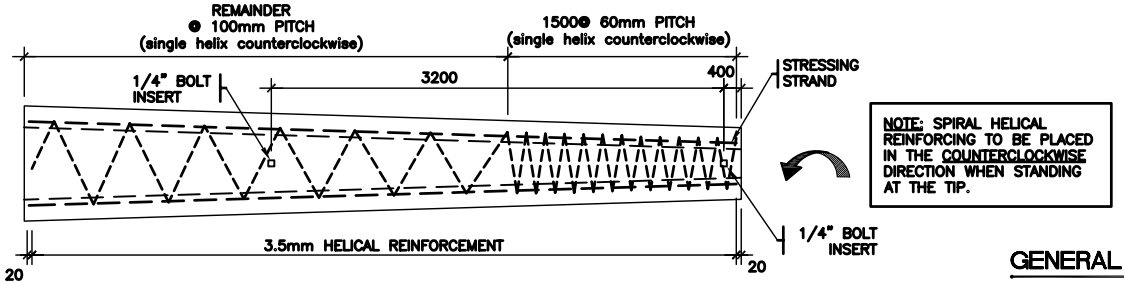

REINFORCING PLAN

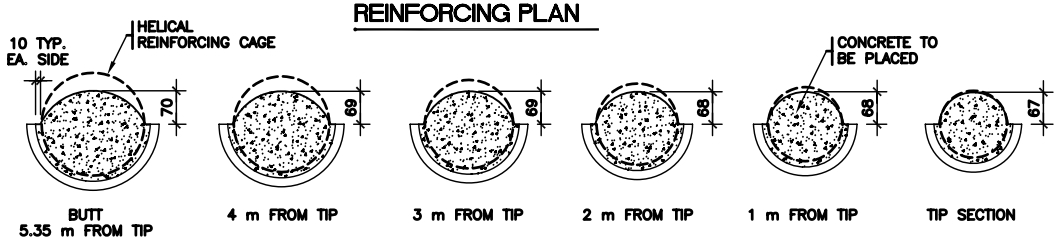

CONCRETE FILL SECTIONS

GENERAL NOTES

1. PRESTRESSING STRANDS TO BE LOW RELAXATION STEEL
2. PRESTRESSING STRANDS TO BE TENSIONED TO 80% OF ULTIMATE STRAND STRENGTH.
3. REINFORCING AND PRESTRESSING STRANDS TO HAVE 20mm CLEAR COVER.
4. CLAMP LENGTH IS 1830mm (72") OR 10% OF POLE LENGTH (WHICHEVER IS GREATER)
5. CAPACITIES BASED ON PRESTRESS LOSSES OF 10% AT TRANSFER AND 21% LONG TERM. MOMENTS TAKEN AT TOP OF CLAMP LENGTH, TORQUE TAKEN AT 600mm FROM TIP.
6. SPIRAL REINFORCING TO BE COLD DRAWN STEEL WIRE CONFORMING TO A.S.T.M. A641 OR C.S.A. G30.3 WITH CLASS 'A' GALVANIZED COATING AS PER A.S.T.M. A641

DESIGN DATA

REINFORCING					LOAD RESISTANCE DATA			CONCRETE	
PRESTRESS STRAND NUMBER & DIAMETER (mm)	STRAND GRADE (MPa)	REINFORCING BARS NUMBER & SIZE	REBAR GRADE (MPa)	BAR LENGTH (m)	CRACKING MOMENT @3.6m Mcr (kNm)	UNFACTORED MOMENT CAPACITY@3.6m Mr (kNm)	CRACKING TORQUE @0.6m Tcr (kNm)	REQUIRED COMPRESSIVE STRENGTH at TRANSFER (MPa)	28 DAY COMPRESSIVE STRENGTH (MPa)
4 – 9mm / (3/8")	1860				13.0	32.8	7.1	25	60

PROJECT NAME
UNIVERSITY OF WATERLOO
TORSIONAL TEST SPECIMENS

DRAWING TITLE
FIGURE 4.7: 165 SINGLE CCW HELIX NORMAL SPACED SPECIMEN (165-CCW-N)

SCALE	N.T.S.
DATE	JUN. 24/07
JOB No.	00–00–00
CAD FILE	
SHEET No.	165-6

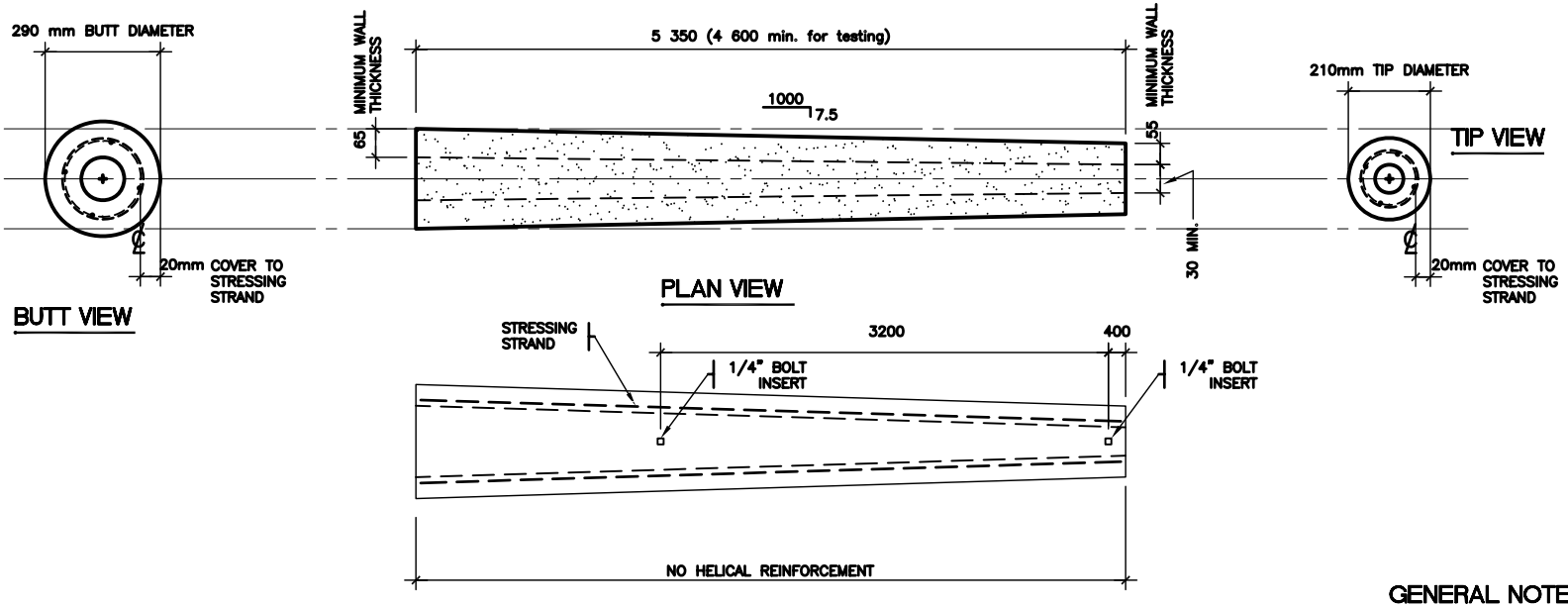

REINFORCING PLAN

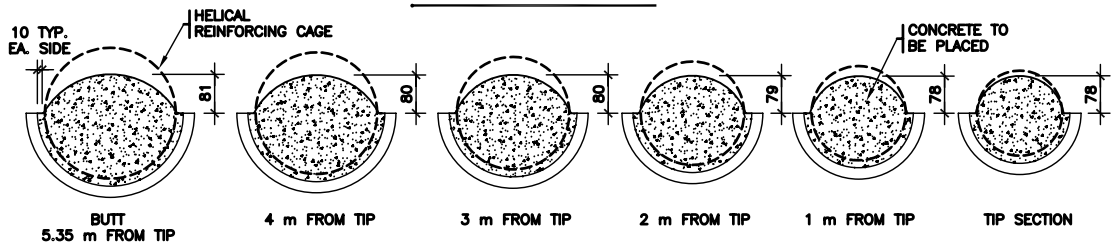

CONCRETE FILL SECTIONS

GENERAL NOTES

1. PRESTRESSING STRANDS TO BE LOW RELAXATION STEEL
2. PRESTRESSING STRANDS TO BE TENSIONED TO 80% OF ULTIMATE STRAND STRENGTH.
3. REINFORCING AND PRESTRESSING STRANDS TO HAVE 20mm CLEAR COVER.
4. CLAMP LENGTH IS 1830mm (72") OR 10% OF POLE LENGTH (WHICHEVER IS GREATER)
5. CAPACITIES BASED ON PRESTRESS LOSSES OF 10% AT TRANSFER AND 21% LONG TERM. MOMENTS TAKEN AT TOP OF CLAMP LENGTH, TORQUE TAKEN AT 600mm FROM TIP.
6. SPIRAL REINFORCING TO BE COLD DRAWN STEEL WIRE CONFORMING TO A.S.T.M. A641 OR C.S.A. G30.3 WITH CLASS 'A' GALVANIZED COATING AS PER A.S.T.M. A641

DESIGN DATA

REINFORCING					LOAD RESISTANCE DATA			CONCRETE	
PRESTRESS STRAND NUMBER & DIAMETER (mm)	STRAND GRADE (MPa)	REINFORCING BARS NUMBER & SIZE	REBAR GRADE (MPa)	BAR LENGTH (m)	CRACKING MOMENT @3.6m Mcr (kNm)	UNFACTORED MOMENT CAPACITY@3.6m Mr (kNm)	CRACKING TORQUE @0.6m Tcr (kNm)	REQUIRED COMPRESSIVE STRENGTH at TRANSFER (MPa)	28 DAY COMPRESSIVE STRENGTH (MPa)
4 – 9mm / (3/8")	1860				18.1	41.3	12.0	25	60

PROJECT NAME
UNIVERSITY OF WATERLOO
TORSIONAL TEST SPECIMENS

DRAWING TITLE
FIGURE 4.8: 210 CONTROL SPECIMEN (210-C)

SCALE	N.T.S.
DATE	JUN. 24/07
JOB No.	00–00–00
CAD FILE	
SHEET No.	210-1

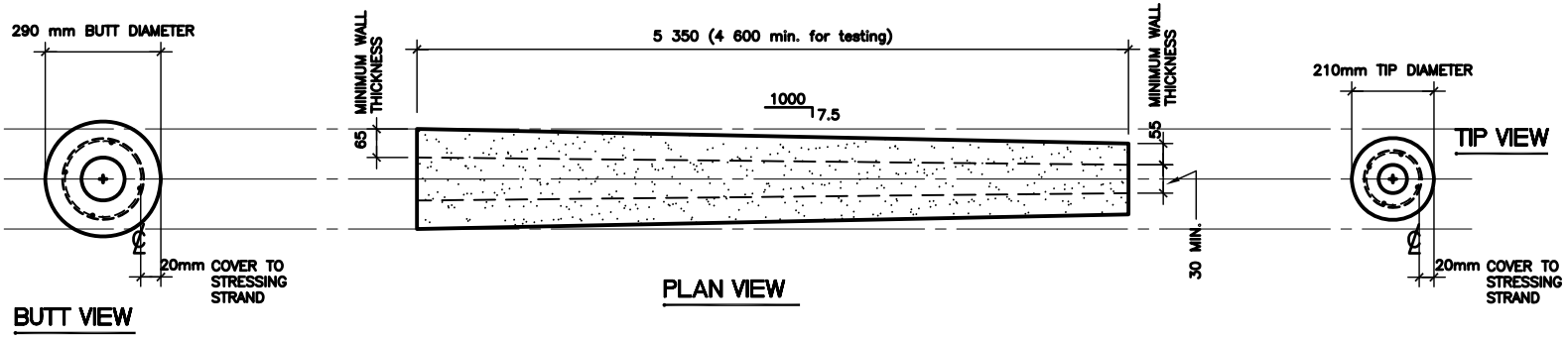

BUTT VIEW

PLAN VIEW

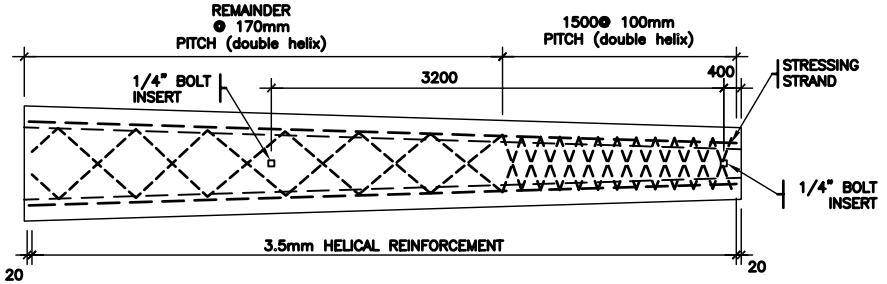

REINFORCING PLAN

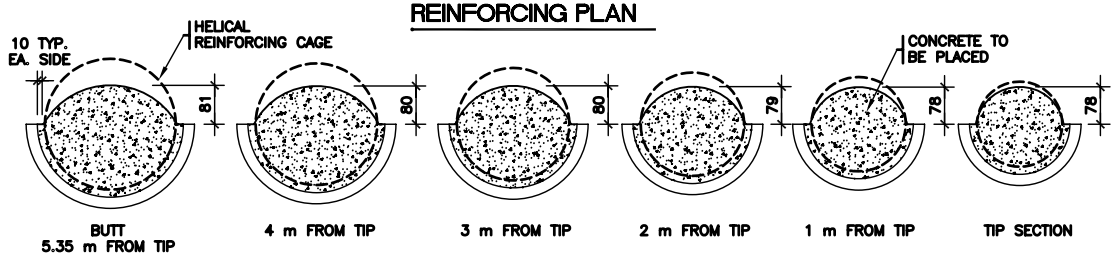

CONCRETE FILL SECTIONS

GENERAL NOTES

1. PRESTRESSING STRANDS TO BE LOW RELAXATION STEEL
2. PRESTRESSING STRANDS TO BE TENSIONED TO 80% OF ULTIMATE STRAND STRENGTH.
3. REINFORCING AND PRESTRESSING STRANDS TO HAVE 20mm CLEAR COVER.
4. CLAMP LENGTH IS 1830mm (72") OR 10% OF POLE LENGTH (WHICHEVER IS GREATER)
5. CAPACITIES BASED ON PRESTRESS LOSSES OF 10% AT TRANSFER AND 21% LONG TERM. MOMENTS TAKEN AT TOP OF CLAMP LENGTH, TORQUE TAKEN AT 600mm FROM TIP.
6. SPIRAL REINFORCING TO BE COLD DRAWN STEEL WIRE CONFORMING TO A.S.T.M. A641 OR C.S.A. G30.3 WITH CLASS 'A' GALVANIZED COATING AS PER A.S.T.M. A641

DESIGN DATA

REINFORCING					LOAD RESISTANCE DATA			CONCRETE	
PRESTRESS STRAND NUMBER & DIAMETER (mm)	STRAND GRADE (MPa)	REINFORCING BARS NUMBER & SIZE	REBAR GRADE (MPa)	BAR LENGTH (m)	CRACKING MOMENT @3.6m Mcr (kNm)	UNFACTORED MOMENT CAPACITY@3.6m Mr (kNm)	CRACKING TORQUE @0.6m Tcr (kNm)	REQUIRED COMPRESSIVE STRENGTH at TRANSFER (MPa)	28 DAY COMPRESSIVE STRENGTH (MPa)
4 – 9mm / (3/8")	1860				18.1	41.3	12.0	25	60

PROJECT NAME
UNIVERSITY OF WATERLOO
TORSIONAL TEST SPECIMENS

DRAWING TITLE
FIGURE 4.9: 210 DOUBLE HELIX SPECIMEN (210-D)

SCALE	N.T.S.
DATE	JUN. 24/07
JOB No.	00–00–00
CAD FILE	
SHEET No.	210-2

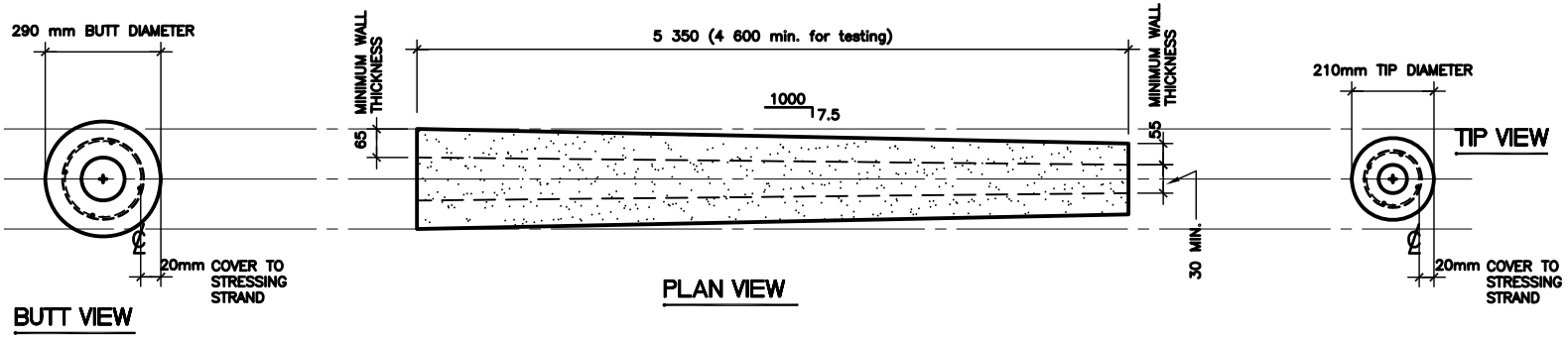

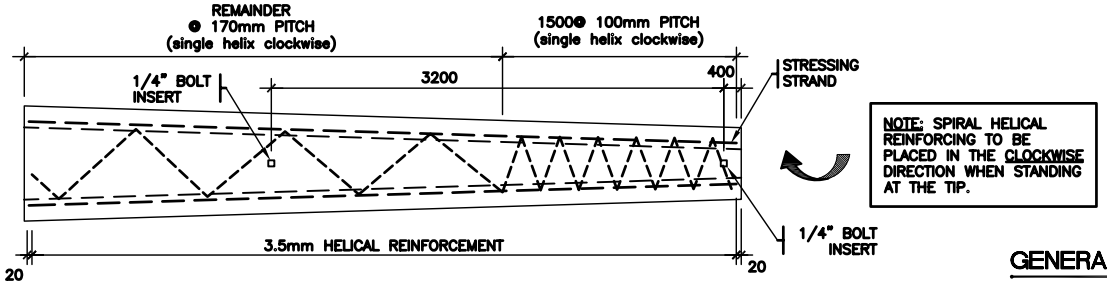

REINFORCING PLAN

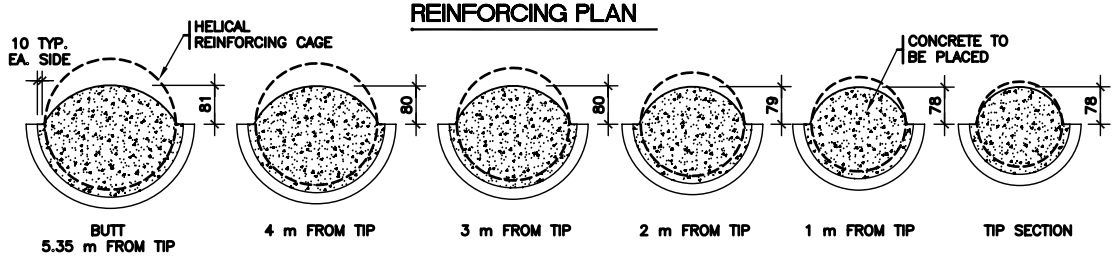

CONCRETE FILL SECTIONS

GENERAL NOTES

1. PRESTRESSING STRANDS TO BE LOW RELAXATION STEEL
2. PRESTRESSING STRANDS TO BE TENSIONED TO 80% OF ULTIMATE STRAND STRENGTH.
3. REINFORCING AND PRESTRESSING STRANDS TO HAVE 20mm CLEAR COVER.
4. CLAMP LENGTH IS 1830mm (72") OR 10% OF POLE LENGTH (WHICHEVER IS GREATER)
5. CAPACITIES BASED ON PRESTRESS LOSSES OF 10% AT TRANSFER AND 21% LONG TERM. MOMENTS TAKEN AT TOP OF CLAMP LENGTH, TORQUE TAKEN AT 600mm FROM TIP.
6. SPIRAL REINFORCING TO BE COLD DRAWN STEEL WIRE CONFORMING TO A.S.T.M. A641 OR C.S.A. G30.3 WITH CLASS 'A' GALVANIZED COATING AS PER A.S.T.M. A641

DESIGN DATA

REINFORCING					LOAD RESISTANCE DATA			CONCRETE	
PRESTRESS STRAND NUMBER & DIAMETER (mm)	STRAND GRADE (MPa)	REINFORCING BARS NUMBER & SIZE	REBAR GRADE (MPa)	BAR LENGTH (m)	CRACKING MOMENT @3.6m Mcr (kNm)	UNFACTORED MOMENT CAPACITY@3.6m Mr (kNm)	CRACKING TORQUE @0.6m Tcr (kNm)	REQUIRED COMPRESSIVE STRENGTH at TRANSFER (MPa)	28 DAY COMPRESSIVE STRENGTH (MPa)
4 – 9mm / (3/8")	1860				18.1	41.3	12.0	25	60

SCALE	N.T.S.
DATE	JUN. 24/07
JOB No.	00–00–00
CAD FILE	
SHEET No.	210-3

PROJECT NAME
UNIVERSITY OF WATERLOO
TORSIONAL TEST SPECIMENS

DRAWING TITLE
FIGURE 4.10: 210 SINGLE CW HELIX LARGE SPACED SPECIMEN (210-CW-L)

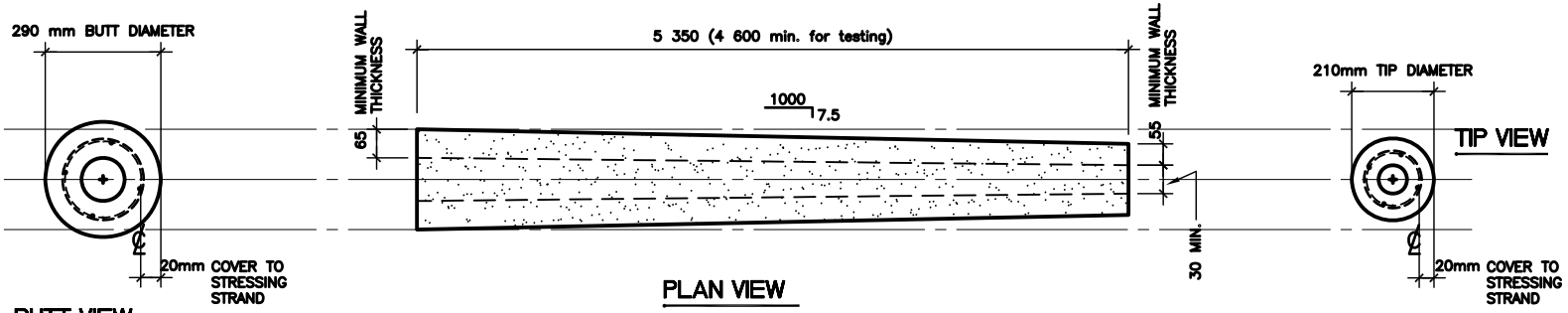

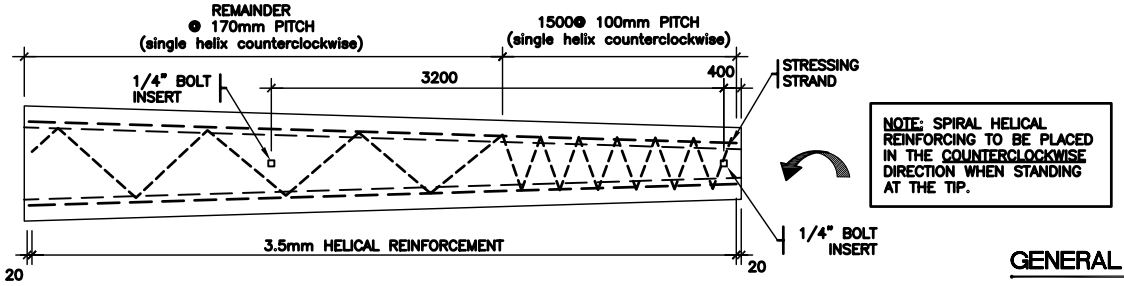

REINFORCING PLAN

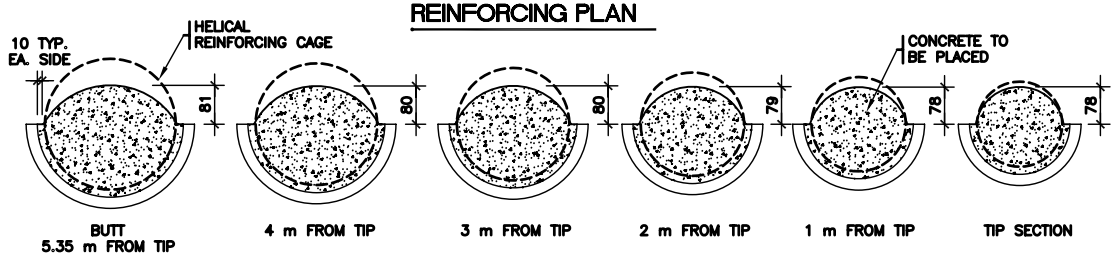

CONCRETE FILL SECTIONS

GENERAL NOTES

1. PRESTRESSING STRANDS TO BE LOW RELAXATION STEEL
2. PRESTRESSING STRANDS TO BE TENSIONED TO 80% OF ULTIMATE STRAND STRENGTH.
3. REINFORCING AND PRESTRESSING STRANDS TO HAVE 20mm CLEAR COVER.
4. CLAMP LENGTH IS 1830mm (72") OR 10% OF POLE LENGTH (WHICHEVER IS GREATER)
5. CAPACITIES BASED ON PRESTRESS LOSSES OF 10% AT TRANSFER AND 21% LONG TERM. MOMENTS TAKEN AT TOP OF CLAMP LENGTH, TORQUE TAKEN AT 600mm FROM TIP.
6. SPIRAL REINFORCING TO BE COLD DRAWN STEEL WIRE CONFORMING TO A.S.T.M. A641 OR C.S.A. G30.3 WITH CLASS 'A' GALVANIZED COATING AS PER A.S.T.M. A641

DESIGN DATA

REINFORCING					LOAD RESISTANCE DATA			CONCRETE	
PRESTRESS STRAND NUMBER & DIAMETER (mm)	STRAND GRADE (MPa)	REINFORCING BARS NUMBER & SIZE	REBAR GRADE (MPa)	BAR LENGTH (m)	CRACKING MOMENT @3.6m Mcr (kNm)	UNFACTORED MOMENT CAPACITY@3.6m Mr (kNm)	CRACKING TORQUE @0.6m Tcr (kNm)	REQUIRED COMPRESSIVE STRENGTH at TRANSFER (MPa)	28 DAY COMPRESSIVE STRENGTH (MPa)
4 – 9mm / (3/8")	1860				18.1	41.3	12.0	25	60

SCALE	N.T.S.
DATE	JUN. 24/07
JOB No.	00–00–00
CAD FILE	
SHEET No.	210-4

PROJECT NAME
UNIVERSITY OF WATERLOO
TORSIONAL TEST SPECIMENS

DRAWING TITLE
FIGURE 4.11: 210 SINGLE CCW HELIX LARGE SPACED SPECIMEN (210-CCW-L)

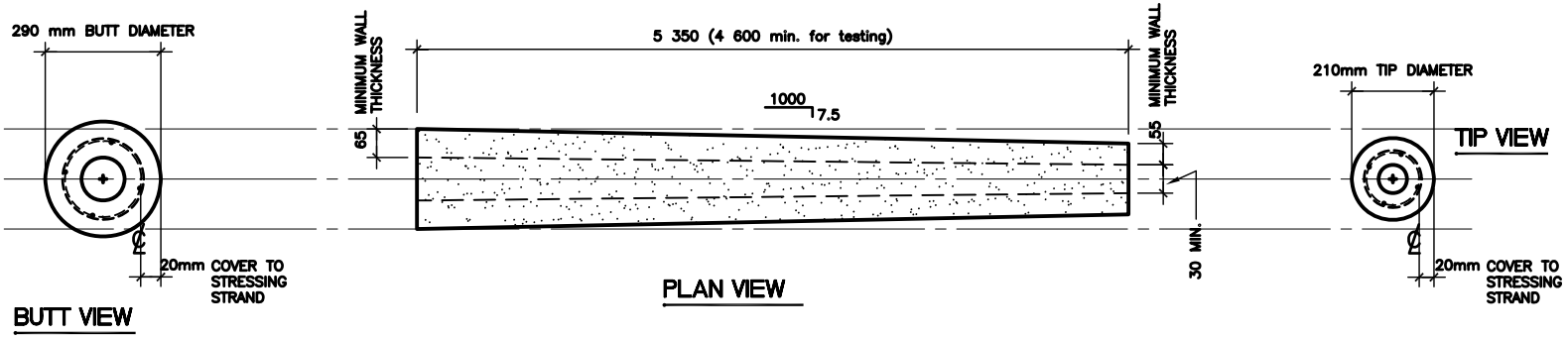

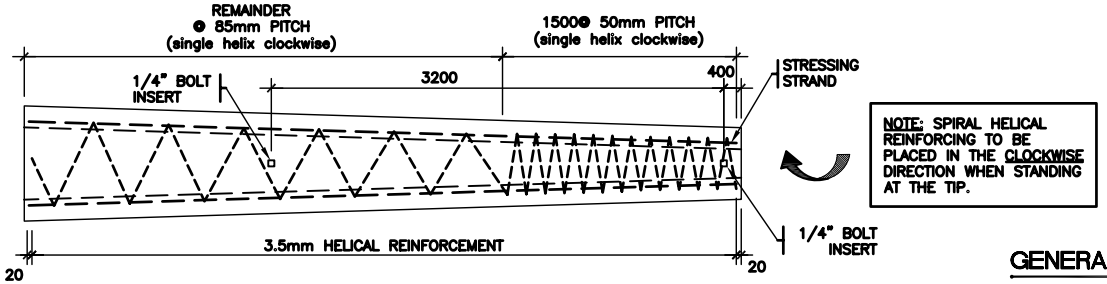

REINFORCING PLAN

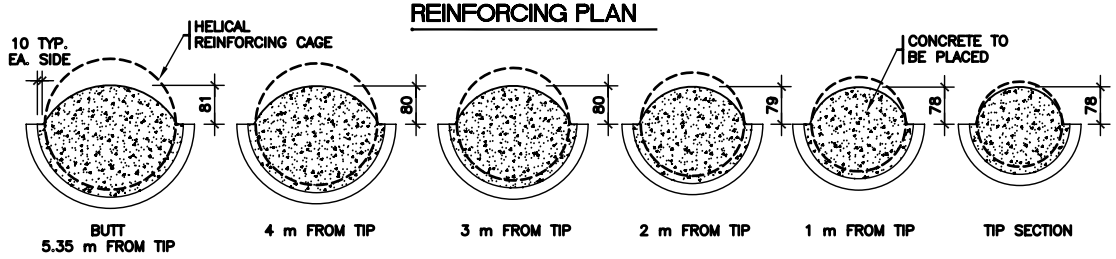

CONCRETE FILL SECTIONS

GENERAL NOTES

1. PRESTRESSING STRANDS TO BE LOW RELAXATION STEEL
2. PRESTRESSING STRANDS TO BE TENSIONED TO 80% OF ULTIMATE STRAND STRENGTH.
3. REINFORCING AND PRESTRESSING STRANDS TO HAVE 20mm CLEAR COVER.
4. CLAMP LENGTH IS 1830mm (72") OR 10% OF POLE LENGTH (WHICHEVER IS GREATER)
5. CAPACITIES BASED ON PRESTRESS LOSSES OF 10% AT TRANSFER AND 21% LONG TERM. MOMENTS TAKEN AT TOP OF CLAMP LENGTH, TORQUE TAKEN AT 600mm FROM TIP.
6. SPIRAL REINFORCING TO BE COLD DRAWN STEEL WIRE CONFORMING TO A.S.T.M. A641 OR C.S.A. G30.3 WITH CLASS 'A' GALVANIZED COATING AS PER A.S.T.M. A641

DESIGN DATA

REINFORCING					LOAD RESISTANCE DATA			CONCRETE	
PRESTRESS STRAND NUMBER & DIAMETER (mm)	STRAND GRADE (MPa)	REINFORCING BARS NUMBER & SIZE	REBAR GRADE (MPa)	BAR LENGTH (m)	CRACKING MOMENT ⊙3.6m Mcr (kNm)	UNFACTORED MOMENT CAPACITY⊙3.6m Mr (kNm)	CRACKING TORQUE ⊙0.6m Tcr (kNm)	REQUIRED COMPRESSIVE STRENGTH at TRANSFER (MPa)	28 DAY COMPRESSIVE STRENGTH (MPa)
4 – 9mm / (3/8")	1860				18.1	41.3	12.0	25	60

PROJECT NAME
UNIVERSITY OF WATERLOO
TORSIONAL TEST SPECIMENS

DRAWING TITLE
FIGURE 4.12: 210 SINGLE CW HELIX NORMAL SPACED SPECIMEN (210-CW-N)

SCALE	N.T.S.
DATE	JUN. 24/07
JOB No.	00–00–00
CAD FILE	
SHEET No.	210-5

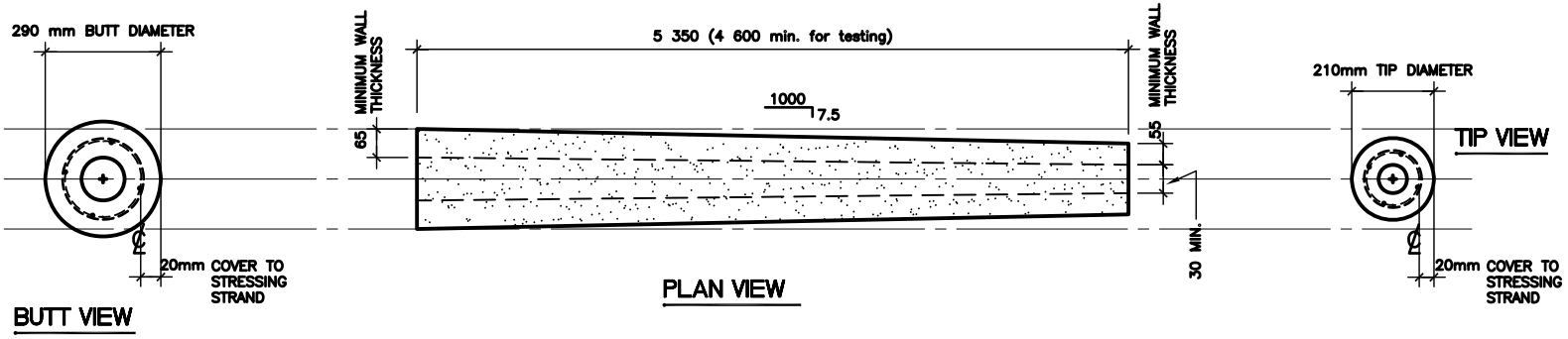

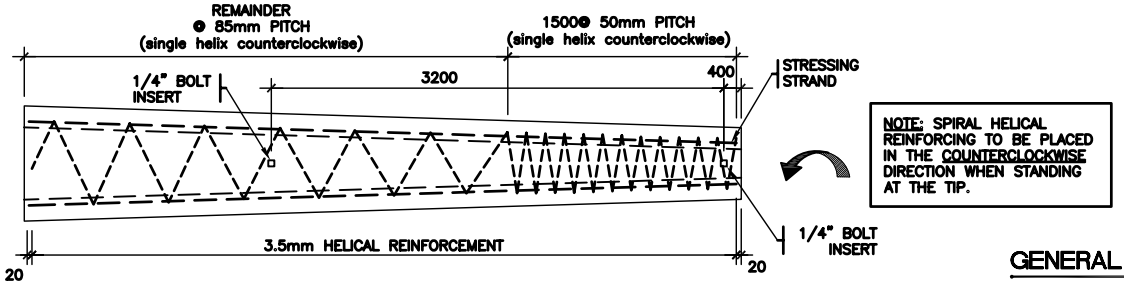

REINFORCING PLAN

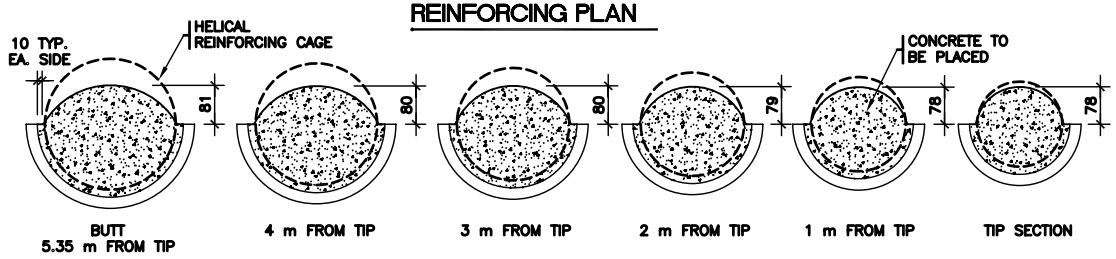

CONCRETE FILL SECTIONS

GENERAL NOTES

1. PRESTRESSING STRANDS TO BE LOW RELAXATION STEEL
2. PRESTRESSING STRANDS TO BE TENSIONED TO 80% OF ULTIMATE STRAND STRENGTH.
3. REINFORCING AND PRESTRESSING STRANDS TO HAVE 20mm CLEAR COVER.
4. CLAMP LENGTH IS 1830mm (72") OR 10% OF POLE LENGTH (WHICHEVER IS GREATER)
5. CAPACITIES BASED ON PRESTRESS LOSSES OF 10% AT TRANSFER AND 21% LONG TERM. MOMENTS TAKEN AT TOP OF CLAMP LENGTH, TORQUE TAKEN AT 600mm FROM TIP.
6. SPIRAL REINFORCING TO BE COLD DRAWN STEEL WIRE CONFORMING TO A.S.T.M. A641 OR C.S.A. G30.3 WITH CLASS 'A' GALVANIZED COATING AS PER A.S.T.M. A641

DESIGN DATA

REINFORCING					LOAD RESISTANCE DATA			CONCRETE	
PRESTRESS STRAND NUMBER & DIAMETER (mm)	STRAND GRADE (MPa)	REINFORCING BARS NUMBER & SIZE	REBAR GRADE (MPa)	BAR LENGTH (m)	CRACKING MOMENT ⊙3.6m Mcr (kNm)	UNFACTORED MOMENT CAPACITY⊙3.6m Mr (kNm)	CRACKING TORQUE ⊙0.6m Tcr (kNm)	REQUIRED COMPRESSIVE STRENGTH at TRANSFER (MPa)	28 DAY COMPRESSIVE STRENGTH (MPa)
4 – 9mm / (3/8")	1860				18.1	41.3	12.0	25	60

PROJECT NAME
UNIVERSITY OF WATERLOO
TORSIONAL TEST SPECIMENS

DRAWING TITLE
FIGURE 4.13: 210 SINGLE CCW HELIX NORMAL SPACED SPECIMEN (210-CCW-N)

SCALE	N.T.S.
DATE	JUN. 24/07
JOB No.	00–00–00
CAD FILE	
SHEET No.	210-6

4.4 CSA A23.3-4 Specimen Design Moment, Shear and Torsion Values

The specimens were analyzed using the pole capacity analysis program presented in section 3.2. According to the CSA A14-07 classification system a Class C pole is required to hold a 5.3 kN load at 0.6 m from the tip. Typical ground embedment for concrete poles is 10 percent of the pole length plus 2 feet (~ 0.66 m). For a 10.7 m design pole length, the corresponding classification ground line moment at 9 m from the tip of the pole is 44.5 kN-m. The unfactored and factored design moment, shear, and torsional capacities are given in Table 4-4 and Table 4-5 respectively. Comparing the unfactored moments at 9 m from the tip to the required classification ground line moment confirms that the specimens are all Class C poles.

Table 4-4: Calculated unfactored 165 and 210 specimen moment, shear, and torsional capacities

Unfactored Resistances		Specimen					
		165 Tip			210 Tip		
	Location (m from tip):	0.6 m	3.6 m	9 m	0.6 m	3.6 m	9 m
Moment (kN-m)	M_{cr}		13.0	23.2		18.1	30.7
	M_r		32.8	48.1		41.3	56.7
Shear (kN)	V_c	11.4	15.8		16.7	21.8	
	V_s	8.7	8.5		8.5	9.3	
	V_r	20.1	24.3		25.2	31.1	
Torsion (kN-m)	T_{cr}	7.1	12.2		12.0	18.8	
	T_r	1.2	1.6		1.5	2.2	
Transfer release strength (MPa)	f_{ci}	25.2			16.2		

Table 4-5: Calculated factored 165 and 210 specimen moment, shear, and torsional capacities

Factored Resistances		Specimen					
		165 Tip			210 Tip		
	Location (m from tip):	0.6 m	3.6 m	9 m	0.6 m	3.6 m	9 m
Moment (kN-m)	M_{cr}		13.0	23.2		18.1	30.7
	M_r		28.3	41.8		35.8	49.5
Shear (kN)	V_c	8.0	11.1		11.7	15.2	
	V_s	7.4	7.2		7.2	7.9	
	V_r	15.4	19.3		18.9	23.1	
Torsion (kN-m)	T_{cr}	5.6	9.4		9.2	14.4	
	T_r	1.0	1.3		1.3	1.9	
Transfer release strength (MPa)	f_{ci}	25.2			16.2		

The calculated ultimate torsion resistances are lower than the cracking torques in all cases since the ultimate resistance is based on the transverse reinforcement alone. The concrete transfer release strength required for the 165 mm specimens is 25.2 MPa and 16.2 MPa for the 210 mm specimens. The shear capacity of the concrete is greater than the applied shear force indicating that the concrete is adequate to resist the shear force. The output from the pole analysis program has been included in Appendix A.

4.5 Specimen Preparation

The test specimens were produced by Sky Cast Inc. between August 22nd, 2007 and August 30th, 2007. The spun cast concrete pole production process is summarized in this section.

The moulds are first cleaned and then setup according to the Sky Cast specifications. The mould design allows multiple mould sections to be assembled to produce a variety of pole lengths and diameters. To save material costs the test specimens were produced shorter than normal poles at 5.345 m long, and therefore specially made wood tip and butt plates were fastened in the moulds at the required diameters.

Once the setup of the mould is complete it is moved to the reinforcing and pouring stations. The reinforcing and pouring steps in spun cast pole production uses the bottom half of the mould only. Depending on the applied loads, 4 or 8 prestressing strands are spaced evenly within the pole section and stressed initially to 20% of the final stressing to tighten the strands. The end plates on the mould are left 3 to 5 mm away from the bottom mould half to allow enough room for the top mould to be placed prior to the spinning process.

The helical reinforcing is wound by hand tightly against the stressing strands and spaced according to the specifications of the pole (Figure 4.14). When a double helix of reinforcing is required an additional coil is added in the opposite direction of the first. To ensure the required spacing of the specimen helix was achieved for all specimens, a wooden ruler was used to indicate the spacing needed (Figure 4.15). Typically the helical reinforcing is spaced by eye. The helical reinforcing is typically a 3.5 mm cold drawn wire with a yield stress between 500 and 600 MPa (CSA A14-07).

Figure 4.14: Placing the helical reinforcing

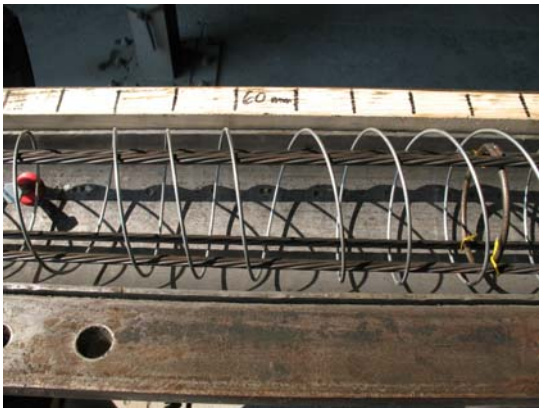

Figure 4.15: Spacing the helical reinforcing

Pouring of the concrete is accomplished using a hopper on rails. The hopper travels the length of the pole and the amount of concrete placed is controlled by the operator. A second operator follows behind the hopper and places the concrete by hand while ensuring enough concrete is added in each section (Figure 4.16). The wall thickness of the pole is directly affected by the judgment of the operator placing the concrete. If the pile of concrete is not high enough, a thinner wall section will be produced, which may cause problems during prestress transfer and reduce the overall capacity of the pole.

Ensuring consistent wall thickness for all specimens is a difficult part of the production process. It relies on the experience of the operator placing the concrete and can be altered by changes in the concrete properties or spinning speed. To reduce the variability in wall thicknesses, volume calculations were completed prior to pouring to determine how much concrete would be needed at each section of the pole. Typically a mound of concrete is placed on top of the full half mould. Using the required concrete volumes, the area of the moulds, and an estimated size of the mound on top, the distance to the top of the mound is calculated. It is determined to achieve the required wall thicknesses; the distance from the mould to the top of the mound should be 70 mm for the 165 mm tip poles and 80 mm for the 210 mm tip poles.

After the concrete is poured, and the excess concrete is removed from the bottom mould flanges, the top mould is placed on top. The mould is then bolted down along the length and the end plates are tightened into place (Figure 4.17). The prestressing strands are then stressed to the final stressing values. During stressing, the elongation is measured and recorded for each strand. Following the final assembly of the mould, the pole is moved to the spinning machine (Figure 4.18).

Figure 4.16: Pouring and placing of concrete

Figure 4.17: Tightening bolts on mould

Figure 4.18: Mould on spinning machine

Figure 4.19: Kiln and curing process

Figure 4.20: De-moulding machine

Figure 4.21: Releasing pole from mould

The poles are then spun for approximately 8 minutes at 15 m/s. The spinning process pushes the concrete outwards and thereby consolidating it against the mould creating the hollow centre of the pole. The hollow centre is called the raceway and is used for electrical conduits. Once the poles have been spun, the moulds are moved to the kiln area (Figure 4.19). The poles remain in the moulds during the curing process, which takes approximately 6 to 8 hours. The steam curing kilns achieve a temperature of approximately 60 degrees Celsius during the curing process.

The moulds are removed from the kiln following the curing process and moved to the de-moulding area. A concrete mix with high early strength development is used to allow transfer of the prestressing forces to the concrete. The prestressing strands are cut and the bolts are removed from the mould. To strip the poles, the top of the mould is removed and placed aside while the bottom is placed in the pole stripping machine (Figure 4.20). The poles are released from the mould by flipping the mould bottom on its side and vibrating it (Figure 4.21).

4.6 Concrete Mix

The concrete mix used for the production of the experimental specimens was the typical mix used by Sky Cast Inc. for round grey poles. The mixes at Sky Cast Inc. are all based on the research conducted by Wang, Dilger, and Kuebler (2001) (section 2.1.4). The target mix for the specimens is summarized in Table 4-6 and detailed batch records, concrete and kiln reports are located in Appendix B. The batches were mixed on consecutive work days starting on August 22nd, 2007.

All batches were fairly consistent with one another however there were some variations due to the visual batching technique employed. The coarse aggregate content was within 20-30 kg/m^3 of the target value with the highest in Batch 4 (1085 kg/m^3) and lowest in Batch 7 (1035 kg/m^3). The sand content varied from 822 kg/m^3 in batch 3 to 763 kg/m^3 used in Batch 6. All batches contained approximately the target value of 426 kg/m^3 of cement, except for Batch 4 which had more at 448 kg/m^3. Total water added was the similar for all batches, the lowest being 7 kg/m^3 below the target value (batch 3). Water-cement ratios ranged between 0.30 and 0.33. Batch 4 also contained the highest quantities of air entraining agent and super plasticizer. Due to the extra super plasticizer added to Batch 4, the resulting slump of 65 mm was higher than the target value of 20-50 mm. The air content was also high for Batch 4 at 8.2%. The remaining values were within acceptable ranges of one another.

Table 4-6: Summary of target mix and actual specimen concrete mixes

Mix	Targets		Actual						
Batch number (#):	1	2 - 7	1 (-C)	2 (-D)	3 (-C-2)	4 (-CCW-L)	5 (-CW-L)	6 (CW-N)	7 (CCW-N)
Batch size (m^3)	0.38	0.46	0.38**	0.46	0.46	0.46	0.46	0.46	0.46
13 mm Coarse Aggregate (kg/m^3)	1057		1045	1054	1048	1085	1052	1052	1035
Sand (kg/m^3)	774		803	807	822	798	807	763	774
Type 30 HSF Cement (kg/m^3)*	426		426	422	422	448	426	426	424
Total Water (kg/m^3)	135		137	137	128	139	135	135	137
Air Entraining Agent (mL)	646	782	688	813	812	963	813	813	813
Super Plasticizer (mL)	2109	2553	2150	2600	2600	2650	2600	2600	2600
Water Reducing Agent (mL)	408	494	450	550	500	500	500	500	500
w/c ratio	0.32		0.32	0.33	0.30	0.31	0.32	0.32	0.32
Slump (mm)	20-50		35	35	40	65	55	55	45
Temperature (°C)	25 minimum		25	27.5	28	28	28.5	28	27
Air Content (%)	5 - 8		4.8	6.1	6.7	8.2	6.4	6.5	6.6
Moisture Content (%)	-		7	7.1	N/A	6.7	6.8	6.4	6.3
Fresh Density (kg/m^3)	-		2449	2391	2384	2354	2419	2427	2380
Kiln #			2	1	1	3	5	2	9
Average Curing Temperature over 4 hours (°C)	60 +/- 5		62	61	61	59	59	61	54
Density of Hardened Concrete (kg/m^3)	-		2425	2394	2419	2321	2373	2395	2371

* = 82 % Type 30, 10 % silica fume, 8% slag ** = second batch made, more concrete was needed

4.6.1 Prestressing Strand

Each specimen was reinforced with 4 - 3/8" (9.5 mm) diameter prestressing strands spaced 90 degrees around the pole cross section. The use of the same strand size for both poles allowed the double-pole manufacturing process to be simplified since only one set of strands needed to be placed for two poles. The prestressing strand had the following properties according to quality control test reports (provided in Appendix B: Coil No. C-8944): area of 55.22 mm^2, breaking load of 110.7 kN, yield load of 102.3 kN, and modulus of elasticity of 199 534 MPa. The strands are initially stressed to 40% of the final stressing force, which corresponds to 16.7 kN for the 3/8" strands. Afterwards, when final stress values are applied, the resulting force is 80 kN for the 3/8" strands. The jacks used to stress the prestressing strands are calibrated and stop when the design stressing stress of 80% f_{pu} (1488 MPa, resulting in 1176 MPa after 21% losses) is reached. Measurements of the strand elongation and tilt in the end plates are typically taken between the initial and final stressing steps to confirm the stress in

each strand. Using the initial stressing force, actual area of the strand, and the modulus of elasticity allows the initial strain in the strand to be calculated. Adding the initial strain to the measured elongation of the strands during final stressing and subtracting the shrinkage of the mould due to the prestressing forces gives the measured prestressing strains recorded in Table 4-7. Converting the measured strain values into stress and assuming losses of 21 percent, the final stresses in the experimental specimens can be calculated.

Table 4-7: Summary of prestressing strand strains and stress values

Specimen	3/8" Prestressing Strand		
	Measured Prestressing Strain	**Initial Prestressing Stress (MPa)**	**Prestressing Stress after 21% Losses (MPa)**
210-C / 165-C	0.0071	1413	1116
210-C-2 / 165-C-2	0.0068	1355	1070
210-D / 165-D	0.0067	1341	1059
210-CW-L / 165-CW-L	0.0067	1332	1052
210-CCW-L / 165-CCW-L	0.0067	1341	1059
210-CW-N / 165-CW-N	0.0069	1378	1089
210-CCW-N / 165-CCW-N	0.0067	1341	1059
Average:	**0.0068**	**1357**	**1072**
Note: Assumed stressing of 80%(1860 MPa) gives 1176 MPa after losses			

The assumed design prestressing stress value is 1176 MP after losses. The measured stress values in the strands are all lower than the assumed design value. The final stressing values range from 1116 MPa for the -C specimens to 1052 MPa for the -CW-L specimens. The average final stressing value for specimens was 1072 MPa.

4.6.2 Helical (Transverse) Reinforcement and Wall Thickness

The test specimens were designed as Class C and contained helical reinforcement ratios as given in CSA A14-07 Table 2: 0.35% for the first 1.5 m of the pole, and 0.2% for the remaining length. Since the process of calculating the spacing of the helical reinforcing is highly dependant on the wall thickness, target values were set for all specimens. The third reinforcing percentage given in CSA A14-07 Table 2 for section of the pole 4.5 m from the tip was not required since the test poles were only produced 5.75 m long. The helical reinforcing steel was 3.5 mm diameter smooth galvanized cold drawn wire with a yield stress of 500 MPa. A test report of the material used is located in Appendix B.

Table 4-8: Target helical reinforcing spacing/percentages and concrete wall thickness

Specimen	Helical Reinforcing Spacing - Tip Section (mm)*	Helical Reinforcing Spacing - Butt Section (mm)*	Target Tip Thickness (mm)	Target Butt (@5.75 m) Thickness (mm)	Target Helical Reinforcing Tip Section	Target Helical Reinforcing Butt Section
165-C	-	-	45	55	-	-
165-C-2	-	-	45	55	-	-
165-D	60[#]	100[#]	45	55	0.35%	0.20%
165-CW-L	120	200	45	55	0.18%	0.10%
165-CCW-L	120	200	45	55	0.18%	0.10%
165-CW-N	60	100	45	55	0.35%	0.20%
165-CCW-N	60	100	45	55	0.35%	0.20%
210-C	-	-	55	65	-	-
210-C-2	-	-	55	65	-	-
210-D	50[#]	85[#]	55	65	0.35%	0.20%
210-CW-L	100	170	55	65	0.18%	0.10%
210-CCW-L	100	170	55	65	0.18%	0.10%
210-CW-N	50	85	55	65	0.35%	0.20%
210-CCW-N	50	85	55	65	0.35%	0.20%

* = Tip section refers to the first 1.5 m from tip, butt section refers to 1.5 m to 5.75 m from tip of pole
[#] = 210-D/165-D spacing is double the value for each half helix; two halves combined values shown

Table 4-9: Actual helical reinforcing spacing/percentages and concrete wall thickness

Specimen	Helical Reinforcing Spacing - Tip Section (mm)*	Helical Reinforcing Spacing - Butt Section (mm)*	Actual Tip Thickness (mm)	Actual Butt (@5.75 m) Thickness (mm)	Actual Helical Reinforcing Steel – Tip Section	Actual Helical Reinforcing Steel – Butt Section
165-C	-	-	44	64	-	-
165-C-2	-	-	44	70	-	-
165-D	60[#]	100[#]	46	69	0.35%	0.18%
165-CW-L	120	200	46	66	0.17%	0.09%
165-CCW-L	120	200	46	72	0.17%	0.09%
165-CW-N	60	100	48	67	0.33%	0.18%
165-CCW-N	60	100	45	70	0.36%	0.18%
210-C	-	-	45	74	-	-
210-C-2	-	-	50	77	-	-
210-D	50[#]	85[#]	52	77	0.37%	0.19%
210-CW-L	100	170	50	78	0.19%	0.10%
210-CCW-L	100	170	53	85	0.18%	0.09%
210-CW-N	50	85	50	75	0.39%	0.19%
210-CCW-N	50	85	55	80	0.35%	0.18%

* = Tip section refers to the first 1.5 m from tip, butt section refers to 1.5 m to 5.75 m from tip of pole
[#] = 210-D/165-D spacing is double the value for each half helix; two halves combined values shown

It should be noted that the smooth cold drawn wire provides less anchorage and bar development than normal deformed reinforcing steel bar used in other concrete members. The target wall thicknesses at the tip and butt were 45 mm and 55 mm respectively, for the 165 mm tip specimens and 55 mm and 65 mm for the 210 mm tip specimens. Due to the manual manufacturing process the actual values varied slightly. A summary of the spacing targets for the helical reinforcing and target values for the concrete wall thickness are presented in Table 4-8. Actual values are given in Table 4-9. Helical reinforcing spacing values were checked with a template prior to pouring.

Due to changes in wall thickness during production, the target percentages of reinforcement were not always obtained. An increase in the wall thickness will cause an effective decrease in the percentage of helical reinforcement. It should be noted however that CSA A14-07 recommends that a nominal wall thickness of 45 mm be used for the calculation of the helical steel spacing. Using the 45 mm nominal thickness the percentages would be higher than the target values in all cases.

4.6.3 Curing Cycle

Heat during the curing process enables the concrete strength to develop quicker and the poles to be removed from the moulds within 6 - 8 hours after pouring. The curing cycle (Figure 4.22) is separated into two parts: the ramp up period and the curing period. The ramp up period brings the temperature surrounding the mould and concrete from 25 degrees Celsius up to 40 degrees in 1.5 hours and then to 60 degrees Celsius at the 3 hour mark. Once the ramp up period is complete the temperature is held constant at 60 degrees Celsius for a 3 hour period. The sustained 60 degree Celsius temperature allows for proper curing of the concrete. The average temperature for each specimen curing cycle was near 60 degrees (Table 4-6). After the 3 hour curing period is finished the temperature drops back down to 25 degrees and the pole can be removed from the mould. The mix design ensures that the minimum concrete strength is achieved to avoid failure during prestressing transfer.

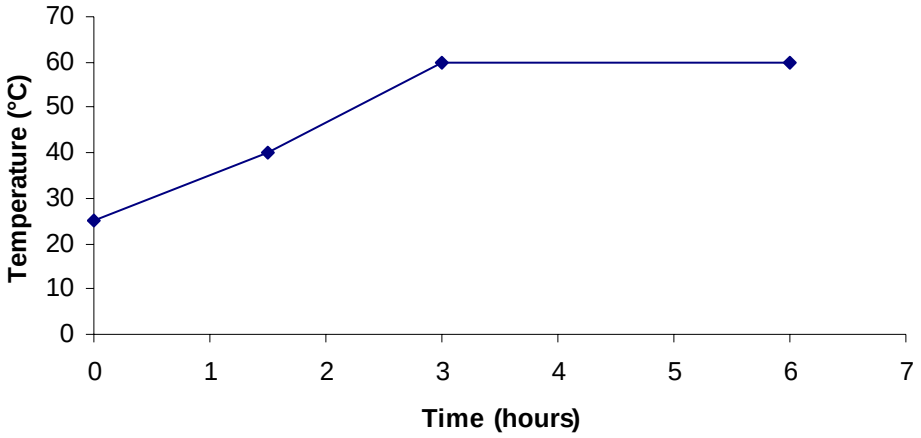

Figure 4.22: Typical prestressed concrete steam curing cylcle

4.6.4 Concrete Compressive and Tensile Strengths

A total of 16 (200 mm high by 100 mm wide) cylinders were cast from each concrete batch to determine the compressive and tensile strength of the mixture. Two cylinders were tested in compression after one day to ensure the proper prestressing concrete transfer strength was achieved. After 28 days another two cylinders were tested in compression to give an indication of the strength progression of the concrete. In addition, three compressive and three tensile cylinders were tested to determine the strengths at the time of testing. Average measurements of the diameter and height were taken for each cylinder tested. Standard compressive and splitting tensile tests were performed and the strengths were determined using the following formulae:

$$\text{Compression: } \sigma_c = \frac{P}{A} \qquad \text{Splitting Tension: } \sigma_t = \frac{2P}{\pi L d}$$

where σ_c is the compressive strength of the concrete and P is the force applied to the cross sectional area of the cylinder, A, σ_t is the tensile strength of the concrete, P is the splitting force applied to the cylinder of length L and diameter d.

The high strength at one day is required for production purposes and to allow transfer of the prestressing forces to the concrete poles. The typical 28 day strength of the concrete mix used for the specimens is around 60 MPa. The target strength at one day was governed by the 25.2 MPa transfer release strength of the 165 mm tip specimens.

Table 4-10: Summary of concrete cylinder compressive and tensile strengths

Specimen	1 Day Compressive Strength (MPa)	28 Day Compressive Strength (MPa)	Time of Testing	
			Compressive Strength (MPa)	Tensile Strength (MPa)
165-C	39.5	41.0	50.6	3.5
165-C-2	59.6*	67.1	72.3	4.7
165-D	52.2	63.9	66.4	4.4
165-CW-L	49.0	59.5	64.7	4.1
165-CCW-L	35.6	39.3	45.8	2.9
165-CW-N	55.0	57.1	63.7	4.5
165-CCW-N	49.5	62.0	66.0	4.4
210-C	42.9	61.0	61.5	3.3
210-C-2	53.5*	63.8	68.1	3.8
210-D	47.3	63.0	65.3	4.3
210-CW-L	42.5	57.4	62.6	3.9
210-CCW-L	41.6	57.4	57.0	4.2
210-CW-N	55.0	66.7	67.5	4.9
210-CCW-N	53.9	57.3	63.6	4.4
* = 3 day cylinder test result				

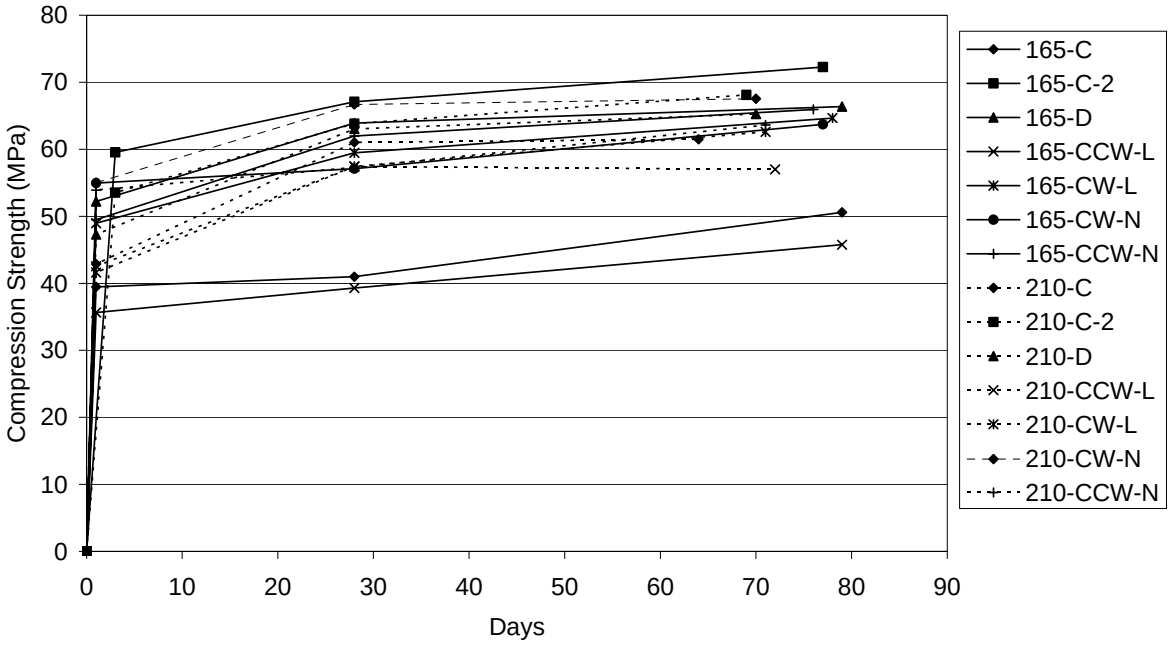

Figure 4.23: Specimen compression strength development to time of testing

At one day, all specimens achieved the required transfer strength (Table 4-10). The strength at prestressing transfer ranged from 35.6 to 59.6 MPa (three day result). Compression testing results at 28 days ranged from 39.3 MPa to 67.1 MPa (Table 4-10). The low value of the 165-CCW-L specimen (39.3 MPa) can be traced to mix differences and variations in the kiln curing temperatures from one end to the other. The CCW-L mixture could have been altered due to the higher air entrainment and super plasticizer volume, which resulted in a higher slump. Only two specimens (165-C and 165-CCW-L) had 28 day compression results well below the target 60 MPa concrete strength. The remaining specimens had values over or just under the target concrete strength. At the time of testing compressive strengths ranged from 45.8 MPa to 68.1 MPa. Tensile strengths ranged from 2.9 MPa to 4.9 MPa. It should be noted that both the 165-C and 165-CCW-L specimens had significantly lower values (~15-20 MPa) at the time of testing and may be reflected in their torsional performance.

It should also be noted that even though the 165-CCW-L mix achieved the lowest concrete strengths, the same mix used in the 210-CCW-L specimen achieved acceptable strengths. This confirms the fact that variations in the kiln temperatures played a role in the strength development of the concrete in the 165-CCW-L specimen. Figure 4.23 shows the compression strength development of the specimens from the time of casting to the time of testing. All time of testing specimen compression results, except the 165-C and 165-CCW-L specimens lie between 55 MPa and 72 MPa and show similar strength development curves.

Chapter 5
Experimental Setup and Procedures

5.1 Test Setup and Apparatus

The pole specimens were tested on-site at Sky Cast Inc. in Guelph, Ontario (see Figure 5.1). The testing facilities at Sky Cast Inc. were used to avoid transporting the pole specimens. A testing clamp fixed to an exterior concrete slab was used to hold the butt end of pole rigid during testing (Figure 5.2 a)). One side of the testing clamp moves on rails and is fastened to the other side using four steel rods. The pole specimen is loaded into the clamp using a forklift and held in place. The four bolts on the rods are tightened until the pole is firmly held in place. To ensure no movement or slippage occurs at the clamp end, a mark is made on the pole and clamp and checked throughout the testing process.

The loads were applied from the pulling bench which is located approximately 11.5 m from the clamp. A 16.3 mm steel cable and a two-speed manual winch with a rating of 50 kN (25 kN-m maximum torque for test setup) were used (Figure 5.2 b)). The low speed of the winch pulls at a rate of 9 mm of cable per crank rotation, whereas the high speed pulls at a rate of 18 mm per crack rotation. During testing of the specimens, the high speed was only used to tighten the slack in the cable. Once the slack was removed the slow speed was used until cracking and failure of the pole.

The poles were loaded with a counter clockwise torque for each specimen allowing the differences between the clockwise and counter clockwise helical steel layouts to be observed. The manual winch allowed the testing to be displacement controlled. Rotation was applied in increments as governed by the winch and the resulting load in the cable was measured. The steel cable was attached to the pole using a steel collar located 0.6 m from the tip of the pole as required by CSA A-14-07 (Figure 5.2 a) and c)). The collar bolts were tightened, which clamped the collar around the pole. Slippage and movement of the collar was monitored by applying a mark on the collar and the pole (Figure 5.2 d) and e)). The torque arm from the collar cable connection point to the middle of the pole was 0.5 m.

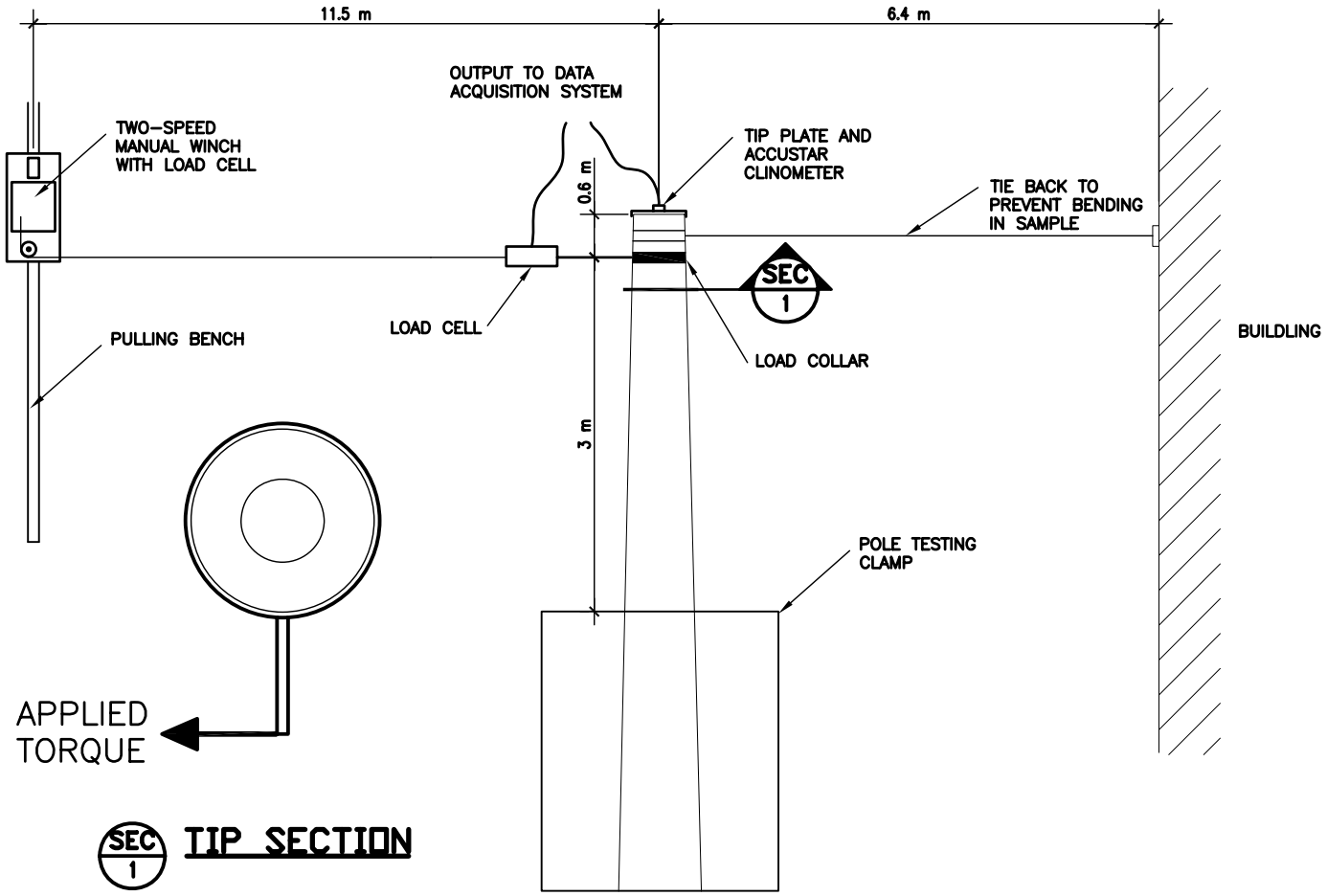

SCALE	N.T.S.
DATE	JUN. 01/07
JOB No.	00-00-00
CAD FILE	TESTING SETUP.DWG
SHEET No.	1

PROJECT NAME
UNIVERSITY OF WATERLOO
TORSIONAL TEST SPECIMENS

DRAWING TITLE
FIGURE 5.1: TESTING BED LAYOUT AND TEST SETUP

a) Pole testing clamp

b) Application of loads using two-speed manual winch

c) Loading and tie-back collar setup

d) monitoring movement at pole clamp end

e) monitoring movement at loading collar

Figure 5.2 a) - e): Pictures of test setup

To ensure pure torsional loads were applied to the specimens a tie back cable was attached to the plant building (6.4 m in the opposite direction of the pulling bench). The tie back cable was tightened using a griphoist and an 11 mm steel cable prior to testing. A loose steel collar was placed on the pole near where the loading collar was fastened (Figure 5.2 c)).

Applied loads were recorded using a 44.5 kN (10000 lbs.) load cell attached between the loading collar and the 16.3 mm steel cable. Twist values were recorded using an electronic clinometer attached at the tip end of the pole.

5.2 Instrumentation

5.2.1 Data acquisition system

The data acquisition system consisted of a laptop, and a four input Onset HOBO micro station datalogger. Two S-VIA-CM14 Onset 0-5 V adapters were used to input the applied load and twist data values. The HOBO datalogger system was chosen as the data acquisition system since the testing would be done onsite. A simple and easy to use system was needed to reduce the electronic devices required on site. The data logger was easily launched using the HOBOware Pro software and was downloaded to the laptop using a serial cable connection.

The use of the HOBO data loggers caused limitations on the data acquisition system. The 0-5 V input adapters limited the input voltages from the instrumentation to 5 V. The HOBO data logger could only record every 0.1 mV difference, and sample from the instrumentation every second. To overcome these limitations the instrumentation output voltage was kept below 5 V and the loading was applied slowly to ensure enough voltage values were recorded at each step.

5.2.2 Load Cells and Single Channel Signal Conditioner

Two load cells were used to record the applied loads. The first load cell was attached to the pulling bench behind the winch to give the winch operator an indication of the load level. No data was recorded from the first load cell.

The second load cell was placed between the steel cable and the load collar to obtain the most accurate recording of the load applied to the pole specimen. The second load cell had a capacity of 44.5 kN (10000 lbs.) and an output of 3 mV/V. The load cell was excited with a 10.22 V signal.

The load cell output was limited at 5 V due to the HOBO data logger adapters. It was determined that the use of a 10 V input signal and the load cell output of 3 mV/V would give an applied load recorded in increments of 0.41 kN. Since the accuracy needed to be much lower than the increment provided, a Sensotec Model GM Single Channel Signal Conditioner was needed to lower the perceived load increment. The signal conditioner allowed increments of approximately 0.001 kN to be measured. Since the maximum output of the Sensotec device was 10 V at a load cell input of 44.5 kN (10000 lbs.) and the maximum voltage the HOBO adapter could record was 5 V, a limit on the load cell data acquisition was placed at 22.2 kN (5000 lbs.) initially. For each calibration the Sensotec device displayed a calibration reading of 22.0 kN.

To calibrate the 44.5 kN (10000 lbs.) load cell to be used for testing, a known calibrated load cell rated at 22.2 (5000 lbs.) was setup in series with the 44.5 kN (10000 lbs.) load cell. The calibrated load cell was loaded at 2.22 kN (500 lbs.) increments up to 22.2 kN (5000 lbs.) and the associated voltage output from the 44.5 kN (10000 lbs.) load cell was measured. Each increment was held for a predetermined length of time to establish an average voltage output. The average output voltage for each increment was then plotted versus the known load increments. A linear regression was then completed to relate the load cell output voltage and the applied load in kN (Figure 5.4).

Figure 5.3: Signal conditioner with voltage divider

A second calibration was performed when a larger applied torque was needed for the larger pole diameters. Since the output voltage still needed to be 5 V to be recorded by the HOBO adapter, a voltage divider was added to the output of the load cell. The voltage divider used two 16k ohm +/- 5% resistors to halve the 10 V load cell output to a value below 5 V (Figure 5.3). The two resistors were 16.55k ohm and 16.84k ohm and within 0.29k ohms or 1.5% of each other. The 16.55k ohm resistor was used from the negative output terminal to the NC terminal, whereas the 16.84k ohm resistor was used from the positive terminal to the NC terminal. The resulting linear calibration related the output voltage to the applied load (Figure 5.5).

The output from the load cell placed between the load collar and the steel cable was recorded using the data acquisition system. During post-processing of the data, the voltages recorded were converted to applied torques using the equations below:

$$T_a = (0.5m)(5.0159kN/V)(x) \text{ without voltage divider} \quad (5\text{-}1)$$

$$T_a = (0.5m)(10.139kN/V)(x) \text{ with voltage divider} \quad (5\text{-}2)$$

where T_a is the applied load in kN-m, and x is the load cell output voltage in V.

5.2.3 Electronic Clinometer

The rotation of the pole specimens were recorded using a Schaevitz AccuStar electronic clinometer with an accuracy of 0.001 degrees, a range of +60 degrees to -60 degrees, and a variability of 10%. The data logger limitation of 0.1 mV allowed changes of 0.00167 degrees to be recorded. The clinometer was powered using an excitation voltage of 12.75 VDC from a battery supply. The clinometer outputted 60 mV/degree and therefore the voltage at the maximum +/-60 degrees was +/- 3.6 V. The clinometer was mounted to a plastic tip plate and placed on the tip end of the pole. The output was recorded using the data acquisition system and converted to degrees using the following formula:

$$\Phi = 60mV/\text{degrees}(1000x) \quad (5\text{-}3)$$

where Φ is the rotation in degrees, and x is the clinometer output voltage in mV.

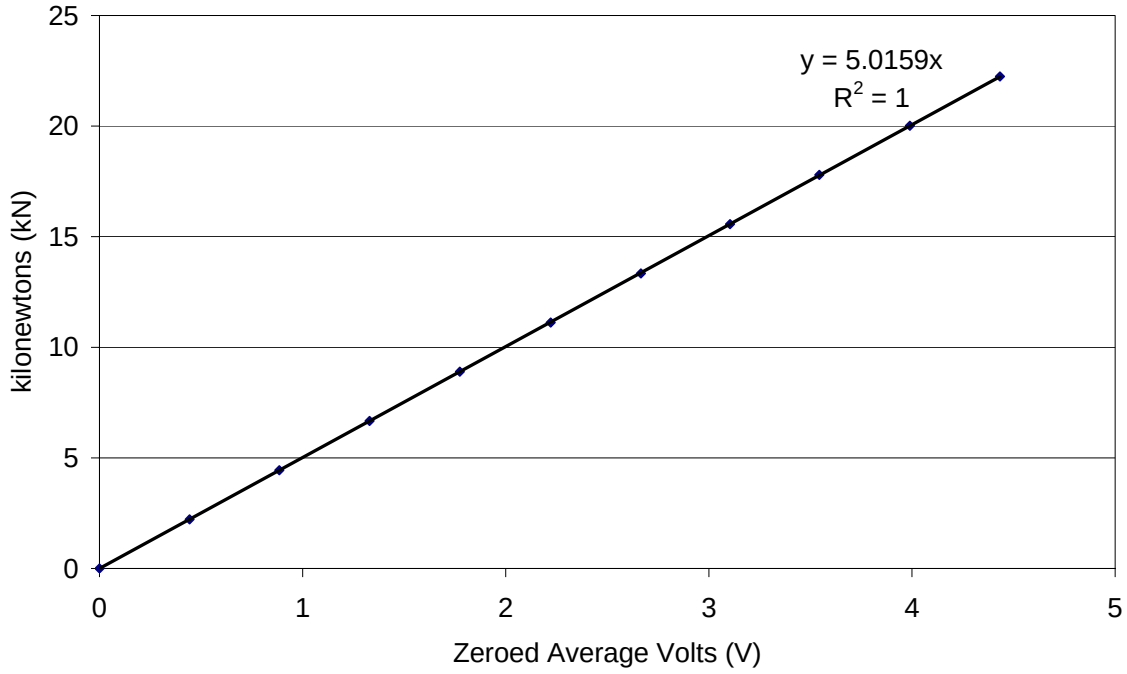

Figure 5.4: Load cell calibration 1

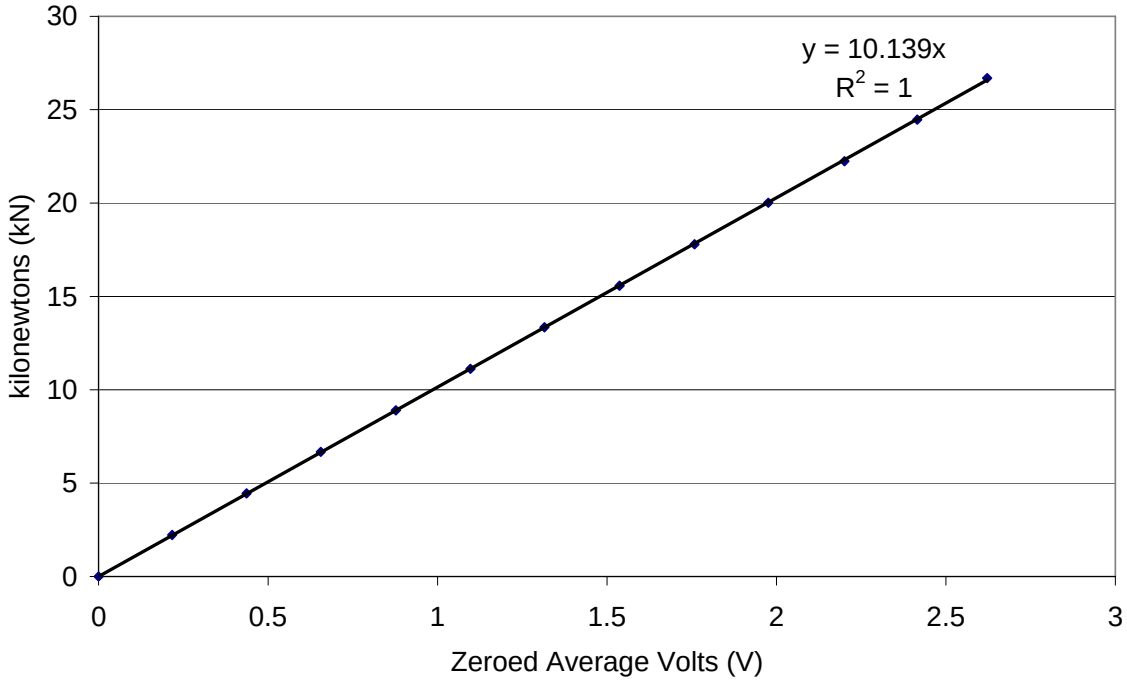

Figure 5.5: Load cell calibration 2 (with voltage divider)

5.2.4 Documentation Equipment

A video camera and digital camera was used to record each test. Prior to cracking, the video camera was setup to record the entire pole movement. After cracking the video camera was moved to the crack location to document the crack development and mode of failure. Notes were taken during testing to correlate with the data, video, and pictures taken.

5.3 Testing Procedures

The specimens were placed in the test frame using a forklift and a side loader. The tested length of 3.6 m was kept constant for each specimen, measured from the tip to the butt clamp (Figure 5.6). The clamp was tightened until the specimen was held snug against the wood bearing blocks. Measurements were taken to determine the overall length of the specimen and the exact dimension from the tip to the butt clamp. The loading collar was then placed at 0.6 m from the tip end and the bolts were tightened until snug. The tie-back collar was put on the specimen next to the loading collar. The clinometer was placed on the tip of the pole using the manufactured tip plate. Zero measurements were recorded for both the load cell and clinometer as the data acquisition system was started. Marks were made on the specimen, butt clamp, and loading collar to observe any slippage in the specimen.

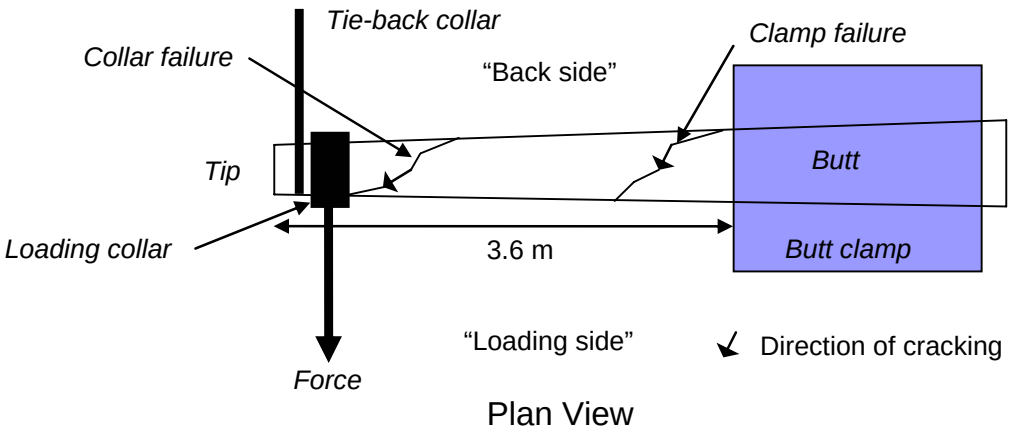

Figure 5.6: Diagram of cracking patterns, failure locations, and loading terminology

The load cell and the loading cable were then attached to the loading collar to begin testing of the specimen. The load cell calibration shown in Figure 5.4 was used in testing of specimens 210-C, 210-C-2, and the pre-cracking portion of 210-D. Since the 210-D specimen required larger loads, the load cell output was split using a voltage divider and the remaining 210 specimens and all of the 165 specimens were tested using the second calibration presented in Figure 5.5.

Since the load was applied manually, the best method for ensuring an approximate constant loading rate was to have one person crank the winch slowly. The testing was performed in displacement control mode using the two gears of the manual winch. After the cable slack was removed the low speed of the winch was used, which pulled 9 mm of cable per full crank rotation. The loading rate was difficult to maintain perfectly constant, however a rate of 0.7 degrees/min was calculated from the data afterwards. As the specimen cracked and rotated, the cable slacked, meaning the slow crank rotation allowed only the necessary amount of displacement and load to be applied. Load was applied post-peak to record the behaviour after cracking. Specimen testing was completed once substantial rotation occurred or the specimen fell to the ground. Measurements were also taken after testing to determine the failure location, wall thickness, and cover to the prestressing steel.

Chapter 6
Experimental Results

6.1 Test Observations

Generally, the 165 specimens cracked and failed at the loading collar whereas the 210 specimens began to fail at the butt clamp (Figure 5.6). Cracking was initiated on the back side for all specimens and moved up towards the tip of the pole spiralling to the loading side of the specimen (Figure 5.6) indicating that perhaps not all of the flexure was eliminated by the restraining cable. A summary of the test results and observations are presented in Table 6-2 and Table 6-3. Specimens were tested in the same order as presented in the following sections. The total length and tested specimen length (distance from tip to clamp) were measured. Prior to each test the calibration of the electronic equipment was checked and values for the excitation voltages for the load cell and clinometer, and the Sensotec signal conditioner reading were recorded. Differences were noted between the excitation voltages, and calibration readings. These differences can be contributed to the change in temperature between tests and warming up of the electronic equipment. The recorded values for each specimen have been summarized in Table 6-1. Raw test observation sheets are included in Appendix C.

Table 6-1: Summary of initial test excitation and calibration readings

Specimen	Date and Time Tested	Total Specimen Length (m)	Tested Length (m)	Excitation Voltage load cell (V)	Sensotec Calibration reading (kN)	Accustar Clinometer Excitation Voltage (V)
210-C	Oct. 25, 10:30 AM	5.345	3.627	10.22	22.00	12.75
210-C-2	Oct. 30 11:01 AM	5.350	3.613	10.21	22.00	12.75
210-D	Oct. 30 1:30 PM	5.350	3.605	10.22	21.95	12.75
210-CCW-L	Nov. 6 10:55 AM	5.360	3.610	10.22	21.98	12.73
210-CW-L	Nov. 6 11:55 AM	5.357	3.615	10.22	21.98	12.70
210-CCW-N	Nov. 8 10:12 AM	5.350	3.622	10.22	21.97	12.74
210-CW-N	Nov. 6 1:51 PM	5.347	3.608	10.22	22.03	12.69
165-C	Nov. 8 11:15 AM	5.345	3.63	10.22	22.01	12.69
165-C-2	Nov. 8 12:07 PM	5.345	3.61	10.22	22.00	12.68
165-D	Nov. 10 12:15 PM	5.350	3.608	10.22	21.99	12.73
165-CCW-L	Nov. 13 10:35 AM	5.343	3.605	10.22	22.00	12.72
165-CW-L	Nov. 13 11:35 AM	5.340	3.608	10.22	21.98	12.71
165-CW-N	Nov. 13 1:45 PM	5.345	3.610	10.22	21.99	12.72
165-CCW-N	Nov. 13 2:50 PM	5.344	3.604	10.22	22.00	12.71

After the maximum torque had been reached, loads were sustained to observe behaviour. The behaviour was noted in the torque-twist figures when the curve looped back upon itself (Figure 6.3; 0.065 rad/m). The torque-twist loops can be attributed to increased cracking and movement in the specimens. As an excess amount of torque is applied, the specimen releases energy post-peak through rotation and increased cracking. The applied torque decreases suddenly causing slack in the loading cable. The slack allows specimen relaxation and the torque-twist curve loop back behaviour.

6.1.1 Test Observations for 210 mm Tip Specimens

6.1.1.1 Specimen 210-C

The 210-C and 165-C specimens were the first to be produced. There was a shortage of concrete during the production of the 210-C specimen which caused the wall thickness at the tip end of the pole to be thinner on one side of the pole (Figure 6.1 a)). The cover from the inside wall of the pole to the strand was only 5 to 10 mm. The wall thickness was only 45 mm, 10 mm thinner than the 55 mm needed. Due to the thinner wall and the lack of helical reinforcement in the 210-C control specimen, a 400 mm longitudinal crack formed along the strand starting at the tip (Figure 6.1 b)).

Since the loading collar relies on friction resistance between the steel collar and the concrete pole, slippage can occur if the bolts on the loading collar are not tightened adequately. Zero readings were initially taken as 0.0006 V for the load cell, and 0.3961 V for the clinometer. Loading collar slippage occurred at 10:48 AM and zero readings were re-established as 0.0006 V for the load cell and 0.3961 V for the clinometer.

The cracking torque of the specimen was determined from the torque-twist curve. Cracking of 210-C specimen occurred at 5.1 kN-m and a twist of 0.0011 rad/m. This corresponds to a stiffness of 4733.11 kN-m^2/rad. Cracking was observed at the butt of the pole near the clamp. Ultimate torque capacity of the specimen was 8.5 kN-m at 0.0029 rad/m of twist. Failure was sudden and brittle and located at the butt clamp (Figure 6.1 c)). The failure crack extended 2.8 m from the butt clamp and 1.7 m into the clamped section. The bottom of the pole held in the clamp was cracked and large pieces had spalled. Post failure, the specimen sustained approximately 1.5 kN-m. Large cracking and twist deformation continued as the specimen continued to hold 1.5 – 2.0 kN-m load. Ultimately the specimen fell to ground. The measured wall thickness at failure was 57 mm with a 20 mm cover to the prestressing strands.

Table 6-2: Summary of 210 mm tip Experimental Results

Specimen	Specimen Properties							Experimental Results						
	Helical Reinforcing Spacing Tip Section (mm)*	Helical Reinforcing Spacing Butt Section (mm)*	Tip Thickness (mm)	Butt (@5.75m) Thickness (mm)	Compressive Strength (MPa)	Tensile Strength (MPa)	Final Prestressing Stress (MPa)	Cracking Torque (kN-m)	Twist at Cracking (rad/m)	Stiffness (kN-m^2/rad)	Ultimate Torque (kN-m)	Twist at Ultimate Torque (rad/m)	Failure Location and Position from tip (m)	Wall Thickness at Failure (mm)
210-C	-	-	45	74	61.5	3.3	1116	5.1	0.0011	4733.11	8.5	0.0029	clamp (2.2 m)	57
210-C-2	-	-	50	77	68.1	3.8	1070	7.3	0.0016	4647.77	8.7	0.0028	clamp (3.2 m)	62
210-D	50#	85#	52	77	65.3	4.3	1059	12.5	0.0030	4243.44	13.3	0.0070	clamp (3.3 m)	63
210-CCW-L	100	170	50	78	62.6	3.9	1052	6.5	0.0016	4164.90	9.5	0.0084	clamp (3.3 m)	71
210-CW-L	100	170	53	85	57.0	4.2	1059	11.5	0.0029	3894.70	12.9	0.0063	clamp (3.4 m)	68
210-CW-N	50	85	50	75	67.5	4.9	1089	9.8	0.0024	4132.63	12.9	0.0087	collar (0.9 m)	55
210-CCW-N	50	85	55	80	63.6	4.4	1059	7.1	0.0013	5561.17	10.7	0.0041	clamp (3.0 m)	71

* = Tip section refers to the first 1.5 m from tip, butt section refers to 1.5 m to 5.75 m from tip of pole
# = 210-D spacing is double the value for each half helix; two halves combined values shown

Table 6-3: Summary of 165 mm tip Experimental Results

Specimen	Specimen Properties							Experimental Results						
	Helical Reinforcing Spacing Tip Section (mm)*	Helical Reinforcing Spacing Butt Section (mm)*	Tip Thickness (mm)	Butt (@5.75m) Thickness (mm)	Compressive Strength (MPa)	Tensile Strength (MPa)	Final Prestressing Stress (MPa)	Cracking Torque (kN-m)	Twist at Cracking (rad/m)	Stiffness ($kN-m^2/rad$)	Ultimate Torque (kN-m)	Twist at Ultimate Torque (rad/m)	Failure Location and Position from tip (m)	Wall Thickness at Failure (mm)
165-C	-	-	44	64	50.6	3.5	1116	2.8	0.0022	1281.71	2.8	0.0088	collar (1.05 m)	48
165-C-2	-	-	44	70	72.3	4.7	1070	2.6	0.0011	2363.96	-	-	collar (0.8 m)	52
165-D	60#	100#	46	69	66.4	4.4	1059	6.7	0.0032	2123.09	8.1	0.0071	collar (0.9 m)	50
165-CCW-L	120	200	46	66	64.7	4.1	1052	5.9	0.0032	1876.12	-	-	collar (0.8 m)	49
165-CW-L	120	200	46	72	45.8	2.9	1059	6.1	0.0032	1930.75	6.4	0.0047	clamp (3.21 m)	53
165-CW-N	60	100	48	67	63.7	4.5	1089	8.5	0.0041	2057.28	8.9	0.0073	clamp (3.31 m)	56
165-CCW-N	60	100	45	70	66.0	4.4	1059	7.5	0.0036	2055.06	7.5	0.0067	collar (0.8 m)	50

* = Tip section refers to the first 1.5 m from tip, butt section refers to 1.5 m to 5.75 m from tip of pole
# = 165-D spacing is double the value for each half helix; two halves combined values shown

a) 210-C tip with thinner wall

b) Longitudinal crack at tip

c) Cracking and spalling in butt clamp

d) Failure at butt (back side)

e) Crack pattern (back side)

f) Crack pattern (loading side)

Figure 6.1: a) – f) 210-C test observation photos

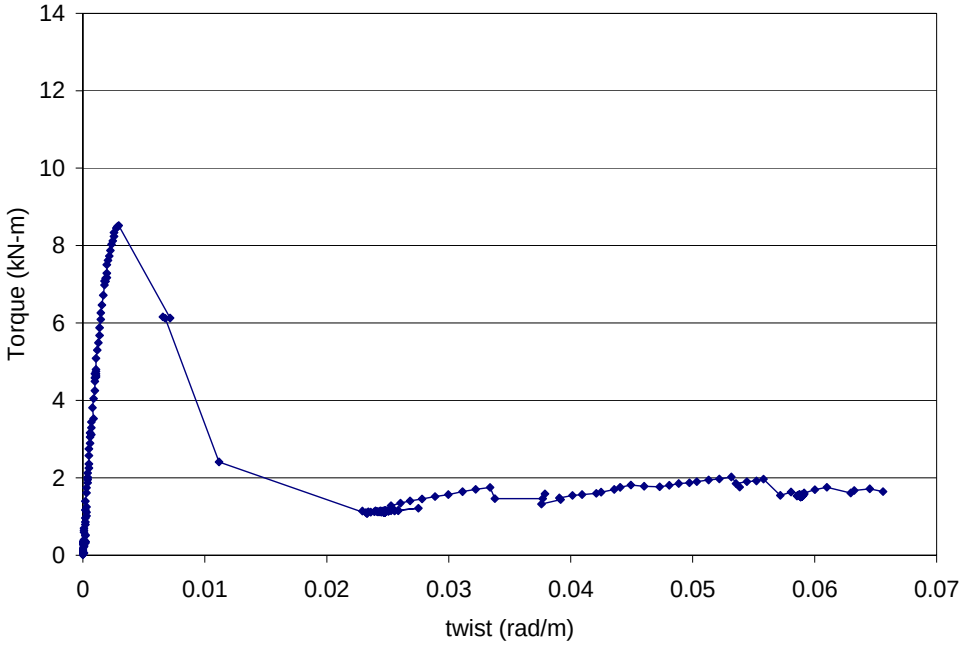

Figure 6.2: Torque-twist history for 210-C

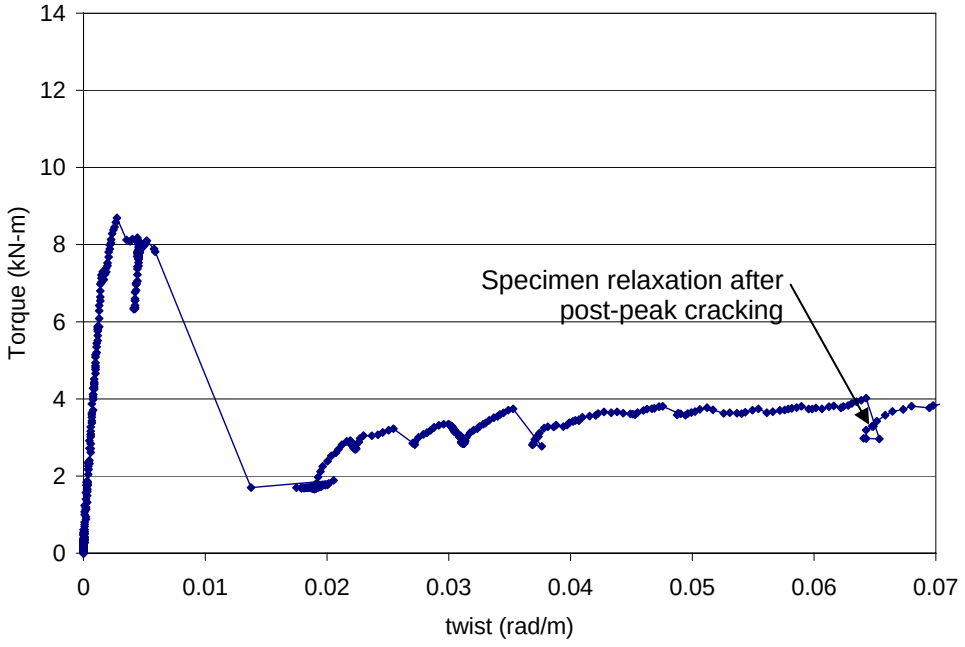

Figure 6.3: Torque-twist history for 210-C-2

6.1.1.2 Specimen 210-C-2

Similar to the 210-C specimen, initial longitudinal cracking was observed at the tip end prior to testing (Figure 6.4 e)). The cracking was most likely caused by the prestressing loads and either lack of helical reinforcing and/or segregation of the concrete. Zero readings were taken as 0.0006 V for the load cell, and 0.2765 V for the clinometer. Torsional cracking was initiated from the butt clamp, similar to the 210-C specimen. The cracking torque was determined to be 7.3 kN-m at a twist of 0.0016 rad/m. The calculated stiffness was therefore 4647.77 kN-m^2/rad. Sudden brittle failure and major spalling was observed quickly once the cracking torque was exceeded. Ultimate torque was recorded as 8.7 kN-m at a twist of 0.0028 rad/m. The failure crack occurred 3.2 m from the tip and measured approximately 0.9 m in length. Cracks at the bottom of the pole were observed 0.2 m into the butt clamp. Spalling of the concrete occurred on the top surface and on the loading side of the pole. After the ultimate load was achieved the pole sustained approximately 3.5 kN-m until excessive cracks widening and spalling caused the pole to fall to the ground. The measured wall thickness at failure was 62 mm with a 24 mm cover to the prestressing strands.

6.1.1.3 Specimen 210-D

Testing of the 210-D specimen began using the load cell calibration shown in Figure 5.4. Zero readings were taken as 0.0006 V for the load cell, and 0.2594 V for the clinometer. The maximum torque that could be recorded using the initial load cell calibration was 12.5 kN-m. During testing, the first signs of cracking were observed at the butt clamp once the maximum recordable torque was applied. The cracking torque was therefore recorded as 12.5 kN-m at a twist value of 0.0030 rad/m giving a stiffness of 4243.44 kN-m^2/rad. Once the maximum recordable torque was reached, it was decided that the signal conditioner output would need reducing so the additional post-cracking torque could be recorded. The post-cracking behaviour was therefore recorded on the second day of testing, November 3, 2007, after the calibration had been completed. To maintain consistency between the two testing periods the twist voltage after the pre-cracking test was recorded and used as the zero reading for the post-cracking test. The twist voltage was recorded as 0.285 V, which corresponds to 0.427 degrees. Testing of the 210-D specimen was suspended at 1:45 PM on October 30. The specimen was left in the testing clamp and shored to prevent large deformations and stresses.

a) Initial cracking at butt

b) Torsional cracks at butt

c) Failure pattern (back side)

d) Failed section from above (at butt)

e) Longitudinal cracking at strand

Figure 6.4: a) – e) 210-C-2 test observation photos

a) Initial torsional cracking at butt

b) Torsional failure showing helical steel

c) Failed section (loading side)

d) Failed section (back side)

e) Failed section (from top)

Figure 6.5: a) – e) 210-D test observation photos

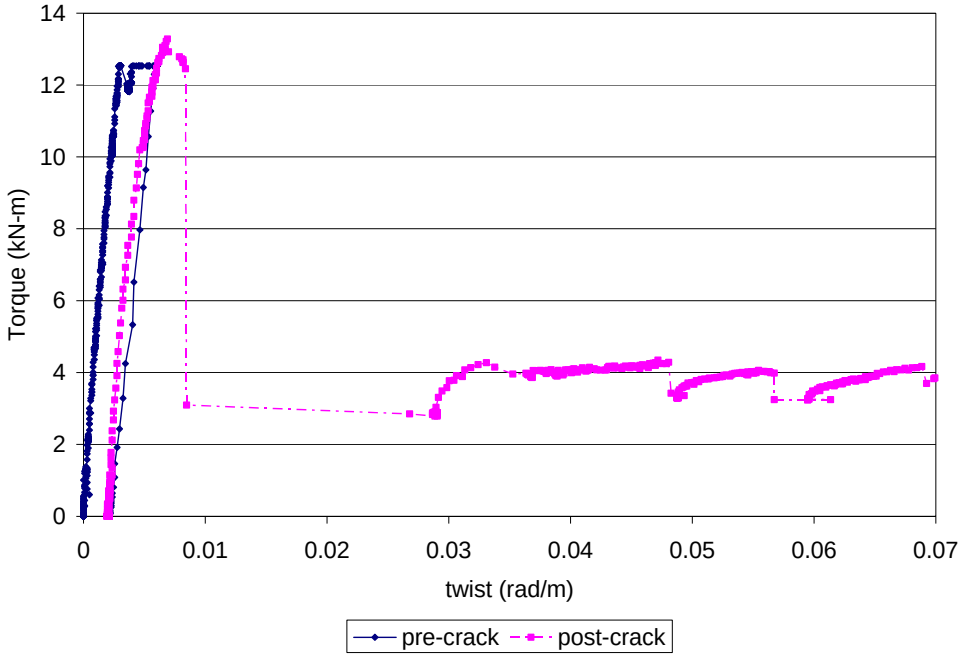

Figure 6.6: Torque-twist history for 210-D

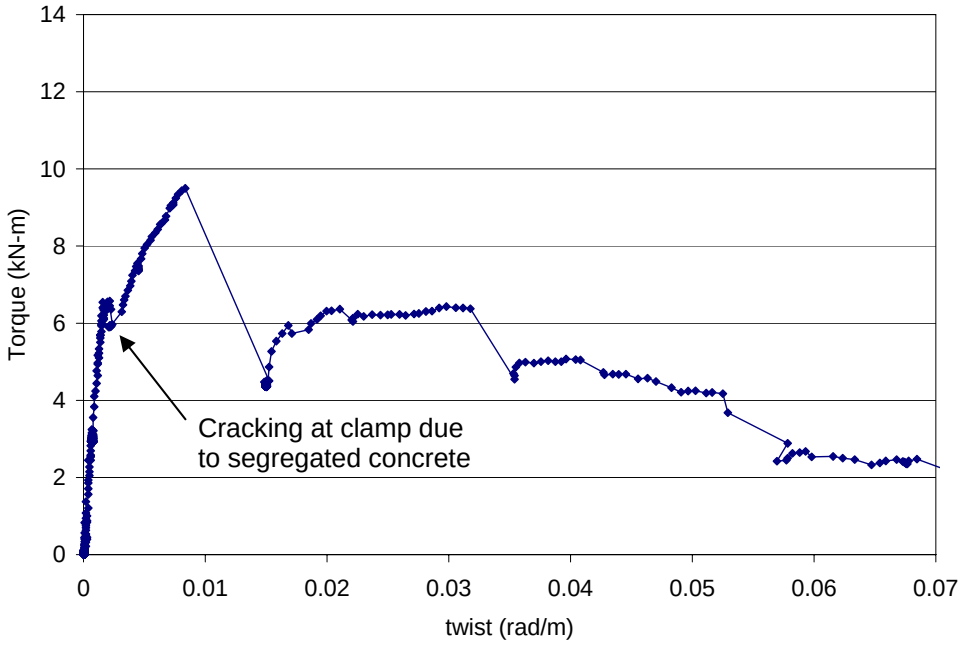

Figure 6.7: Torque-twist history for 210-CCW-L

Post-cracking testing for the 210-D specimen was continued on November 3 at 11:30 AM using the load cell calibration as shown in Figure 5.5. The excitation voltage for the load cell was recorded as 10.22 V. The calibration reading from the Sensotec device was 21.98 kN. The battery providing excitation to the AccuStar clinometer was outputting 12.75 V. Zero readings were taken as 0.0006 V for the load cell, and 0.2863 V for the clinometer.

Due to the pre-cracked nature of the specimen a reduced stiffness was observed once loading was continued. The post-cracking curve met the pre-cracking curve very closely indicating that post-cracking testing would give acceptable torsional results. As the applied load was increased the crack observed initially at the butt clamp continued to grow in size. Spalling, continued increase in crack width, and yielding and necking of the helically steel was observed as the ultimate torque of 13.3 kN-m was reached. The ultimate torque was found to occur at a twist of 0.0070 rad/m. Spalling occurred 0.8 m from the butt clamp, while the major crack causing failure was located at 3.3 m from the tip. After the peak torque the specimen sustained 4 kN-m as the twist angle continually increased. Spacing of the helical reinforcement in the failed portion was measured to be 100 mm. The measured wall thickness at failure was 63 mm with a 30 mm cover to the prestressing strands.

6.1.1.4 Specimen 210-CCW-L

The zero readings for the 210-CCW-L specimen were taken as 0.0006 V for the load cell, and 0.4889 V for the clinometer. Cracking at the butt of the pole was observed at 6.5 kN-m and a twist of 0.0016 rad/m, giving a stiffness value of 4164.9 kN-m^2/rad. Two cracks were observed at the butt of the pole. One crack was located at the clamp, whereas the second crack formed approximately 200 mm from the clamp. As the load was increased both cracks linked together, possibly due to additional longitudinal cracking down the prestressing strand.

Increasing cracks widths near the butt of the pole and spalling of the concrete to 0.3 m from the butt clamp (3.3 m from the tip) caused the failure of the specimen. Failure of the helical steel could also be heard (popping sound) at this time. The ultimate torque was recorded as 9.5 kN-m at 0.0084 rad/m. Examination of the specimen after failure indicated that the helical steel did not arrest the developing cracks. Instead, the cracks formed alongside the helical steel. Failure occurred when the longitudinal cracking linked the torsional cracks together and caused a single piece of helical steel to hold the load. Since the failure of the steel was heard at the same time as the specimen failed, it is likely that the steel could not maintain the torsional load.

a) Initial cracking at butt

b) Torsional/longitudinal cracking at strand

c) Crack pattern (back side)

d) Crack pattern (loading side)

e) Failure at butt (loading side)

f) Torsional cracks running along helical steel and failed helical piece

Figure 6.8: a) – f) 210-CCW-L test observation photos

After the ultimate torque was reached the specimen held 6 kN-m, 4 kN-m, and 2.5 kN-m as the condition of the pole degraded. The measured wall thickness at failure was 71 mm with a 26 mm cover to the prestressing strands. At the point of failure, a 20 mm thick cement paste was observed on the inside of the wall. The larger cement paste and segregation at the point of failure likely caused the early cracking observed during tested.

6.1.1.5 Specimen 210-CW-L

Zero readings were taken as 0.0006 V for the load cell, and 0.5695 V for the clinometer. Cracking was first observed for the 210-CW-L specimen at the butt clamp at a torque of 11.5 kN-m and a twist of 0.0029 rad/m giving a stiffness of 3894.70 kN-m^2/rad. Two cracks were noted at the butt, one close to the clamp and another along the same crack angle approximately 200 mm from the clamp. Following a decrease in torsional stiffness due to cracking, the ultimate torsional capacity was reached at 12.9 kN-m. The twist at ultimate torque was recorded as 0.0063 rad/m. Failure was caused by the second crack from the butt clamp crossing over a single helix of reinforcement (confirmed spacing 170 mm; Figure 6.9 d)). The subsequent necking and failure of the steel reinforcement caused large spalling of the concrete on the top and loading side of the pole. Due to the loss of concrete on the top, the pole began bending upwards while maintaining approximately 4 kN-m of applied torque. The measured wall thickness at failure was 68 mm with a 23 mm cover to the prestressing strands. A 20 mm thick segregated cement paste was observed on the inner wall of the pole.

6.1.1.6 Specimen 210-CCW-N

The 210-CCW-N zero readings were taken as 0.0006 V for the load cell, and 0.3326 V for the clinometer. Cracking started at the butt at a torque of 7.1 kN-m and twist of 0.0013 rad/m. The stiffness of the specimen was therefore 5561.17 kN-m^2/rad. A second crack was noted approximately 300 mm away (towards the tip) from the first one, at a torque of 9.5 kN-m. The ultimate torque was recorded shortly after at 10.7 kN-m and 0.0041 rad/m. Failure of the specimen was caused by the fracture of a single piece of helical steel located 0.65 m from the clamp. The subsequent spalling on the loading side and cracking caused the pole to break and bend downwards prior to total loss of integrity. After the post-peak torque was achieved, the specimen sustained approximately 2.5 to 3 kN-m torque. Detailed inspection of the specimen confirmed the spacing of the helical steel to be 110 mm.

a) Initial cracking at butt

b) Failed section at butt (back side)

c) Failed section at butt (loading side)

d) Failed section and cracking crossing helical steel

e) Helical steel at failed section

f) Failed section (loading side)

Figure 6.9: a) – f) 210-CW-L test observation photos

a) Initial cracking at butt

b) Two sets of torsional cracks at butt

c) Failed section (back side)

d) Failed section (loading side)

e) Close up torsional cracks crossing failed helical steel

Figure 6.10: a) – e) 210-CCW-N test observation photos

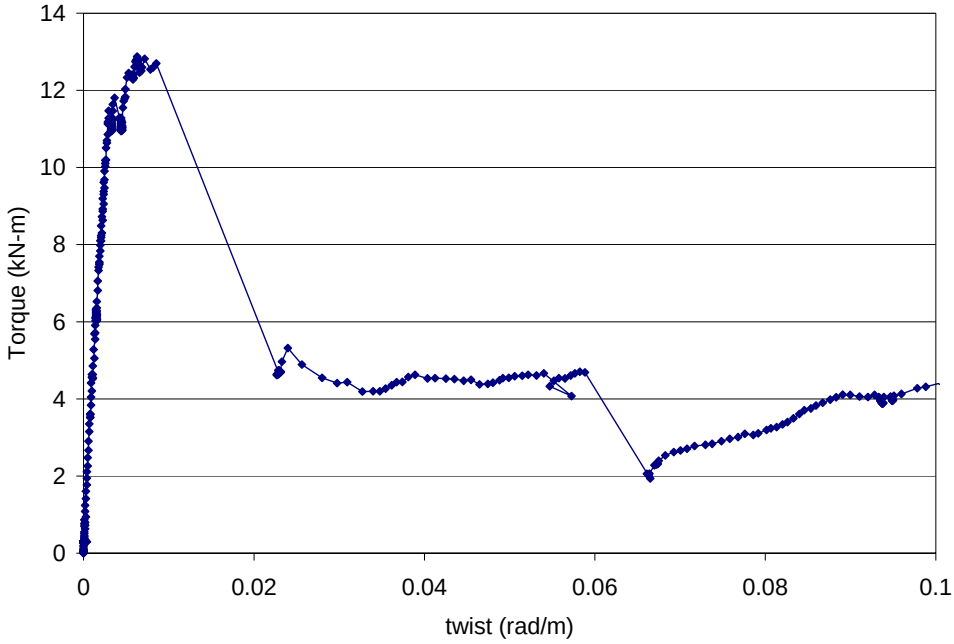

Figure 6.11: Torque-twist history for 210-CW-L

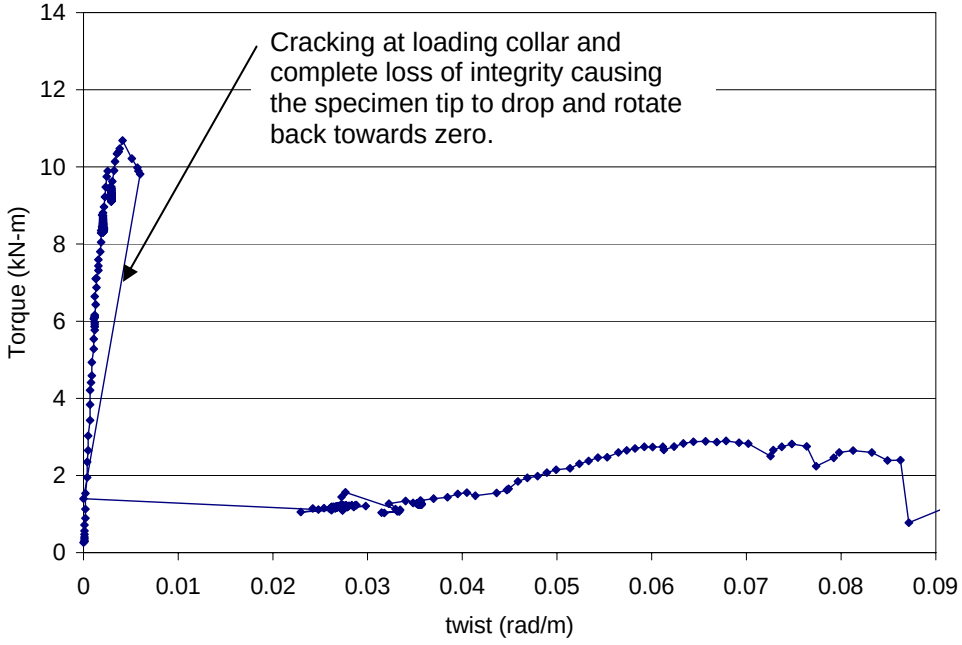

Figure 6.12: Torque-twist history for 210-CCW-N

The cracks propagated along the helical steel similar to the cracking observed for the 210-CCW-L specimen. Failure was caused when the crack crossed over the helical steel and opened large enough to cause the necking and failure of the steel (Figure 6.10 e)). The measured wall thickness at failure was 71 mm with a 24 mm cover to the prestressing strands.

6.1.1.7 Specimen 210-CW-N

For the 210-CW-N specimen zero readings were taken as 0.0018 V for the load cell, and 0.1068 V for the clinometer. Cracking was first observed at the butt of the pole with an applied torque of 9.8 kN-m and a twist value of 0.0024 rad/m. The stiffness value was calculated as 4123.63 rad/m. As the torsional load was increased sudden failure due to cracking and spalling occurred at the load collar (1.2 m from the tip). The ultimate torque recorded prior to the specimen failure was 12.9 kN-m at 0.0087 rad/m. Three pieces of helical steel were fractured between the loading collar and 300 mm from the collar. At the middle of the failure (300 mm from the loading collar) larger spacing between helical steel was noted. The typical spacing was to be 50 mm and the measured spacing in that location was closer to 100 mm (Figure 6.13 e)). This error was likely caused during production as the concrete was placed into the mould from the hopper. The helical reinforcing can get dragged if the labourers are not careful during pouring. The change in spacing may have caused the failure of the specimen to be at the loading collar instead of the at the clamp. The collar failure caused large torsional rotations of approximately 0.04 rad/m and a drop in torsional resistance to 1 kN-m. The initial crack at the butt of the pole increased in width as the load was increased. The crack at the butt was approximately 600 mm long at the time of failure. The measured wall thickness at failure was 55 mm with a 27 mm cover to the prestressing strands.

a) Initial cracking at butt

b) Loading collar failure (loading side)

c) Failed section at loading collar

d) Cracks at butt after failure at collar

e) Larger spaced helical steel
at collar failure location

Figure 6.13: a) – e) 210-CW-N test observation photos

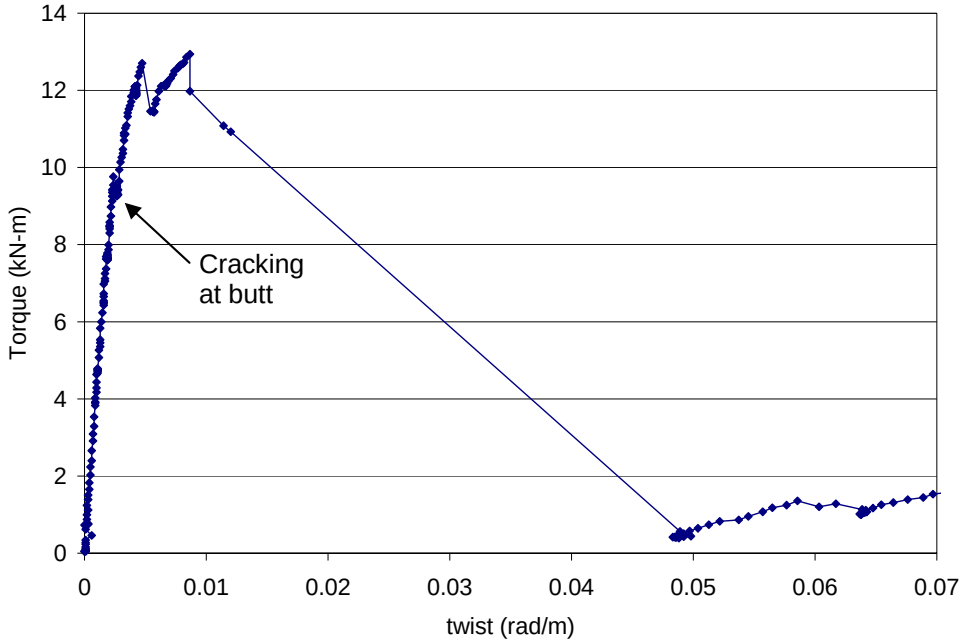

Figure 6.14: Torque-twist history for 210-CW-N

6.1.2 Test Observations for 165 mm Tip Specimens

6.1.2.1 Specimen 165-C

Prior to testing, longitudinal cracks were observed above the strands measuring approximately 0.6 m from the tip down (Figure 6.15 a) and f)). Strand slippage of 2 – 4 mm was also observed at the tip of the pole (Figure 6.15 e)). Widening of the longitudinal cracks could be seen as the loading collar was tightened and the testing began. Zero readings were taken as 0.0006 V for the load cell, and 0.3363 V for the clinometer. Torsional cracking was initiated from the longitudinal cracking at the loading collar location (0.6 m from tip). A sudden failure was observed which caused cracking and spalling of the concrete around the loading collar. The failed section extended from 0.6 m to 1.5 m from the tip. A cracking torque of 2.8 kN-m was recorded at a twist value of 0.0022 rad/m. The corresponding stiffness was calculated as 1281.71 kN-m^2/rad. Immediately after cracking the torque dropped to 2 kN-m and slipped to a twist value of 0.005 rad/m. Under post-cracking loading, the cracks continued down the pole above the strand locations. A post-cracking ultimate torque of 2.8 kN-m was achieved at a twist of 0.0088 rad/m. The measured wall thickness at failure was 48 mm with a 21 mm cover to the prestressing strands.

a) Longitudinal transfer crack along strand

b) Torsional cracking prior to failure

c) Cracking pattern (back side)

d) Cracking Pattern (front side)

e) Strand slippage and longitudinal cracking

f) Longitudinal strand cracks post failure

Figure 6.15: a) – f) 165-C test observation photos

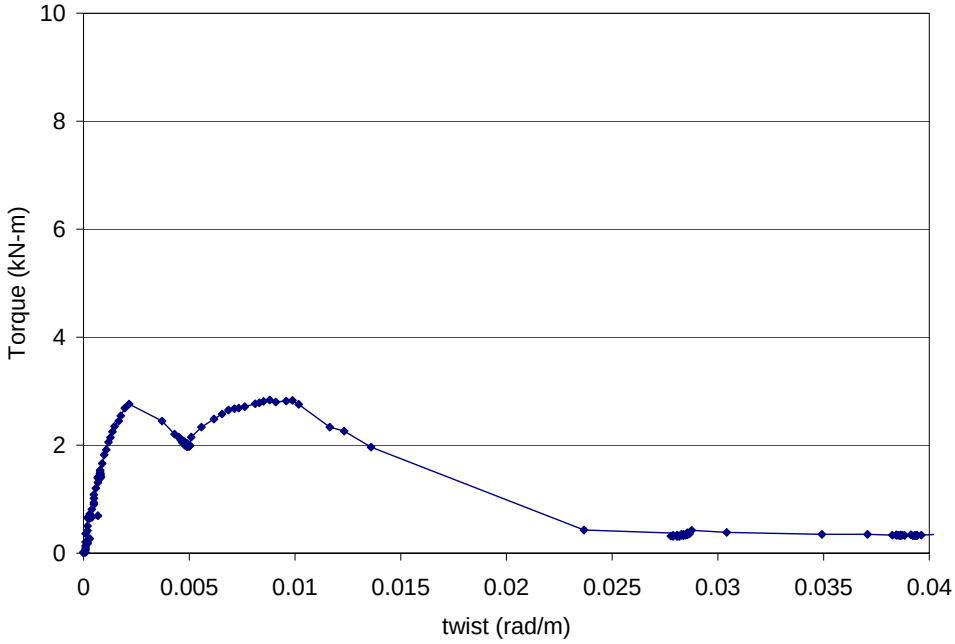

Figure 6.16: Torque-twist history for 165-C

6.1.2.2 Specimen 165-C-2

Strand slippage of about 2 – 4 mm was noted at the tip end of the pole prior to testing. Zero readings were taken as 0.0006 V for the load cell, and 0.2826 V for the clinometer. During testing of the specimen, the loading collar slipped as the applied torque reached 2.6 kN-m and 0.0011 rad/m. Retightening of the collar was performed with the load removed from the specimen. A slight increase in the crack width was observed after retightening of the collar (Figure 6.17 a) and b)). As the torque was reapplied to the specimen, the same stiffness was observed and permanent twist was recorded due to the collar not being reset perfectly (Figure 6.18). An edited torque-twist plot zeroed to remove the collar slippage was created (Figure 6.19). The results indicate the specimen reached a cracking torque of 2.6 kN-m at a twist value of 0.0011 rad/m as determined prior to the collar slippage. The corresponding stiffness was calculated as 2363.96 kN-m^2/rad. Failure was observed to extend 0.5 m from the loading collar. Immediately after cracking, the torque dropped continuously indicating failure of the specimen was occurring. Ultimately failure of the entire tip portion of the specimen occurred ending the testing (Figure 6.17 f)). The measured wall thickness at failure was 52 mm with a 24 mm cover to the prestressing strands.

a) Longitudinal transfer crack at collar

b) Longitudinal cracking along strand

c) Cracking pattern (front side)

d) Cracking Pattern (collar bottom)

e) Failure and cracking at collar

f) Ultimate failure of 165-C-2 specimen

Figure 6.17: a) – f) 165-C-2 test observation photos

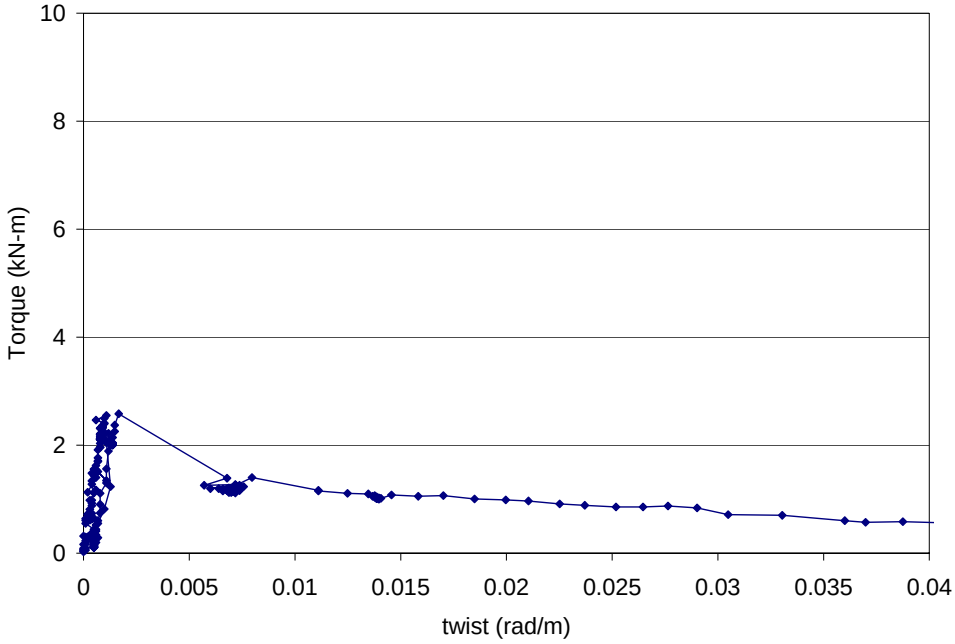

Figure 6.18: Torque-twist history for 165-C-2

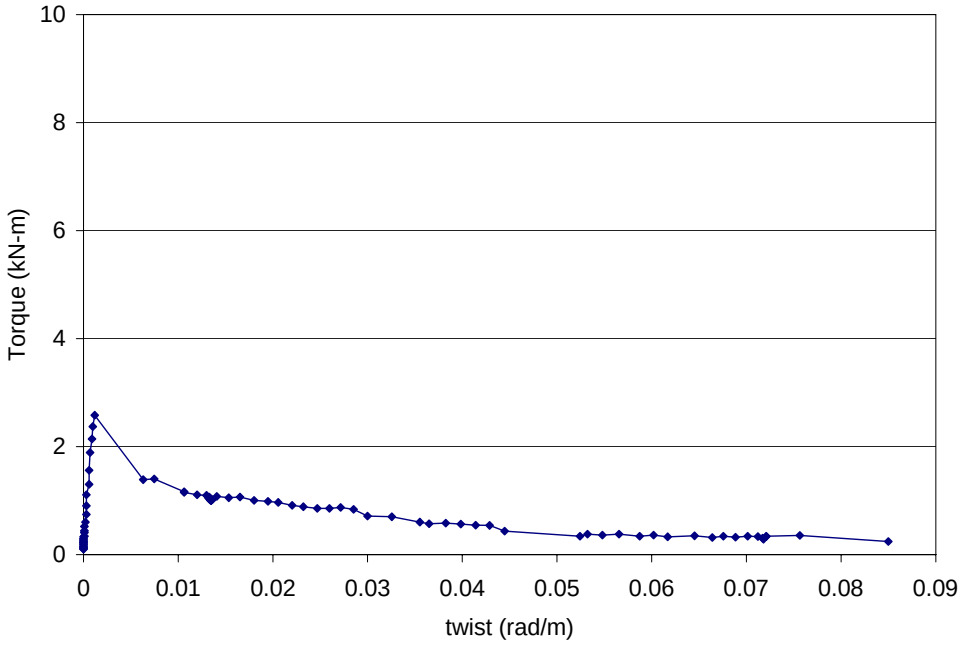

Figure 6.19: Specimen 165-C-2 load history without collar slip

6.1.2.3 Specimen 165-D

The 165-D specimen zero readings were initially taken as 0.0006 V for the load cell, and 0.2118 V for the clinometer. The loading collar slipped and was reset at 12:31 PM, and the new zero readings were recorded as 0.0006 V for the load cell and 0.2130 V for the clinometer. The first torsional cracks were observed at the butt of the pole with a torsional load of 6.5 kN-m at 0.0032 rad/m. The corresponding stiffness was calculated as 2123.09 kN-m^2/rad. The load was held constant and a slight drop to 6.25 kN-m was noted. As the torsional load was increased the loading collar slipped near 7.4 kN-m. The loading collar was reset and testing continues at 12:48 PM. The torque-twist curve during reloading showed an expected difference in stiffness and matched the previous curve at the point of loading collar slippage. Post-cracking loading caused the crack at the butt to grow in width and length (40 cm from the butt clamp), and new cracks to develop near the loading collar. The pole reached an ultimate cracking torque of 8.1 kN-m at a twist value of 0.0071 rad/m. Failure was caused by spalling and torsional cracks near the loading collar (0.9 m from the tip). The third spiral of the helical reinforcing (approximately 350 mm from the loading collar) showed signs of a necking failure and suggests that the post-cracking failure was ultimately caused by the failure of the reinforcing spiral. Spacing of the helical reinforcement was measured to be 120 mm. Immediately after the maximum torque was reached the pole failed suddenly. No additional torsional load was sustained and rotation dropped to zero as the tip of the pole fell down and rotated in a reverse direction due to the applied load. The measured wall thickness at failure was 50 mm with a 28 mm cover to the prestressing strands.

6.1.2.4 Specimen 165-CCW-L

Zero readings were taken as 0.0006 V for the load cell, and 0.2972 V for the clinometer. The first cracks were noted at the loading collar. The cracking torque was recorded as 5.9 kN-m at a twist value of 0.0032 rad/m. The stiffness was calculated as 1876.12 kN-m^2/rad. Following cracking at the collar the pole quickly lost all torsional strength due to cracking and sudden concrete spalling. Large twist deformation was observed and the pole ultimately fell to the ground. Examination of the failure section indicated that the second and third helical spirals from the loading collar had failed. The spacing of the spirals was confirmed to be 120-140 mm. The total length of the failure section was roughly 0.6 m. The measured wall thickness at failure was 49 mm with a 24 mm cover to the prestressing strands. 15 mm of segregated cement paste was measured on the inner surface of the wall.

a) Initial cracking at butt

b) Cracking at loading collar (loading side)

c) Cracking at collar (back side)

d) Failure at collar (back side)

e) Failure at collar (loading side)

f) Double helix and confined concrete

Figure 6.20: a) – f) 165-D test observation photos

a) Cracking at collar (loading side)

b) Cracking at collar (back side)

c) Failure at collar (back side)

d) Failed collar section

e) Failure at collar (loading side)

Figure 6.21: a) – e) 165-CCW-L test observation photos

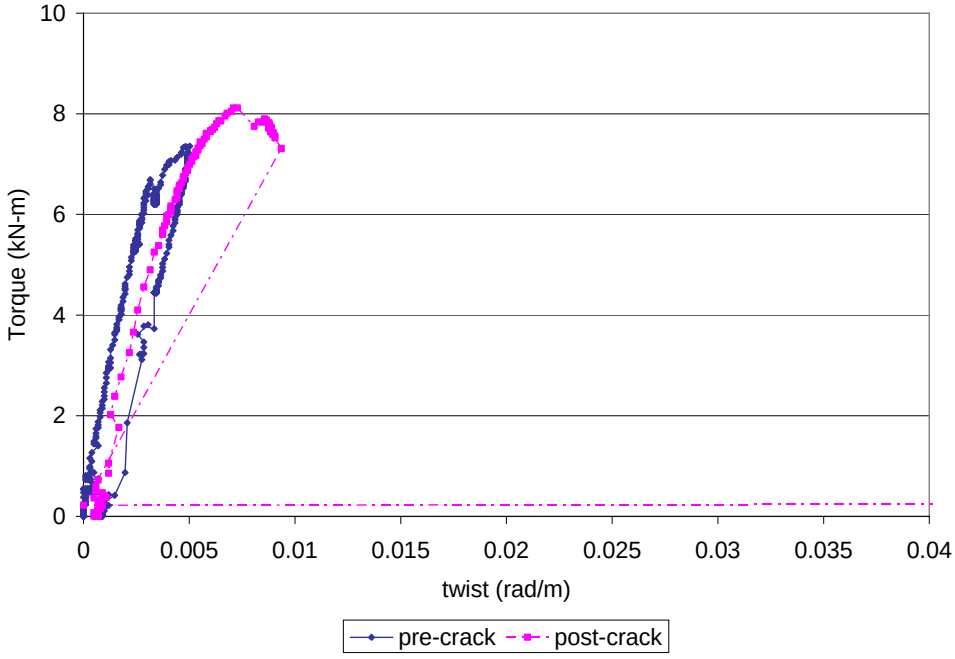

Figure 6.22: Torque-twist history for 165-D

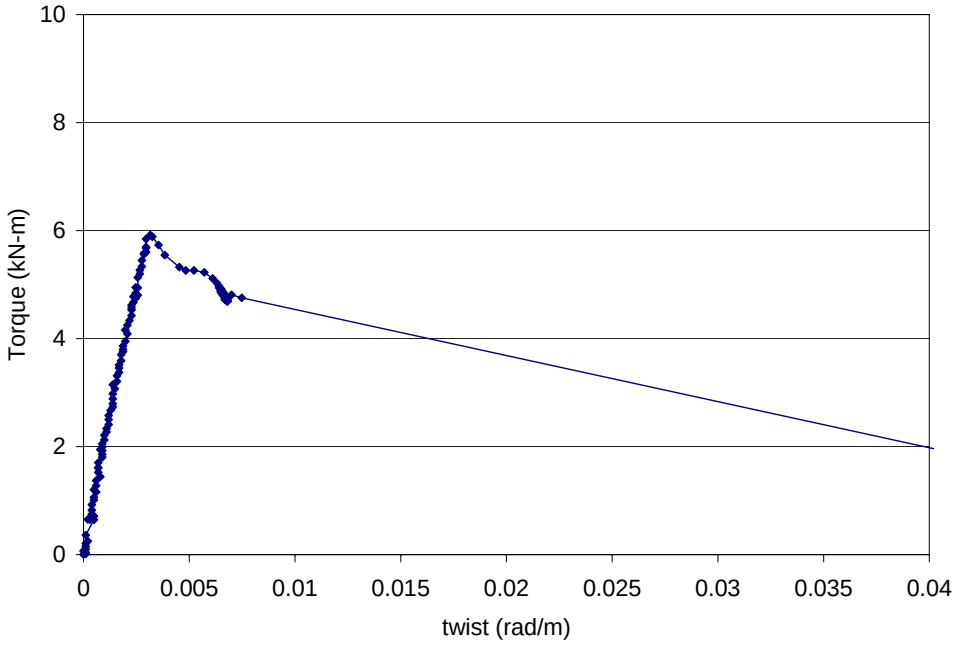

Figure 6.23: Torque-twist history for 165-CCW-L

6.1.2.5 Specimen 165-CW-L

The 165-CW-L specimen zero readings were taken as 0.0006 V for the load cell, and 0.4730 V for the clinometer. A crack appeared during tightening of the loading collar. Torsional cracking was first noted near the butt clamp at a torque of 6.1 kN-m and 0.0032 rad/m twist. The pole held 6.4 kN-m post cracking but ultimately cracking and spalling at the clamp caused the pole to fail and fall to the ground. Failure was measured to be at 3.21 m from the tip and 40 cm from the clamp end. The total length of the failed section was 70 cm. Spalling of the concrete and large torsional cracks on both sides of the pole were observed. The measured wall thickness at failure was 53 mm with a 30 mm cover to the prestressing strands. 15 mm of cement paste was measured on the inner surface of the wall.

6.1.2.6 Specimen 165-CW-N

Zero readings were taken as 0.0128 V for the load cell, and 0.3717 V for the clinometer. The testing was restarted at 1:53 PM due to a loose cable on the back of the signal conditioner with the same zero readings. Initially cracking occurred near the clamp at an applied torque of 8.5 kN-m and 0.0041 rad/m of twist.

Following cracking the torque held dropped slightly to 8 kN-m. Loading collar slippage occurred at 1:58 PM when the applied torque was near 9 kN-m. Prior to collar slippage, the crack was growing near the butt clamp. The specimen was unloaded and the collar was reset. Zero readings were recorded again as 0.0006 V for the load cell and 0.3815 V for the clinometer. The testing continued at 2:04 PM. The reloading path exhibited the same stiffness as the unloading path and matched the pre-cracking curve.

Ultimate torque was reached and failure occurred soon after reaching the previous slippage torque. The ultimate torque was measured as 8.9 kN-m at 0.0073 rad/m of twist. Failure occurred at the butt clamp and measured approximately 0.9 m from the butt end. The first and second helical spirals from the clamp end were showed necking failures. The spacing of the spirals was confirmed as 90 mm in the failure section. Spalling and large twist deformations were observed and indicated the specimen could hold no more torque. The measured wall thickness at failure was 56 mm with a 25 mm cover to the prestressing strands. 15 mm of cement paste was measured on the inner surface of the wall.

a) Crack due to tightening of collar

b) Initial cracking at butt

c) Crack pattern (loading side)

d) Failure crack on back side

e) Failure (loading side)

f) Crack across fail piece of helical steel

Figure 6.24: a) – f) 165-CW-L test observation photos

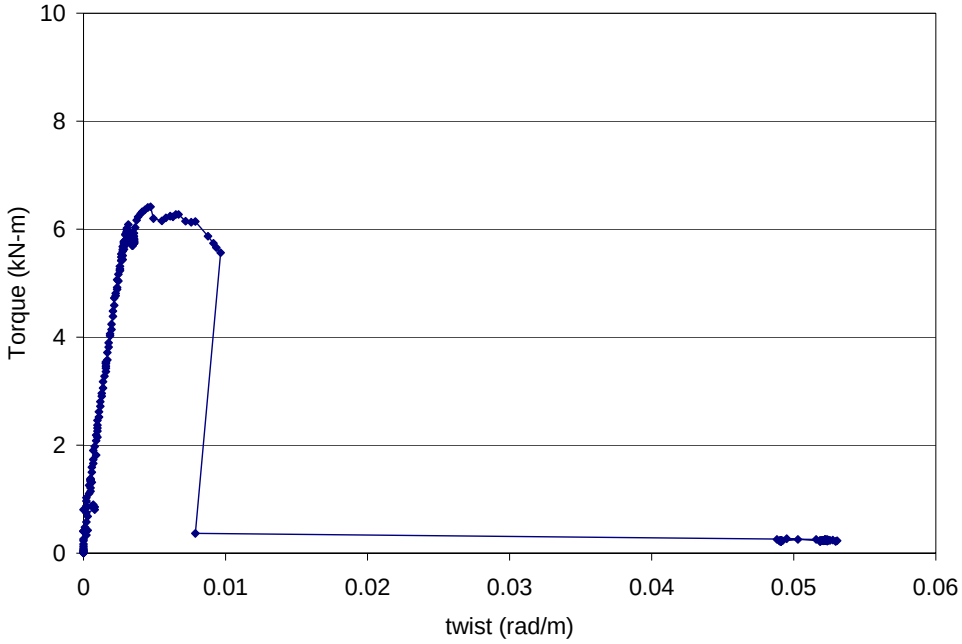

Figure 6.25: Torque-twist history for 165-CW-L

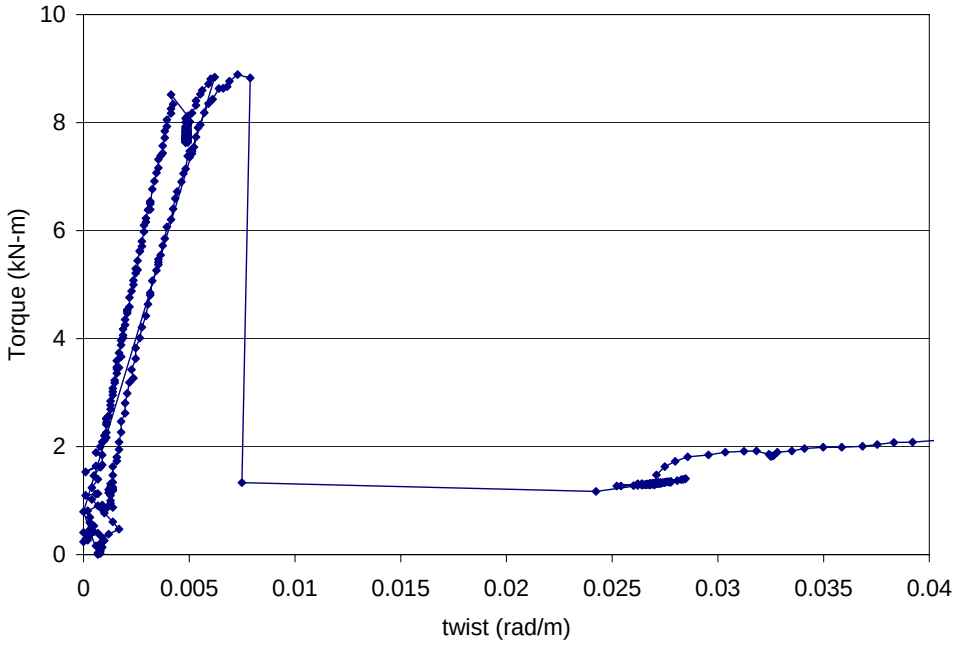

Figure 6.26: Torque-twist history for 165-CW-N

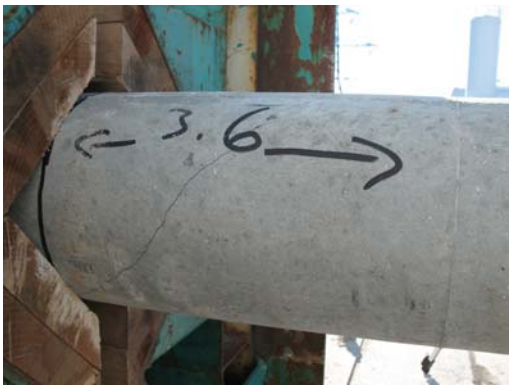

a) Initial crack at butt

b) Failure at butt (loading side)

c) Failure at butt (back side). Note crack crossing failed helical steel

d) Failed section at butt (from bottom)

c) Failed section after removal

Figure 6.27: a) – d) 165-CW-N test observation photos

6.1.2.7 Specimen 165-CCW-N

Zero readings were taken as 0.0006 V for the load cell, and 0.3033 V for the clinometer. First signs of cracking near the loading collar were noted at an applied torque of 7.5 kN-m and 0.0036 rad/m of twist. A decrease in torque resistance to 6.75 kN-m was observed as the load was held constant on the specimen. As the specimen was reloaded, spalling of the concrete in the loading collar area was noted and popping sounds from failure of the helical steel could be heard. Ultimate failure of the specimen was recorded at 7.5 kN-m and 0.0067 rad/m of twist. The total length of the failed section was 0.45 m from the loading collar. Examination of the failure section indicated that the cracks were inline with the helical steel (Figure 6.29 d)). This indicates that the steel was not providing any resistance to the opening of the cracks. The torsional cracks crossed through only the second spiral from the loading collar (25 cm from the collar) and caused the steel to fracture and the subsequent failure of the specimen. Spacing of the helical steel was confirmed as 100-110 mm. The measured wall thickness at failure was 50 mm with a 26 mm cover to the prestressing strands. 10 mm of cement paste was measured on the inner surface of the wall.

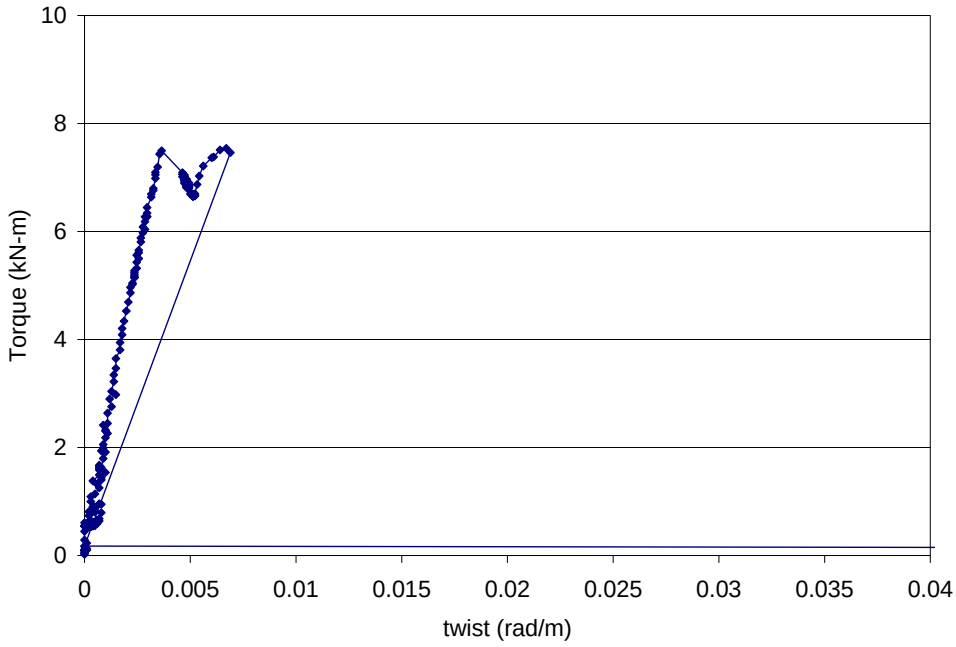

Figure 6.28: Torque-twist history for 165-CCW-N

a) Torsional cracking at collar

b) Failure at collar (loading side)

c) Failed section (loading side)

d) Cracking along helical steel

Figure 6.29: a) – d) 165-CCW-N test observation photos

Chapter 7
Analysis of Experimental Results

7.1 General Experimental Results

This chapter contains the analysis of the results, which are used to determine the influence that helical reinforcing spacing, direction, wall thickness, and other factors have on the cracking torque of prestressed concrete poles. The results are also compared to two torsion models (presented in section 2.6) and analyzed to determine how well the models can predict the experimental results. Cracking torque formulae are presented and compared to the experimental data to establish whether the torsion capacity of concrete poles can be accurately calculated. The variation in the experimental results is analyzed and the potential causes for the variations discussed. Finally, strut and tie models are used to determine the required spacing of the helical reinforcing in the prestressing transfer zone and minimum transverse reinforcement requirements from the concrete codes and literature will be discussed.

The data collected during the testing allowed the entire torque-twist history of each pole to be plotted (Figure 7.1 and Figure 7.2). All experimental data figures present the torque and twist response of the pole specimens at 0.6 m from the tip. The torque is given in kN-m and the twist in rad/m. The twist angle measured was divided by the length of each specimen to account for slight variations in the tested length of the specimens. All CCW labelled specimens were tested in the counter clockwise direction indicating that the helical steel was theoretically ineffective (see Section 4.2). The CW specimens were tested in the clockwise direction and had effective helical steel.

In general, the larger 210 mm specimens sustained an additional amount of torque after cracking. The post-cracking additional load was in the range of 0.3 kN-m for the 165 mm tip poles and 2.4 kN-m for the 210 mm tip poles. Failure in all cases was sudden and coincided with substantial rotation. The load sustained after maximum torque had been achieved was less than half of the maximum torque. The lower results of the CCW-L specimens may have been skewed due to the higher air content and lower concrete strengths.

Figure 7.1 displays the 165 mm specimens. It should be noted that since all except for two of the failures (165-CW-N and 165-CW-L) occurred at the loading collar. The torque-twist curves all

typically have a sudden drop off where the rotation ends up going to zero. This behaviour is caused by the concrete in the pole failing at the collar and the strands pulling the remaining concrete at the tip back into alignment with the rest of the pole. The 210 mm specimens (Figure 7.2) all failed at the clamp except for one specimen (210-CCW-N) and therefore they typically exhibit a load path of increasing rotation while holding a fraction of the maximum torque.

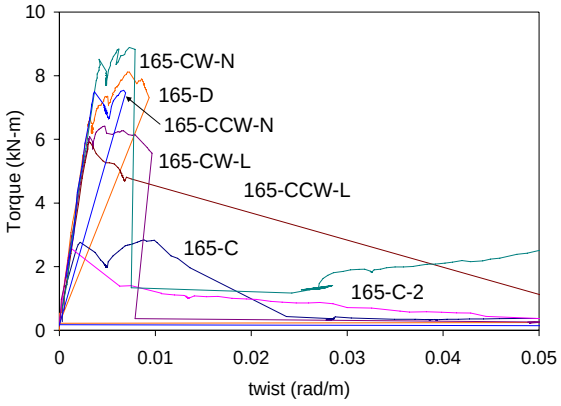

Figure 7.1: Torque-twist history of 165 specimens

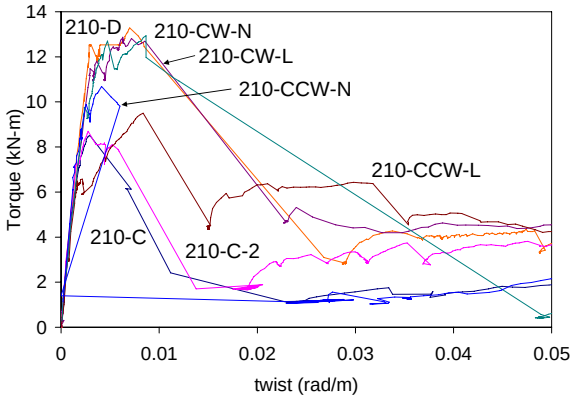

Figure 7.2: Torque-twist history of 210 specimens

7.2 Graphical Experimental Results Comparison

7.2.1 Cracking Torque Comparison

The plots of the 165 and 210 mm specimens were truncated at the cracking point for each specimen and plotted to a twist of 0.01 rad/m to allow for better analysis of the elastic region and the post-cracking behaviour of each pole (Figure 7.3 and Figure 7.4). The differences in cracking torque between specimens were unexpected since cracking torque is typically thought to be related to the area of concrete present and not to the reinforcement. The control (un-reinforced) specimens cracked earlier than the reinforced specimens. Generally the results indicate that the helical reinforcing is required to ensure pre-cracking and early failure does not occur. However the helical steel seemed to delay the cracking torque in some situations. From the observations during testing it was noticed that at nearly the same time as cracking of the concrete and ultimate failure, the pole specimen made popping sounds which were thought to be the helical steel yielding and ultimately rupturing. The helical steel may impact the cracking torque values by confining the concrete core or by intercepting micro cracking occurring prior to failure.

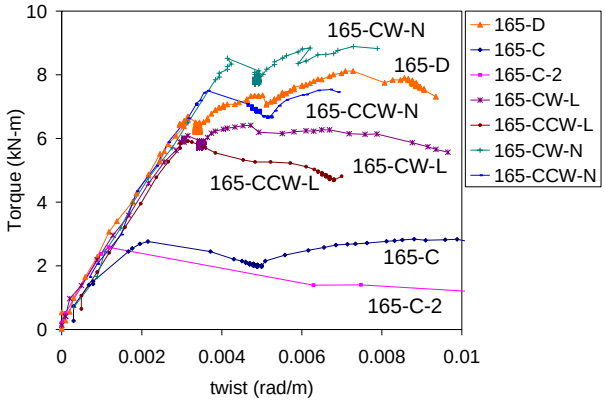

Figure 7.3: Torque-twist response of 165 mm specimens

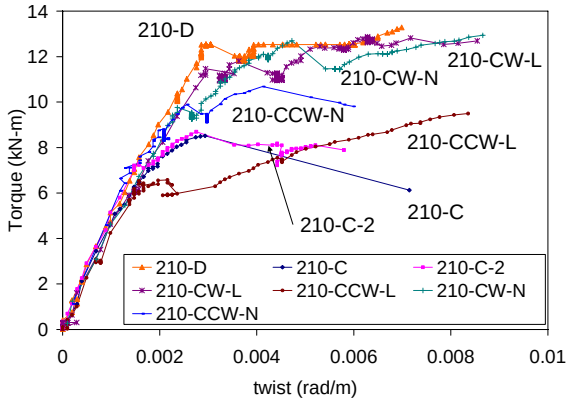

Figure 7.4: Torque-twist response of 210 mm Specimens

7.2.2 Influence of Diameter and Wall Thickness on Torsional Capacity

Differences in torsional cracking strength were found between the 165 mm and 210 mm tip specimens (Figure 7.5). As expected, the larger 210 mm tip specimens had larger cracking torques than the smaller 165 mm tips. The increase in cracking strength is due to the increase in concrete volume from the larger diameter and wall thickness of the 210 mm specimens. The double helix specimens (-D) were found to be stronger than the control specimens.

It was also determined that the 165-D specimen cracking and ultimate strength was close to that of the 210 mm control specimens (210-C and 210-C-2). If the difference in maximum torque between 210 mm control specimens and 210-D is compared to the difference in maximum torque between the 165 mm control specimens and 165-D, it can be concluded that the 165 mm control poles are relatively weaker. Longitudinal cracking in the control specimens and strand slippage leading to reduced prestressing stress in the concrete could account for the lower torsional capacities for the control specimens.

7.2.3 Stiffness Difference between 165 and 210 Specimens

The elastic stiffness of the specimens increased for the 210 mm specimens as compared to the 165 mm specimens. A larger volume of concrete contributed to a stiffer pole (Table 7-1). Increasing the tip diameter and the wall thickness to the larger 210 mm specimens increased the stiffness by 217%, or approximately 2400 kN-m^2/rad (from 2068 kN-m^2/rad to 4483 kN-m^2/rad).

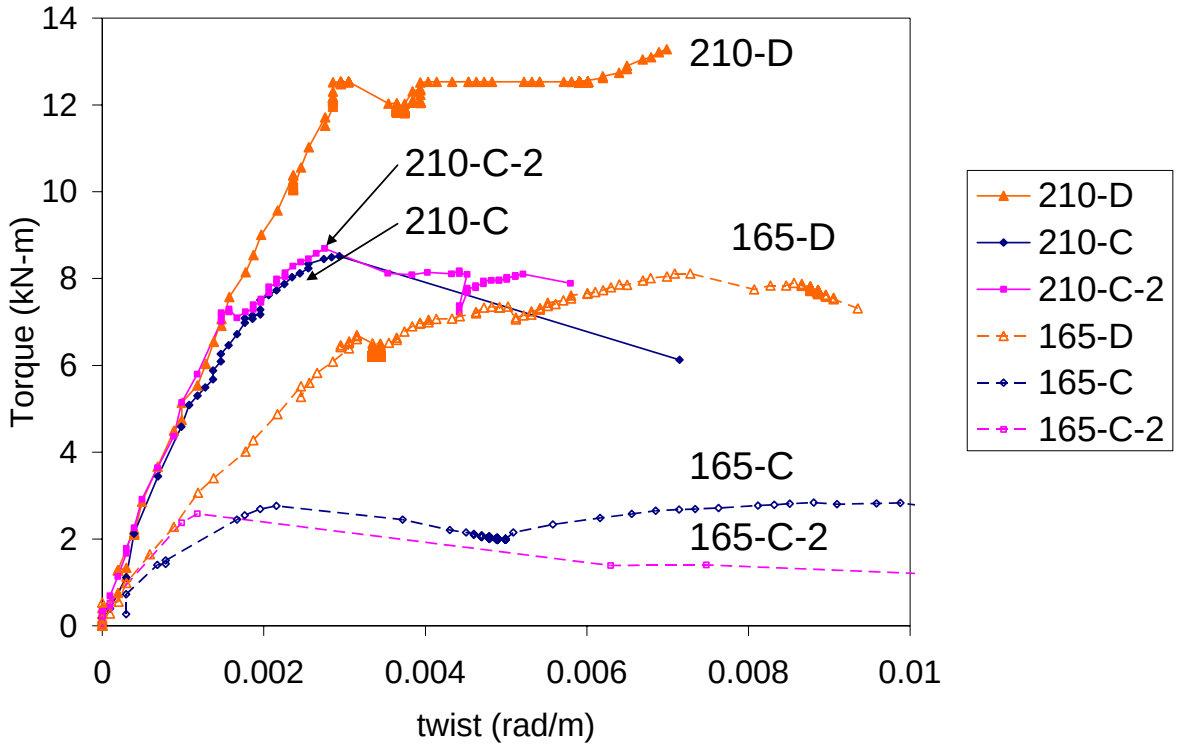

Figure 7.5: 210 vs. 165 mm tip cracking torques

Figure 7.6 illustrates the difference in stiffness between all specimens. The dashed lines are the 165 mm specimens whereas the solid lines are the 210 mm specimens. The figure shows that the 210 mm specimens demonstrated consistent elastic stiffness values. The 165 mm specimens exhibit similar consistent elastic stiffness values except for the pre-cracked 165-C specimen. The pre-cracked 165-C specimen had a significantly lower elastic stiffness value than the other 165 specimens at 1282 kN-m^2/rad.

Table 7-1: Comparison of average stiffness for 165 and 2 10 specimens

Pole Group	Average Stiffness (kN-m^2/rad)
165*	2068
210	4483
* = average stiffness excluding 165-C	

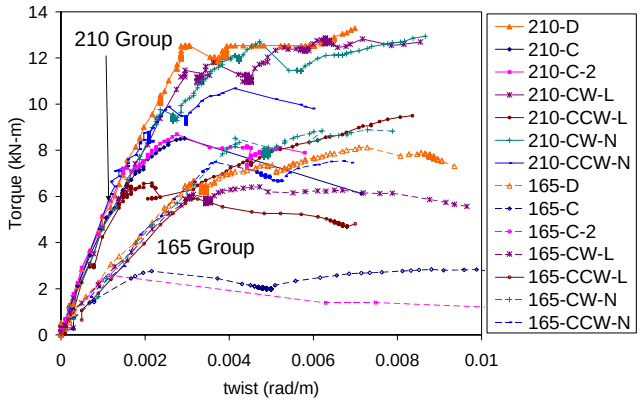

Figure 7.6: Torque-twist curves for all specimens

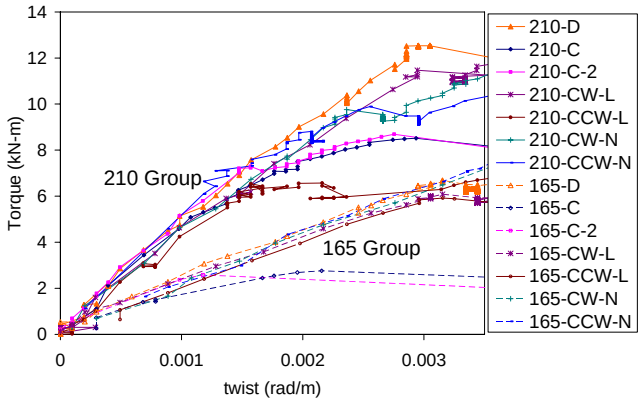

Figure 7.7: Linear portion of specimen results

The analysis of the linear portion of the curves is shown in Figure 7.7. While the 165 mm specimens remain fairly close and within a consistent band until failure, the 210 mm specimen behaviour shows a point where the stiffness diverges for the specimens. The torque at which this divergence in the 210 mm specimens occurs is around 5 kN-m. If the divergence point represents the point where the 210 mm specimens cracked and became non-linear than the predicted value of 12.9 kN-m from the CSA A23.3-04 (2004) T_{cr} equation (Equation 2-8) is unconservative and suggests the cracking torque equation may need to be revisited for application with concrete poles. The stiffness and torsional response differences due to the pre-cracked 165-C and 165-C-2 control specimens are clearly seen in Figure 7.7.

Linear elastic torsional responses for the 210 and 165 diameter tips were modelled and compared to the test results (Figure 7.8). The linear elastic responses were calculated using the design values (concrete strength of 60 MPa, design wall thickness, etc…) and the following mechanics formulae common to all codes:

$$T = \frac{J}{c}\tau\sqrt{1+\frac{f_{pc}}{\tau}} \tag{7-1}$$

$$\phi = \frac{TL}{JG} \tag{7-2}$$

where T is the applied torque (kN-m), c is the outside radius of the pole (m), L is the length of the pole (m), G is the shear modulus of concrete in MPa (taken as $G = 0.5E_c$), and J is the polar moment of inertia calculated as $J = \frac{1}{2}\pi\left(c_2^{\,4} - c_1^{\,4}\right)$, where c_2 is the radius to the outside of the cross section and c_1 is the radius of the inner hole of the pole. E_c is taken as $4500\sqrt{f_c'}$ (CSA A23.3-04 Clause 8.6.2.3) and τ is the shear stress on the section. The biaxial stress added due to prestressing is included using the factor described in section 2.4.1, where f_{pc} is the stress in the concrete section due to the prestressing force.

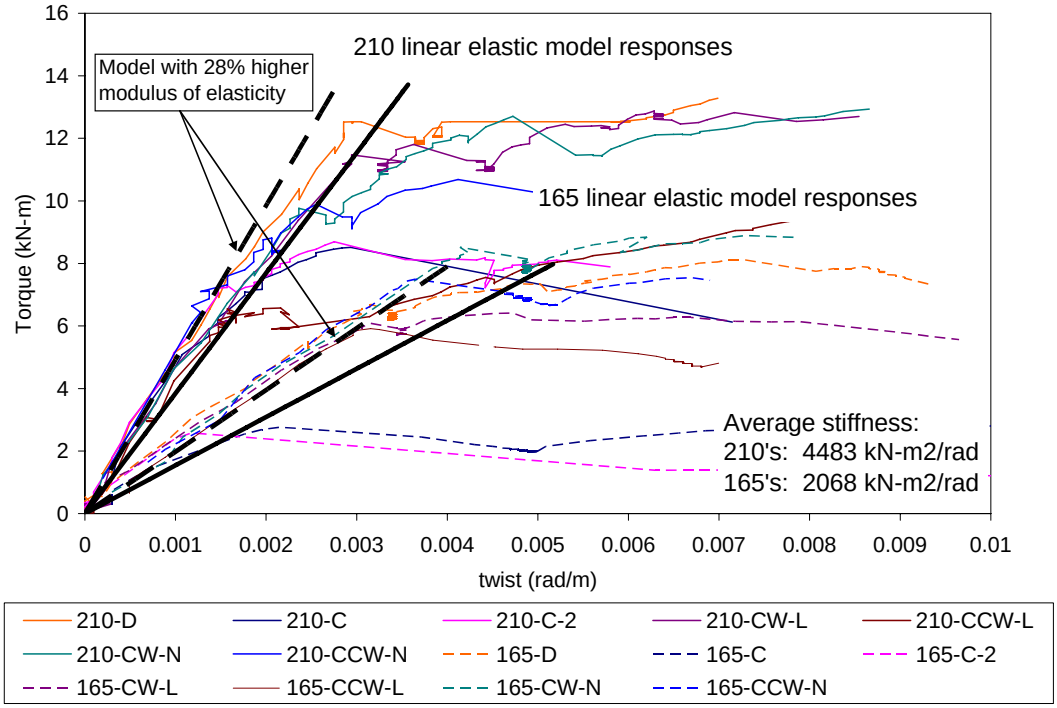

Figure 7.8: Linear elastic torsional predicted response compared to test results

The linear elastic response approximates the 210 test specimen results very well and is also below the test results indicating a conservative prediction. The linear elastic theory does not predict the 165 mm test specimens as well but still provides a conservative prediction. The 165 mm specimen test results indicate that the smaller tip poles were stiffer than elastic theory predicts. The variation in predicted results versus the test results can be explained by the assumed shear modulus value (relating to E_c) and differences in the wall thickness (Terrasi and Lees, 2003). Spun cast concrete poles can

have a modulus of elasticity 28 percent higher than regular concrete (Fouad et al., 1994). Increasing the assumed E_c coefficient to 5760 from 4500 (28 % higher) brings the predictions even closer to the test results for both the 165 and 210 mm tip specimens. The apparent linear response of prestressed concrete poles indicates that the specimens likely fail due to cracking torque (concrete failure) under torsional loading and the helical steel is likely insignificant.

7.2.4 Helical Reinforcing Direction

Prior to testing, it was assumed that helical reinforcing direction would have a large impact on the torsional capacity of the pole. For the larger spaced specimens, the specimen with the helical steel not engaged (CCW-L) should have similar behaviour as the control specimens. The opposite direction specimen (-CW-L) where the steel is engaged, would have increased capacity. Since the single helix normal spacing (-N) specimens are allowed by CSA-A14-07, the theory was that both the counter clockwise and clockwise specimens (-CW-N and –CCW-N) would behave similar to each other due to the tighter spacing of the spirals and their increased ability to intercept torsional cracks.

Analyzing the influence of helical reinforcing direction on the torque capacity of the 165 mm poles yielded inconclusive results. While both methods of reinforcing (-CW and –CCW) increased the torque capacity when compared to the control specimens, very little difference was observed between the two methods (Figure 7.9, Figure 7.10, and Figure 7.13). The same can be said for the larger 210 mm specimens (Figure 7.11, Figure 7.12, and Figure 7.14). The 210-CW-N specimen actually cracked earlier than the 210-CW-L specimen but ultimately achieved the same ultimate torque while the 210-CCW-L specimen cracked earlier than the 210-CCW-N specimen and reached the same ultimate torque as well. The early cracking of the 210-CCW-L specimen is explained further in 7.7.

Comparing Figure 7.9 and Figure 7.10 we can see some trends with the behaviour of the 165 mm poles after cracking in regards to direction of helix reinforcing. The CCW specimens show an immediate decrease after cracking indicating the helix reinforcing is not engaging and provide some additional post-cracking ductility. The 165-CCW-N specimen does exhibit some post-cracking ability to resist torque; however the added capacity is insignificant when compared to the cracking torque.

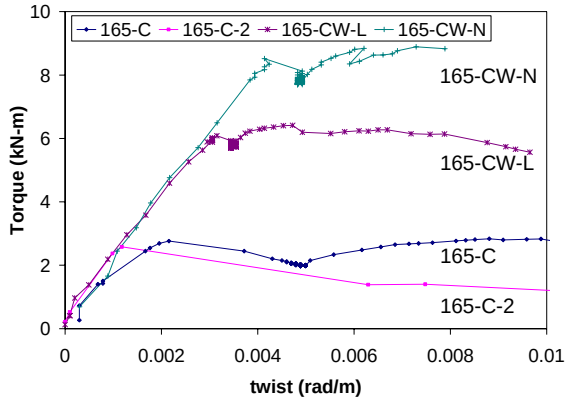

Figure 7.9: 165 mm clockwise reinforced specimens

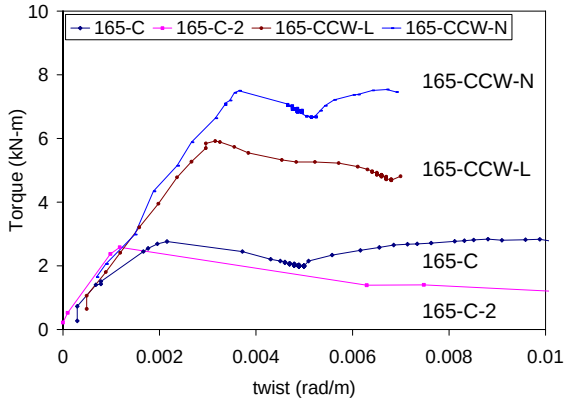

Figure 7.10: 165 mm counter clockwise reinforced specimens

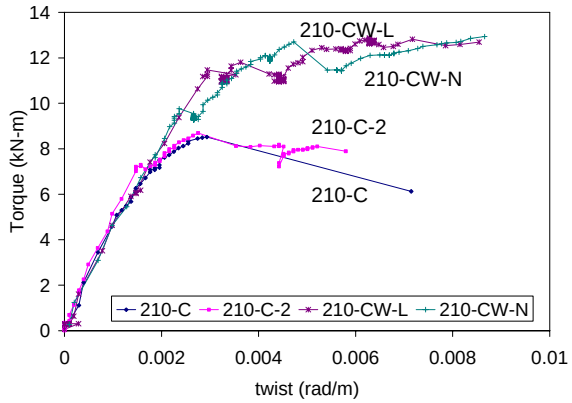

Figure 7.11: 210 mm clockwise reinforced specimens

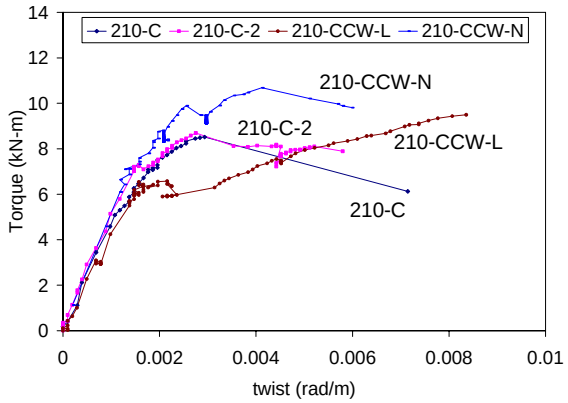

Figure 7.12: 210 mm counter clockwise reinforced specimens

The increase in torque capacity after cracking observed in the 165-CCW-N specimen can be explained by the tighter spacing of the helical reinforcing holding the concrete together and providing interlock between the cracked concrete pieces. The CW specimens on the other hand, show a slight increase after cracking or an ability to maintain the cracking torque with increasing twist. The observed decrease after cracking is not seen with the CW specimens. Analyzing Figure 7.13, it can be noted that the normal spaced specimens demonstrated a greater capacity than the larger spaced specimens. The 210 mm specimens do not show the behaviour seen in the 165 mm specimens. All the 210 specimens actually increase in capacity post cracking until the ultimate failure point is reached. The cracking torque values for both the large and normal spacing specimens, regardless of

the direction of the helix reinforcement, are close to each other and therefore it can be concluded that for the 165 mm tip specimens, the direction of the helix reinforcement has very little influence on the torsional capacity. Similarly for the 210 mm specimens, excluding the 210-CCW-L specimen which seems to have cracked early, it appears that direction of reinforcement also has very little influence on the torsional capacity of the pole.

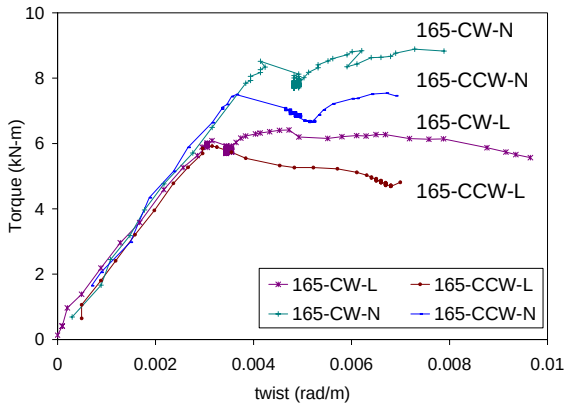

Figure 7.13: Comparison between 165 mm clockwise and counter clockwise specimens

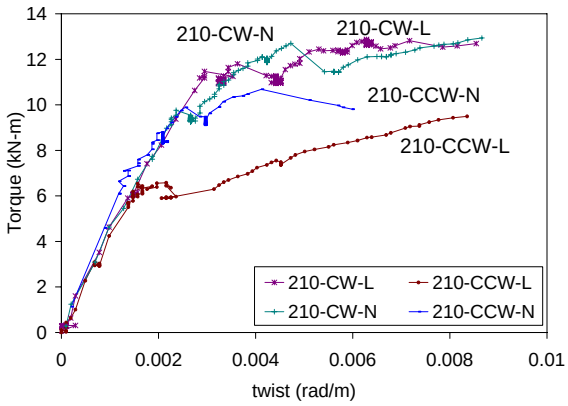

Figure 7.14: Comparison between 210 mm clockwise and counter clockwise specimens

7.2.5 Helical Reinforcing Spacing

The spacing of the helical reinforcement appears to have more of an influence on the cracking torque of the 165 mm specimens than the direction of the reinforcing. The 210 mm specimens, however, do not follow the same trend as the 165 mm specimens. Prior to testing, it was thought that the tighter spaced specimens (CW-N and CCW-N) would perform better than the larger spaced specimens (CW-L and CCW-L). It was also thought that the double helix specimen (-D) would perform similar to the CW-L specimens since the double helix is produced by adding a CW-L reinforcing helix to a CCW-L helix. Only the CW helix was thought would engage during testing since the torque was applied in the CCW direction.

The cracking torques of the -L specimens were found to be very similar (Figure 7.15). The 165-CW-L and 165-CCW-L specimens cracked at 6.1 and 5.9 kN-m respectively. The double helix specimen, 165-D, which can be considered similar to the 165-CW-L specimen, cracked at a torque of

6.7 kN-m. While the cracking torques of each specimen was similar, the behaviour after cracking differed. The 165-D specimen was able to hold additional post-cracking torque, increasing to 8.1 kN-m. The large spaced specimens on the other hand held no additional load (165-CCW-L) or maintained approximately the cracking torque value while the twist continued to increase (165-CW-L). The increase in torque after cracking observed for the 165-D specimen is likely caused by the increased ratio of helical reinforcement. Since the 165-D specimen contained the same volume of helical steel as the normal spaced specimens, an increase in ultimate torsional capacity for the double helix specimen is expected when compared to the large spaced specimens.

The results of the 165 mm pole testing suggest that the normal spaced specimens have higher cracking torque values than the larger spaced specimens. Respectively the 165-CW-N and 165-CCW-N specimens cracked at 8.5 and 7.5 kN-m (Figure 7.16). Both normal spaced specimen showed very little ability to hold additional load after cracking and held about the same torque as the 165-D specimen after cracking. Compared to the approximate 6 kN-m achieved with the larger spaced specimens, the tighter spaced specimens crack at a higher torque. The results for the 165 mm tip specimens appear to be consistent with the pre-testing theory, and logically suggest that with tighter spacing specimens the torsional capacity of the pole increases.

The 210 poles on the other hand exhibited different behaviour than the 165 mm poles (Figure 7.17 and Figure 7.18. In fact, the larger spaced 210 specimens actual had higher torsional capacities than the normal spaced specimens. The tighter spaced 210 specimens actually had lower cracking torques and only the 210-CW-N specimen actually achieved the same ultimate, post-cracking torsional capacity as the larger spaced specimens.

7.2.6 Analysis of Failure Location (Clamp vs. Collar Failure)

As discussed earlier in Chapter 6, two locations of failure were observed. Prior to testing the location of failure was thought to be where the smallest loaded cross section is located. Since the load was applied at 0.6 m from the tip and the torsion is constant throughout the length, logically the failure would occur just after the loading collar.

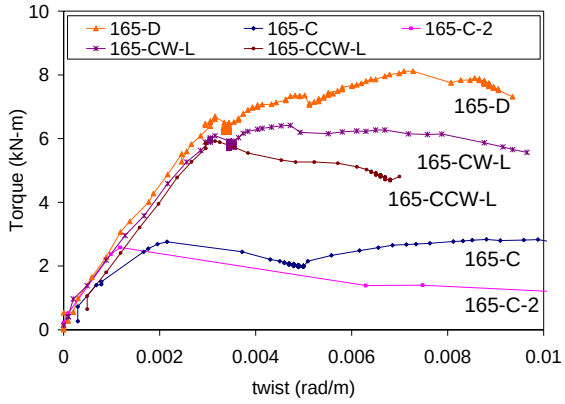

Figure 7.15: 165 mm large spaced specimens (-L)

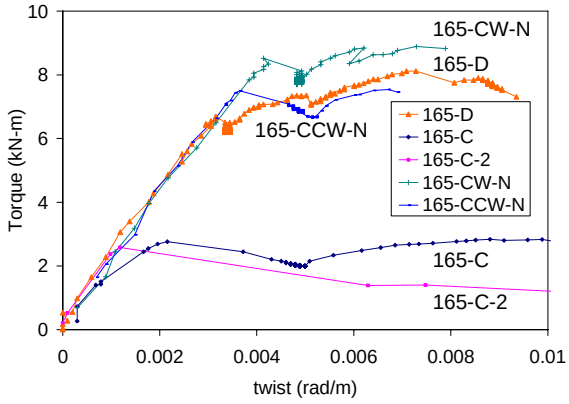

Figure 7.16: 165 mm normal spaced specimens (-N)

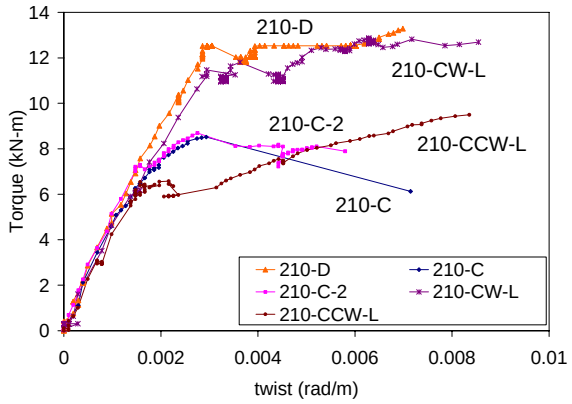

Figure 7.17: 210 mm large spaced specimens (-L)

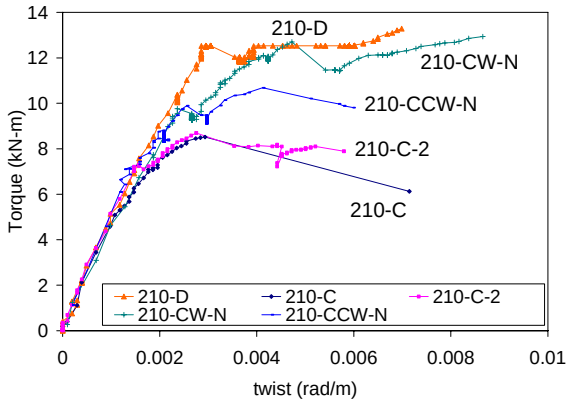

Figure 7.18: 210 mm normal spaced specimens (-N)

For the 165 mm specimens five of the seven poles tested failed at the loading collar while the remaining two failed at the clamp location. It is interesting to note that the CW specimens (165-CW-N and 165-CW-L), while having different cracking torque values, both failed at the clamp end (Figure 7.19). This observation suggests that the engaging steel (in the CW direction) provides enough resistance to the applied torque that the location of failure is moved from the collar to the clamp. If this were the case, the double helix specimens would have also failed at the clamp since it has one half of the helix engaged. Cracking of the 165-D specimen was observed to occur first at the clamp location suggesting that the theory is correct, however ultimately the failure was observed to occur at the collar. Also interestingly to note is that while the clamp failures occurred in both of the CW specimens, the clamp failure did not have substantially higher cracking torque values than the collar

failures (Figure 7.20). It would be logical that if the failure occurred at the clamp end then the cracking torque of the specimen would be larger due to the larger diameter and volume of concrete present.

Conversely, nearly all the 210 mm specimens failed at the butt clamp (Figure 7.21). Only the 210-CW-N specimen failed at the loading collar (Figure 7.22). The 210-CW-N specimen likely only failed at the loading collar due to a helical reinforcing spacing error. While the 210 specimens contradict the CW theory above, there may be other reasons that the majority of the 210 mm specimens failed at the butt. For example, due to the CSA A14-07 minimum torsional reinforcement percentages, the 210 mm specimens contained tighter spaced spirals than the 165 mm specimens (50 vs. 60 mm). The increased number of spirals may have intercepted more of the cracking occurring near the loading collar and caused the failure to move to the butt end of the pole.

Table 4-8 and Table 4-9 show that due to the variations in wall thickness caused by the manual pouring method the 210 mm specimens contained a lower percentage of reinforcement than suggested by CSA A14-07 in the butt section. Conversely the percentage is also slightly higher in the tip section. The change in percentages from the target values are because the wall thickness was either decreased (tip section) or increased (butt section). For the 165 mm specimens the tip values are close to the targets whereas the butt section has slightly lower values similar to the 210 poles. It is unclear why the 165-CW-N and 165-CW-L specimens were the only smaller specimens to fail at the clamp. The difference in percentages of reinforcement between the two sections in the 210 mm specimens could be the reason why the failure moved from the tip section to the butt. Shrinkage effects due to segregation and longitudinal cracking may have also played a role.

It is likely however that the 165 mm specimens were all pre-cracked due to prestressing transfer (see section 7.7). If the 165 mm specimens were all pre-cracked at the tip, torsional failure near the loading collar would be more likely to occur. The larger diameter and thicker wall thickness of the 210 mm specimens may have reduced the pre-cracking enough to cause failure to occur at the clamp.

It should also be noted that during testing some bending moments could have been introduced since the pole specimens were not held in the vertical direction. While the videos of the testing only reveal large vertical deflections occurring after cracking and spalling of the concrete, some small bending moments may have been introduced. Since the deflections in the vertical direction were not recorded it is unknown how large the bending moments may have been. Prestressing concrete poles have large bending moment capacities however and should be able to resist the applied loads during

torsional testing. The combination of torsional and moments may have caused the failure of the 210 mm specimens to occur at the butt instead of the loading collar and may explain why most the failures also had failures occurring at the bottom of the pole (tension side of the bending moment) within the butt clamp.

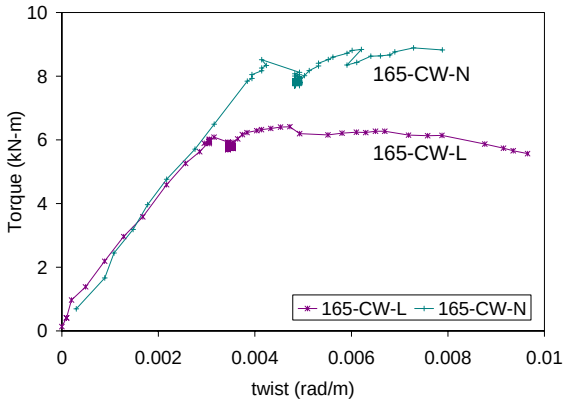

Figure 7.19: Clamp failures for 165 mm specimens

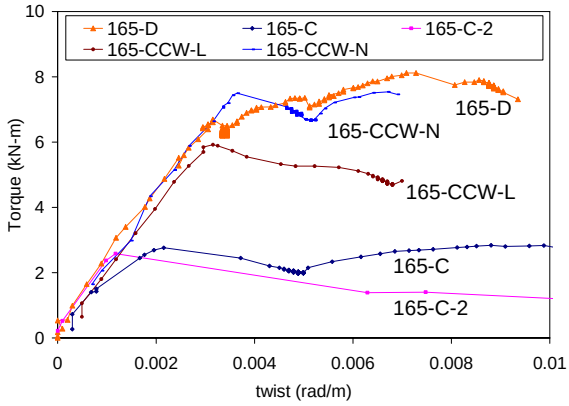

Figure 7.20: Collar failures of 165 mm specimens

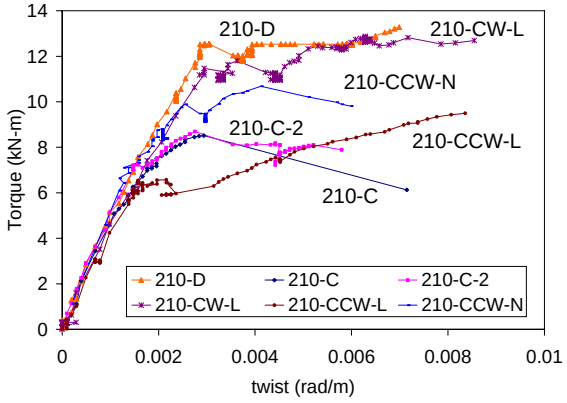

Figure 7.21: Clamp failures for 210 mm specimens

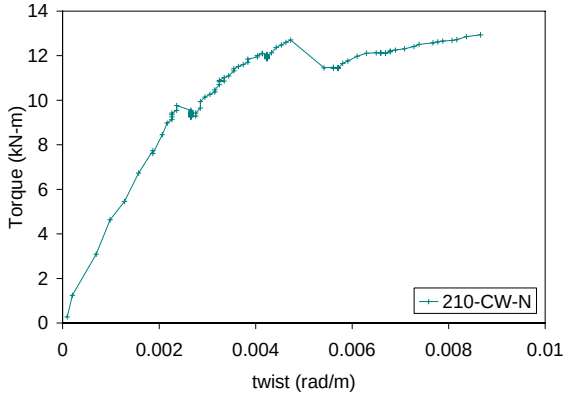

Figure 7.22: Collar failures for 210 mm specimens

7.3 Comparison of Softened Truss and Spalled Models to Test Results

The softened truss model and compression field theory (spalled model) programs discussed in Chapter 3 were modified for use with the concrete pole cross section and reinforcement. The torsion models allow the post-cracking behaviour of the poles to be compared to the actual test results. While the models do not predict the cracking torques and associated twist values, it can predict the

post-crack behaviour, torque, and failure mode. Since the post-crack torsion theories rely on the transverse reinforcement to carry the torsion loads, the post-cracking behaviour for prestressed concrete poles represents the curve for the 3.5 mm diameter (modulus of elasticity, 500 MPa) helical steel reinforcing. The failure mode is due to yielding of the transverse reinforcement.

Only the clockwise specimens were modelled since theoretically the counter clockwise specimens should have similar behaviour as the control specimens (without helical reinforcement). The double helix specimens are included since theoretically only half of the helical steel is effective in resisting the torsion load and therefore should behave similar to the clockwise specimens.

The load histories are labelled using the specimen name and additional letters in brackets to distinguish between the spalled model, softened truss model, and experimental results. The compression field theory (spalled model) results are labelled as CFT, while the softened truss model is labelled as STM. The experimental test results are labelled as T.

Figure 7.23 shows the comparison between the 165-N and -D experimental results and the torsion models. It is interesting to note that the 165-CW-N specimen, which failed at the butt clamp, follows closely to the spalled model prediction. The softened truss model meanwhile predicts torsional strengths approximately double of that predicted by the spalled model. The 165-D specimen failed suddenly at the loading collar and does not exhibit any behaviour similar to the theories presented. The 165-CW-L specimen also failed at the butt clamp but unlike the 165-CW-N specimen does not show any post-cracking behaviour (Figure 7.24). The spalled and softened truss models predict lower torsional strengths (~ 1 – 1.5 kN-m lower) at smaller twist values since the helical steel is spaced at twice the –N specimens.

Unlike the other 210 specimens, the 210-CW-N specimen failed at the collar and the experimental results show a sharp decrease and lose of torque. As a result the predicted softened truss and spalled model load histories cannot be compared to the experimental results (Figure 7.25). Even though the 210-D specimen is considered equivalent to the 210-CW-N specimen according to CSA A14-07, the load history is 2 kN-m below the predictions of the spalled model and 5 kN-m below the softened truss model. Both the 210-CW-L and 210-D specimens failed at the butt clamp allowing for post-crack torque to be held and comparison to be made to the model predictions (Figure 7.26). Better results are observed if the 210-CW-L specimens and 210-D specimens are compared to the larger spaced model predictions.

The 210-CW-L specimen actual follows the CFT model nearly exactly for 0.03 rad/m. The 210-D specimen follows the CFT model but fluctuates to a greater extent. The close agreement between the model and the experimental results could indicate that the 210-D specimen is actually behaving similarly to the 210-CW-L specimen as originally expected and the other half helix of reinforcement is not contributing unless a reversed torque is applied. Again in the case of the 210 specimens the softened truss model predicts a larger torque value than the experimental results indicate.

While the 210-CCW-L specimen was not modelled using the CFT and STM theories, the 210-CCW-L specimen test results curiously matched the modelled 210-CW-L results briefly. As the 210-CCW-L specimen failed and the torsional capacity dropped, the test results sustained loads at levels matching both the STM and CFT models (Figure 7.26).

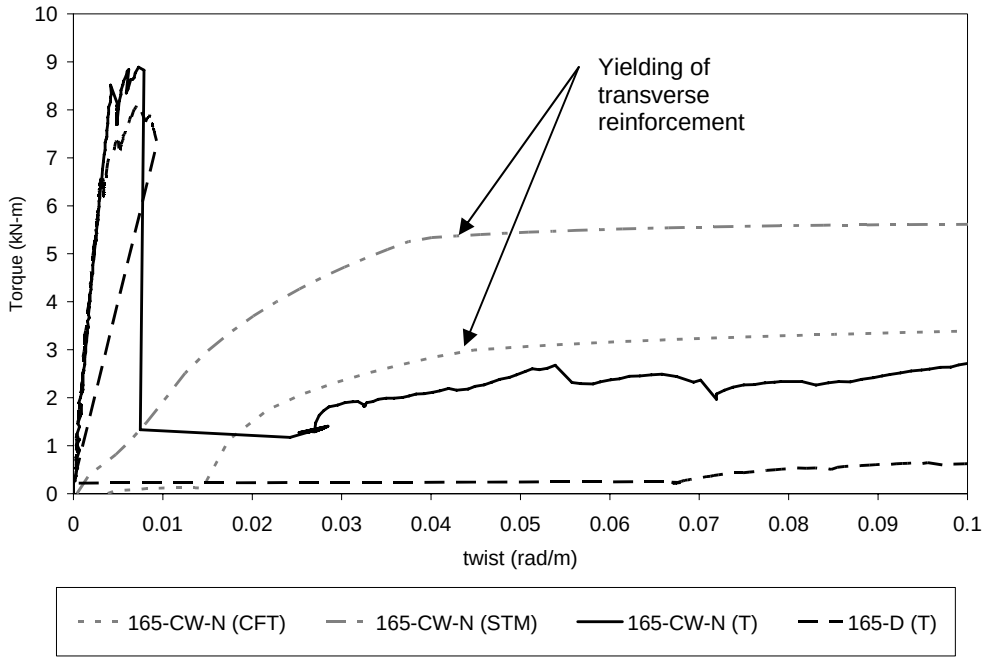

Figure 7.23: Comparison between 165-N and 165-D specimens and torsion models

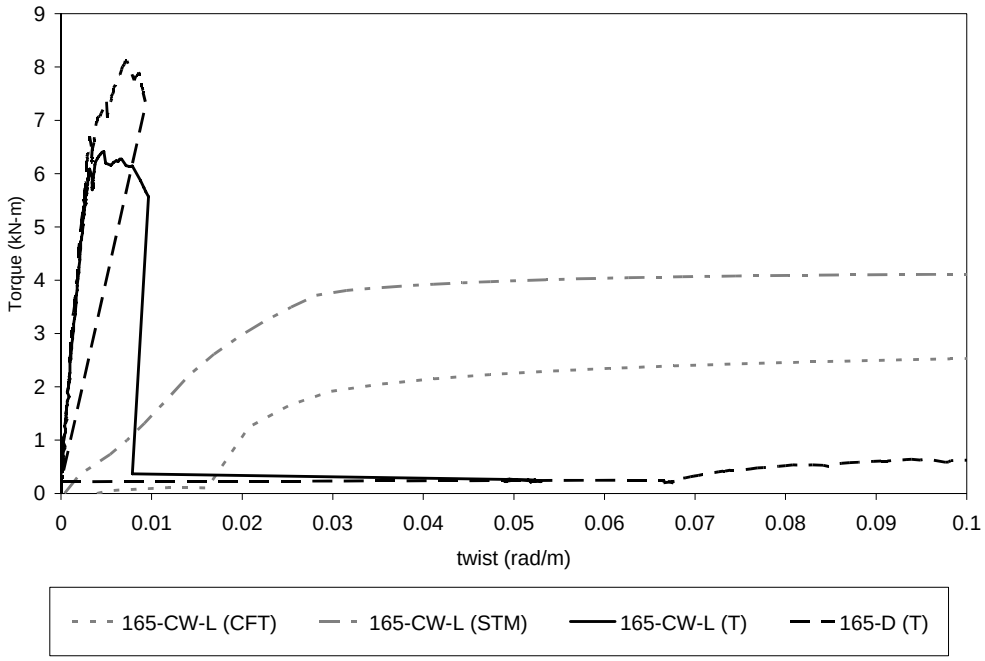

Figure 7.24: Comparison between 165-L and 165–D specimens and torsion models

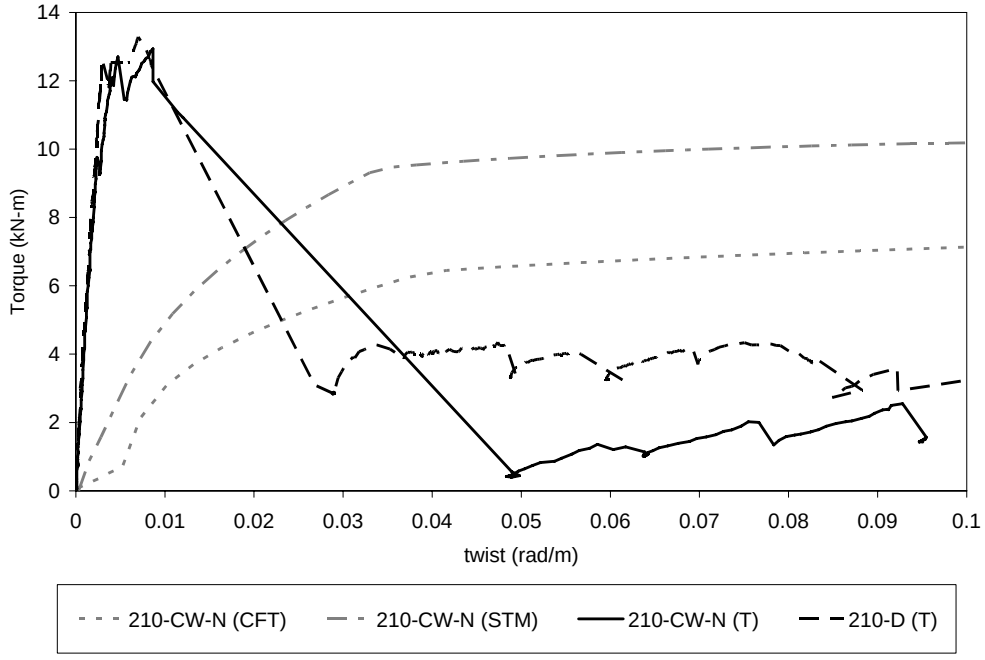

Figure 7.25: Comparison between 210-N and 210-D specimens and torsion models

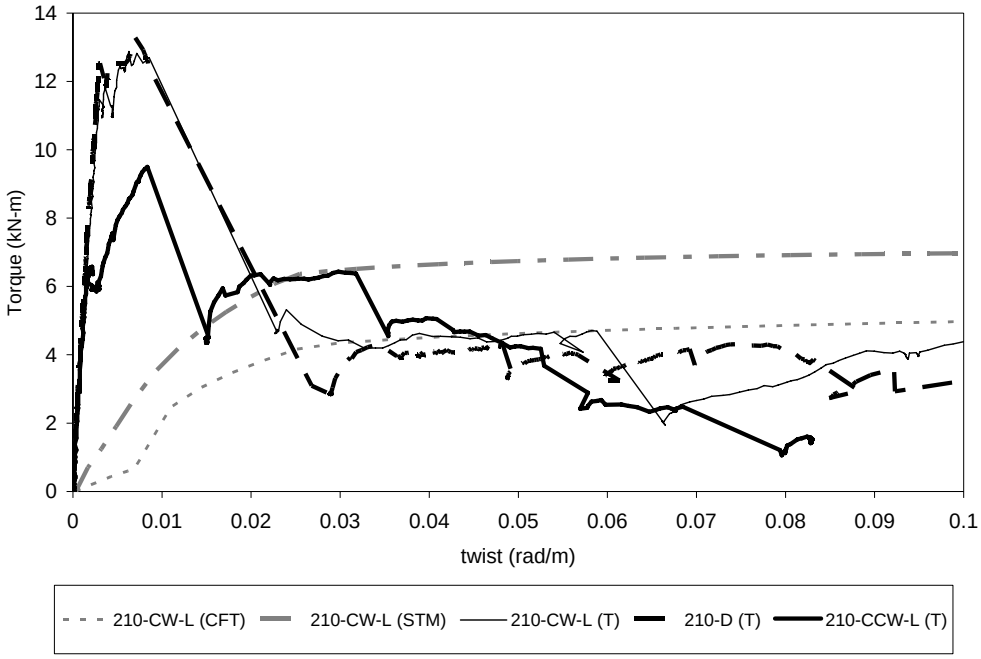

Figure 7.26: Comparison between 210-L and 210-D specimens and torsion models

From the limited amount of experimental data, the CFT model appeared predict the experimentally results better. Several papers have been written on the subject of torsion and the spalling of the concrete cover (Rahal, 2000; Rahal and Collins, 1996; and Rahal and Collins, 1995). Rahal (2000) explains that while it is conservative to assume that the cover spalls off, experimental evidence indicates that spalling will occur when the cover is larger. However, when the cover is small the concrete cover contributes in resisting the applied torque. Rahal and Collins (1996) suggested that if the cover is greater than or equal to $0.3A_c/p_c$, where A_c is the area of the concrete section including holes and p_c is the perimeter of area A_c, concrete spalling is likely to occur. At the design section (0.6 m from the tip) the average value of $0.3A_c/p_c$ for the 165 mm diameter pole specimens was calculated to be around 13 mm, while for the 210 mm diameter specimens it was 16.4 mm. At the point of failure for each specimen the value ranged from 13.3 to 16 mm for the 165 specimens and 16.8 to 19.5 mm for the 120 specimens. The cover to the helical steel in the pole specimens was typically around 20 - 23 mm. Since the cover is greater than the calculated values it can be concluded that the concrete cover spalls off at ultimate torque for prestressed concrete poles and gives an explanation as to why the CFT (spalled) model provides more accurate predictions of the load history in the post-cracking region.

7.4 Minimum Transverse Reinforcement Requirements

7.4.1 Prestressing Transfer Zone Strut and Tie Model

A strut and tie model was used to get an idea of the helical reinforcement required for the transfer of the prestressing force (Figure 7.27 and Figure 7.28). The prestressing force causes a wedging action perpendicular to the strands which can cause cracking longitudinally along the strand. A calculation sheet was created using the requirements outlined in CSA A23.3-04 on strut and tie models.

The model consisted of a uniformly distributed prestressing force which would be gradually transferred into the concrete using concrete struts and steel ties at each point along the development length of the strand. The prestressing load was assumed to act on an effective prestressing area of width p and depth w. The prestressing force, P_i, is taken as a uniformly distributed load, $P_i/50d$, along the development length and transferred in section into the concrete (Figure 7.27). The concrete strut angle, θ from the longitudinal axis of the pole is first assumed to lie between 25 and 65 degrees. Using the known angle of the concrete strut the spacing required for the tension tie can be calculated. Knowing the spacing of the ties, the prestressing load to be transferred by the strut and tie model for this section can be calculated as $P_i\ s\ /\ 50d$ (Figure 7.27). The components of the prestressing load can be calculated from the angle of the strut and therefore forces in the strut and tie are known. Assuming the force in the tie is taken by helical steel we must account for the angle of the steel and find the reduced tensile resistance. Knowing the resistance of the helical steel and the tensile force to be resisted, the required number of helical steel reinforcement can be determined. The concrete struts are sized to ensure enough concrete is present in the section to resist the compressive forces in the strut and to ensure the nodes of the truss are sized large enough.

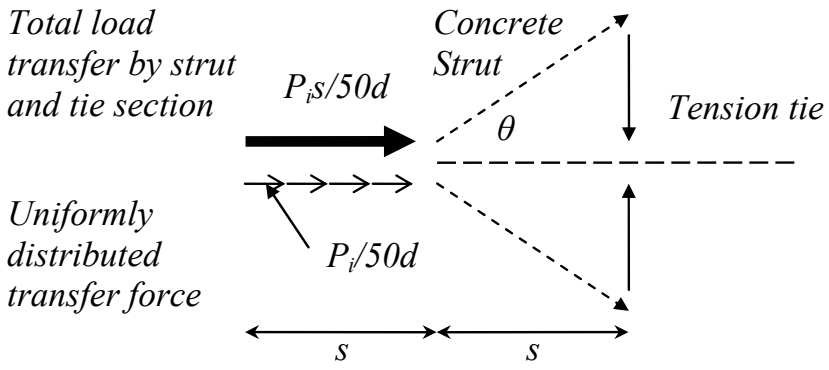

Figure 7.27: Strut and tie model

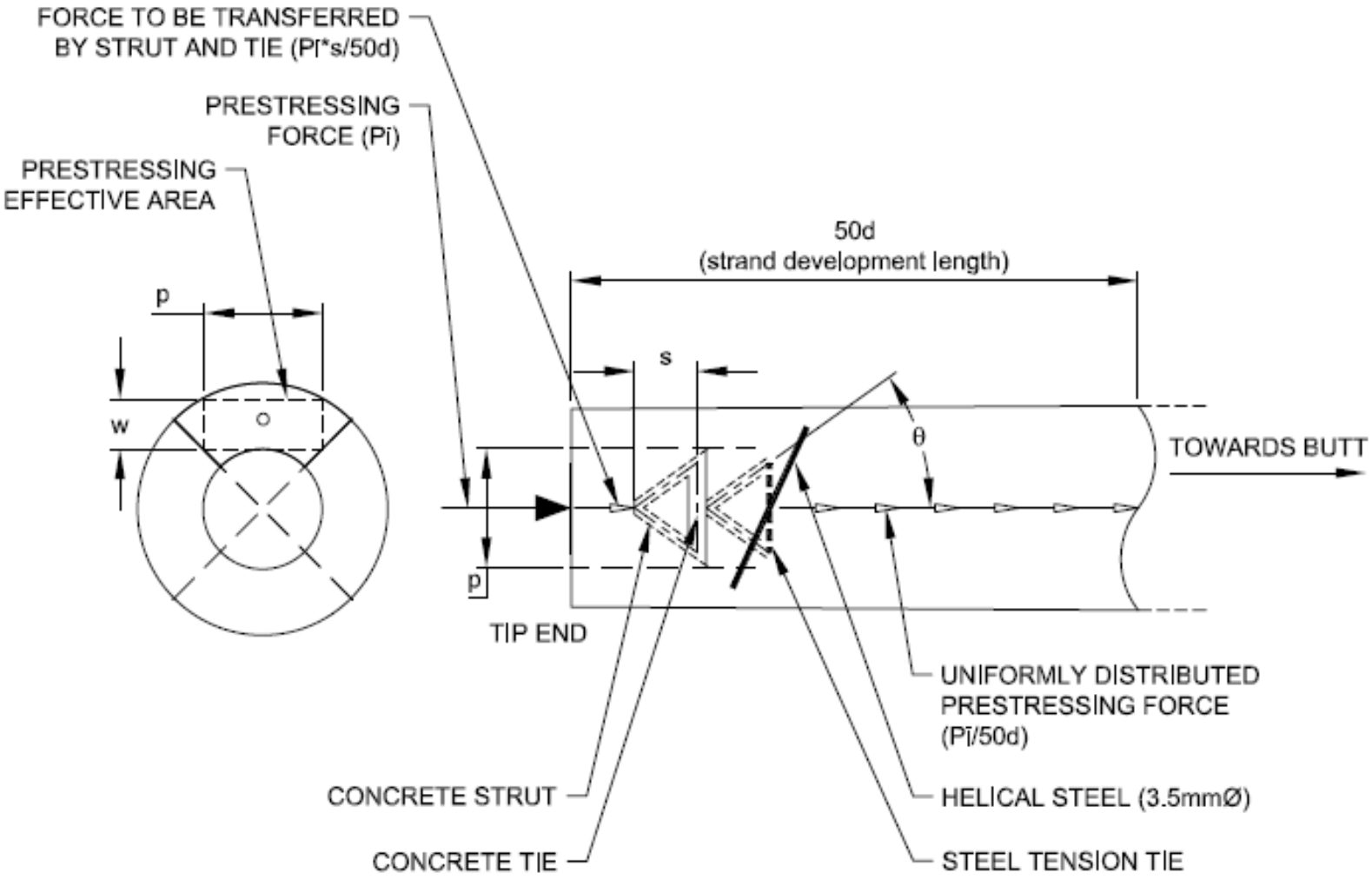

Figure 7.28: Strut and tie model for transfer length zone

Samples of the strut and tie calculation sheet can be found in Appendix D. The strut and tie model determined that the maximum concrete strut size required was 11.7 mm while the minimum was 6.4 mm. It was also found that the maximum spacing of the helical steel in the transfer zone for the 165 mm tips was 40 mm while the minimum associated with the largest strut width was 9 mm. In each strut and tie truss along the development length, a single helical steel piece was sufficient to resist the tensile forces developed due to transfer. An equivalent concrete tie width was calculated using the effective depth, *w* and assuming a tensile strength of the concrete as 2 MPa. It was found that instead of using steel tension ties, and equivalent concrete tie width of 12.9 mm could also be used. This conclusion indicates that the concrete may be able to withstand the tension forces only without the helical reinforcing steel. It also may be the reason why the German pole standard, DIN EN 12843 suggests that only 0.05% helical steel is required for spun cast prestressed concrete poles and none at all for non-spun prestressed concrete poles. The 210 mm tip pole results are similar to the results from the 165 mm poles. The maximum concrete strut size increases to 13.3 mm, while the minimum is 7.3 mm. The spacing of the ties ranges from a maximum of 53 mm to a minimum of 12 mm and the equivalent concrete tie width increased slightly to 17.0 mm.

The strut and tie helical model suggestions for the reinforcement spacing within the transfer zone are summarized in Table 7-2.

Table 7-2: Strut and tie transfer zone model spacing results

165 mm tip pole					
Strut Angle θ (degrees)	**Compression Strut Width**		**Number of Ties required (#)**	**Spacing of Ties (mm)**	**Equivalent Concrete Tie Width* (mm)**
	at prestressing force (mm)	**at tension tie (mm)**			
25	7.6	7.9	12	40	12.9
45	6.4	6.4	26	19	12.9
65	11.7	11.7	54	9	12.9
210 mm tip pole					
Strut Angle θ (degrees)	**Compression Strut Width**		**Number of Ties required (#)**	**Spacing of Ties (mm)**	**Equivalent Concrete Tie Width* (mm)**
	at prestressing force (mm)	**at tension tie (mm)**			
25	8.6	8.9	9	53	17.0
45	7.3	7.3	20	25	17.0
65	13.3	13.3	41	12	17.0
* = equivalent concrete tie sized using 2 MPa as tensile strength of concrete					

7.4.2 Code Required Maximum Transverse Reinforcement Spacing

To determine the spacing required for the helical steel according to the ACI-318-05, CSA A23.3-04, and Eurocode 2 (EC2) the minimum shear reinforcement requirements presented in section 2.5 were used. The detailed calculations of the clauses are included with the strut and tie results in Appendix C. The calculations were done assuming the use of 3.5 mm diameter helical steel as the transverse/torsional reinforcement. The diameter of the pole was taken as the effective width, b_w.

For the 165 mm tip poles the CSA clauses suggested a maximum spacing of 62 mm whereas the ACI and EC2 clauses suggested lower values of 51 mm and 47 mm respectively. In the case that the factored torsional moment is larger than a quarter of the cracking torque the CSA requirement decreases to 45.5 mm. The requirements for the 210 mm poles were lower since the effective width increased from 165 mm to 210 mm. The CSA recommended maximum spacing for the 210 mm poles is 49 mm while ACI and EC2 suggested 47 mm and 40 mm respectively.

The alternative equations for minimum transverse reinforcement for torsion presented by Ali and White (1999) and Koutchoukali and Belarbi (2001) were also used to calculate the maximum spacing permitted. The formula suggested by Ali and White gave a spacing of 19 mm for the 165 mm tip poles and 26 mm for the 210 mm poles. Similarly, the equation suggested by Koutchoukali and Belarbi suggested 28 and 23 mm for the 165 and 210 mm poles respectively. The equations are developed assuming $T_r = \lambda T_{cr}$ and the tighter spacing requirements suggested by these equations are due to the assumed value λ. Ali and White and Koutchoukali and Belarbi assumed a value greater than 1 for λ. If λ is assumed to be 1 and the calculations are repeated for maximum spacing of the transverse reinforcement a value of 36 mm results for the 165 mm poles and 29 for the 210 mm poles. In either case the transverse reinforcement equations presented in the literature give tighter spacing requirements than the codes. It is possible that theses equations should only be used for large concrete members and cannot be used in the case of prestressed concrete poles. It should also be noted that a spacing of less than 20 mm is not feasible for manufacturing purposes since concrete must be able to pass through the helical reinforcing during pouring and spinning of the concrete pole.

Similar to the strut and tie model results, the helical reinforcement spacing for all experimental specimens were all larger than the recommended concrete code maximum transverse reinforcement spacing.

7.5 Comparison of Experimental and Theoretical Cracking Torque Results

During the design of the specimens (section 4.4) it was noted that the equations given in the CSA A23.3-04 (2004) and ACI 318-05 (2005) code for ultimate torsional capacity resulted in lower values than the values based on the cracking torque formulae. The ultimate torsional capacity equations are not really applicable since they are based on the space truss model and are dependent on the transverse/helical reinforcing steel and ignore the concrete contribution. In the case of prestressed concrete poles, the helical reinforcing steel area is so small that the calculated ultimate torsional capacity is lower than the cracking torque, indicating that the poles fail at cracking loads. Given this, the equations presented in section 2.4.2 were not used.

Using the cracking torque formulae presented in section 2.4.1, a comparison between theoretical and experimental results were made. The experimental cracking torque (taken at the point when the torque-twist curve became non-linear) was used for comparison as well as the maximum torque sustained by each specimen. In addition, comparisons were made at the theoretical minimum torsional resistance location on the pole at 0.6 m from the tip (Table 7-3, Table 7-5) and at the recorded failure location (loading collar or butt clamp) using the measured wall thickness at the failure location (Table 7-4, Table 7-6). The same tables were then reproduced using two different sets of prestressing values. The first set was calculated from measurements taken of the strand elongation between the initial prestressing to tighten the strand and the final prestressing during manufacturing (Table 7-3 and Table 7-4). The measured change in length of the strands, recorded by the manufacturers was typically around 140 mm. Using the strand elongation measurements and taking into account the length changes in the pole mould and tip/butt plates prestressing stresses were calculated for each specimen. Since the stressing jack doesn't allow overstressing, theoretically each pole should have been stressed to the same prestressing value. The second prestressing value used for all pole specimens assumed a prestressing stress of $0.8f_{pu}$ and final prestressing losses of 21% as given in codes (Table 7-5 and Table 7-6).

Ratios of experimental to theoretical values were produced to predict the accuracy and conservativeness of each formula. Statistical information presented below the tables allows for comparison between the theoretical methods. Figure 7.29, Figure 7.30, and Figure 7.31 summarize the predictions by ACI 318-05, CSA A23.3-04 and EC2 respectively. The code summarizes provide a visual interpretation of the Table 7-3 to Table 7-6. Ratios above 1.0 in the tables and figures represent a conservative code prediction of the experimental cracking torque.

Table 7-3: Comparison of experimental and theoretical cracking torque results (at 0.6 m and using measured prestressing)

Specimen	T_{test} (kN-m)	$T_{test-max}$ (kN-m)	f'_c (MPa)	Diameter at 0.6 m (mm)	Wall Thickness at 0.6m (mm)	Final Prestressing Stress (MPa)	ACI 318-05*			CSA-A23.3-04			EUROCODE 2 (EC 2-1-1:2004)		
							T_{cr}^{ACI}	T_{test}/T_{cr}^{ACI}	$T_{test-max}/T_{cr}^{ACI}$	T_{cr}^{CSA}	T_{test}/T_{cr}^{CSA}	$T_{test-max}/T_{cr}^{CSA}$	T_{cr}^{EC2}	T_{test}/T_{cr}^{EC2}	$T_{test-max}/T_{cr}^{EC2}$
165-C	2.8	2.8	50.6	174	46	1116	6.3	0.44	0.45	6.8	0.41	0.42	7.9	0.35	0.36
165-C-2	2.6	2.6	72.3	174	47	1070	6.8	0.37	0.38	7.4	0.34	0.35	8.8	0.29	0.29
165-D	6.7	8.1	66.4	174	49	1059	6.6	1.02	1.23	7.1	0.94	1.14	8.4	0.79	0.96
165-CW-L	6.1	6.4	64.7	174	48	1052	6.5	0.93	0.98	7.1	0.86	0.91	8.4	0.73	0.77
165-CCW-L	5.9	5.9	45.8	174	49	1059	5.9	1.01	1.01	6.4	0.93	0.93	7.2	0.83	0.83
165-CW-N	8.5	8.9	63.7	174	50	1089	6.5	1.31	1.36	7.1	1.21	1.26	8.3	1.02	1.07
165-CCW-N	7.5	7.5	66.0	174	48	1059	6.6	1.14	1.14	7.1	1.05	1.06	8.5	0.89	0.89
210-C	5.1	8.5	61.5	219	48	1116	11.6	0.44	0.73	12.6	0.40	0.68	14.1	0.36	0.60
210-C-2	7.3	8.7	68.1	219	53	1070	11.5	0.64	0.76	12.5	0.58	0.70	14.6	0.50	0.59
210-D	12.5	13.3	65.3	219	55	1059	11.2	1.12	1.19	12.2	1.03	1.09	14.4	0.87	0.92
210-CW-L	11.5	12.9	62.6	219	53	1052	11.1	1.03	1.16	12.1	0.95	1.07	14.1	0.81	0.91
210-CCW-L	6.5	9.5	57.0	219	57	1059	10.6	0.62	0.89	11.6	0.57	0.82	13.6	0.48	0.70
210-CW-N	9.8	12.9	67.5	219	53	1089	11.5	0.85	1.12	12.5	0.78	1.03	14.7	0.67	0.88
210-CCW-N	7.1	10.7	63.6	219	58	1059	10.9	0.65	0.98	11.9	0.60	0.90	14.1	0.51	0.76
						Average:		0.83	0.96		0.76	0.88		0.65	0.75
						Standard Deviation:		0.30	0.29		0.28	0.27		0.23	0.22
						High:		1.31	1.36		1.21	1.26		1.02	1.07
						Low:		0.37	0.38		0.34	0.35		0.29	0.29
						COV:		0.36	0.30		0.36	0.30		0.36	0.30

Specimen	AASHTO (1994)			Ghoneim and Macgregor (1993)			Rahal and Collins (1996)			Hsu and Mo (1985)			Hsu (1968)		
	$T_{cr}^{AASHTO,94}$	T_{test}/T_{cr}	$T_{test-max}/T_{cr}$	T_{cr}^{GM}	T_{test}/T_{cr}^{GM}	$T_{test-max}/T_{cr}^{GM}$	T_{cr}^{RC}	T_{test}/T_{cr}^{RC}	$T_{test-max}/T_{cr}^{RC}$	T_{cr}^{HM}	T_{test}/T_{cr}^{HM}	$T_{test-max}/T_{cr}^{HM}$	T_{cr}^{HMeff}	T_{test}/T_{cr}^{HMeff}	$T_{test-max}/T_{cr}^{HMeff}$
165-C	2.9	0.96	0.99	8.2	0.34	0.34	7.2	0.39	0.40	6.2	0.45	0.46	6.4	0.43	0.44
165-C-2	3.4	0.74	0.75	9.0	0.28	0.29	7.8	0.33	0.33	7.4	0.35	0.35	7.6	0.33	0.34
165-D	3.3	2.04	2.47	8.6	0.78	0.94	7.5	0.89	1.08	7.2	0.93	1.12	13.0	0.52	0.63
165-CW-L	3.2	1.88	1.98	8.5	0.71	0.75	7.4	0.82	0.86	7.1	0.86	0.91	10.0	0.61	0.64
165-CCW-L	2.7	2.17	2.17	7.7	0.77	0.77	6.7	0.88	0.88	6.0	0.98	0.98	8.5	0.69	0.69
165-CW-N	3.2	2.65	2.76	8.5	1.00	1.04	7.4	1.14	1.19	7.3	1.16	1.21	13.2	0.65	0.68
165-CCW-N	3.3	2.29	2.30	8.6	0.87	0.87	7.5	1.00	1.00	7.1	1.05	1.06	12.8	0.59	0.59
210-C	6.3	0.81	1.35	15.2	0.33	0.56	13.3	0.38	0.64	10.0	0.51	0.85	10.3	0.49	0.83
210-C-2	6.6	1.10	1.31	15.1	0.48	0.58	13.2	0.55	0.66	11.2	0.65	0.77	11.5	0.64	0.76
210-D	6.5	1.93	2.05	14.7	0.85	0.90	12.9	0.97	1.03	11.2	1.11	1.18	23.1	0.54	0.58
210-CW-L	6.4	1.80	2.02	14.6	0.79	0.88	12.8	0.90	1.01	10.7	1.07	1.20	16.5	0.70	0.78
210-CCW-L	6.1	1.08	1.57	14.0	0.47	0.68	12.2	0.53	0.78	10.8	0.61	0.88	16.6	0.40	0.57
210-CW-N	6.6	1.48	1.96	15.2	0.64	0.85	13.3	0.74	0.98	11.2	0.87	1.16	23.0	0.42	0.56
210-CCW-N	6.4	1.11	1.67	14.4	0.49	0.74	12.6	0.56	0.85	11.6	0.61	0.92	23.8	0.30	0.45
Average:		1.57	1.81		0.63	0.73		0.72	0.83		0.80	0.93		0.52	0.61
Standard Deviation:		0.61	0.57		0.23	0.22		0.26	0.25		0.27	0.27		0.13	0.14
High:		2.65	2.76		1.00	1.04		1.14	1.19		1.16	1.21		0.70	0.83
Low:		0.74	0.75		0.28	0.29		0.33	0.33		0.35	0.35		0.30	0.34
COV:		0.39	0.31		0.36	0.30		0.36	0.30		0.34	0.28		0.25	0.22

* = ASCE/PCI Guide and AASHTO (2001) formulas give the same results as ACI 318-05

Table 7-4: Comparison of experimental and theoretical cracking torque results (at failure location and using measured prestressing)

Specimen	T_{test} (kN-m)	$T_{test-max}$ (kN-m)	f'_c (MPa)	Diameter at failure (mm)	Wall Thickness at failure (mm)	Final Prestressing Stress (MPa)	ACI 318-05			CSA-A23.3-04			EUROCODE 2 (EC 2-1-1:2004)		
							T_{cr}^{ACI}	T_{test} / T_{cr}^{ACI}	$T_{test-max} / T_{cr}^{ACI}$	T_{cr}^{CSA}	T_{test} / T_{cr}^{CSA}	$T_{test-max} / T_{cr}^{CSA}$	T_{cr}^{EC2}	T_{test} / T_{cr}^{EC2}	$T_{test-max} / T_{cr}^{EC2}$
165-C	2.8	2.8	50.6	181	48	1116	6.8	0.40	0.42	7.4	0.37	0.38	8.6	0.32	0.33
165-C-2	2.6	2.6	72.3	177	52	1070	6.9	0.37	0.37	7.5	0.34	0.34	9.0	0.28	0.29
165-D	6.7	8.1	66.4	178	50	1059	6.9	0.96	1.17	7.5	0.89	1.08	8.9	0.75	0.91
165-CW-L	6.1	6.4	64.7	213	53	1052	10.5	0.58	0.61	11.4	0.53	0.56	13.4	0.45	0.48
165-CCW-L	5.9	5.9	45.8	177	49	1059	6.1	0.97	0.97	6.6	0.89	0.89	7.5	0.79	0.79
165-CW-N	8.5	8.9	63.7	215	56	1089	10.6	0.80	0.84	11.5	0.74	0.77	13.6	0.63	0.65
165-CCW-N	7.5	7.5	66.0	177	50	1059	6.8	1.10	1.11	7.4	1.02	1.02	8.7	0.86	0.86
210-C	5.1	8.5	61.5	243	57	1116	14.4	0.35	0.59	15.7	0.32	0.54	18.1	0.28	0.47
210-C-2	7.3	8.7	68.1	257	62	1070	16.6	0.44	0.52	18.1	0.40	0.48	21.1	0.35	0.41
210-D	12.5	13.3	65.3	259	63	1059	16.6	0.76	0.80	18.1	0.69	0.73	21.1	0.59	0.63
210-CW-L	11.5	12.9	62.6	260	68	1052	16.2	0.71	0.80	17.7	0.65	0.73	20.8	0.55	0.62
210-CCW-L	6.5	9.5	57.0	259	71	1059	15.4	0.42	0.62	16.9	0.39	0.56	19.8	0.33	0.48
210-CW-N	9.8	12.9	67.5	223	55	1089	12.0	0.81	1.08	13.1	0.75	0.99	15.4	0.63	0.84
210-CCW-N	7.1	10.7	63.6	255	71	1059	15.3	0.46	0.70	16.8	0.42	0.64	19.8	0.36	0.54
						Average:		0.65	0.76		0.60	0.70		0.51	0.59
						Standard Deviation:		0.25	0.25		0.23	0.24		0.20	0.20
						High:		1.10	1.17		1.02	1.08		0.86	0.91
						Low:		0.35	0.37		0.32	0.34		0.28	0.29
						COV:		0.39	0.34		0.39	0.34		0.39	0.34

Specimen	AASHTO (1994)			Ghoneim and Macgregor (1993)			Rahal and Collins (1996)			Hsu and Mo (1985)			Hsu (1968)		
	$T_{cr}^{AASHTO,94}$	T_{test} / T_{cr}	$T_{test-max} / T_{cr}$	T_{cr}^{GM}	T_{test} / T_{cr}^{GM}	$T_{test-max} / T_{cr}^{GM}$	T_{cr}^{RC}	T_{test} / T_{cr}^{RC}	$T_{test-max} / T_{cr}^{RC}$	T_{cr}^{HM}	T_{test} / T_{cr}^{HM}	$T_{test-max} / T_{cr}^{HM}$	T_{cr}^{HMeff}	$T_{test} / T_{cr}^{HMeff}$	$T_{test-max} / T_{cr}^{HMeff}$
165-C	3.2	0.86	0.88	8.9	0.31	0.32	7.8	0.36	0.36	6.7	0.41	0.42	7.0	0.40	0.41
165-C-2	3.6	0.71	0.72	9.1	0.28	0.28	7.9	0.32	0.33	8.2	0.31	0.32	8.5	0.30	0.30
165-D	3.5	1.89	2.29	9.1	0.73	0.89	7.9	0.84	1.02	7.7	0.87	1.06	13.9	0.48	0.59
165-CW-L	6.0	1.02	1.08	13.8	0.44	0.47	12.0	0.51	0.53	10.4	0.58	0.62	13.3	0.46	0.48
165-CCW-L	2.9	2.06	2.06	8.0	0.74	0.74	7.0	0.85	0.85	6.2	0.96	0.96	8.8	0.67	0.67
165-CW-N	6.0	1.41	1.47	14.0	0.61	0.64	12.2	0.70	0.73	11.0	0.77	0.81	16.9	0.50	0.53
165-CCW-N	3.4	2.18	2.19	8.9	0.84	0.85	7.8	0.97	0.97	7.6	0.99	1.00	13.6	0.55	0.55
210-C	8.6	0.59	0.98	19.0	0.27	0.45	16.7	0.31	0.51	13.5	0.38	0.63	13.8	0.37	0.62
210-C-2	10.8	0.68	0.81	21.9	0.33	0.40	19.2	0.38	0.45	16.5	0.44	0.53	16.8	0.44	0.52
210-D	10.8	1.16	1.23	21.9	0.57	0.61	19.2	0.65	0.69	16.5	0.76	0.80	27.5	0.46	0.48
210-CW-L	10.7	1.07	1.21	21.4	0.54	0.60	18.8	0.61	0.69	17.3	0.66	0.74	23.2	0.49	0.56
210-CCW-L	10.1	0.65	0.94	20.4	0.32	0.47	17.9	0.37	0.53	17.0	0.38	0.56	22.9	0.29	0.42
210-CW-N	7.0	1.39	1.84	15.8	0.62	0.82	13.8	0.71	0.94	11.9	0.82	1.08	24.6	0.40	0.53
210-CCW-N	10.1	0.70	1.05	20.3	0.35	0.53	17.8	0.40	0.60	17.5	0.41	0.61	29.1	0.24	0.37
Average:		1.17	1.34		0.50	0.57		0.57	0.66		0.62	0.72		0.43	0.50
Standard Deviation:		0.54	0.54		0.19	0.19		0.22	0.22		0.24	0.24		0.11	0.10
High:		2.18	2.29		0.84	0.89		0.97	1.02		0.99	1.08		0.67	0.67
Low:		0.59	0.72		0.27	0.28		0.31	0.33		0.31	0.32		0.24	0.30
COV:		0.47	0.40		0.39	0.34		0.39	0.34		0.38	0.33		0.26	0.20

* = ASCE/PCI Guide and AASHTO (2001) formulas give the same results as ACI 318-05

Table 7-5: Comparison of experimental and theoretical cracking torque results (at 0.6 m and using assumed prestressing)

Specimen	T_{test} (kN-m)	$T_{test-max}$ (kN-m)	f'_c (MPa)	Diameter at 0.6 m (mm)	Wall Thickness at 0.6m (mm)	Final Prestressing Stress (MPa)	ACI 318-05			CSA-A23.3-04			EUROCODE 2 (EC 2-1-1:2004)		
							T_{cr}^{ACI}	T_{test} / T_{cr}^{ACI}	$T_{test-max} / T_{cr}^{ACI}$	T_{cr}^{CSA}	T_{test} / T_{cr}^{CSA}	$T_{test-max} / T_{cr}^{CSA}$	T_{cr}^{EC2}	T_{test} / T_{cr}^{EC2}	$T_{test-max} / T_{cr}^{EC2}$
165-C	2.8	2.8	50.6	174	46	1176	6.4	0.43	0.44	6.9	0.40	0.41	8.1	0.34	0.35
165-C-2	2.6	2.6	72.3	174	47	1176	7.1	0.36	0.36	7.7	0.33	0.34	9.2	0.28	0.28
165-D	6.7	8.1	66.4	174	49	1176	6.9	0.98	1.18	7.4	0.90	1.09	8.8	0.76	0.92
165-CW-L	6.1	6.4	64.7	174	48	1176	6.8	0.89	0.94	7.4	0.82	0.87	8.7	0.70	0.73
165-CCW-L	5.9	5.9	45.8	174	49	1176	6.2	0.96	0.96	6.6	0.89	0.89	7.5	0.79	0.79
165-CW-N	8.5	8.9	63.7	174	50	1176	6.7	1.27	1.32	7.3	1.17	1.22	8.6	0.99	1.03
165-CCW-N	7.5	7.5	66.0	174	48	1176	6.9	1.09	1.10	7.4	1.01	1.01	8.8	0.85	0.85
210-C	5.1	8.5	61.5	219	48	1176	11.8	0.43	0.72	12.8	0.40	0.66	14.4	0.35	0.59
210-C-2	7.3	8.7	68.1	219	53	1176	11.9	0.61	0.73	12.9	0.56	0.67	15.1	0.48	0.57
210-D	12.5	13.3	65.3	219	55	1176	11.6	1.08	1.14	12.6	0.99	1.05	14.9	0.84	0.89
210-CW-L	11.5	12.9	62.6	219	53	1176	11.6	0.99	1.11	12.6	0.91	1.02	14.7	0.78	0.88
210-CCW-L	6.5	9.5	57.0	219	57	1176	11.1	0.59	0.86	12.0	0.54	0.79	14.1	0.46	0.67
210-CW-N	9.8	12.9	67.5	219	53	1176	11.9	0.82	1.09	12.9	0.76	1.00	15.1	0.65	0.86
210-CCW-N	7.1	10.7	63.6	219	58	1176	11.4	0.62	0.94	12.4	0.57	0.86	14.6	0.49	0.73
						Average:		0.79	0.92		0.73	0.85		0.63	0.73
						Standard Deviation:		0.29	0.28		0.26	0.26		0.22	0.22
						High:		1.27	1.32		1.17	1.22		0.99	1.03
						Low:		0.36	0.36		0.33	0.34		0.28	0.28
						COV:		0.36	0.30		0.36	0.30		0.36	0.30

Specimen	AASHTO (1994)			Ghoneim and Macgregor (1993)			Rahal and Collins (1996)			Hsu and Mo (1985)			Hsu (1968)		
	$T_{cr}^{AASHTO,94}$	T_{test} / T_{cr}	$T_{test-max} / T_{cr}$	T_{cr}^{GM}	T_{test} / T_{cr}^{GM}	$T_{test-max} / T_{cr}^{GM}$	T_{cr}^{RC}	T_{test} / T_{cr}^{RC}	$T_{test-max} / T_{cr}^{RC}$	T_{cr}^{HM}	T_{test} / T_{cr}^{HM}	$T_{test-max} / T_{cr}^{HM}$	T_{cr}^{HMeff}	$T_{test} / T_{cr}^{HMeff}$	$T_{test-max} / T_{cr}^{HMeff}$
165-C	2.9	0.96	0.99	8.4	0.33	0.34	7.3	0.38	0.39	6.3	0.44	0.45	6.5	0.42	0.43
165-C-2	3.4	0.74	0.75	9.3	0.27	0.28	8.1	0.32	0.32	7.6	0.34	0.34	7.9	0.32	0.33
165-D	3.3	2.04	2.47	9.0	0.74	0.90	7.8	0.85	1.04	7.5	0.89	1.08	13.5	0.50	0.60
165-CW-L	3.2	1.88	1.98	8.9	0.68	0.72	7.8	0.78	0.82	7.4	0.83	0.87	10.4	0.58	0.61
165-CCW-L	2.7	2.17	2.17	8.0	0.74	0.74	7.0	0.85	0.85	6.3	0.95	0.95	8.9	0.67	0.67
165-CW-N	3.2	2.65	2.76	8.8	0.97	1.01	7.7	1.11	1.16	7.5	1.13	1.18	13.5	0.63	0.66
165-CCW-N	3.3	2.29	2.30	9.0	0.83	0.84	7.8	0.96	0.96	7.4	1.02	1.02	13.3	0.57	0.57
210-C	6.3	0.81	1.35	15.5	0.33	0.55	13.6	0.38	0.63	10.2	0.50	0.83	10.5	0.49	0.81
210-C-2	6.6	1.10	1.31	15.6	0.47	0.56	13.7	0.53	0.64	11.6	0.63	0.75	11.8	0.62	0.73
210-D	6.5	1.93	2.05	15.3	0.82	0.87	13.4	0.94	0.99	11.6	1.08	1.14	23.8	0.53	0.56
210-CW-L	6.4	1.80	2.02	15.2	0.75	0.85	13.3	0.86	0.97	11.1	1.03	1.16	17.1	0.67	0.75
210-CCW-L	6.1	1.08	1.57	14.6	0.45	0.65	12.7	0.51	0.75	11.1	0.59	0.85	17.1	0.38	0.55
210-CW-N	6.6	1.48	1.96	15.6	0.62	0.83	13.6	0.72	0.95	11.5	0.85	1.13	23.6	0.41	0.55
210-CCW-N	6.4	1.11	1.67	15.0	0.47	0.71	13.1	0.54	0.82	12.0	0.59	0.89	24.5	0.29	0.44
Average:		1.57	1.81		0.61	0.70		0.69	0.80		0.78	0.90		0.51	0.59
Standard Deviation:		0.61	0.57		0.22	0.21		0.25	0.24		0.26	0.26		0.12	0.13
High:		2.65	2.76		0.97	1.01		1.11	1.16		1.13	1.18		0.67	0.81
Low:		0.74	0.75		0.27	0.28		0.32	0.32		0.34	0.34		0.29	0.33
COV:		0.39	0.31		0.36	0.30		0.36	0.30		0.33	0.28		0.25	0.23

* = ASCE/PCI Guide and AASHTO (2001) formulas give the same results as ACI 318-05

Table 7-6: Comparison of experimental and theoretical cracking torque results (at failure location and using assumed prestressing)

Specimen	T_{test} (kN-m)	$T_{test-max}$ (kN-m)	f'_c (MPa)	Diameter at failure (mm)	Wall Thickness at failure (mm)	Final Prestressing Stress (MPa)	ACI 318-05			CSA-A23.3-04			EUROCODE 2 (EC 2-1-1:2004)		
							T_{cr}^{ACI}	T_{test} / T_{cr}^{ACI}	$T_{test-max} / T_{cr}^{ACI}$	T_{cr}^{CSA}	T_{test} / T_{cr}^{CSA}	$T_{test-max} / T_{cr}^{CSA}$	T_{cr}^{EC2}	T_{test} / T_{cr}^{EC2}	$T_{test-max} / T_{cr}^{EC2}$
165-C	2.8	2.8	50.6	181	48	1176	7.0	0.40	0.41	7.5	0.37	0.38	8.8	0.31	0.32
165-C-2	2.6	2.6	72.3	177	52	1176	7.2	0.35	0.36	7.8	0.33	0.33	9.3	0.27	0.28
165-D	6.7	8.1	66.4	178	50	1176	7.2	0.92	1.12	7.8	0.85	1.03	9.3	0.72	0.87
165-CW-L	6.1	6.4	64.7	213	53	1176	10.9	0.56	0.59	11.9	0.51	0.54	14.0	0.43	0.46
165-CCW-L	5.9	5.9	45.8	177	49	1176	6.4	0.92	0.92	6.9	0.85	0.85	7.8	0.76	0.76
165-CW-N	8.5	8.9	63.7	215	56	1176	10.9	0.78	0.81	11.9	0.72	0.75	14.0	0.61	0.63
165-CCW-N	7.5	7.5	66.0	177	50	1176	7.1	1.06	1.06	7.7	0.98	0.98	9.1	0.82	0.83
210-C	5.1	8.5	61.5	243	57	1176	14.7	0.35	0.58	16.0	0.32	0.53	18.4	0.28	0.46
210-C-2	7.3	8.7	68.1	257	62	1176	17.1	0.43	0.51	18.7	0.39	0.46	21.8	0.33	0.40
210-D	12.5	13.3	65.3	259	63	1176	17.2	0.73	0.77	18.8	0.67	0.71	21.9	0.57	0.61
210-CW-L	11.5	12.9	62.6	260	68	1176	16.8	0.68	0.77	18.3	0.63	0.70	21.6	0.53	0.60
210-CCW-L	6.5	9.5	57.0	259	71	1176	16.0	0.41	0.59	17.5	0.37	0.54	20.5	0.32	0.46
210-CW-N	9.8	12.9	67.5	223	55	1176	12.4	0.79	1.05	13.4	0.73	0.96	15.8	0.62	0.82
210-CCW-N	7.1	10.7	63.6	255	71	1176	15.9	0.45	0.67	17.4	0.41	0.62	20.5	0.35	0.52
						Average:		0.63	0.73		0.58	0.67		0.50	0.57
						Standard Deviation:		0.24	0.24		0.22	0.22		0.19	0.19
						High:		1.06	1.12		0.98	1.03		0.82	0.87
						Low:		0.35	0.36		0.32	0.33		0.27	0.28
						COV:		0.38	0.33		0.39	0.34		0.39	0.33

Specimen	AASHTO (1994)			Ghoneim and Macgregor (1993)			Rahal and Collins (1996)			Hsu and Mo (1985)			Hsu (1968)		
	$T_{cr}^{AASHTO,94}$	T_{test} / T_{cr}	$T_{test-max} / T_{cr}$	T_{cr}^{GM}	T_{test} / T_{cr}^{GM}	$T_{test-max} / T_{cr}^{GM}$	T_{cr}^{RC}	T_{test} / T_{cr}^{RC}	$T_{test-max} / T_{cr}^{RC}$	T_{cr}^{HM}	T_{test} / T_{cr}^{HM}	$T_{test-max} / T_{cr}^{HM}$	T_{cr}^{HMeff}	$T_{test} / T_{cr}^{HMeff}$	$T_{test-max} / T_{cr}^{HMeff}$
165-C	3.2	0.86	0.88	9.1	0.30	0.31	7.9	0.35	0.36	6.9	0.40	0.41	7.1	0.39	0.40
165-C-2	3.6	0.71	0.72	9.5	0.27	0.27	8.2	0.31	0.31	8.5	0.30	0.31	8.8	0.29	0.29
165-D	3.5	1.89	2.29	9.5	0.70	0.85	8.3	0.81	0.98	8.0	0.84	1.02	14.4	0.46	0.56
165-CW-L	6.0	1.02	1.08	14.4	0.42	0.45	12.6	0.48	0.51	10.8	0.56	0.59	13.8	0.44	0.46
165-CCW-L	2.9	2.06	2.06	8.4	0.71	0.71	7.3	0.81	0.81	6.4	0.92	0.92	9.1	0.65	0.65
165-CW-N	6.0	1.41	1.47	14.4	0.59	0.62	12.5	0.68	0.71	11.3	0.75	0.79	17.3	0.49	0.51
165-CCW-N	3.4	2.18	2.19	9.3	0.81	0.81	8.1	0.93	0.93	7.8	0.96	0.96	14.1	0.53	0.53
210-C	8.6	0.59	0.98	19.4	0.26	0.44	17.0	0.30	0.50	13.7	0.37	0.62	14.0	0.36	0.61
210-C-2	10.8	0.68	0.81	22.6	0.32	0.38	19.8	0.37	0.44	16.9	0.43	0.51	17.2	0.42	0.50
210-D	10.8	1.16	1.23	22.7	0.55	0.59	19.9	0.63	0.67	17.0	0.74	0.78	28.3	0.44	0.47
210-CW-L	10.7	1.07	1.21	22.2	0.52	0.58	19.4	0.59	0.66	17.8	0.64	0.72	23.9	0.48	0.54
210-CCW-L	10.1	0.65	0.94	21.1	0.31	0.45	18.5	0.35	0.51	17.5	0.37	0.54	23.5	0.28	0.40
210-CW-N	7.0	1.39	1.84	16.3	0.60	0.80	14.2	0.69	0.91	12.2	0.80	1.06	25.2	0.39	0.51
210-CCW-N	10.1	0.70	1.05	21.0	0.34	0.51	18.4	0.39	0.58	18.0	0.39	0.59	30.0	0.24	0.36
Average:		1.17	1.34		0.48	0.55		0.55	0.63		0.61	0.70		0.42	0.49
Standard Deviation:		0.54	0.54		0.18	0.19		0.21	0.21		0.23	0.23		0.11	0.10
High:		2.18	2.29		0.81	0.85		0.93	0.98		0.96	1.06		0.65	0.65
Low:		0.59	0.72		0.26	0.27		0.30	0.31		0.30	0.31		0.24	0.29
COV:		0.47	0.40		0.39	0.34		0.39	0.34		0.38	0.33		0.26	0.20

* = ASCE/PCI Guide and AASHTO (2001) formulas give the same results as ACI 318-05

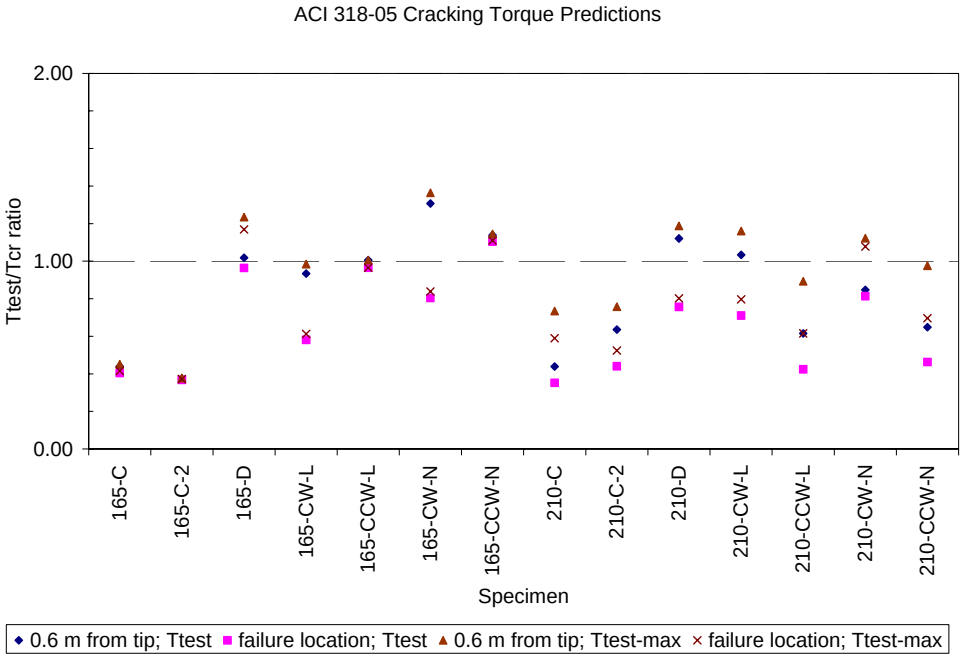

Figure 7.29: Variation and accuracy of ACI 318-05 code predictions

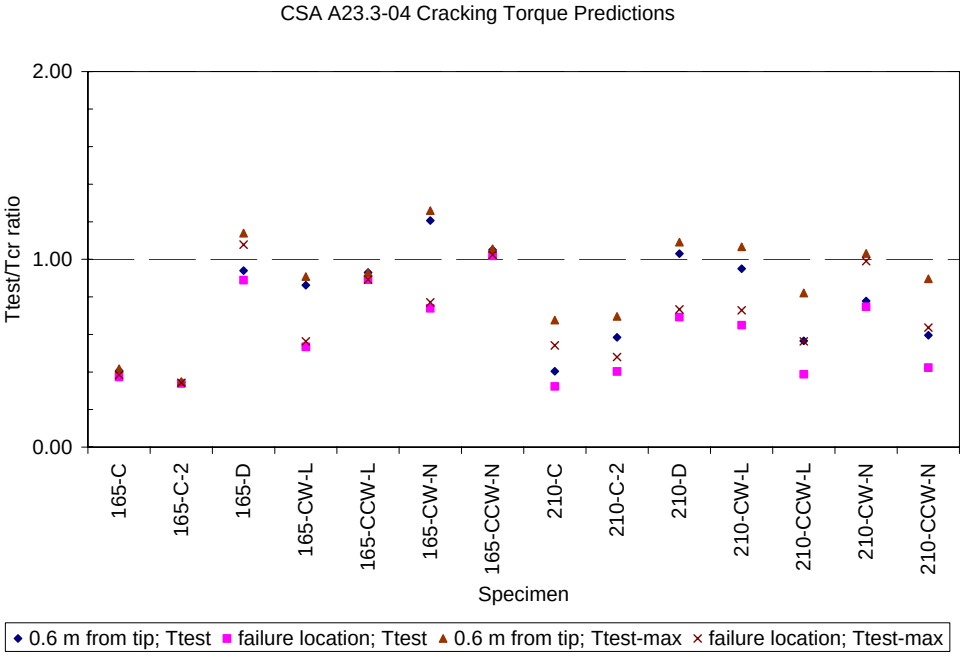

Figure 7.30: Variation and accuracy of CSA A23.3-04 code predictions

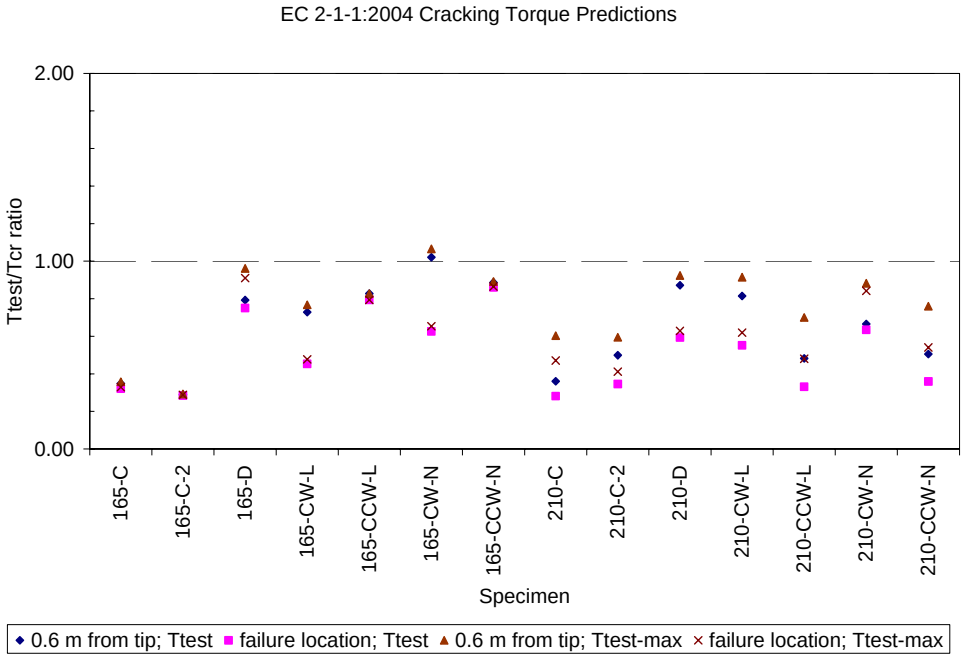

Figure 7.31: Variation and accuracy of EC2 code predictions

Table 7-3 presents the comparison between experimental and theoretical cracking torque values using the design section at 0.6 m from the top and measured strain prestressing values. Generally the averages of the ratio between the experimental and theoretical values were below 1.0 (unconservative). The average ratios were higher for the maximum torque values and all the data had low variance (COV values < 1). Only the AASHTO (1994) code formula, which is now no longer in use, gave conservative average ratios (1.57 for the cracking torques and 1.81 for the maximum torques). A larger variation in the AASHTO (1994) predicted data is evident by the higher standard deviation value. Next to the AASHTO (1994) results, the ACI predictions (see Figure 7.29) gave the second highest average for the experimental cracking torque values at 0.83. CSA and Eurocode 2 predictions were lower at 0.76 and 0.65, respectively (see Figure 7.30 and Figure 7.31). As previously stated, the ratios between the maximum torque and the predicted values were all higher than the ratios calculated with the experimental cracking torque values. The average ratios were 0.1 to 0.13 higher for the maximum torque ratios. Similar to the cracking torque ratios ACI produced the second highest average ratio at 0.96 (after the AASHTO (1994) results). The cracking torque equations presented by Ghoneim and MacGregor, Rahal and Collins, and Hsu and Mo produced similar average results to the code equations. The effective cracking torque equation presented by

Hsu (1968) and based on the amount of longitudinal and transverse reinforcement, gave the lowest ratios averages, however, also had the lowest standard deviation (lowest coefficient of variation, COV). Hsu's effective cracking torque formula predicted the test results poorly but reduced the standard deviation by taking into account the variation caused by the reinforcing steel (both longitudinal and transverse).

The average ratios decreased when the actual failure location and wall thicknesses were used to predict the theoretical cracking torque values (Table 7-4). The ACI average ratios decreased to 0.65 and 0.76 for the experimental cracking torque and maximum torque, respectively. Each method gave less accurate results even though the actual location of failure was used in the calculation of the theoretical cracking torque values. During testing, the location of failure occurred in two places, at the loading collar or at the butt clamp. It was thought that using the actual wall thickness and helical reinforcing (in the case of Hsu's effective cracking equation) at the location of failure would yield better results. In general, the equations had lower average ratios and standard deviation values indicating that the methods were predicting less conservative values using the actual failure location data.

The same tables were reproduced using an assumed constant prestressing force for all specimens of $0.8f_{pu}$ and assuming 21% final losses. Table 7-5 displays the comparison between experimental and theoretical cracking torque values calculated at the design section (0.6 m from tip), while Table 7-6 shows the theoretical cracking torque values calculated at the specific failure location. In general, the average ratios were very similar to those calculated using the measured prestressing stresses but were 0.3 – 0.4 lower. It is interesting to note that the effective cracking torque formula by Hsu (1968) was less influenced by the prestressing value change exhibiting a average ratio decrease of only 0.1 – 0.2. The standard deviation was fairly constant for all cracking torque prediction methods dropping only slightly by 0.1 or 0.2. It should also be noted that the AASHTO (1994) formula is independent of prestressing and gives conservative results. The predicted values using the assumed prestressing stress are anywhere from 0.5 to 1.0 kN-m higher depending on the method of calculation. This explains the decrease in average ratios noted when the prestressing stress was assumed.

Since the 165-C, 165-C-2, 210-C and 210-C-2 specimens were cracked longitudinally prior to testing we can remove the values from the analysis. The average ratios increase, as expected, when the low torsional results of the controls specimens are removed. As an example, the ACI values (presented in Table 7-7) increase to 0.97 while the standard deviation value decreases to 0.22. The

same trend is observed when the predicted results calculated at the failure location are compared to the test results. It is apparent that without the control specimens the average becomes more accurate and closer to a conservative value. The range of ratios is still significant (0.62 to 1.31) and indicates that either the helical steel may be contributing or the formula cannot predict the values when applied to concrete poles. The high and low values correspond to specimens with different concrete compressive strength or wall thicknesses, however, there is no general trend that explains the spread of ratio observed. The variation of results is discussed further in section 7.8.

Table 7-7: Comparison of ACI-318-05 Statistical Data with and without control specimens

	With Control specimens		Without Control Specimens	
	0.6 m from Tip	Failure Location	0.6 m from Tip	Failure Location
Average	0.83	0.65	0.97	0.76
Standard Deviation	0.30	0.25	0.22	0.22
High	1.31	1.10	1.31	1.10
Low	0.37	0.35	0.62	0.42
COV	0.36	0.39	0.22	0.29

7.6 Factors Affecting Theoretical Cracking Torque Formulae

Wall thickness, concrete compressive strength, and prestressing stress are all important factors to the calculation of the theoretical cracking torque. Percentage of reinforcement could also be significant depending on the amount of longitudinal and transverse reinforcement present (see Hsu's effective cracking torque formula). The sensitivity of the predicted values to the variables in the ACI-318-05 cracking torque formula was determine and are summarized in Figure 7.32. It is apparent that as the wall thickness increases, the prestressing compressive stress in the concrete is lower, resulting in a decrease in the cracking torque. The decrease is significant as a change in the wall thickness from 30 mm to 75 mm reduces the cracking torque, as predicted by the ACI equation, from approximately 7.7 kN-m to 6.1 kN-m. Intuitively the amount of prestressing can reduce the torsional capacity of a pole as well. A decrease from 80% stressing to 60% will change the torsional capacity by nearly 1 kN-m. Concrete strength is also important and reduces the torsional strength by roughly 0.3 kN-m. Of course segregation, as discussed in section 2.1.4, caused by improper batches or concrete placement can also reduce the capacity by introducing longitudinal cracking and weaker areas of concrete

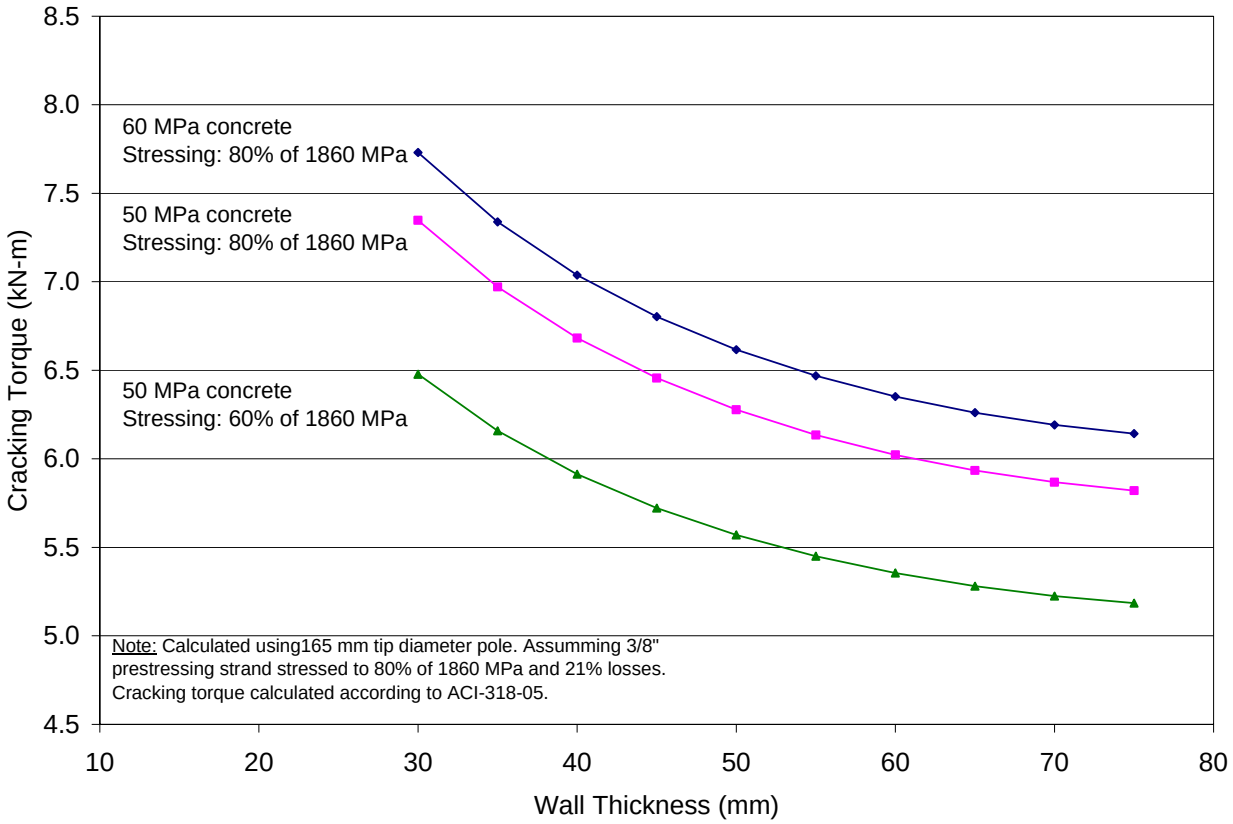

Figure 7.32: Effects of wall thickness, compressive strength, and prestressing stress on cracking torque

7.7 Influence of Longitudinal Cracking, Segregation, and Concrete Quality on Cracking Torque

Longitudinal cracking was observed in all control specimens produced. The 165 mm control specimens (165-C and 165-C-2) were much weaker compared to the 210 mm controls in relation to the rest of the tested specimens. The lower torsional capacities are likely due to the longitudinal cracking observed along the prestressing strands (Figure 7.33 (a)). It appears that without any helical reinforcing, the thinner 165 mm tip poles are more susceptible to cracking due to the transfer of the prestressing force than the 210 mm tip poles. Since the 210-C specimen failed at the butt clamp however, it is possible that the longitudinal crack at the tip end was not the cause of the pole's premature failure.

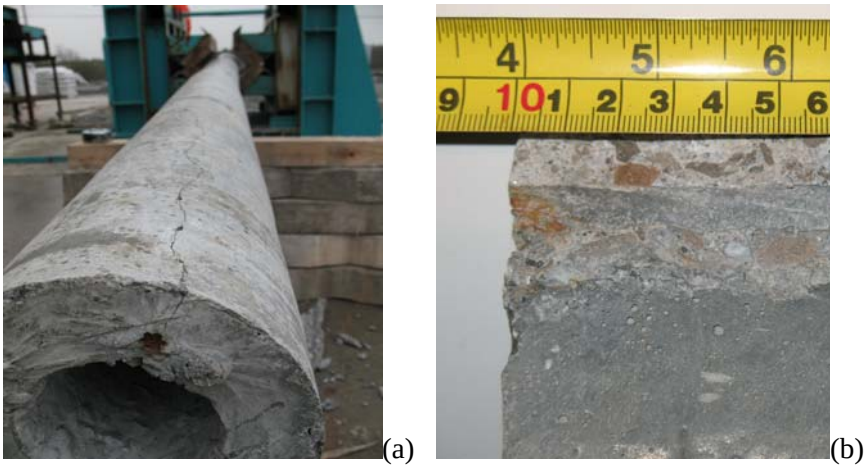

(a) (b)

Figure 7.33: Longitudinal cracking (a) and strand slip (b) due to prestressing (165-C)

As shown in Figure 7.33 (a) and in more detail in (b), the specimens without helical reinforcement showed signs of strand slip. It was determined that the strand had sunk into the concrete by 2-4 mm. The strand slip and pre-cracking of the control specimens can explain the poor performance observed for the two control specimens. To control the strand slip, the specimens can be cast with a plate at the tip attaching to each of the prestressing strands. This would spread the prestressing force over the entire cross section and decrease the likeliness of longitudinal cracks forming. The addition of an end plate, however, could lead to concrete crushing problems under the end plate since the prestressing force is immediately transferred to the concrete. Without the end plate the prestressing force is uniformly distributed to the concrete over the development length of the strand.

While the helical reinforcing will help to reduce the longitudinal cracking due to prestressing transfer, other issues can also cause longitudinal cracking in prestressed concrete poles. As discussed earlier in section 2.1.4, it was proven that differential shrinkage due to segregation of paste from aggregate can cause longitudinal cracking to occur in spun cast concrete poles. Thus the longitudinal cracking can attributed to concrete quality and not necessarily the lack of helical reinforcing steel. A 10 cm paste wedge was seen in some specimens during post-failure inspections (Figure 7.34 a)). It is believed that the early cracking torque observed in the 210-CCW-L specimen was caused by the wetter mix and excess air entrainment agent (Table 4-6). A thicker wall thickness in the 210-CCW-L specimen and therefore larger quantity of concrete (Table 4-9) caused more segregation (20 mm of paste was noted during testing, Figure 7.34 c)). The load held post-cracking by the 210-CCW-L specimen could be attributed to the helical steel and concrete interaction. Normally with a proper

concrete mix the concrete cracking torque is higher than observed with the 210-CCW-L specimen and the helical steel fails immediately after cracking.

The presence of longitudinal cracking along the strands prior to testing decreases the torsional capacity or cracking torque of concrete poles. If prestressed concrete pole were to be produced without any helical reinforcing steel, the concrete quality (no segregation) and strength would need to be very high. It also may not be possible to completely remove the helical reinforcing since issues like vehicle impact, shear forces, and construction requirements may make it unfeasible.


a)


b)


c)

Figure 7.34 a)-c): a) Typical paste wedge and segregation along inner wall of specimens b) segregation of 210-CCW-L specimen c) extreme example from Chahrour and Soudki (2006) pole testing

7.8 Discussion on the Variation in the Results

7.8.1 Sky Cast Inc. Database and Experimental Specimen Comparison

The experimental results discussed in Chapter 6 were compared to a database of test results provided by Sky Cast Inc. to determine if the specimens were representative of previous findings. The Sky Cast Inc. database contained many test results ranging from smaller Class A poles to larger Class O poles. The database provided information on the class, length, helical reinforcement type (single, double, none), prestressing strand size, wall thickness at failure for bending, and tip diameter. Specimen specific concrete strengths, wall thickness at torsion failure, and prestressing levels were not recorded and therefore theoretical calculations were not completed on the database. While the missing information could have be estimated, the theoretical calculations were not completed since cracking torque is greatly affected by wall thickness, concrete strength, and prestressing level (as shown previously in section 7.5 and 7.6).

The database was sorted and plotted into 5 figures with tip diameters of 165 mm and 210 mm and stressing strand sizes of 3/8", 7/16" and 1/2". Poles classified as A through F were used since the CSA A14-07 standard gives the same spacing and percentage of helical reinforcement as the experimental specimens tested. The class of a pole relates only to the length and bending capacity of the pole and does not affect the torsional result as long as wall thickness, tip diameter, and strand sizes are kept constant. Testing of database single helical reinforcement poles were always completed in the CCW direction according to the CSA A14-M1979 standard, clause 7.5.4 (torsional load creates compressive principal stresses along the direction of spirals).

Figure 7.35 plots the database results of 150 mm tip poles with 3/8" prestressing strand. The results include Class A and B poles and double helix, single helix, and no helical reinforcement. The single helically reinforced poles results are between 4 and 10 kN-m with the majority between 5 and 8 kN-m. The results of the few double helically reinforced and non reinforced poles tested also fall between 5 and roughly 8.5 kN-m. The database results suggest that the single helical poles behave similarly to the double helical and non-reinforced poles. The results also suggest that helical reinforcement did not increase the torsional capacity of the 150 mm tip poles, and the torsional results vary between 4 and 9 kN-m regardless of the helical reinforcement type.

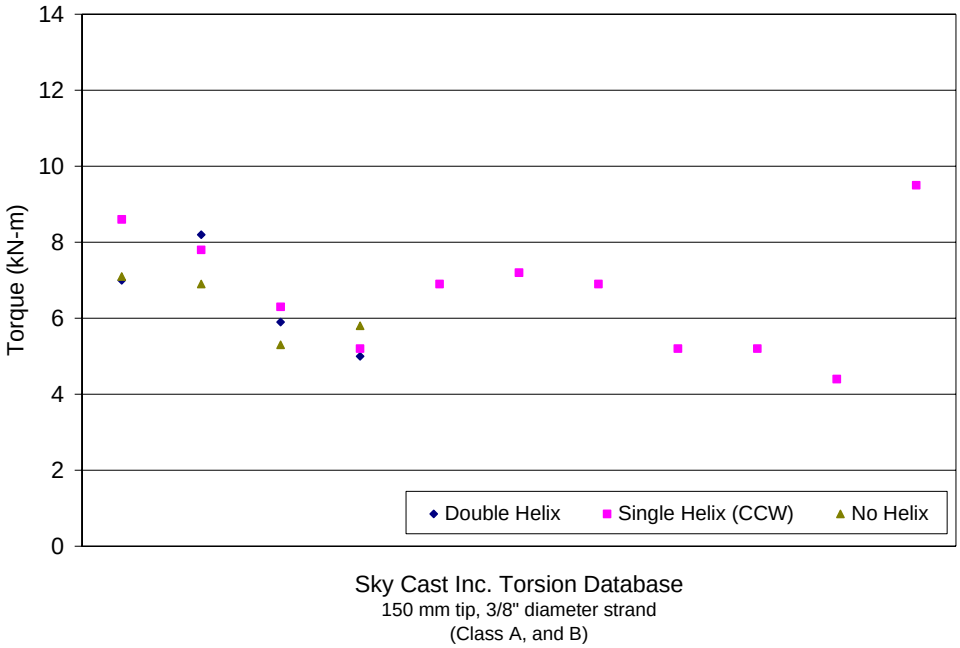

Figure 7.35: Sky Cast Inc. Torsion Database Results - 150 mm tip, 3/8" prestressing strand

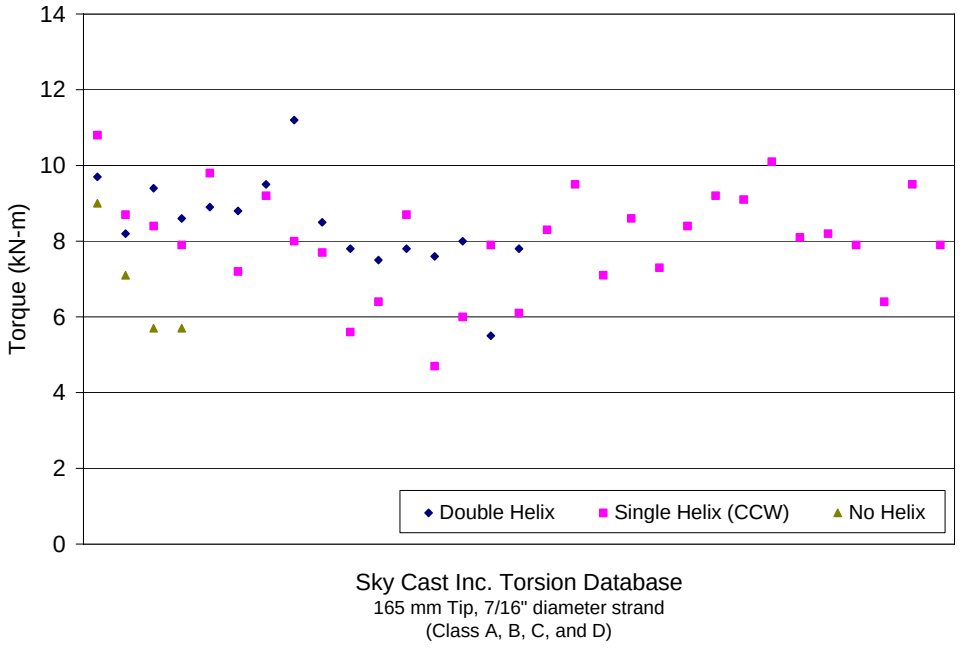

Figure 7.36: Sky Cast Inc. Torsion Database Results - 165 mm tip, 7/16" prestressing strand

The database also contained 165 mm tip poles with stressing strands sizes of 3/8", 7/16", and 1/2". The majority of the poles tested used 7/16" strand (Figure 7.36). Similar to the 150 mm tip pole results, the 165 mm tip poles with 7/16" strand lie within a band of roughly 5 to 10 kN-m with a few outliers. Again, no significant difference in torsional capacity was observed between the double helical poles and the single/no helix poles. The results indicate further that the helical reinforcement does not contribute significantly to the torsional capacity of the pole tested. The variation in the torsional capacities (5 to 10 kN-m) is slightly higher, but very similar to the band determined from the 150 mm tip poles (4 to 9 kN-m). The similar results can be explained by the concrete area difference between a 150 mm tip pole and 165 mm tip pole being small. It should be noted that the prestressing strand size, while doubled from 3/8" to 7/16" strand, increased the torsional capacity only slightly.

Figure 7.37 shows the 165 mm tip poles tested with 1/2" prestressing strand. Similarly to Figure 7.35 and Figure 7.36, the double helix and single helix specimens do not show a difference in torsional capacity and all the results lie within a band of 6 – 9 kN-m. Again, similar to the 165 mm tip - 7/16" strand results, it appears that the prestressing strand size does not affect the torsional capacity very much. Failure of the specimens may be caused by some other phenomenon and as a result the increased strand size does not cause a noticeable increase in the torsional capacity.

To determine if the experimental results were in agreement with the Sky Cast Inc. database results, poles with the same tip diameter as the 14 experimental specimens were selected and plotted together with the experimental results (Figure 7.38 and Figure 7.39). Due to the lack of results to compare to the 210 mm specimens with 3/8", 7/16", and 1/2" strands were plotted together with the 210 experimental specimens since it was determined in the previous figures that prestressing strand size does seem to affect the torsional capacity of the pole to a great extent.

The 165 mm tip experimental specimens all behaved similarly to the database results (Figure 7.38). While the 165-D specimen had a lower torsional capacity than the database results, the specimen still fell within the 6 to 10 kN-m band observed. According to the database results the double helix does not seem to hold more torsional load than the single/non-reinforced specimens. The 165-CCW-N and 165-CW-N specimens were found to lie in the middle of the database results as expected since the single helix (CCW) poles were reinforced and tested in the same manner. Even though the engaged reinforcing direction (CW) yielded larger torsional capacities in the experimental testing, the database results (tested in the CCW direction) do not support this result.

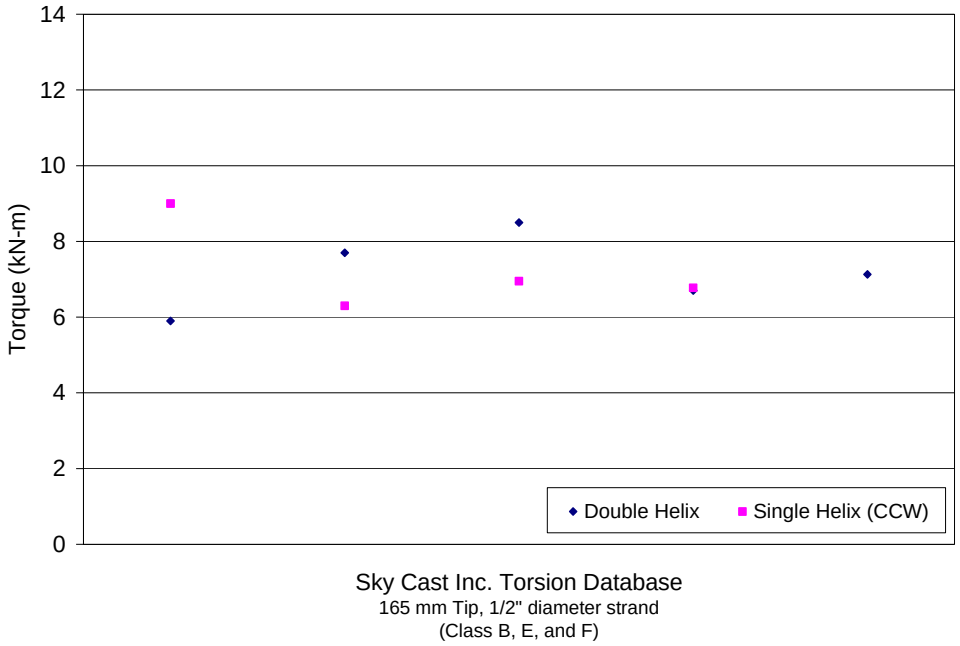

Figure 7.37: Sky Cast Inc. Torsion Database Results - 165 mm tip, 1/2" prestressing strand

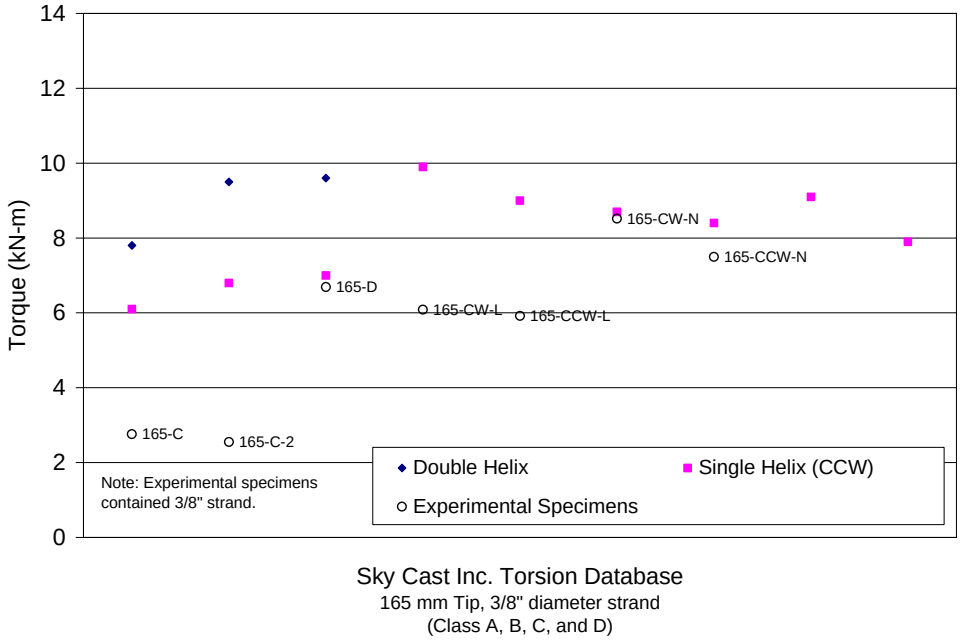

Figure 7.38: Sky Cast Inc. Torsion Database and Experimental Results - 165 mm tip, 3/8"strand

The database had several poles, tested in the CCW direction, which gave larger torsional results than the 165-CW-N specimen. This fact seems to suggest that the direction of the reinforcement does not affect the capacity of the pole. The large spaced, non CSA A14-07 conforming poles, 165-CW-L and 165-CCW-L, interestingly enough also behaved similar to the low end single helix results from the database. This suggests that the spacing of the helical reinforcement is also insignificant to the overall variation observed in the database. The non reinforced experimental specimens (165-C and 165-C-2) behaved significantly below the other database results. While no non-helical reinforced specimens were tested with 3/8" strand in the database, previous figures suggest that the non-reinforced specimens typically lie within the band 5 – 10 kN-m band. The poor performance of the 165-C and 165-C-2 specimens can likely be linked to the longitudinal cracking observed. Concrete strength and wall thickness differences may also have contributed.

Since there are fewer Sky Cast Inc. database results for the 210 mm tip poles, less can be conclusively derived. The 210 mm tip experimental specimens are compared with 10 poles from the database in Figure 7.39. While one of the non-reinforced specimens (210-C-2) was in the middle of the database results, the other specimen (210-C) was lower than all the other database results. The low result observed by the 210-C specimen is still within 2 kN-m of the other results and could seem further removed due to the lower number of results available for comparison. The 210-CCW-L, 210-CCW-N, and 210-CW-N specimens all were relatively close to the database results. The results further the suggestion presented in the 165 mm tip data that the spacing of the helical reinforcement does not affect the torsional capacity. However, the 210-D, 210-CW-L and 210-CW-N poles appear to have increased torsional capacity compared to the database results. This result suggests that the direction may have an influence on the larger sized poles or that not enough database results are available for comparison and the band of results is actually wider. The increased capacity exhibited by the 210-D and 210-CW-L may be due to differences in concrete and is unlikely related to the helical reinforcement as the specimens with more helical reinforcement actually exhibited smaller torsional capacities.

Without further testing the observations made can not be conclusively stated, however from the experimental results both differences in wall thickness and concrete strength can not explain the increase in torsional capacities observed. It is apparent that helical steel affects the cracking torque of the specimen, however the mechanism and how much the steel contributes is unknown.

Figure 7.39: Sky Cast Inc. Torsion Database and Experimental Results - 210 mm tip

7.8.2 Experimental Variation and the CSA A14-07 Spacing Provisions

Of the seven 165 mm poles tested, only three were acceptable according to current CSA A14-07 standards (165-D, 165-CW-N, and 165-CCW-N). The remaining poles were not designed based on CSA A14-07; 165-C and 165-C-2 contained no reinforcing and the spacing was too large for the 165-CW-L and 165-CCW-L specimens. The variation and scatter observed during testing of the specimens and in the Sky Cast Inc. database results could be explained by insufficient transfer zone helical steel.

The three specimens designed based on the code displayed similar behaviour after cracking, adding approximately 0.5 to 1.5 kN-m to the torque sustained in post-cracking region (Figure 7.40). The cracking torques ranged from 6.7 to 8.5 kN-m for the 165-D and 165-CW-N specimens respectively. The remaining poles, excluding the control specimens, exhibited cracking torques of 6.1 and 5.9 kN-m and held the cracking torque or maintained no additional post-crack torque (Figure 7.41). The results suggest that for the 165 mm specimens the code designed poles have a better ability to maintain the cracking torque in the post-cracking region and have larger cracking torques in general.

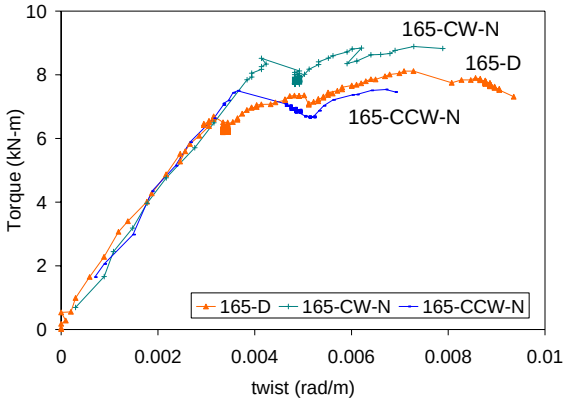

Figure 7.40: 165 mm specimens designed to CSA A14

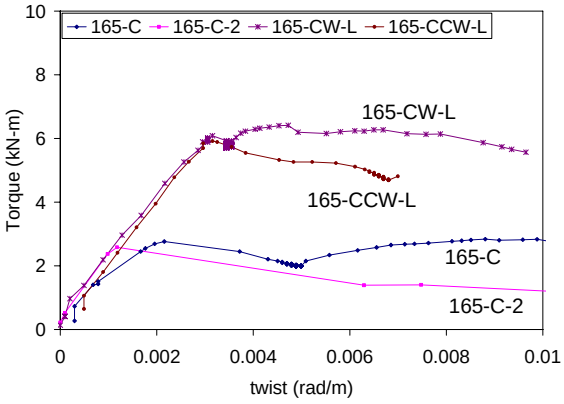

Figure 7.41: 165 mm specimens against CSA A14

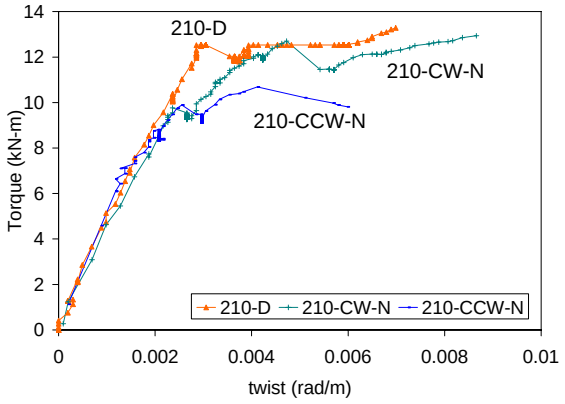

Figure 7.42: 210 mm specimens designed to CSA A14

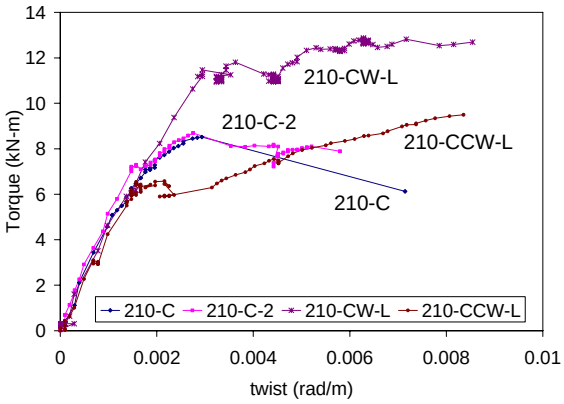

Figure 7.43: 210 mm specimens against CSA A14

However, the difference between the highest cracking torque for the non-code designed poles (165-CW-L) and the lowest cracking torque for the code designed poles (165-D) is only 0.6 kN-m.

The 210 mm specimens behaved differently than the 165 mm specimens. Two of the code allowable poles (210-D and 210-CW-N) displayed similar ultimate torque values of 12 kN-m. Both normal spaced specimens (210-CW-N and 210-CCW-N) however cracked 3 kN-m below the 210-D specimen. In fact, the 210-CW-L exhibited a larger cracking torque value indicating that the code designed poles may in fact not be better than the non-code designed poles. However, it cannot be conclusively stated since the 210-CCW-L specimen cracked much lower than all the specimens.

Unlike the 165 mm specimens, all the 210 specimens were able to hold additional post cracking torque load. The reason why the 210 mm poles may be demonstrating different behaviour than the 165 mm poles is that they failed at different ends of the pole. The 210 mm specimens have a greater likelihood of holding post-crack load since there is a larger amount of concrete at the butt failure zone, which increases concrete interlock. Also the failure at the loading collar, typical of the 165 mm specimens is sudden and causes destruction of the surrounding concrete and the entire tip of the pole to fall to the ground.

Comparing the strut and tie model spacing suggestions to the specimen spacing gives the best explanation of the scatter of results recorded and modes of failure observed (Table 7-8). In the case of the 165 mm tip specimens the spacing suggests by the strut and tie model is 20 mm tighter than the CSA A14-07 (2007) requirements and the large specimen spacing (165-CW-L and 165-CCW-L) are three times the spacing of the strut and tie model. The 165 mm specimens therefore were likely pre-cracked (visible or invisible) regardless if they were designed to CSA A14-07 spacing requirements. The fact that the specimens were pre-cracked may explain the spread of results obtained during testing (see section 7.5), the variation observed in the Sky Cast Database (see section 7.8.1), and the fact that nearly all the 165 specimens failed at the collar. Therefore, the degree to which a specimen is pre-cracked determines the cracking torque of the specimen and longitudinal cracking due to segregation of the concrete and transfer of prestressing forces cause variation in torsional capacities of the poles.

The 210 mm tip CSA A14-07 (2007) spacing requirements are close to the value suggested by the strut and tie model and therefore the 210-D, 210-CW-N, and 210-CCW-N specimens may or may not have been pre-cracked. The 210-CCW-L and 210-CW-L specimens were not reinforced adequately according to the strut and tie model and yet the 210-CW-L specimen performed as well as the CSA A14-07 designed specimens. The combination of the larger spaced helical steel and the greater volume of concrete present for the 210 mm tip specimens may have reduced or eliminated the pre-cracking of the reinforced 210 specimens causing failure to occur at the clamp and more consistent results between specimens.

Table 7-8: Comparison between strut and tie spacing requirements and specimen spacing

165 mm tip Specimens			210 mm tip Specimens		
Strut and Tie Model Spacing (mm)	Experimental Specimen Spacing		Strut and Tie Model Spacing (mm)	Experimental Specimen Spacing	
	CSA A14-07 Designed Spacing (mm)	Large Specimen Spacing (mm)		CSA A14-07 spacing (mm)	Large Specimen Spacing (mm)
40	60	120	53	50	100

7.9 Economic Analysis of Helical Reinforcing

An approximate economic analysis was performed at Sky Cast Inc. in Guelph to determine the cost reduction associated with using larger spaced helical reinforcement or single versus double helical reinforcing. Using an assumed labour cost per minute and measured labour times, approximate savings can be determined (Table 7-9). The material savings comes from the fact that approximately half the helical steel is required when the spacing is doubled. The production is also halved since only half the coil is needed. The placement of the coil does not decrease by exactly half because the number of coils does not decrease by exactly half and the coils must still be hand wound.

Table 7-9: Savings due to helical spacing changes

Helix Type	Material cost helical reinforcement ($)	Labour cost per minute:		$ 0.58 /min		
		Production of helical reinforcement (minutes)	Placement of helical reinforcement (minutes)	Total Labour (minutes)	Labour costs ($)	Total Savings ($)
Single Helix (-N)	$ 1.60	1.5	3.75	5.25	$ 3.06	-
Double Helix (-D)	$ 3.19	3	6.56	9.56	$ 5.58	-
Single Helix (-L)	$ 0.80	0.75	1.875	2.625	$ 1.53	-
Savings using single helix (-N) over double helix (-D)	$ 1.60	1.50	2.81	4.31	$ 2.52	$ 4.11
Savings using larger single helix (-L) spacing over normal helix (-N)	$ 0.80	0.75	1.88	2.63	$ 1.53	$ 2.33
Savings using larger single helix (-L) spacing over double helix (-D)	$ 2.39	2.25	4.69	6.94	$ 4.05	$ 6.44

It can be approximated that $2.33 can be saved per pole using the larger spaced single helical spacing (-L). Using a similar method, approximately $4.11 can be saved using the single helix (-N) over the double helix (-D). When the single helix at the large spacing is compared against the double helix spacing we get a total savings of approximately $6.44. The savings may not be significant when it is compared to the $300 total production cost of a single pole. When large volumes of poles are produced, savings may be more substantial.

7.10 Analysis and Comparison of Typical Applied Torques on Lighting Poles

Typical applied loads on lighting poles were calculated to determine if the torque capacity of the tested poles was adequate. A standard cobra head fixture with an Effective Projected Area (EPA) of 0.093 m^2 (1 ft^2) and a fixture arm length of 2.4 m (8 ft) and EPA of 0.055 m^2 (0.6 ft^2) were used to calculated wind torque loads due to 80 and 160 mph wind speeds using the AASHTO LTS-4-M (2001) static wind pressure formula below:

$$P = 0.613 K_Z G V^2 I_r C_d \tag{7-3}$$

where K_Z is a height and exposure factor, G is the gust effect factor of 1.14, V is the design wind velocity in mph, I_r is a wind importance factor, C_d is the drag coefficient, and P is the static wind pressure in Pa. Appendix E contains the product sheets showing where the EPA values were taken from and a print out of the wind load calculation spreadsheet.

Calculating the height and exposure factor for 10.7 m gave a value of 1.09. The gust factor was calculated to be 1.14. Since the poles were near 10 m in height, the wind importance factor was taken as 1. A drag coefficient of 1 was used since the EPA values given by the manufacturers already incorporate the fixture's drag coefficient. The 80 mph wind speed was considered as a design wind speed for non-hurricane regions (Waterloo, Ontario) whereas the 160 mph wind speed was assumed for hurricane regions. The factored calculated values of applied torque for the 80 mph and 160 mph wind speeds were calculated as 0.4 kN-m, and 1.84 kN-m respectively.

The ACI (Clause 11.6.1) and CSA (Clause 11.2.9.1) code indicate that if the factored torsional loads are below $0.25T_{cr}$ than the torsional loads can be ignored for design. The clauses in both codes can be linked to a report by ACI Committee 438 (1969). The report suggests that torsion can be neglected in design if the nominal ultimate stress due to torsion is less than $1.5\phi\sqrt{f_c'}$. The stress suggested is approximately 25 percent of the pure torsional strength of a member without web

reinforcement. The simplification for design is considered allowable since a torsional moment applying a stress of $1.5\phi\sqrt{f_c'}$ will not cause a significant reduction in ultimate strength in flexure of shear. In beams without stirrups, a torsional moment of 30 percent of the pure torsional strength causes no reduction in the flexural strength, and reduces the shear strength by about 5-15 percent. It is suggested that the reduction in shear strength can be compensated by the post-cracking shear strength, since shear strength is based on diagonal cracking and is less than the actual ultimate shear strength. Beams with stirrups the stress corresponds to a torsional moment much less than 25 percent of the pure torsional strength. The flexural strength is reduced by a few percent only and shear strength is reduced by about 15 percent.

The associated factored resistance (calculated using CSA cracking torque equations and including factors of safety (ϕ_c = 0.7)) for the lowest 165 mm tip diameter specimen can be calculated as 5.18 kN-m and 9.29 kN-m for the 210 mm specimen. The $0.25T_{cr}$ values are 1.3 kN-m and 2.3 kN-m respectively. This indicates that even the lowest strength specimen could have been designed neglecting torsion in non-hurricane areas. Only in the 210 mm lighting pole specimens however, can the torsional forces be neglected in hurricane areas (Figure 7.44 and Figure 7.45).

In hurricane areas torsion effects must be considered in addition to bending and shear, however the torsional loads are still well below the tested cracking torque values. The specimens have adequate reserve strength for torsional loads however the torsional loads above $0.25T_c$ may cause a reduction in the shear or moment capacities. For torsional resistance, poles have better geometry and control of material properties than beams cast on site and since the design recommendation of $0.25T_{cr}$ was developed for structural beam elements, it is likely too conservative for concrete lighting poles. It should be noted that the difference between the cracking torques of the CSA A14-07 acceptable and unacceptable specimens is insignificant when compared to the torques typically applied to street lighting poles. As a result, the spacing of the helical reinforcement is insignificant compared to the applied torques and the CSA A14-07 requirements can likely be simplified.

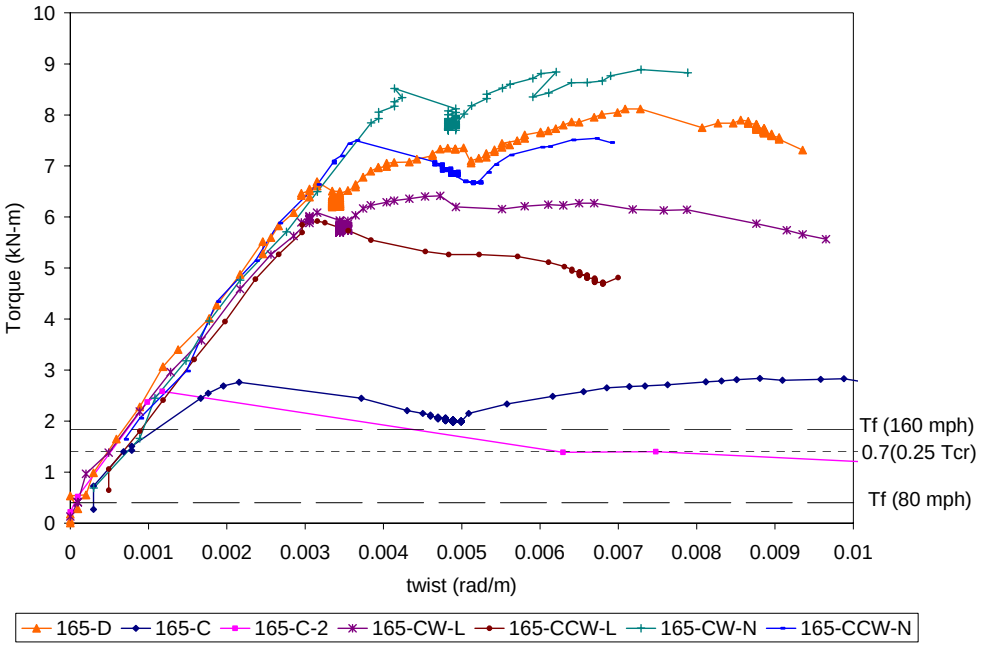

Figure 7.44: Applied factored torque versus 165 cracking torques

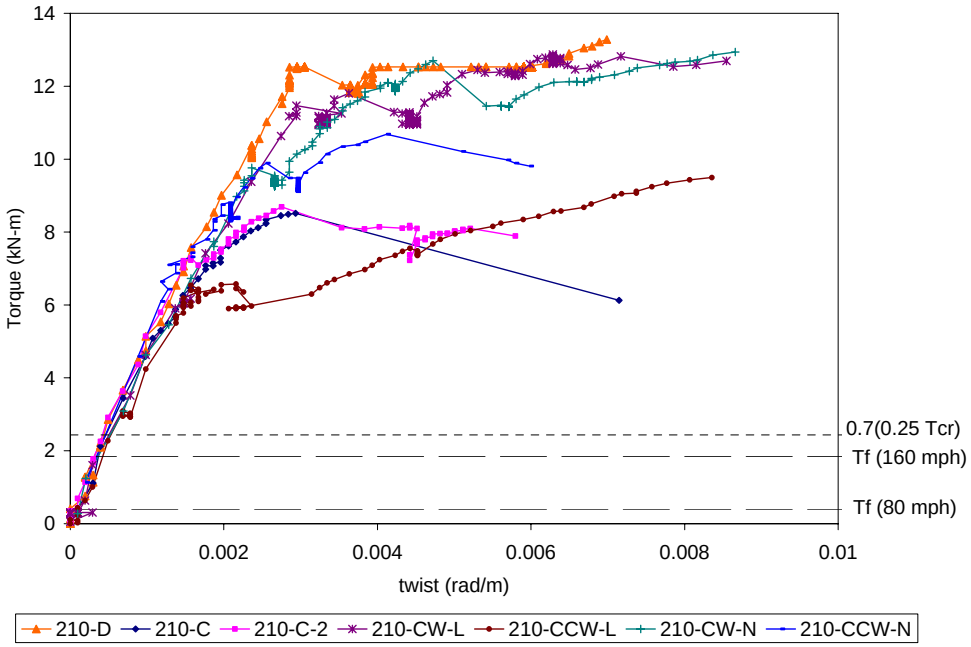

Figure 7.45: Applied factored torque versus 210 cracking torques

Chapter 8
Conclusions and Recommendations for Future Work

An investigation into the effect of helical reinforcement on the torsional capacity of prestressed concrete poles was completed. The objectives of the investigation were to analyze the Canadian code (CSA A14-07) and compare the minimum helical reinforcing requirements to other concrete pole codes. Spacing requirements and direction of the helical steel reinforcing effects on torsional capacity were determined and double and single helix reinforcement methods analyzed. The mode of failure and post-cracking behaviour were also presented and analyzed. The reason for inclusion of helical reinforcement in prestressed concrete poles and the main factors influencing the torsional capacity of prestressed concrete poles were determined. The investigation yielded the conclusions and results.

- The response of the poles could be modelled closely using a linear elastic torsion model, suggesting that the failure is at the cracking torque of the concrete. The model was dependent on the assumed modulus of elasticity and wall thickness. The torsional failure mode for concrete poles is brittle and sudden with no post-cracking ductility provided by the helical reinforcing steel. It appears that the added torsional capacity from the helical reinforcement is insignificant when compared to the torsional capacity contributed by the concrete.

- The helical reinforcing may influence the cracking torque capacity of the prestressed concrete pole. The helical steel provides some confinement to the inner concrete and also intercepts cracks and increases the cracking torque.

- Little difference in torsional capacity was observed between the clockwise (CW; engaged helical steel) and counter clockwise (CCW) helically reinforced specimens. For the smaller 165 mm tip specimens, the CW specimens had slightly higher cracking torque values. The trend was not observed with the 210 mm specimens. The helix direction was determined to be insignificant to the torsional capacity of the concrete pole.

- Spacing of the helical reinforcement as suggested by the CSA A14-07 code and twice the code spacing had little effect on the torsional capacity of the pole. Higher results were noted with 165 mm specimens when tighter spaced helical reinforcement was used.

- Quality assurance of the concrete, prestressing levels and wall thickness are all important factors for the torsional capacity of prestressed concrete poles. Segregation caused by poor concrete, low concrete strengths, and insufficient reinforcement for the transfer of prestressing loads cause longitudinal cracks to develop, which reduce the torsional capacity of the pole.

- The Compression Field Theory was found to better predict the post-cracking region of the concrete pole test results than the Softened Truss Model. For prestressed concrete poles it is apparent that the cover spalls and post-cracking loads are sustained by the helical reinforcement and interlock of the concrete.

- The pole cracking torque was best predicted by the ACI-318-05 code. CSA A23.3-04 and Eurocode 2 were less conservative than ACI. All codes predicted unconservative results on average and a large scatter in the predicted results was noted. The database of previous torsional tests had results scattered over a range of 5 to 10 kN-m regardless of the direction and method of helical reinforcement.

- Strut and tie modeling of the transfer zone determined that a 40 mm helical reinforcement spacing was needed for the 165 mm specimens in the first 500 mm from the tip. The 210 mm specimens required a 53 mm spacing in the prestressing transfer zone. CSA, ACI, and EC2 code determined maximum spacing of the minimum transverse reinforcement was between 47 – 62 mm for the 165 specimens and 40 – 49 mm for the 210 mm specimens. The strut and tie model and code spacing requirements indicate that all the 165 mm specimens and the large spaced 210 mm specimens (210-CW-L and 210-CCW-L) were insufficiently reinforced in the transfer zone. The insufficient reinforcement may explain the scatter of results observed during tested since the specimens could have been pre-cracked to different degrees.

- Torsional loads are typically not a governing factor in the design of concrete lighting poles. In the case of the 165 mm and 210 mm tip specimens the applied loads due to a standard fixture gave negligible or near negligible loads.

Potential exists for the simplification of the CSA A14-07 code in regards to minimum reinforcing requirements and torsional capacities. It is suggested that the requirements be modelled similar to the American (ASTM C 1089-06) requirements. A spacing of 30 mm to 50 mm is recommended in the

transfer zone (approximately 50 times the strand diameter) depending on the pole tip size. The American limit of 102 mm in the remaining portions of the pole requires further investigation. Proper spun cast concrete mixes and adequate concrete strengths, prestressing levels, and wall thickness all have a large impact on the torsional capacity of prestressed concrete poles and therefore should be emphasized in the CSA A14-07 design requirements.

It is recommended that an extensive testing program be undertaken to conclusively determine if direction and spacing have an effect on torsional capacity or to ultimately determine the factors causing the scatter in the results. Further torsional and helical reinforcement research should investigate the performance of prestressed concrete poles reinforced using the suggestions based on the strut and tie model results. If more torsional tests are performed on concrete poles, a method to entirely eliminate the flexural load other than the use of a restraining cable would be beneficial. Reducing the scatter of the results and providing conservative predictions of the cracking torque of prestressed concrete poles is desirable to provide safe, rationale concrete pole designs. A better understanding of the factors that influence the cracking torque in reinforced and prestressed concrete will allow for safer and more economical designs to be produced.

References

AASHTO LTS-3 (1994), “Standard Specification for Structural Supports for Highway Signs, Luminaries and Traffic Signals”, American Association of State Highway and Transportation Officials, Washington, D.C., U.S.A, 1994.

AASHTO LTS-4-M, “Standard Specification for Structural Supports for Highway Signs, Luminaries and Traffic Signals”, American Association of State Highway and Transportation Officials, Washington, D.C., U.S.A, 2001.

ACI Committee 318, “Building Code Requirements for Structural Concrete and Commentary (ACI 318-05)”, American Concrete Institute, Farmington Hills, Detroit, Michigan, U.S.A, 2005.

ACI Committee 438, “Tentative Recommendations for the Design of Reinforced Concrete Members to Resist Torsion”, ACI Journal, January 1969, 8 pp.

ACI Committee 445, State of the Art Report: Design for Torsion in Concrete Structures - Draft Copy, American Concrete Institute, Detroit, 2006, 173 pp.

Ali, M.A., and White, R.N., “Toward a Rational Approach for Design of Minimum Torsion Reinforcement”, ACI Structural Journal, Vol. 96, No. 1, January-February, 1999, pp. 40-46.

ASCE Concrete Pole Task Committee, Guide for the Design and Use of Concrete Poles, American Society of Civil Engineers, New York, 1987, 52 pp.

ASCE-PCI Committee Report, “Guide for the Design of Prestressed Concrete Poles”, PCI Journal, November-December 1997, Vol. 42. No. 6, pp. 93-134.

ASTM C 1089-06, “Standard Specification for Spun Cast Prestressed Concrete Poles”, ASTM International, West Conshohocken, PA., U.S.A, 2006.

ASTM C 1089-97, “Standard Specification for Spun Cast Prestressed Concrete Poles”, ASTM International, West Conshohocken, PA., U.S.A, 1997.

Bolander, J., Sowlat, K., and Naaman, A.E., “Design Considerations for Tapered Prestressed Concrete Poles”, PCI Journal, Vol. 33, No. 1, January-February, 1988, pp. 44-66.

Rosson, B.T., Rohde, J.R., and Klovsky, R., “Behaviour and Design of Static Cast Prestressed Concrete Distribution Poles”, PCI Journal, Vol. 41, No. 5, September-October, 1996, pp. 94-107.

CAN/CSA-S6-06, “Canadian Highway Bridge Design Code (CHBDC)”, Canadian Standards Association International, Mississauga, Ontario, Canada, 2006.

CSA A14-M1979, “Concrete Poles”, Canadian Standards Association International, Mississauga, Ontario, Canada, 1979.

CSA A14-00, “Concrete Poles”, Canadian Standards Association International, Mississauga, Ontario, Canada, 2000.

CSA A14-07, “Concrete Poles”, Canadian Standards Association International, Mississauga, Ontario, Canada, 2007.

Chahrour, A.H., and Soudki, K.A., “Structural Retrofitting of Deteriorated Concrete Lighting Poles Using FRP Sheets in Wet Layup – Field Application”, Journal of Composites for Construction, ASCE, May-June, 2006, pp 234-243.

Collins, M.P. and Mitchell, D., “Shear and Torsion Design of Prestressed and Non-Prestressed Concrete Beams”, Journal of the Prestressed Concrete Institute, Vol. 25, No. 5, September-October, 1980, pp. 32-100.

CSA A23.3-04, “Design of Concrete Structures”, Canadian Standards Association International, Mississauga, Ontario, Canada, 2004.

DIN 1045, “Tragwerke aus Beton, Stahlbeton und Spannbeton – Teil 1: Bemessung und Konstruktion (Concrete, reinforced and prestressed concrete structures – Part 1: Design)”, DIN 1045-1:2001-07, Deutsche Institut für Normung e.V., Berlin, Germany, June 2001.

DIN EN 12843, “ Betonfertigteile – Maste (Precast Concrete Products –Masts and Poles)”, DIN EN 12843:2004, Deutsche Institut für Normung e.V., Berlin, Germany, 2004.

DIN EN 40-4, “Lichtmaste – Teil 4: Anforderungen an Lichtmaste aus Stahl- und Spannbeton (Lighting columns - Part 4: Requirements for reinforced and prestressed concrete lighting columns)”, DIN EN 40-4:2005, Deutsche Institut für Normung e.V., Berlin, Germany, June 2006.

DIN 4228, “Werkmäßig hergestellte Betonmaste”, Deutsche Institut für Normung e.V., Berlin, Germany, February 1989.

Dilger, W.H., and Ghali, A., “Response of Spun Cast Concrete Poles to Vehicle Impact”, PCI Journal, Vol. 31, No. 1, January-February, 1986, pp. 62-82.

Dilger, W.H., Ghali, A., and Rao, S.V.K.M., “Improving the Durability and Performance of Spun-Cast Concrete Poles”, PCI Journal, Vol. 41, No. 2, March-April, 1996, pp. 68-90.

Dilger, W.H., and Rao, S.V.K.M., “High Performance Concrete Mixtures for Spun-Cast Concrete Poles”, PCI Journal, Vol. 42, No. 2, July-August, 1997, pp. 82-96.

EN 1992-1-1:2004, “Eurocode 2: Design of Concrete Structures – Part 1-1: General rules and rules for buildings”, BS EN 1992-1-1:2004, British Standards Institution, December 2004.

Fouad, F.H., Scott, N.L., Calvert, E., and Donovan, M., “Performance of Spun Prestressed Concrete Poles During Hurricane Andrew”, PCI Journal, Vol. 39, No. 2, March-April, 1994, pp. 102-110.

Fouad, F.H., Sherman, D, and Werner, R.J., “Spun Prestressed Concrete Poles – Past, Present, and Future”, Concrete International, Vol. 14 No. 11, November 1992, pp. 25-29.

Ghoneim, M.G., and MacGregor, J.G., “Evaluation of Design Procedures for Torsion in Reinforced and Prestressed Concrete”, *Report* No. 184, Department of Civil Engineering, University of Alberta, Edmonton, February 1993, 301 pp.

Hsu, T. T. C., “Torsion of Structural Concrete – A Summary on Pure Torsion”, Torsion of Structural Concrete, Special Publication No. 18-6, American Concrete Institute, Detroit, 1968.

Hsu, T. T. C., Torsion of Reinforced Concrete, Van Nostrand Reinhold, Inc., New York, 1984, 544 pp.

Hsu, T. T. C. and Mo, Y.L., “Softening of Concrete in Torsional Members – Prestressed Concrete”, ACI Journal, Vol. 82, No. 5, September-October, 1985, pp. 603-615.

Hsu, T. T. C., “Softened Truss Model Theory for Shear and Torsion”, Structural Journal of the American Concrete Institute, Vol. 85, No. 6, November–December, 1988, pp. 624-635.

Hsu, T. T. C. and Zhang, L. X., “Nonlinear Analysis of Membrane Elements by Fixed-Angle Softened-Truss Model”, ACI Structural Journal, Vol. 94, No. 5, 1997, pp. 483-492.

Kaufmann, J.P., Hesselbarth, D., Moser, K., and Terrasi, G.P., “Application of fiber reinforced high performance composites in spun-cast elements”, Materials and Structures, V. 38 No. 279, June, 2005, pp. 549-555.

Koutchoukali, N. and Belarbi, A., “Torsion of High-Strength Reinforced Concrete Beams and Minimum Reinforcement Requirement”, ACI Structural Journal, Vol. 98, No. 4, July-August, 2001, pp. 658-666.

MagGregor, J.G., and Ghoneim, M.G., “Design for Torsion”, ACI Journal, Vol. 92, No. 2, March-April, 1995, pp. 211-218.

McMullen, A.E. and El-Degwy, W.M., “Prestressed Concrete Tests Compared With Torsion Theories”, PCI Journal, Vol. 35, No. 5, September-October, 1985, pp. 96-127.

Mitchell, D., and Collins, M.P., “Diagonal Compression Field Theory – A Rational Model for Structural Concrete in Pure Torsion”, ACI Journal, Vol. 71, August 1974, pp. 396-408.

PCI Committee on Prestressed Concrete Poles, “Guide Specification for Prestressed Concrete Poles”, PCI Journal, Vol. 27, No 3. May-June, 1982, 13 pp.

PCI Committee on Prestressed Concrete Poles, “Guide for the Design of Prestressed Concrete Poles”, PCI Journal, Vol. 28, No. 3, May-June 1983, 67 pp.

Rahal, K. N., “Torsional Strength of Reinforced Concrete Beams”, Canadian Journal of Civil Engineering, Vol. 27, No. 3, 2000, pp. 445–453.

Rahal, K.N. and Collins, M.P., “Simple Model for Predicting Torsional Strength of Reinforced and Prestressed Concrete Sections”, ACI Structural Journal, Vol. 93, No. 6, November-December, 1996, pp. 658-666.

Rodgers, T.E., “Prestressed Concrete Poles – State of the Art”, PCI Journal, Vol. 29, No. 4, September-October 1984, 53 pp.

Smith, P., “Impact Testing of Lighting Poles and Sign Supports, 1967-1968”, *Report* RR158, Department of Highways Ontario Canada, March, 1970, 33 pp.

Terrasi, G.P., Battig, G., and Bronnimann, R., “Pylons made of high-strength spun concrete and prestressed with carbon fiber reinforced plastic for high power transmission lines”, International Journal of Materials and Product Technology, Vol. 17 No. 1-2, 2002, pp. 32-45.

Terrasi, G.P., and Lees, J.M., “CFRP Prestressed Concrete Lighting Columns”, Special Publication No. 215-3, American Concrete Institute, 2003, pp. 55-74.

Wang, M., Dilger, W., and Kuebler, U., “High Performance Concrete for Spun-Cast Utilities Poles”, Proceedings of the 2001 Second International Conference on Engineering Materials Volume 2, Canadian Society of Civil Engineers and Japan Society of Civil Engineers, August 2001, pp. 143 - 154.

Appendix A

Pole Analysis Output for Design of Specimen

165 mm Specimen Graphical Factored Resistances

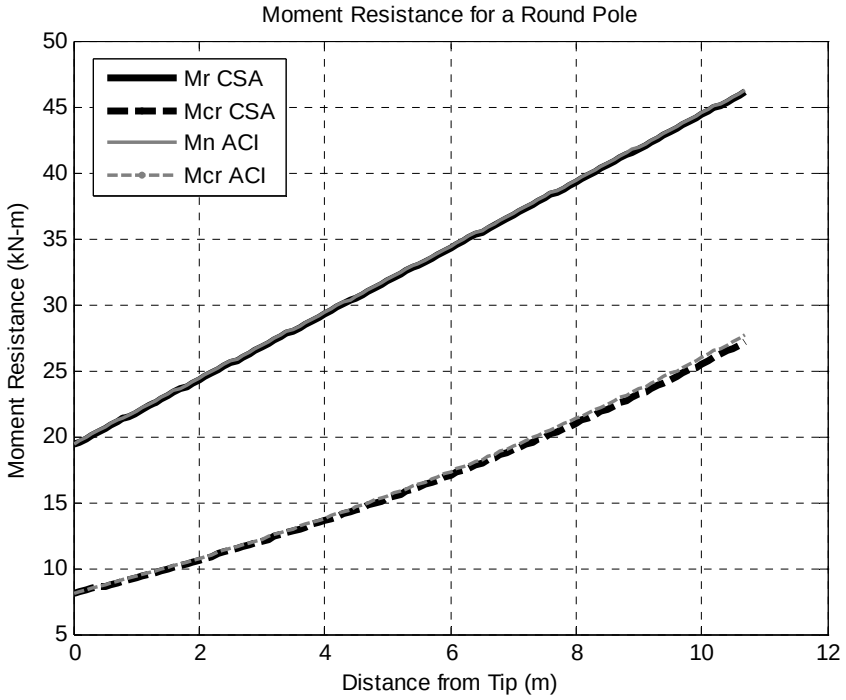

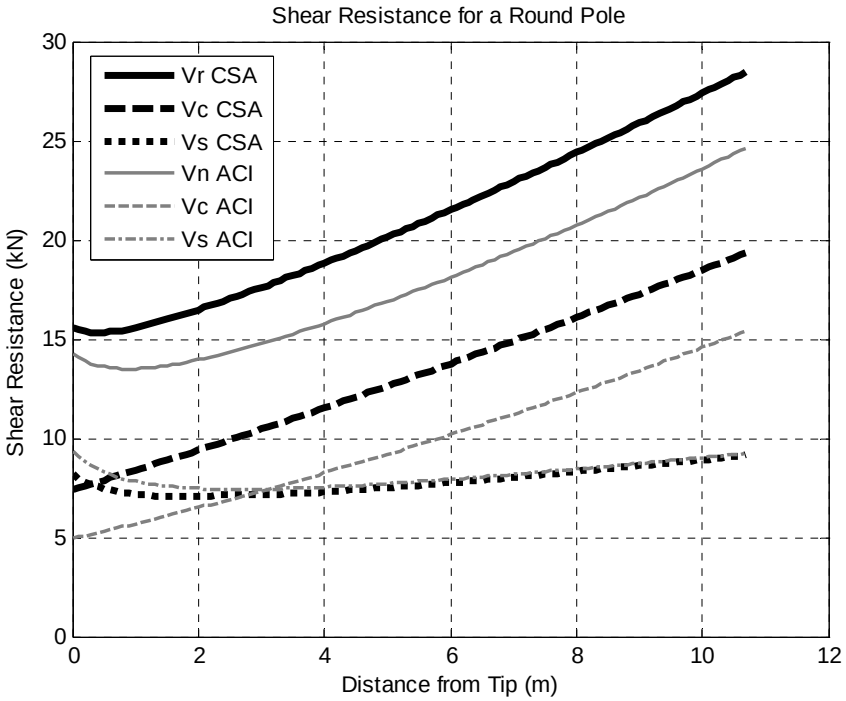

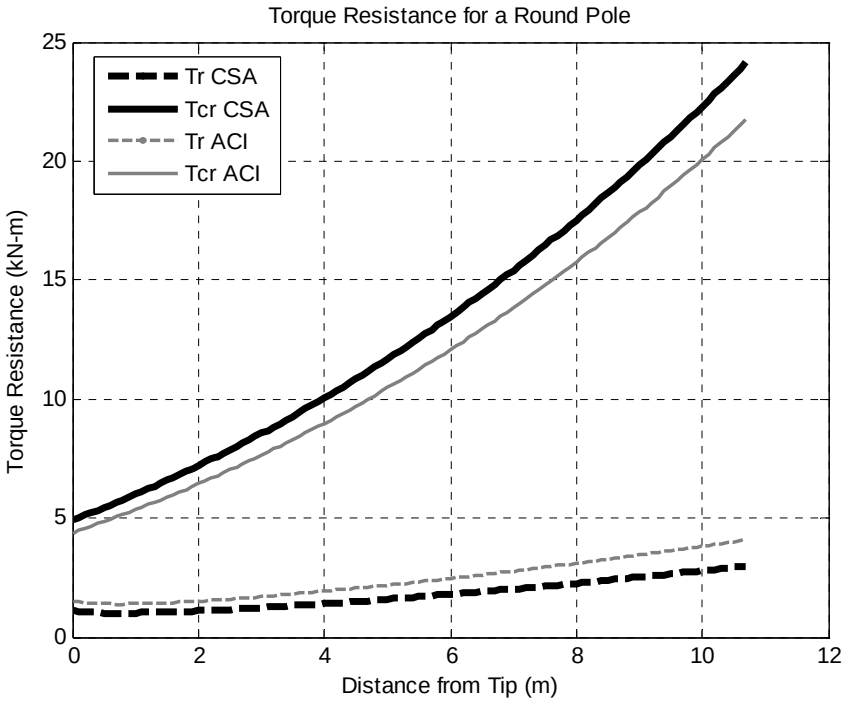

165 mm Specimen Graphical Unfactored Resistances

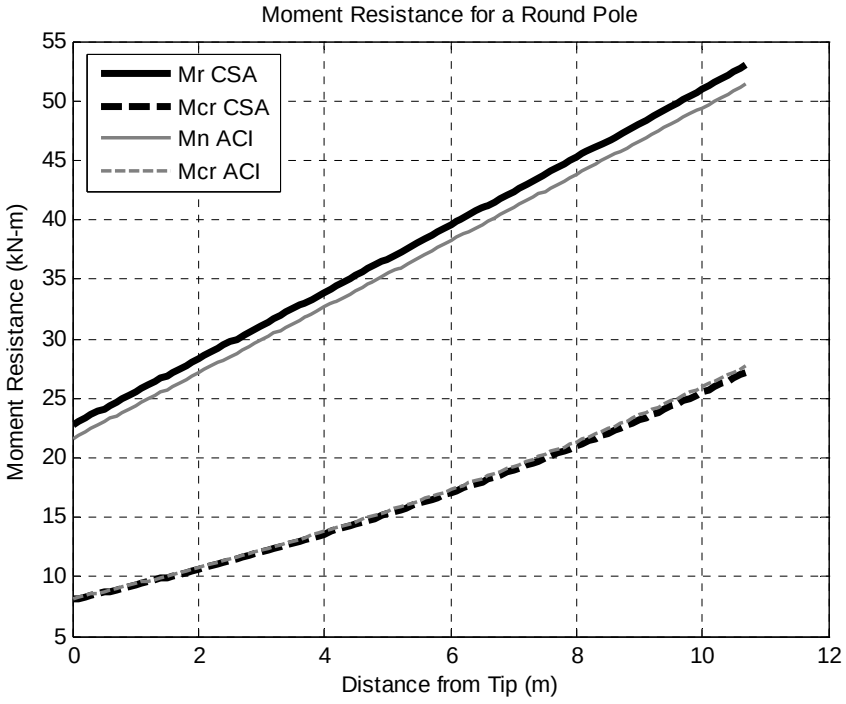

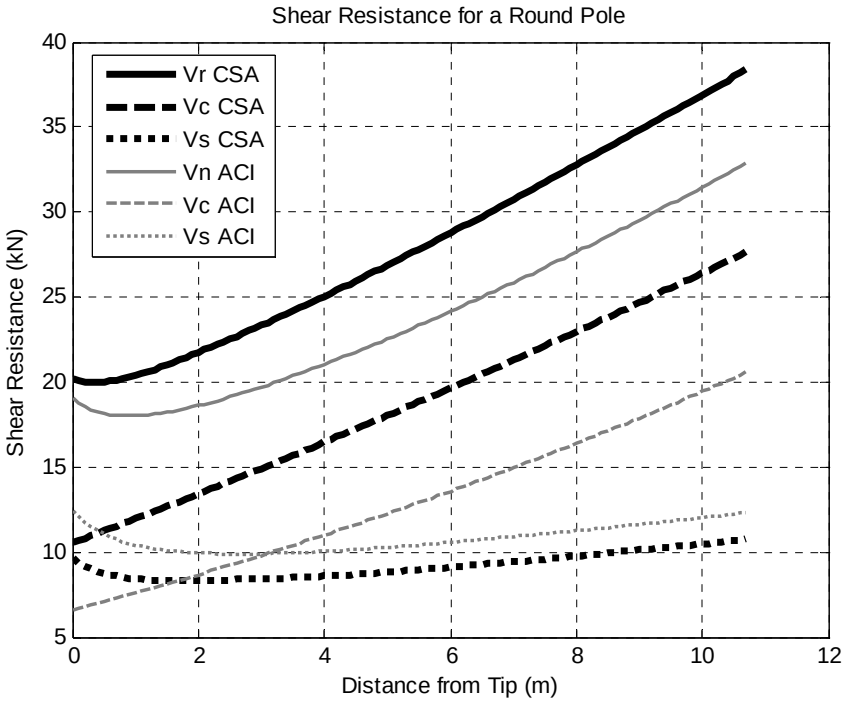
Shear Resistance for a Round Pole
Vr CSA
Vc CSA
Vs CSA
Vn ACI
Vc ACI
Vs ACI
Shear Resistance (kN)
Distance from Tip (m)
40
35
30
25
20
15
10
5
0
2
4
6
8
10
12

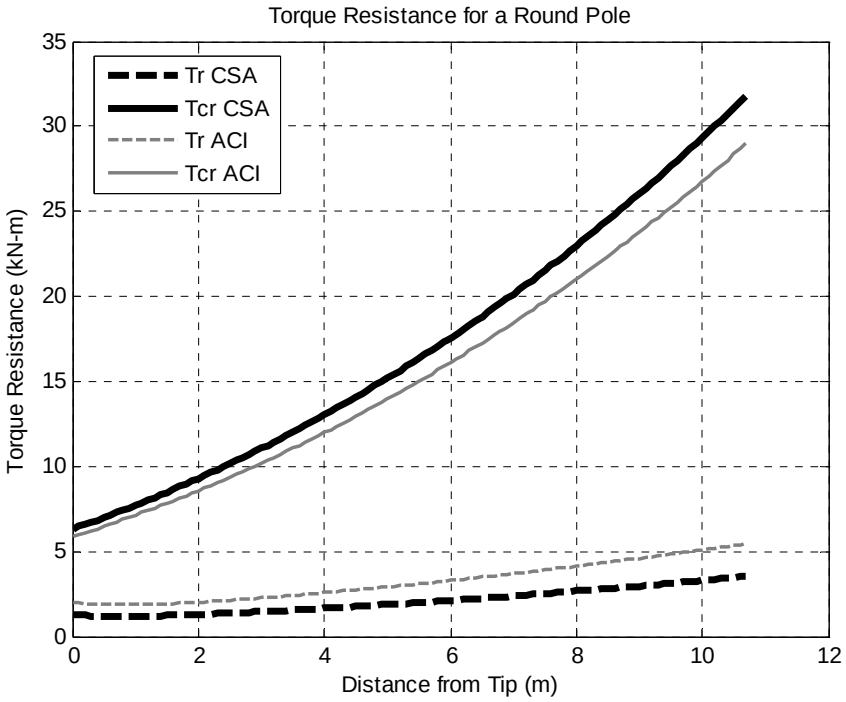
Torque Resistance for a Round Pole
Tr CSA
Tcr CSA
Tr ACI
Tcr ACI
Torque Resistance (kN-m)
Distance from Tip (m)
35
30
25
20
15
10
5
0
0
2
4
6
8
10
12

210 mm Specimen Graphical Factored Resistances

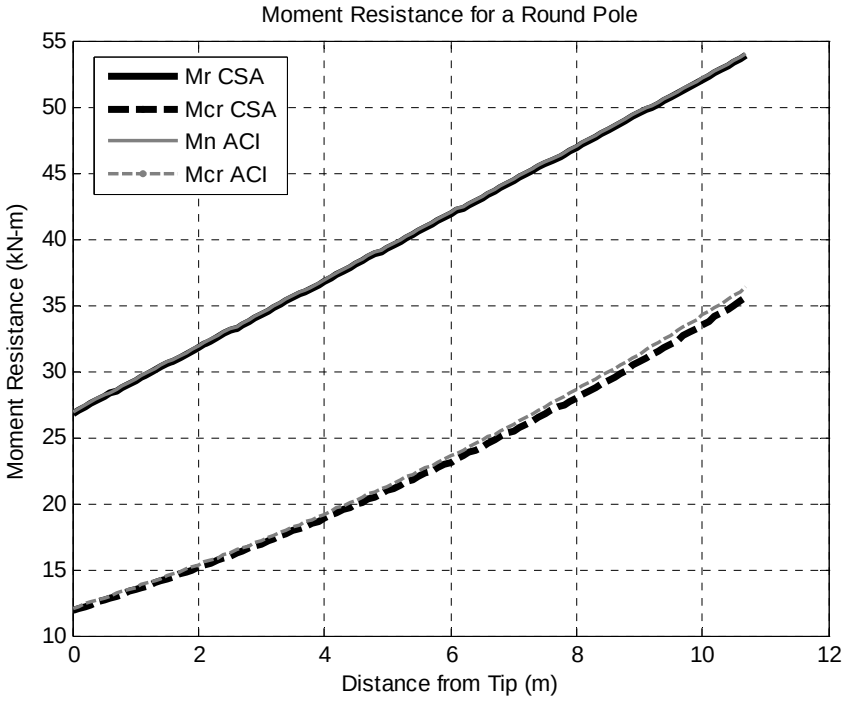

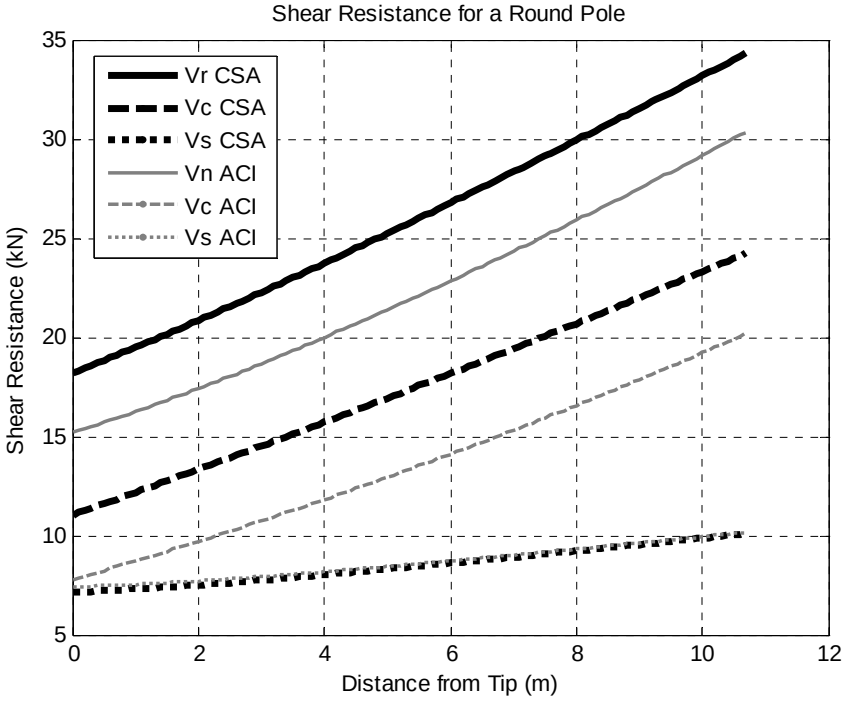

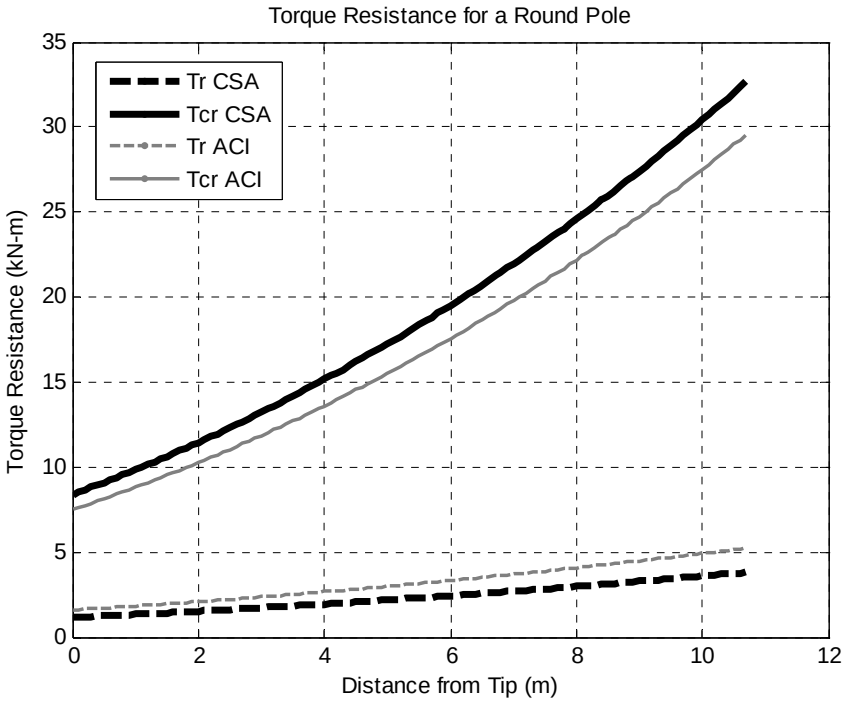

210 mm Specimen Graphical Unfactored Resistances

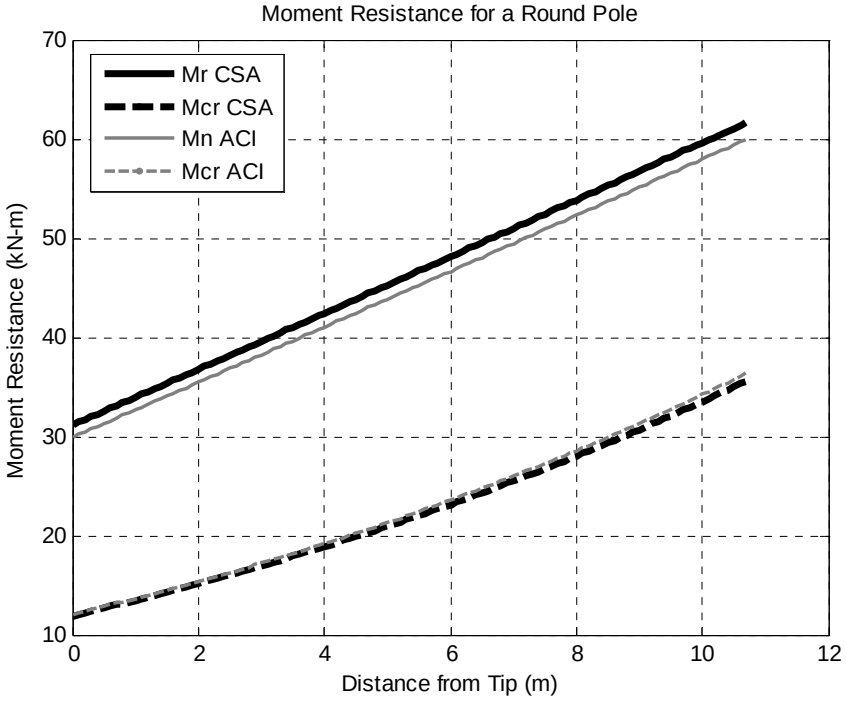

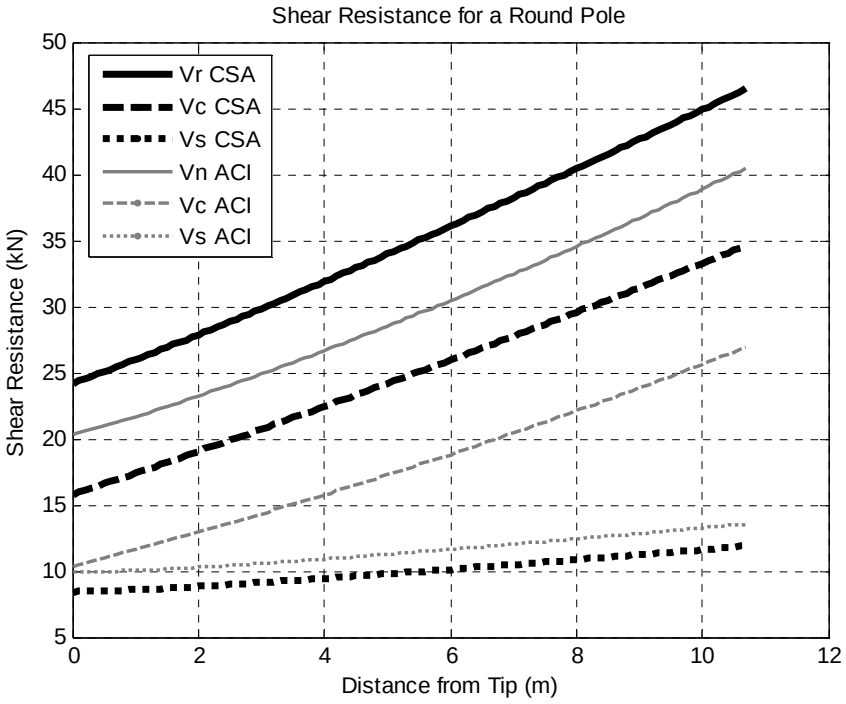
Shear Resistance for a Round Pole
Vr CSA
Vc CSA
Vs CSA
Vn ACI
Vc ACI
Vs ACI
Shear Resistance (kN)
Distance from Tip (m)
50
45
40
35
30
25
20
15
10
5
0
2
4
6
8
10
12

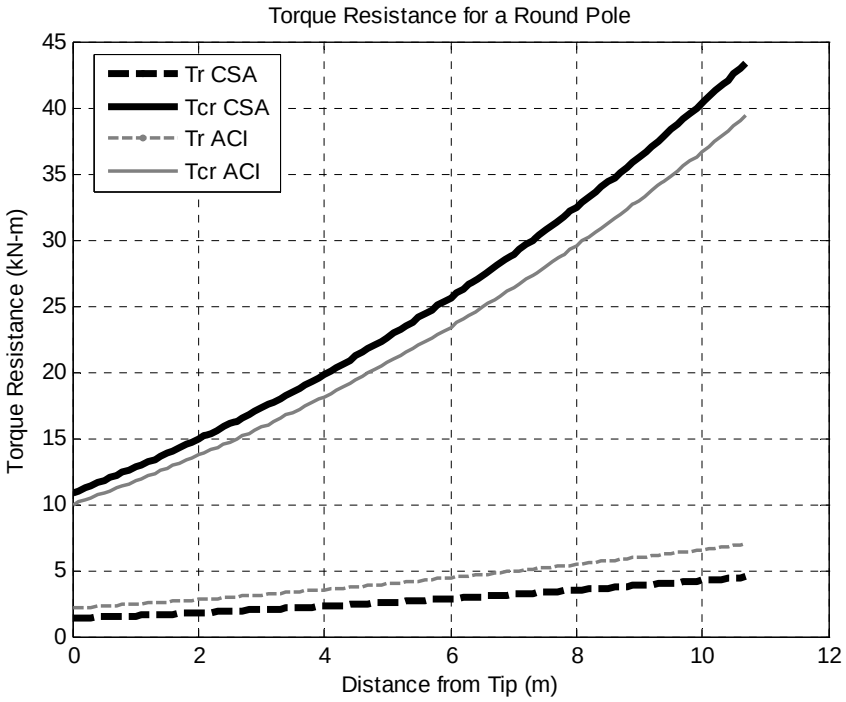
Torque Resistance for a Round Pole
Tr CSA
Tcr CSA
Tr ACI
Tcr ACI
Torque Resistance (kN-m)
Distance from Tip (m)
45
40
35
30
25
20
15
10
5
0
0
2
4
6
8
10
12

Appendix B

Specimen Material Reports

Sky Cast - Daily Batch Record

Work Order: **W000350**

Customer Order: **07-168**

Poles per Mold: **2**

Part ID: **SC-210-ARO-CON-DCG-P-01**

Length: **21**

Tip Size:

Colour: **CO**

Batch Size: **0.38 m³**

Unit	Target	Actual	Ingredients
kg	402	397	Coarse Regular
kg	294	305	Sand Regular
kg	162	161	Type 30 HSF Cement (82:10:8) HEb-SF-S
kg	51	40	Water
mL	646	687	Air Entraining Agent Catexol AE60
mL	2109	2150	Super Plasticizer Catexol 1000 SPMN
mL	408	450	Water Reducing Agent Catexol 900 N
kg	909		**Final Water Added:**

Date: Aug 22/07

Time: (AM) PM

Signature:

BATCH NUMBER: 19200 DESTINATION:CALL #11 STN#3 BATCH: 1 OF 999
: 240
FORMULA #: 18 NAME:POLE375R BATCH SIZE: 909 KG 0.38 CM
START TIME:10:13:18 FINISH TIME:10:19:55 ELAPSED TIME: 397.00 SEC

SCALE	INGREDIENT	TARGET DRY	TARGET WET	ACTUAL DRY	ACTUAL WET
AGGREGATE					
	13MM STONE	400	401	396	397 KG
	SAND	295	306	294	305 KG
CEMENT					
	TYPE 30 HSF	162	162	162	162 KG
WATER					
	WATER	40	40	40	40 KG
					903 KG
ADMIXES:					
AIR ENTRAINMENT		646		688	ML
PLASTCISER		2109		2150	ML
900N		409		450	ML

WATER IN BATCH:
WATER IN AGGREGATE: 12 L
WATER ADDED TO BATCH: 40 L
TOTAL WATER IN BATCH: 52 L
WATER / CEMENT RATIO: 0.32
========== END OF REPORT==========

Daily Compressive Strength Test Report

Date: Aug. 22/07

Fresh Concrete Data					Comments:
Mix No.:	6				
Mix Type:	CO				
Kiln No:	2				
Mould No.:	RO-53				
Length: (ft)	21				
Class:	A				
Type:	RO				
Time of Mould:	10:57				
Slump (50 ±20)	35				
Temperature (10-35°C)	25				
Air Content (5-8 %)	4.8				

Moisture Content (%)					Comments:
Mass of Wet & Tare (A) (g)	1982.1				
Mass of Dry & Tare (B) (g)	1900.5				
Tare (C) (g)	816.5				
Moisture in Mix (A-B) (g)	81.6				
Mass of Wet (A-C) (g)	1165.6				
Moisture Content (A-B)/(A-C)	7.0%				

Density (kg/m^3)					Comments:
Mass & Base Wet (A) (kg)	20.84				
Base (B) (kg)	3.70	3.70	3.70	3.70	
Mass Concrete (A-B) (kg)	17.14				
Volume of Base (C) (m^3)	0.007	0.007	0.007	0.007	
Fresh Density (A-B)/C	2448.6				

Time of Tests: _____

Compressive Strength	Batch #___ Age (h):_____	
Cylinder Location	North	South
Mass (g)		
Strength (kN)		
Strength (MPa)		

Batch #___ Age (h):_____		Compressive Strength
North	South	Cylinder Location
		Mass (g)
		Strength (kN)
		Strength (MPa)

Tested By: SARAH REINHOLT

Signature: _____

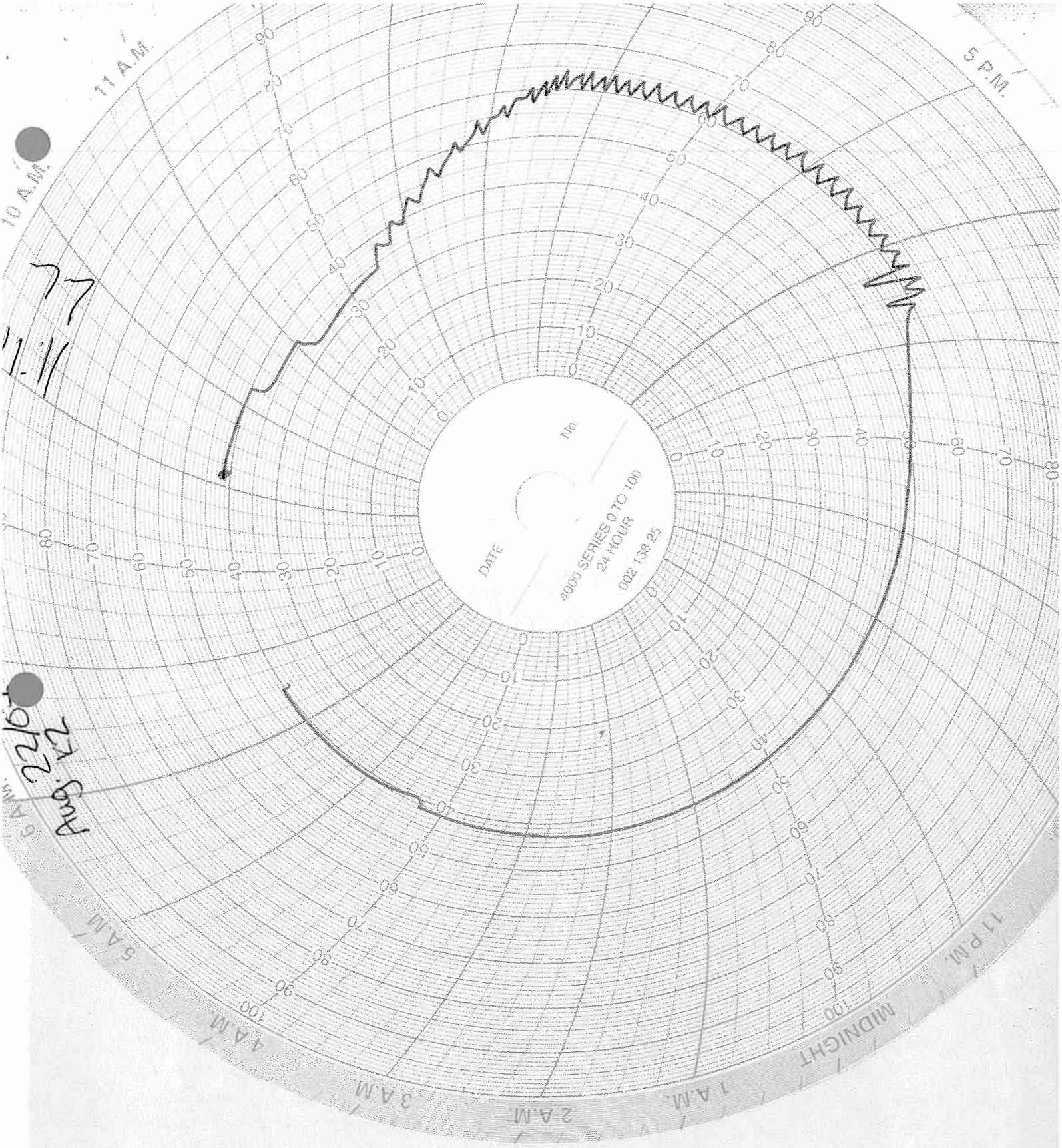
11 A.M.
10 A.M.
5 P.M.
DATE
No.
4000 SERIES 0 TO 100
24 HOUR
002 138 25
MIDNIGHT
1 A.M.
2 A.M.
3 A.M.
4 A.M.
5 A.M.
6 A.M.
11 P.M.

Sky Cast - Daily Batch Record

Work Order: **W000350**

Customer Order: **07-168**

Poles per Mold: **2**

Part ID: **SC-210-ARO-CON-DCG-P-01**

Length: **21**

Tip Size:

Colour: **CO**

Batch Size: **0.46 m³**

Unit	Target	Actual	Ingredients
kg	486	491	Coarse Regular
kg	356	371	Sand Regular
kg	196	194	Type 30 HSF Cement (82:10:8) HEb-SF-S
kg	62	45	Water
mL	782	812	Air Entraining Agent Catexol AE60
mL	2553	2600	Super Plasticizer Catexol 1000 SPMN
mL	494	550	Water Reducing Agent Catexol 900 N
kg	1100		**Final Water Added:**

Date: Aug 23/07

Time: 9:23 (AM) PM

Signature: [signature]

BATCH NUMBER: 19217 DESTINATION:CALL #11 STN#3 BATCH: 1 OF 999
: 240
FORMULA #: 18 NAME:POLE375R BATCH SIZE: 1100 KG 0.46 CM
START TIME:09:11:46 FINISH TIME:09:21:14 ELAPSED TIME: 568.00 SEC

SCALE	INGREDIENT	TARGET DRY	TARGET WET	ACTUAL DRY	ACTUAL WET
AGGREGATE					
	13MM STONE	484	485	484	485 KG
	SAND	357	374	354	371 KG
CEMENT					
	TYPE 30 HSF	196	196	194	194 KG
WATER					
	WATER	45	45	45	45 KG
DELIVERED WEIGHT:					1096 KG
ADMIXES:					
AIR ENTRAINMENT		782		813	ML
PLASTCISER		2553		2600	ML
900N		495		550	ML

WATER IN BATCH:
WATER IN AGGREGATE: 18 L
WATER ADDED IN BATCH: 45 L
TOTAL WATER IN BATCH: 63 L
ACTUAL W/C RATIO: 0.33

========== END OF REPORT==========

Daily Compressive Strength Test Report

Date: Aug. 23/07

Fresh Concrete Data					Comments:
Mix No.:	6				
Mix Type:	CO				
Kiln No:	1				
Mould No.:	RO-53				
Length: (ft)	21				
Class:	A				
Type:	RO				
Time of Mould:	9:49				
Slump (50 ±20)	35				
Temperature (10-35°C)	27.5				
Air Content (5-8 %)	6.1				

Moisture Content (%)					Comments:
Mass of Wet & Tare (A) (g)	1645.9				
Mass of Dry & Tare (B) (g)	1587.3				
Tare (C) (g)	815.7				
Moisture in Mix (A-B) (g)	58.6				
Mass of Wet (A-C) (g)	830.2				
Moisture Content (A-B)/(A-C)	7.06				

Density (kg/m^3)					Comments:
Mass & Base Wet (A) (kg)	20.44				
Base (B) (kg)	3.70	3.70	3.70	3.70	
Mass Concrete (A-B) (kg)	16.74				
Volume of Base (C) (m^3)	0.007	0.007	0.007	0.007	
Fresh Density (A-B)/C	2391.4				

Time of Tests: _____

Compressive Strength	Batch #___ Age (h):_____	
Cylinder Location	North	South
Mass (g)		
Strength (kN)		
Strength (MPa)		

Batch #___ Age (h):_____		Compressive Strength
North	South	Cylinder Location
		Mass (g)
		Strength (kN)
		Strength (MPa)

Tested By: SARAH REINHOLT

Signature: _____

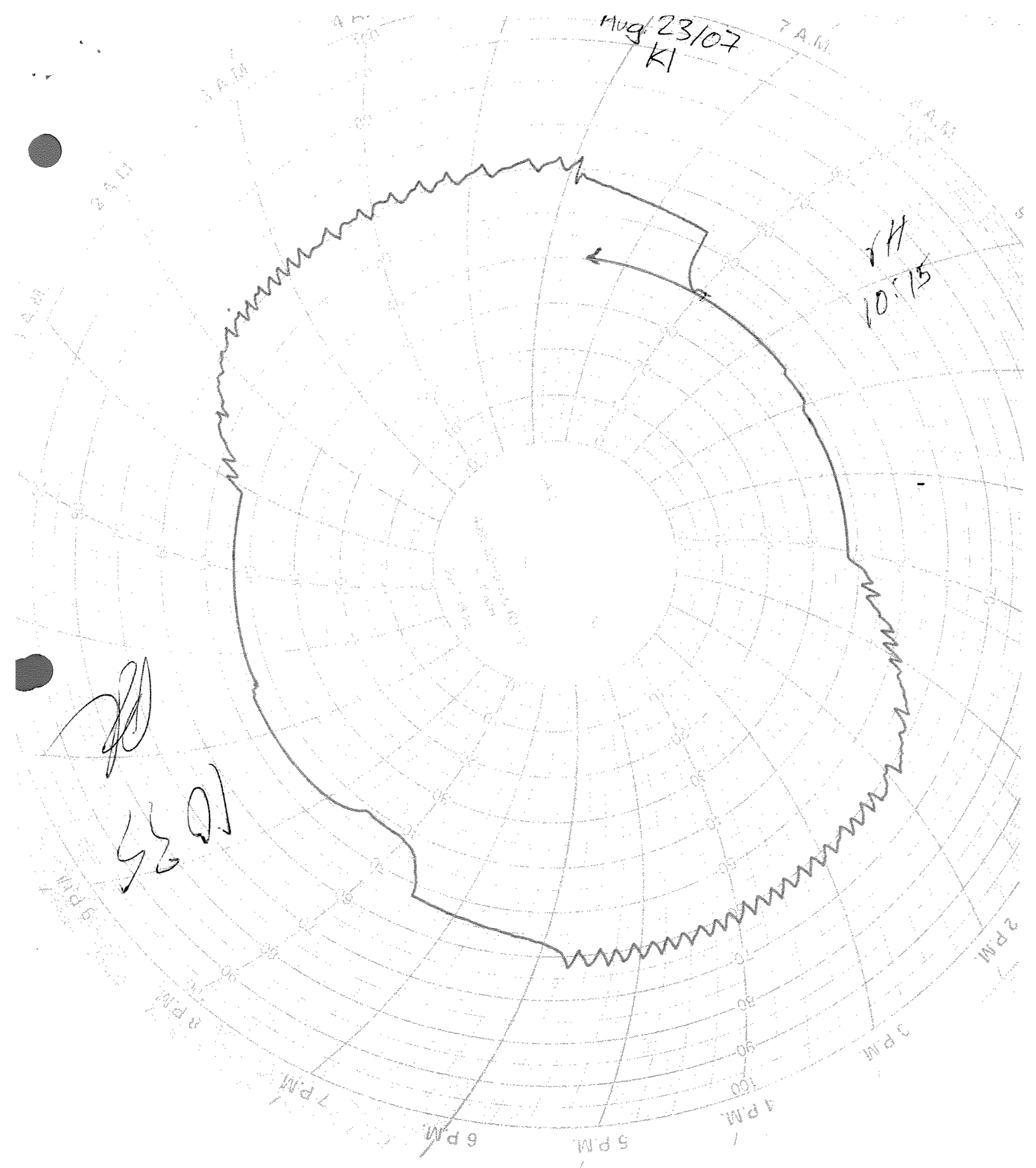
Aug 23/07
KI
VH
10:15
10:45

Sky Cast - Daily Batch Record

Work Order: **W000350**

Customer Order: **07-168**

Poles per Mold: **2**

Part ID: **SC-210-ARO-CON-DCG-P-01**

Length: **21**

Tip Size:

Colour: **CO**

Batch Size: **0.46 m³**

Unit	Target	Actual	Ingredients
kg	486	482	Coarse Regular
kg	356	378	Sand Regular
kg	196	194	Type 30 HSF Cement (82:10:8) HEb-SF-S
kg	62	44	Water
mL	782	812	Air Entraining Agent Catexol AE60
mL	2553	2600	Super Plasticizer Catexol 1000 SPMN
mL	494	500	Water Reducing Agent Catexol 900 N
kg	1100		**Final Water Added:**

Date: Aug 24/07

Time: 11:52 (AM) PM

Signature:

(10)

07-168 RO-53 0.46 18 19° 28° 26.4 22.9 4 good

Sky Cast - Daily Batch Record

Work Order: **W000350**

Customer Order: **07-168**

Poles per Mold: **2**

Part ID: **SC-210-ARO-CON-DCG-P-01**

Length: **21**

Tip Size:

Colour: **CO**

Batch Size: **0.46 m³**

Unit	Target	Actual	Ingredients
kg	486	497	Coarse Regular
kg	356	369	Sand Regular
kg	196	194	Type 30 HSF Cement (82:10:8) HEb-SF-S
kg	62	46	Water
mL	782	812	Air Entraining Agent Catexol AE60
mL	2553	2600	Super Plasticizer Catexol 1000 SPMN
mL	494	500	Water Reducing Agent Catexol 900 N
kg	1100		**Final Water Added:**

Date: Aug 24/07

Time: 11:23 (AM) PM

Signature: [signature]

SCRAPED.

9

07-168 · 80-53 0.46 18 19° 28° 75.9 23.3 2 Good Scrap.

Daily Compressive Strength Test Report

Date: _____

Fresh Concrete Data					Comments:
Mix No.:	8				
Mix Type:	CO				
Kiln No:	1				
Mould No.:	RO-53				
Length: (ft)	21				
Class:	A				
Type:	RO				
Time of Mould:	12:11				
Slump (50 ±20)	40				
Temperature (10-35°C)	28				
Air Content (5-8 %)	6.7				

Moisture Content (%)					Comments:
Mass of Wet & Tare (A) (g)					
Mass of Dry & Tare (B) (g)					
Tare (C) (g)					NOT COMPLETED
Moisture in Mix (A-B) (g)					
Mass of Wet (A-C) (g)					
Moisture Content (A-B)/(A-C)					

Density (kg/m^3)					Comments:
Mass & Base Wet (A) (kg)	20.39				
Base (B) (kg)	3.70	3.70	3.70	3.70	
Mass Concrete (A-B) (kg)	16.69				
Volume of Base (C) (m^3)	0.007	0.007	0.007	0.007	
Fresh Density (A-B)/C	2384.3				

Time of Tests: _____

Compressive Strength	Batch #___ Age (h):_____	
Cylinder Location	North	South
Mass (g)		
Strength (kN)		
Strength (MPa)		

Batch #___ Age (h):_____		Compressive Strength
North	South	Cylinder Location
		Mass (g)
		Strength (kN)
		Strength (MPa)

Tested By: _____

Signature: _____

40 mm.
28°
6.7%

20.39 kg

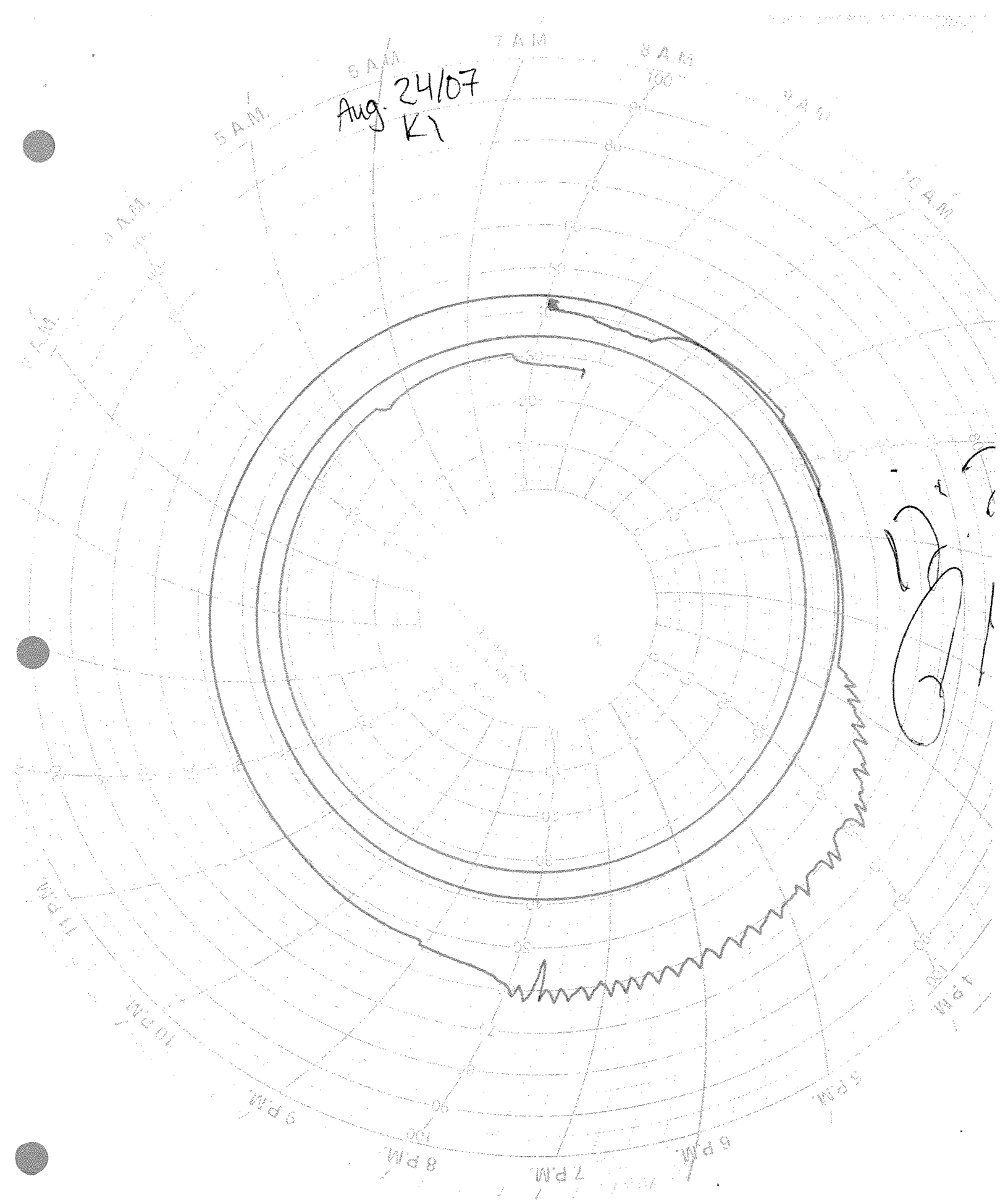
Aug. 24/07
K1
7 A.M.
8 A.M.
9 A.M.
10 A.M.
11 A.M.
12 Noon
1 P.M.
2 P.M.
3 P.M.
4 P.M.
5 P.M.
6 P.M.
7 P.M.
8 P.M.
9 P.M.
10 P.M.
11 P.M.

AUG 27 2007

SKY CAST INC. GENIE-II BATCH REPORT DATE:08-27-1998
ATCH NUMBER: 19713 DESTINATION:CALL #11 STN#3 BATCH: 1 OF 999
240
O[redacted]LA #: 18 NAME:POLE375R BATCH SIZE: 1124 KG 0.47 CM
START TIME:10:56:43 FINISH TIME:11:04:50 ELAPSED TIME: 487.00 SEC

CALE	INGREDIENT	TARGET DRY	TARGET WET	ACTUAL DRY	ACTUAL WET	
GGREGATE						
	13MM STONE	494	496	499	500	KG
	SAND	365	377	367	380	KG
EMENT						
	TYPE 30 HSF	200	200	206	206	KG TOLERANCE ERRO
ATER						
	WATER	50	50	50	50	KG

ELIVERED WEIGHT: 1136 KG
DMIXES:

IR ENTRAINMENT	799	963	ML
LASTCISER	2609	2650	ML
00N	505	500	ML

ATER IN BATCH:

WATER IN AGGREGATE:	14 L
WATER ADDED TO BATCH:	50 L
TOTAL WATER IN BATCH:	64 L
WATER / CEMENT RATIO:	0.31

END OF REPORT

Daily Compressive Strength Test Report

Date: Aug. 27/07

Fresh Concrete Data					Comments:
Mix No.:	7				
Mix Type:	CO				
Kiln No:	3				
Mould No.:	RO-53				
Length: (ft)	21				
Class:	A				
Type:	RO				
Time of Mould:	11:30				
Slump (50 ±20)	65				
Temperature (10-35°C)	28				
Air Content (5-8 %)	8.2?				

Moisture Content (%)					Comments:
Mass of Wet & Tare (A) (g)	1619.7				
Mass of Dry & Tare (B) (g)	1565.5				
Tare (C) (g)	815.8				
Moisture in Mix (A-B) (g)					
Mass of Wet (A-C) (g)					
Moisture Content (A-B)/(A-C)	6.7				

Density (kg/m^3)					Comments:
Mass & Base Wet (A) (kg)	20.18				
Base (B) (kg)	3.70	3.70	3.70	3.70	
Mass Concrete (A-B) (kg)					
Volume of Base (C) (m^3)	0.007	0.007	0.007	0.007	
Fresh Density (A-B)/C	2754.3				

Time of Tests: _____

Compressive Strength	Batch #___ Age (h):_____	
Cylinder Location	North	South
Mass (g)		
Strength (kN)		
Strength (MPa)		

Batch #___ Age (h):_____		Compressive Strength
North	South	Cylinder Location
		Mass (g)
		Strength (kN)
		Strength (MPa)

Tested By: SARAH REINHOLT

Signature: _____

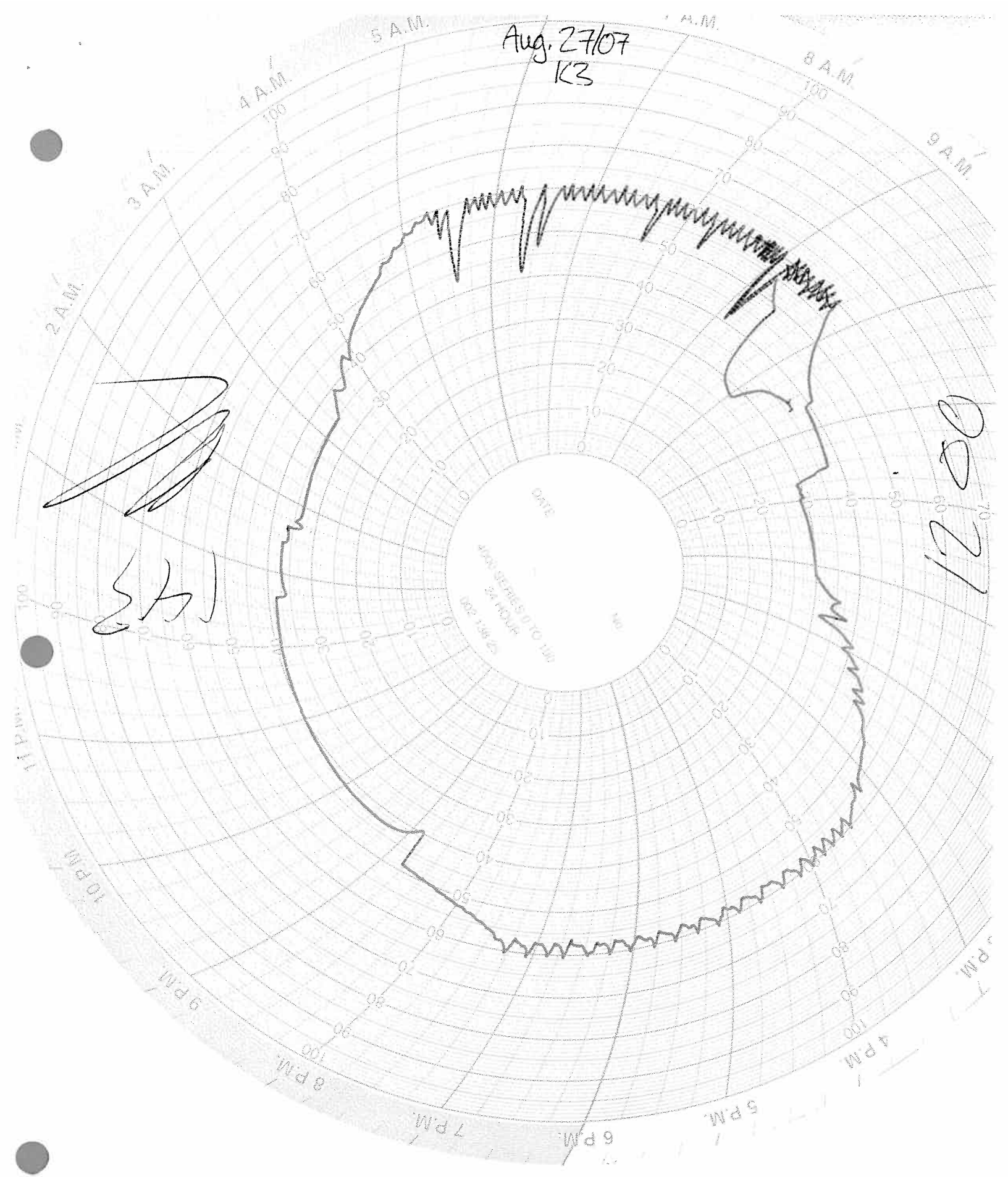
Aug. 27/07
K3
1200
241

AUG 28/07

SKY CAST INC. GENIE-II BATCH REPORT DATE:08-28-1998
ATCH NUMBER: 19968 DESTINATION:CALL #11 STN#3 BATCH: 1 OF 999
240
ORMULA #: 18 NAME:POLE375R BATCH SIZE: 1100 KG 0.46 CM
START TIME:10:43:04 FINISH TIME:10:50:47 ELAPSED TIME: 463.00 SEC

CALE	INGREDIENT	TARGET DRY	TARGET WET	ACTUAL DRY	ACTUAL WET	
GGREGATE						
	13MM STONE	484	485	484	485	KG
	SAND	357	371	361	375	KG
EMENT						
	TYPE 30 HSF	196	196	197	197	KG
ATER						
	WATER	47	47	47	47	KG
ELIVERED WEIGHT:					1104	KG
DMIXES:						
IR ENTRAINMENT		782		813		ML
LASTCISER		2553		2600		ML
00N		495		500		ML

ATER IN BATCH:
WATER IN AGGREGATE: 15 L
WATER ADDED TO BATCH: 47 L
TOTAL WATER IN BATCH: 62 L
WATER / CEMENT RATIO: 0.32
END OF REPORT

Daily Compressive Strength Test Report

Date: August 28/07

Fresh Concrete Data					Comments:
Mix No.:	9				
Mix Type:	CO				
Kiln No:	5				
Mould No.:	RO-53				
Length: (ft)	21				
Class:	A				
Type:	RO				
Time of Mould:	11:13				
Slump (50 ±20)	55				
Temperature (10-35°C)	28.5				
Air Content (5-8 %)	6.4				

Moisture Content (%)					Comments:
Mass of Wet & Tare (A) (g)	1589.0				
Mass of Dry & Tare (B) (g)	1536.4				
Tare (C) (g)	815.6				
Moisture in Mix (A-B) (g)					
Mass of Wet (A-C) (g)					
Moisture Content (A-B)/(A-C)	6.8				

Density (kg/m^3)					Comments:
Mass & Base Wet (A) (kg)	20.63				
Base (B) (kg)	3.70	3.70	3.70	3.70	
Mass Concrete (A-B) (kg)					
Volume of Base (C) (m^3)	0.007	0.007	0.007	0.007	
Fresh Density (A-B)/C	2418.6				

Time of Tests: _____

Compressive Strength	Batch #___ Age (h):_____	
Cylinder Location	North	South
Mass (g)		
Strength (kN)		
Strength (MPa)		

Batch #___ Age (h):_____		Compressive Strength
North	South	Cylinder Location
		Mass (g)
		Strength (kN)
		Strength (MPa)

Tested By: SARAH REINHOLT

Signature: _____

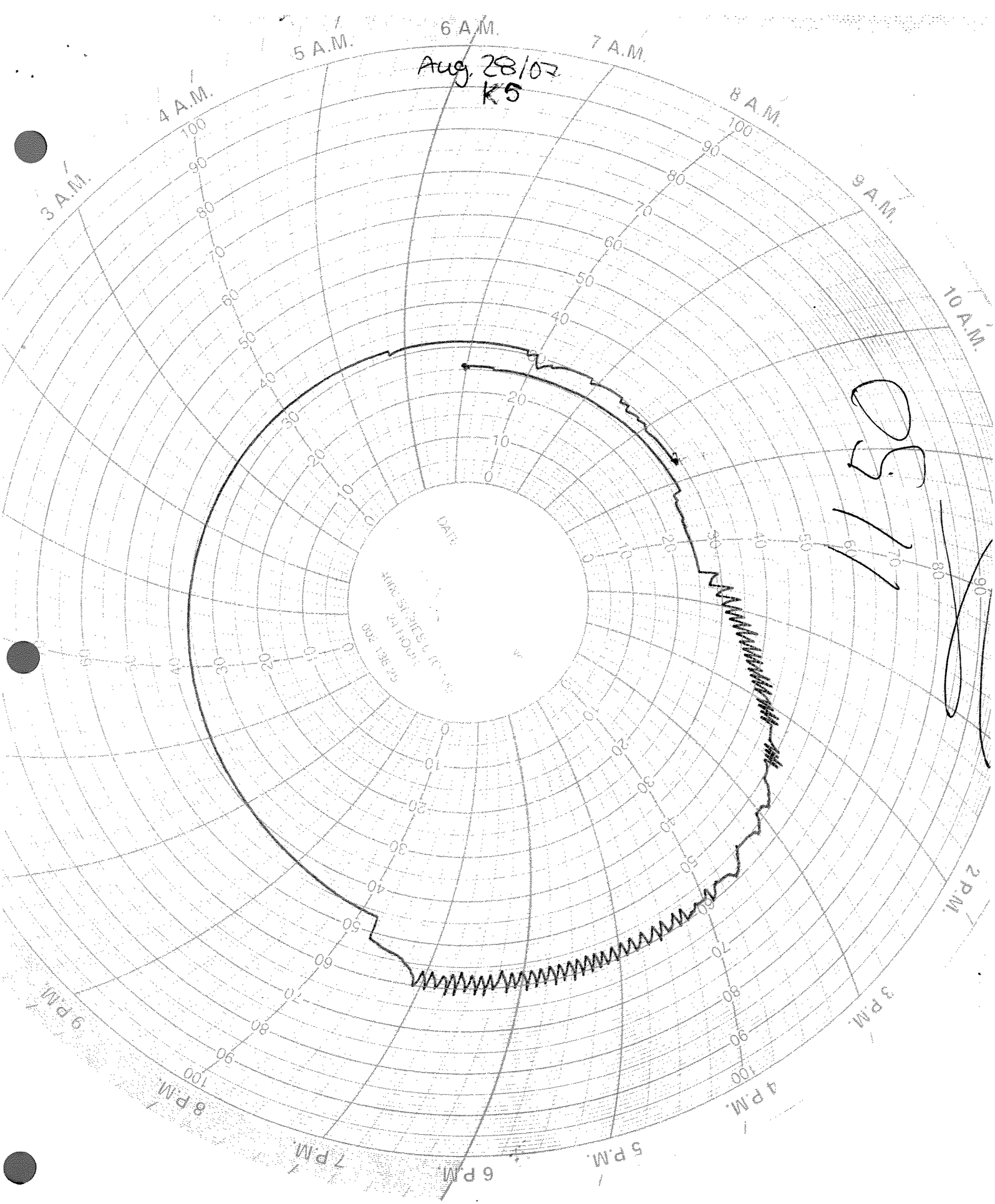
Aug. 28/07
K5
3 A.M.
4 A.M.
5 A.M.
6 A.M.
7 A.M.
8 A.M.
9 A.M.
10 A.M.
2 P.M.
3 P.M.
4 P.M.
5 P.M.
6 P.M.
7 P.M.
8 P.M.
9 P.M.

AUG 29/07

SKY CAST INC. GENIE-II BATCH REPORT DATE:08-29-1998
ATCH NUMBER: 20000 DESTINATION:CALL #11 STN#3 BATCH: 1 OF 999
240
O LA #: 18 NAME:POLE375R BATCH SIZE: 1100 KG 0.46 CM
START TIME:12:03:28 FINISH TIME:12:10:56 ELAPSED TIME: 448.00 SEC

CALE	INGREDIENT	TARGET DRY	TARGET WET	ACTUAL DRY	ACTUAL WET	
GGREGATE						
	13MM STONE	484	485	484	485	KG
	SAND	357	372	351	366	KG
EMENT						
	TYPE 30 HSF	196	196	196	196	KG
ATER						
	WATER	47	47	46	46	KG

ELIVERED WEIGHT: 1093 KG

DMIXES:			
IR ENTRAINMENT	782	813	ML
_ASTCISER	2553	2600	ML
20N	495	500	ML

ATER IN BATCH:

WATER IN AGGREGATE:	16	L
WATER ADDED TO BATCH:	46	L
TOTAL WATER IN BATCH:	62	L
WATER / CEMENT RATIO:	0.32	

END OF REPORT

Daily Compressive Strength Test Report

Date: Aug. 29/07

Fresh Concrete Data					Comments:
Mix No.:	12				
Mix Type:	CO				
Kiln No:	2				
Mould No.:	RD-53				
Length: (ft)	21				
Class:	A				
Type:	RD				
Time of Mould:	12:31				
Slump (50 ±20)	55				
Temperature (10-35°C)	28				
Air Content (5-8 %)	6.5				

Moisture Content (%)					Comments:
Mass of Wet & Tare (A) (g)	1614.5				
Mass of Dry & Tare (B) (g)	1563.4				
Tare (C) (g)	815.8				
Moisture in Mix (A-B) (g)					
Mass of Wet (A-C) (g)					
Moisture Content (A-B)/(A-C)	6.4				

Density (kg/m^3)					Comments:
Mass & Base Wet (A) (kg)	20.69				
Base (B) (kg)	3.70	3.70	3.70	3.70	
Mass Concrete (A-B) (kg)					
Volume of Base (C) (m^3)	0.007	0.007	0.007	0.007	
Fresh Density (A-B)/C	2427.1				

Time of Tests: _____

Compressive Strength	Batch #___ Age (h):_____	
Cylinder Location	North	South
Mass (g)		
Strength (kN)		
Strength (MPa)		

Batch #___ Age (h):_____		Compressive Strength
North	South	Cylinder Location
		Mass (g)
		Strength (kN)
		Strength (MPa)

Tested By: SARAH REINHOLT

Signature: _____

Aug 29/07
KR

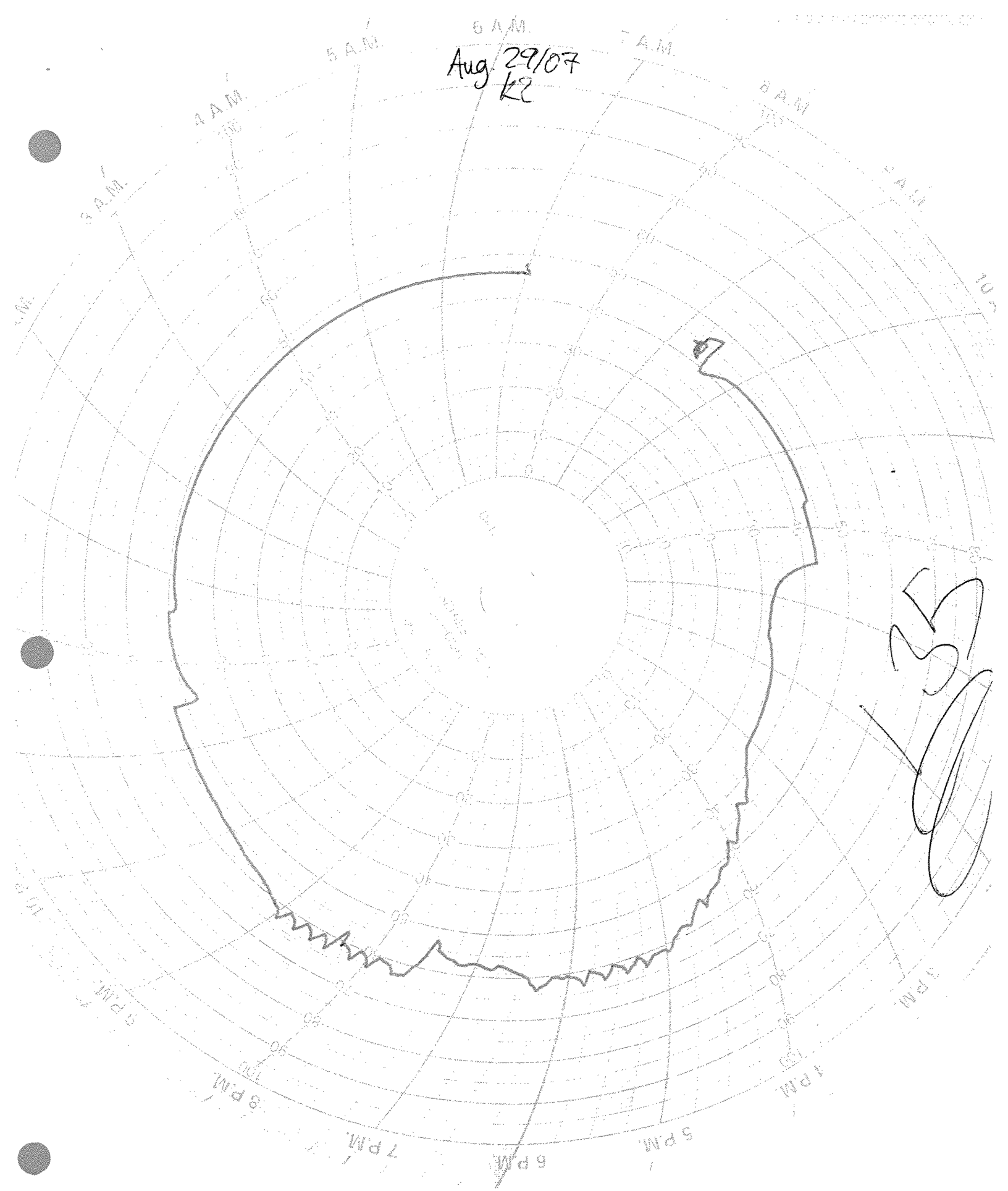
5 A.M.
4 A.M.
3 A.M.
2 A.M.
1 A.M.
12 P.M.
1 P.M.
2 P.M.
3 P.M.
4 P.M.
5 P.M.
6 P.M.
7 P.M.
8 P.M.
9 P.M.
10 P.M.
11 P.M.

SKY CAST INC. GENIE-II BATCH REPORT DATE:08-30-1998
ATCH NUMBER: 20238 DESTINATION:CALL #11 STN#3 BATCH: 1 OF 999
240
O[redacted]LA #: 18 NAME:POLE375R BATCH SIZE: 1100 KG 0.46 CM
S[redacted]RT TIME:12:15:50 FINISH TIME:12:23:09 ELAPSED TIME: 439.00 SEC

CALE INGREDIENT	TARGET DRY	TARGET WET	ACTUAL DRY	ACTUAL WET	
GGREGATE					
13MM STONE	484	485	476	477	KG
SAND	357	373	356	372	KG
EMENT					
TYPE 30 HSF	196	196	195	195	KG
ATER					
WATER	46	46	46	46	KG

ELIVERED WEIGHT:			1091	KG
DMIXES:				
IR ENTRAINMENT	782	813		ML
LASTCISER	2553	2600		ML
20N	495	500		ML

ATER IN BATCH:		
WATER IN AGGREGATE:	17	L
WATER ADDED TO BATCH:	46	L
TOTAL WATER IN BATCH:	63	L
WATER / CEMENT RATIO:	0.32	

END OF REPORT

Daily Compressive Strength Test Report

Date: _____

Fresh Concrete Data					Comments:
Mix No.:					
Mix Type:	CO				
Kiln No:	9				
Mould No.:	RO-53				
Length: (ft)	21				
Class:	A				
Type:	RO				
Time of Mould:	12:23				
Slump (50 ±20)	45 mm				
Temperature (10-35°C)	27				
Air Content (5-8 %)	6.6				

Moisture Content (%)					Comments:
Mass of Wet & Tare (A) (g)	589.0				
Mass of Dry & Tare (B) (g)	551.8				
Tare (C) (g)	-				
Moisture in Mix (A-B) (g)					
Mass of Wet (A-C) (g)					
Moisture Content (A-B)/(A-C)	6.3 %				

Density (kg/m^3)					Comments:
Mass & Base Wet (A) (kg)	20.36				
Base (B) (kg)	3.70	3.70	3.70	3.70	
Mass Concrete (A-B) (kg)					
Volume of Base (C) (m^3)	0.007	0.007	0.007	0.007	
Fresh Density (A-B)/C	2980				

Time of Tests: _____

Compressive Strength	Batch #___ Age (h):_____	
Cylinder Location	North	South
Mass (g)		
Strength (kN)		
Strength (MPa)		

Batch #___ Age (h):_____		Compressive Strength
North	South	Cylinder Location
		Mass (g)
		Strength (kN)
		Strength (MPa)

Tested By: _____

Signature: _____

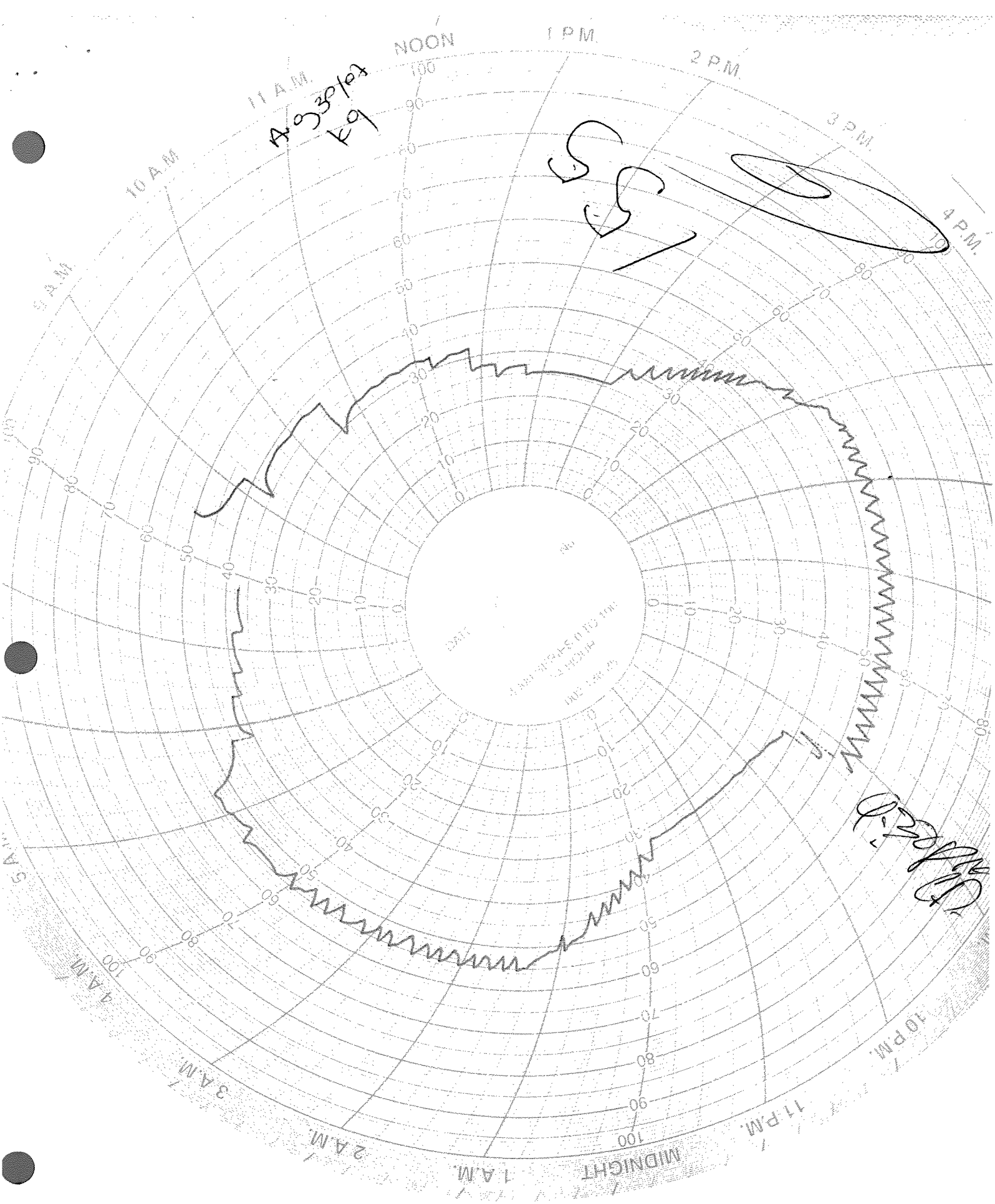
NOON
1 P.M.
2 P.M.
3 P.M.
4 P.M.
11 A.M.
10 A.M.
9 A.M.
5 A.M.
4 A.M.
3 A.M.
2 A.M.
1 A.M.
MIDNIGHT
11 P.M.
10 P.M.

Chia Ta World Co.,Ltd.

TEST REPORT

Report No. ：QC950508
Report Page：1 of 10

Report should not be reproduced except in full.

佳大世界股份有限公司 永康二廠 品管核章 台南縣永康市中正北路965號

與正本相符

HEAD OFFICE：
NO.16, LANE 317, CHUNG CHENG N. ROAD,
YON KAN CITY, TAINAN SHIEN, TAIWAN, R.O.C.
TEL：886-6-2533117-9 FAX:886-6-2533932

TEST RESULT

Chia Ta World Co., Ltd.
HEAD OFFICE : NO.16, LANE 317, CHUNG CHENG NORTH ROAD, YAN HAN.
YON KAN CITY. TAINAN SHIEN. TAIWAN. REPUBLIC OF CHINA.
TEL : 886-6-2533117-9 FAX:886-6-2533932

COIL NO.	LOT NO.	HEAT NO.	STRAND DIA (mm)	AREA ($inch^2$)	BREAKING LOAD (Lbf)	YIELD LOAD (Lbf)	ELONGAT IN24" (%)	MODULUS OF ELASTICITY (Mpsi)	NET WEIGHT (LB)	LENGTH (FT)
C8933	S55053	3B441	9.51	0.0856	25100	23149	5.9	29.72	5892	20040
C8934	S55054	3B441	9.51	0.0856	25100	23149	5.9	29.72	5895	20040
C8935	S55055	3B441	9.51	0.0856	25100	23149	5.9	29.72	3119	10690
C8936	S55056	3B441	9.51	0.0856	25100	23149	5.9	29.72	3119	10690
C8937	S55057	3B441	9.51	0.0856	25100	23149	5.9	29.72	6318	21510
C8938	S55061	3B441	9.52	0.0857	25078	23275	5.2	29.62	6274	21320
C8939	S55062	3B441	9.52	0.0857	25078	23275	5.2	29.62	6276	21320
C8940	S55063	3B441	9.52	0.0857	25078	23275	5.2	29.62	6276	21320
C8941	S55064	3B441	9.52	0.0857	25078	23275	5.2	29.62	6267	21320
C8942	S55065	3B441	9.52	0.0857	25078	23275	5.2	29.62	6272	21320
C8943	S55066	3B441	9.52	0.0857	25078	23275	5.2	29.62	6360	21615
C8944	S55071	3B441	9.50	0.0853	24890	22989	5.3	28.94	6230	21320
C8945	S55072	3B441	9.50	0.0853	24890	22989	5.3	28.94	6245	21320
C8946	S55073	3B441	9.50	0.0853	24890	22989	5.3	28.94	6265	21418
C8947	S55074	3B441	9.50	0.0853	24890	22989	5.3	28.94	6274	21418
C8948	S55075	3B441	9.50	0.0853	24890	22989	5.3	28.94	6267	21418
C8949	S55076	3B441	9.50	0.0853	24890	22989	5.3	28.94	5989	20467
C8950	S55081	3B441	9.51	0.0856	24835	23126	4.9	29.64	6170	20990
C8951	S55082	3B441	9.51	0.0856	24835	23126	4.9	29.64	6177	20990
C8952	S55083	3B441	9.51	0.0856	24835	23126	4.9	29.64	6177	20990
C8953	S55084	3B441	9.51	0.0856	24835	23126	4.9	29.64	6175	20990
C8954	S55085	3B441	9.51	0.0856	24835	23126	4.9	29.64	6117	20795
C8955	S55086	3B441	9.51	0.0856	24835	23126	4.9	29.64	6580	22402
C8956	S55091	3B441	9.54	0.0860	24846	22956	4.6	28.85	6294	21320
C8957	S55092	3B441	9.54	0.0860	24846	22956	4.6	28.85	6296	21320
C8958	S55093	3B441	9.54	0.0860	24846	22956	4.6	28.85	6302	21320
C8959	S55094	3B441	9.54	0.0860	24846	22956	4.6	28.85	6311	21320
C8960	S55095	3B441	9.54	0.0860	24846	22956	4.6	28.85	6302	21320
C8961	S55096	3B441	9.54	0.0860	24846	22956	4.6	28.85	6358	21516
C8962	S55101	3B441	9.52	0.0857	24582	22801	4.7	28.49	6289	21320

STEEL STRAND UNCOATED 7 WIRE POR PRESTRESSED CONCRETE ACCORDING TO ASTM A416-02.
LOW RELAXATION PLAIN GRADE 270K LEFT HAND LAY:3/8 INCH DIAMETER:REEL LENGTH 21320 FT/COIL
PLUS OR MIMUS 2PCT.LIST OP EACH SEPARATELY NUMBERED COIL AND THE WEIGHT AND REEL
LENGTH OF EACH PACKING:REELESS , WRAPPED WITH OIL PAPER AND P.P CLOTH WITHOUT OIL。

與正本相符

NOTE : YIELD LOAD IS THE LOAD AT 1%EXTENSION

DATE: 05-10-2006

佳大世界股份有限公司 永康一廠 品管核章 台南縣永康市中正北路963號

Q.A MANAGER: Lin Tse-Ching

Chia Ta World Co.,Ltd.

3/8" Low PC.STRAND PROGSAN		AREA inch^2:	0.0853	WE HEREBY CERTIFY THAT THE	**Report No. :QC950508**
CUSTOMER:	CRISPIN	MODULUS GPa:	204	PRODUCT BEEN MADE IN	**Report page : 6 of 10**
SPECIFICATION:	ASTM A416-02	MODULUS Mpsi:	28.94	ACCORDING	
ORDER NO:	20-9814	LOAD AT 1%ELONGATION kN:	102.3	WITH THE SPECIFICATION	
COIL NO:	C8944~C8949	LOAD AT 1%ELONGATION lbf:	22989	ASTM A416-02	
HEAT NO.	3B441	ULTIMATE LOAD kN:	110.7	DATE 05-10-2006	
SAMPLE NO:	S55071	ULTIMATE LOAD lbf:	24890		
AREA mm^2:	55.0	FINAL ELONGATION IN 24" %:	5.3		

3/8 inch Strand Tension Test

33070

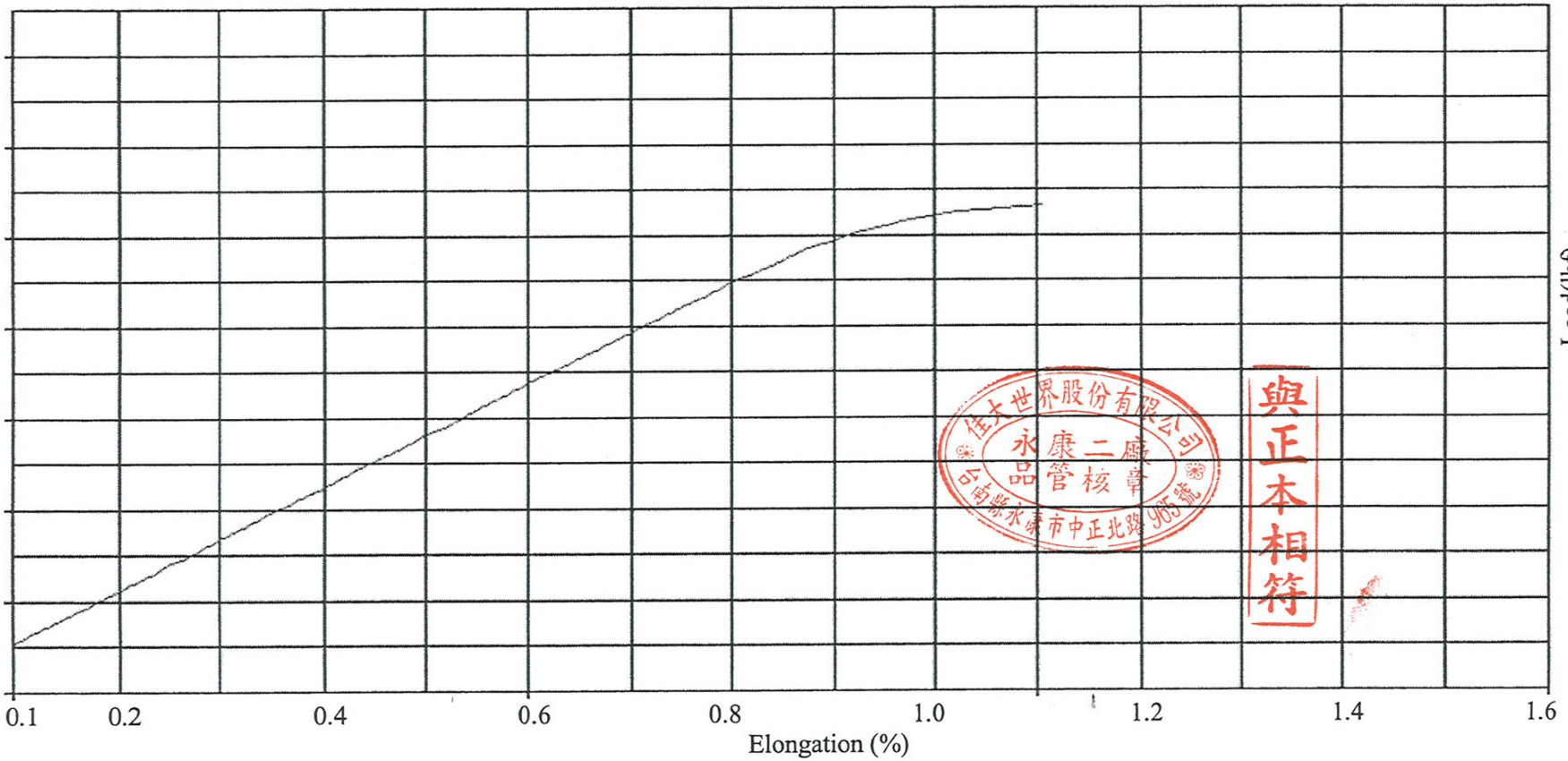

219

QUALITY CERTIFICATE	CHIA TA WORLD CO., LTD NO. 16, LANE 317, CHUNG CHENG N. ROAD, YON KAN CITY, TAINAN SHIEN, TAIWAN, R.O.C. TEL : (06)2533117 FAX : (06)2533932

PURCHASER : THE CRISPIN COMPANY
ORDER NO : 20-9814
MATERIAL : PRESTRESSING STRAND ACCORDING TO ASTM A416-02-GRADE 270K
UNCOATED SEVEN-WIRE STRESS RELIEVED DIAMETER 3/8 INCH
SPECIFICATION : ASTM A416-02-GRADE 270K-LOW RELAXATION

36 COIL : C8933 TO C8968
NET WEIGHT(MT) : 99.159

CHEMICAL ANALYSIS :

HEAT NO	C%	Si%	Mn%	P%	S%
3B441	0.83	0.22	0.72	0.024	0.006

DATE : 05-10-2006
SEND ENCLOSED :
LIST OF TEST RESULT(2 PAGES),
LOAD-ELONGATION GRAPHS(7 PAGES)

佳大世界股份有限公司 永康二廠 品管核章 台南縣永康市中正北路965號

與正本相符

Q.A MANAGER: Lin Tse-Ching

PHYSICAL TEST REPORT

WIRE PRODUCTS

Laurel-LEC Steel
A DIVISION OF HARRIS STEEL LIMITED

DATE ISSUED	23-May-07		
CUSTOMER	Sky Cast Inc.	**PURCHASE ORDER**	PO20914
ADDRESS	299 Brock Road South	**Certificate No.**	195383
SHIP TO LOCATION	Guelph, Ontario N1H 6H9	**Laurel-LEC B/L**	00011739
SHIP DATE	23-May-07		

PRODUCT DESCRIPTION Class III Galv Wire in coil 3.4mm dia

HEAT NUMBER(S) C64373 & C64518

Ultimate Tensile Strength (psi)	**MIN. REQUIREMENT**	**70,000**
	MAX. REQUIREMENT	**90,000**
	LOWEST VALUE	**87,249**
	HIGHEST VALUE	**88,071**

Wire Diameter (inch)	**MIN. REQUIREMENT**	**0.13**	**MAX. REQUIREMENT**	**0.138**
	LOWEST VALUE	**0.1349**		
	HIGHEST VALUE	**0.1356**		

PRODUCED IN ACCORDANCE TO THE APPLICABLE SPECIFICATIONS

ASTM A641/641M Specifications for 3.4mm Clas III Galv Wire

SINCERELY,

JOHN HERRING
Vice President - Operations and Strategic Planning
Laurel-LEC Steel
A Division of Harris Steel Limited

Appendix C
Testing Raw Data Sheets

TL: 5345

-0.02

Specimen:	A65-C	
Date Tested:	Nov 8	
Time Tested:	11:15	
Excitation Voltage (load cell)	10.22	V
Calibration (push button) value	22.01	kN
Excitation Voltage (accustar bat)	12.69	V
Zero reading load cell:	0.0006	V
Zero reading twist:	0.3363	V
Twist at Cracking:		V
		deg
Torque Reading at Cracking:		kN
		kN-m
Twist at Post Crack Hold:		V
		deg
Torque Reading Post Crack Hold:		kN
		kN-m
Wall Thickness at Failure:	46	mm
Cover at Failure:	21	mm
Location of Failure from butt:	see dwg.	mm

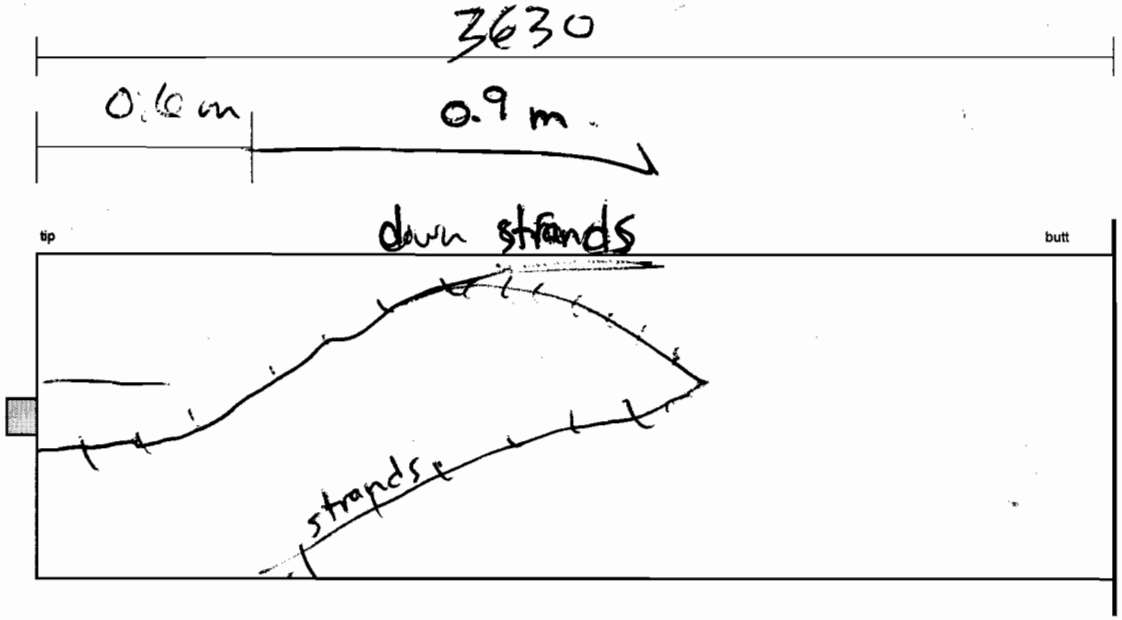

Crack Sketch

223

Comments:

initial cracks @ tip (pics)
- cracking occured down strands after torque crack near collar.

8.5 kN max. → crack near collar.
sudden failure

sinking of strands noticed on ends.
~ 1-2 mm.

TL 5345

3610 TL: 5345

Specimen:	165-C-2	
Date Tested:	Nov 8	
Time Tested:	12:07	
Excitation Voltage (load cell)	10.22	V
Calibration (push button) value	12.00	kN
Excitation Voltage (accustar bat)	12.68	V
Zero reading load cell:	0.006	V
Zero reading twist:	0.282	V
Twist at Cracking:		V
		deg
Torque Reading at Cracking:		kN
		kN-m
Twist at Post Crack Hold:		V
		deg
Torque Reading Post Crack Hold:		kN
		kN-m
Wall Thickness at Failure:	52	mm
Cover at Failure:	24	mm
Location of Failure from butt:	see dwg	mm

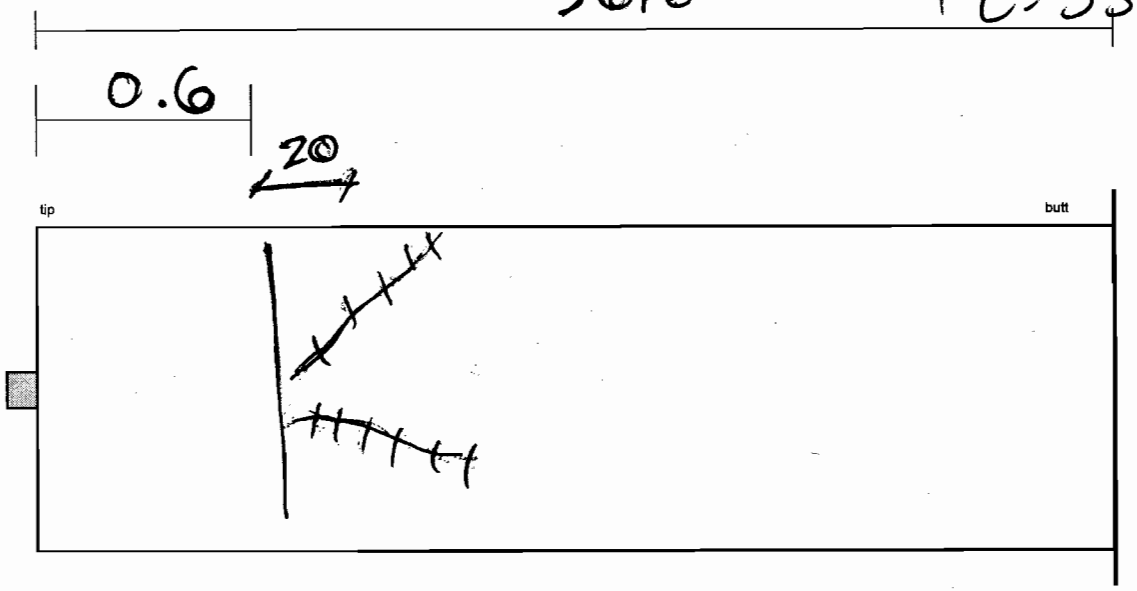

Crack Sketch

Comments:

~4 kN (collar slide) retightened (increase crack)
restart 4+ kN (torsion crack from collar retightened or
failure: no post (like C-1)

sinking of strands noted

TL: 5350

3608

Specimen:	165-D	
Date Tested:	NOV 10	
Time Tested:	12:15	
Excitation Voltage (load cell)	10.22	V
Calibration (push button) value	21.99	kN
Excitation Voltage (accustar bat)	12.73	V
Zero reading load cell:	0.0006	V
Zero reading twist:	0.2118	V
Twist at Cracking:		V
		deg
Torque Reading at Cracking:		kN
		kN-m
Twist at Post Crack Hold:		V
		deg
Torque Reading Post Crack Hold:		kN
		kN-m
Wall Thickness at Failure:	50	mm
Cover at Failure:	28	mm
Location of Failure from butt:	dwg	mm

-0.03

~~0.63m~~

spacing 120 third spiral failed (reading)

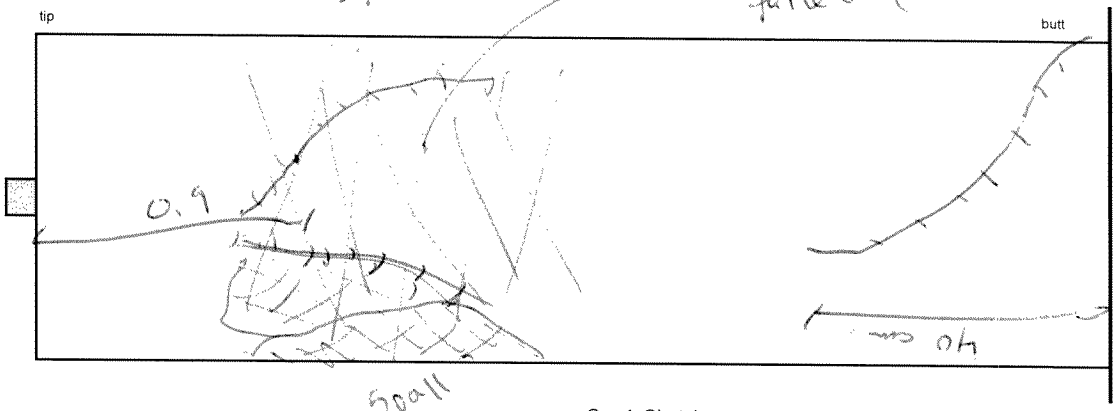

Crack Sketch

225

Comments:

start 12:17 loose collar

restart 12:31 (0.0006, 0.2130) V

12.1 kN first butt crack (11.8 drop) collar slip

restart 12:48

14+ kN Crack growing / crack @ collar

held @ 14 - spall @ collar

failure @ collar.

TZ = 5343

Specimen:	165-ccw-L	
Date Tested:	NOV 13	
Time Tested:	10:35	
Excitation Voltage (load cell)	10.22	V
Calibration (push button) value	22.00	kN
Excitation Voltage (accustar bat)	12.72	V
Zero reading load cell:	0.0006	V
Zero reading twist:	0.2972	V
Twist at Cracking:		V
		deg
Torque Reading at Cracking:		kN
		kN-m
Twist at Post Crack Hold:		V
		deg
Torque Reading Post Crack Hold:		kN
		kN-m
Wall Thickness at Failure:	49	mm
Cover at Failure:	24	mm
Location of Failure from butt:	1.605	mm

1.605

0.6 — 20 cm 40 cm

large piece broke off

tip — butt

helix spaced @ 140 120

these two failed.

Crack Sketch

Comments:	start 10:35 9.5 kN cracking @ collar done 10:39 kN → crack @ collar @ 10 kN spall & twist dropped pole.

226

TL = 1340

Specimen:	165-cw-2	
Date Tested:	Nov 13	
Time Tested:	11:35	
Excitation Voltage (load cell)	10.22	V
Calibration (push button) value	21.98	kN
Excitation Voltage (accustar bat)	12.71	V
Zero reading load cell:	0.0006	V
Zero reading twist:	0.473	V
Twist at Cracking:		V
		deg
Torque Reading at Cracking:		kN
		kN-m
Twist at Post Crack Hold:		V
		deg
Torque Reading Post Crack Hold:		kN
		kN-m
Wall Thickness at Failure:	53	mm
Cover at Failure:	30	mm
Location of Failure from butt:	dug	mm

-0.03

227

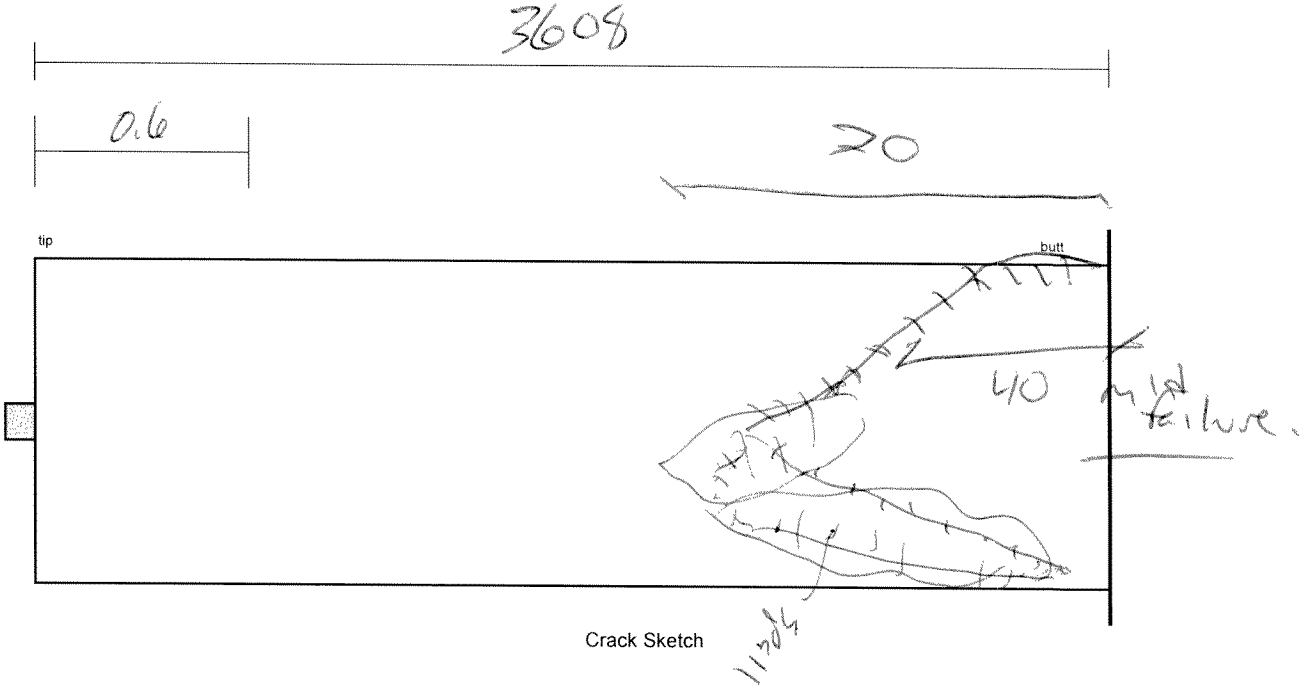

Comments:

start 11:40 ~
crack @ base 11.5 kN
crack @ collar when tightening.
12.6 kN hold. → crack/spalling @ base.
failed @ base
fell to ground. failed - 11:45

TZ: 5344

3604

0.6

20 mid fail

tip

butt

45 to spall max

crack right of helix. (along path)

spall.

2nd helix broken. (25 cm away from mid collar)

Crack Sketch

Spacing ~100 - 110

Specimen:	165 - CCW	
Date Tested:	NOV 13	
Time Tested:	2:50	
Excitation Voltage (load cell)	10.22	V
Calibration (push button) value	22.00	kN
Excitation Voltage (accustar bat)	17.71	V
Zero reading load cell:	0.0006	V
Zero reading twist:	0.3033	V
Twist at Cracking:		V
		deg
Torque Reading at Cracking:		kN
		kN-m
Twist at Post Crack Hold:		V
		deg
Torque Reading Post Crack Hold:		kN
		kN-m
Wall Thickness at Failure:	50	mm
Cover at Failure:	26	mm
Location of Failure from butt:	see drg	mm
Comments:	15.7 kN first crack @ collar. Held load again failed ~ 14.8 kN spall, pop near collar. cracks moved with helix. except 2nd helix from collar. (reading / failure)	

10 mm paste.

-0.02

228

TL 5345

Specimen:	165-CW-N	
Date Tested:	NOV 13	
Time Tested:	1:45	
Excitation Voltage (load cell)	16.22	V
Calibration (push button) value	2199	kN
Excitation Voltage (accustar bat)	12.72	V
Zero reading load cell:	0.0006	V
Zero reading twist:	0.3717	V
Twist at Cracking:		V
		deg
Torque Reading at Cracking:		kN
		kN-m
Twist at Post Crack Hold:		V
		deg
Torque Reading Post Crack Hold:		kN
		kN-m
Wall Thickness at Failure:	56	mm
Cover at Failure:	25	mm
Location of Failure from butt:	see dwg	mm

-0.02

229

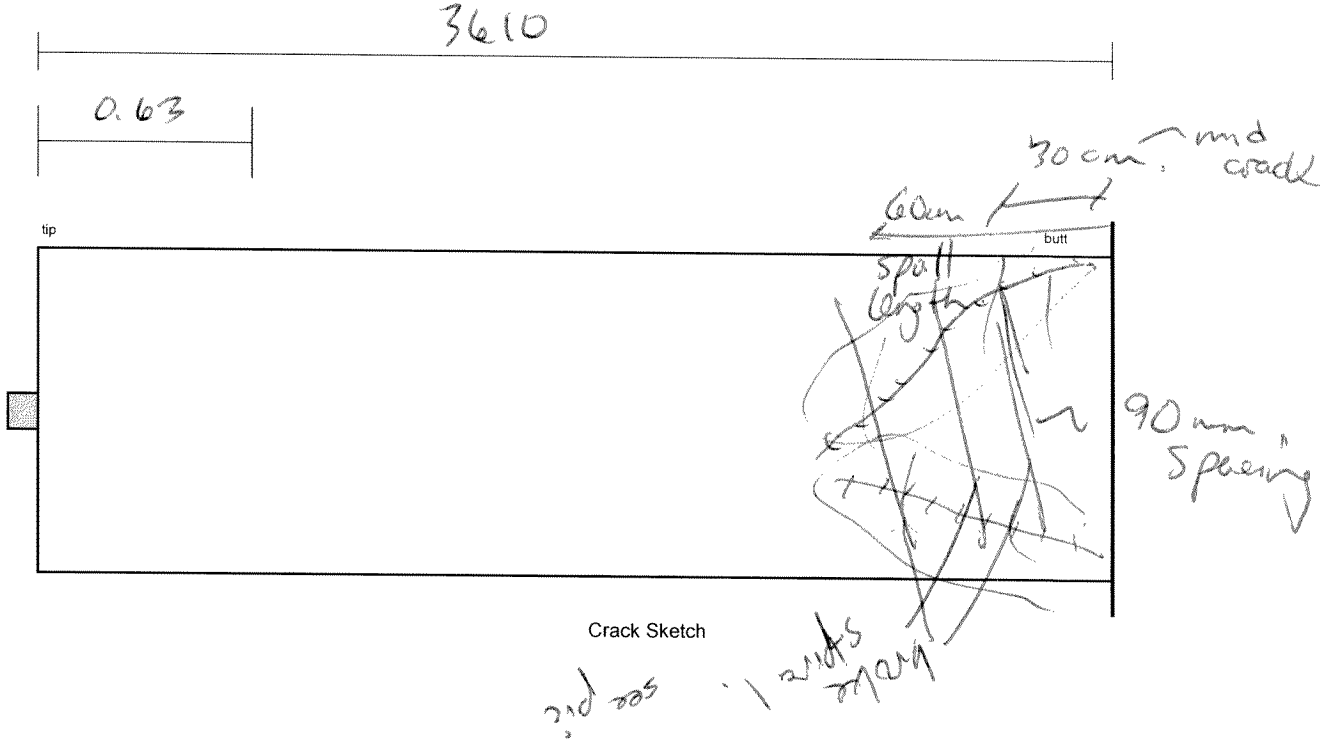

Comments:

Start 1:42
restart electrical wiring problem 1:53 (0.0128, 0.3717)
16.8 kN (crack @ butt.) → down to 16 kN
~17kN collar slip @ 1:58 ~ 1:59 (unload) reload to crack
crack growing @ butt
re-add load zero values (0.0006, 0.3813) restart 2:04

~17.5 spall/failure @ butt (big movement)

stopped (large movement @ butt) 2:10

15 mm paste
(same as others that day).

Specimen:	210-C	
Date Tested:	OCT 25	
Time Tested:	10:30 *	
Excitation Voltage (load cell)	10.22	V
Calibration (push button) value	22.00	kN
Excitation Voltage (accustar bat)	12.75	V
Zero reading load cell:	0.0006	V *
Zero reading twist:	0.3961	V
Twist at Cracking:		V
		deg
Torque Reading at Cracking:		kN
		kN-m
Twist at Post Crack Hold:		V
		deg
Torque Reading Post Crack Hold:		kN
		kN-m
Wall Thickness at Failure:	57	mm
Cover at Failure:	20	mm
Location of Failure from butt:	See D26	mm

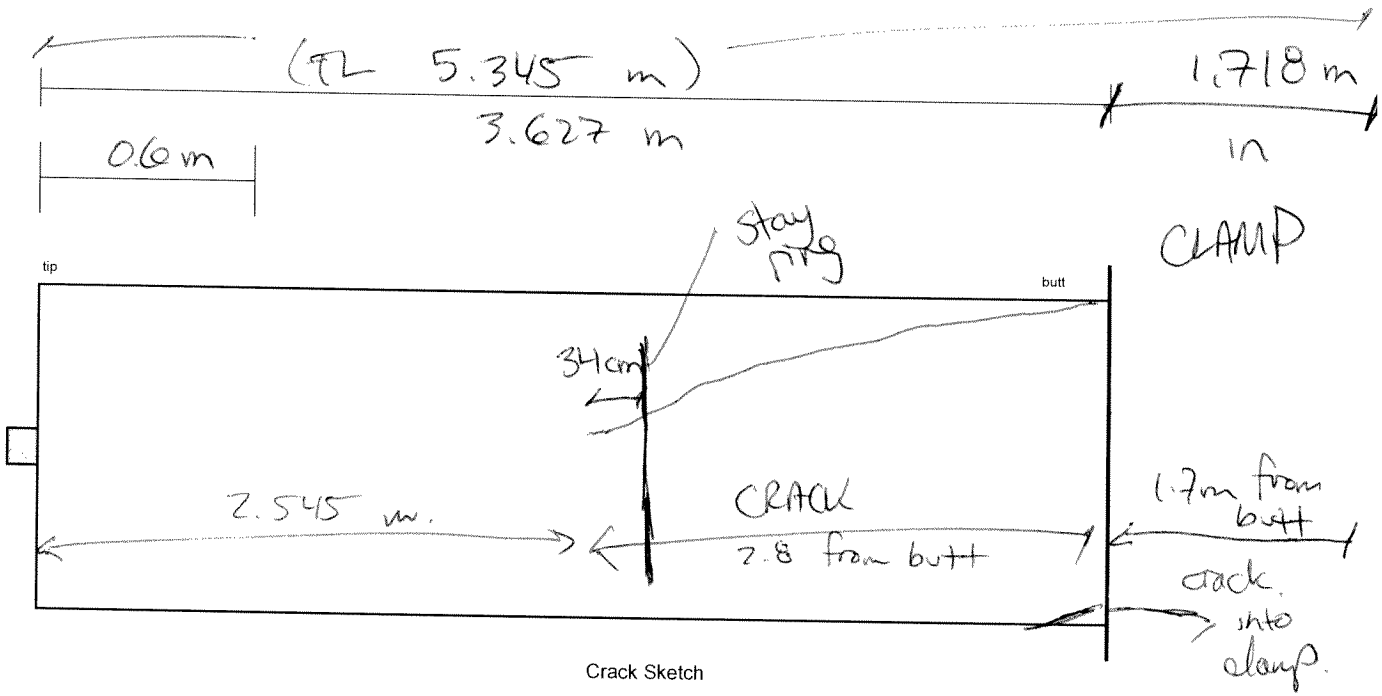

Crack Sketch

Comments:

* restarted (clamp slip) @ 10:48:00 (first 10:35:04)
zero reading (0.03 kN restart \ (0.02 prev.)
load zeros for both 0.0006 V
twist " " " 0.3961 V
14+ kN major first crack
3.1 kN post crack more movement / cracking
10:55 → major failure (pole fell to ground)

1.dco :

T2 = 5330

Specimen:	710-C2	
Date Tested:	Oct 30	
Time Tested:	11:01	
Excitation Voltage (load cell)	10.21	V
Calibration (push button) value	22.00	kN
Excitation Voltage (accustar bat)	12.75	V
Zero reading load cell: 0.0892	~~0.0892~~	V
Zero reading twist:	0.2765	V
Twist at Cracking:		V
		deg
Torque Reading at Cracking:		kN
		kN-m
Twist at Post Crack Hold:		V
		deg
Torque Reading Post Crack Hold:		kN
		kN-m
Wall Thickness at Failure:	62	mm
Cover at Failure:	24	mm
Location of Failure from butt:	560 dwg	mm

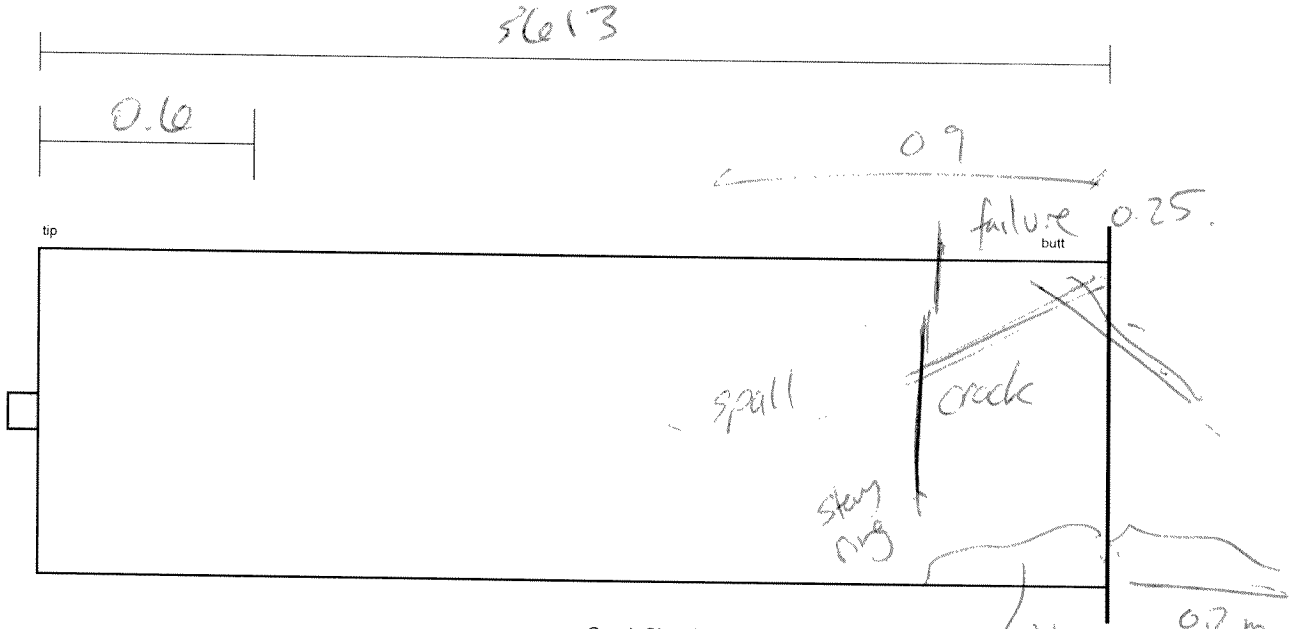

Crack Sketch

Comments:

cracks. (pic). holding @ 15.22 — kN
major spalling holding @ 3 kN
holding 5.2 kN (senso) — widening cracking.
11:21 ultimate failure. pole to ground)
cracking @ clamp
(major spall.

~~Voltage divider.~~
~~Calibration~~
~~Zero~~

senso
0.01

TL = 5550

Specimen:	210-D	
Date Tested:	OCT 30	
Time Tested:	1:30	
Excitation Voltage (load cell)	10.22	V
Calibration (push button) value	21.95	kN
Excitation Voltage (accustar bat)	12.75	V
Zero reading load cell:	2.10006	V
Zero reading twist:	0.7594	V
Twist at Cracking:		V
		deg
Torque Reading at Cracking:		kN
		kN-m
Twist at Post Crack Hold:		V
		deg
Torque Reading Post Crack Hold:		kN
		kN-m
Wall Thickness at Failure:		mm
Cover at Failure:		mm
Location of Failure from butt:		mm

ZERO 0.03

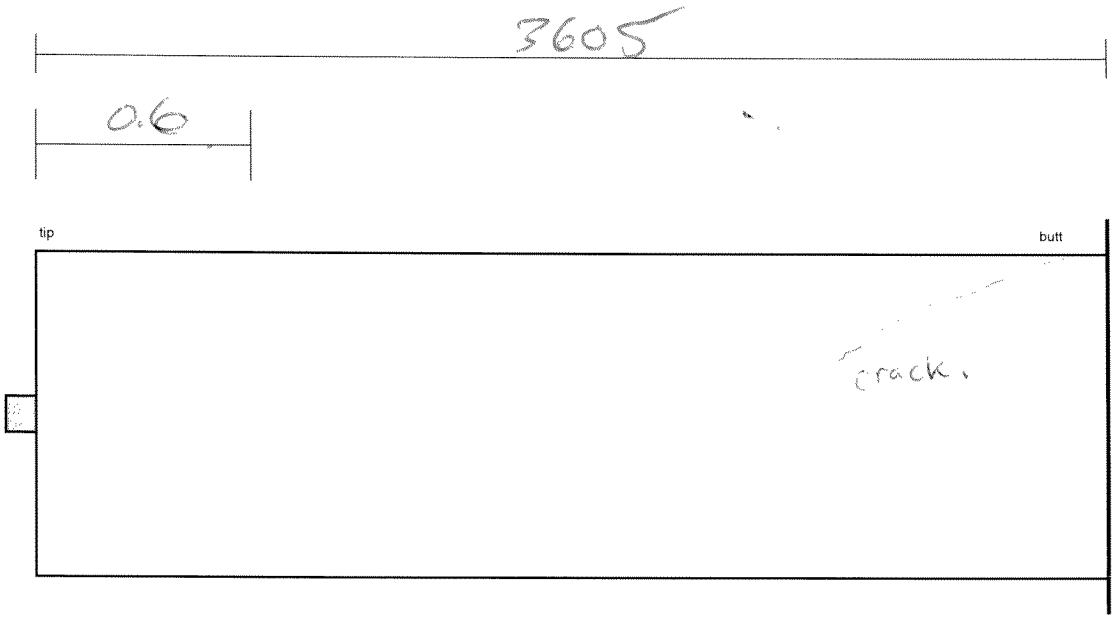

Crack Sketch

Comments:

Crack @ 24.5 kN. 1:37 (max - out.) stopped @ 1:45

bigger crack. (thicker spacing. 26.5 kN)

growing.

retest for post-peak another day.

end twist voltage = 0.285
≈ 0.427°

* with voltage divider
Calib. before 21.98 after 12.02
2.48 → 4.41 (check during test too.)
7.97 = 4.254

NOTE
~~NOT~~ NEEDED
signal conditioner was split into interface

Retest - Post Peak

Specimen:	210-D	
Date Tested:	Nov 3/07	
Time Tested:	11:30	
Excitation Voltage (load cell)	10.22	V
Calibration (push button) value	21.98	kN
Excitation Voltage (accustar bat)	12.75	V
Zero reading load cell:	~~10.22~~	V 0.0006
Zero reading twist:	0.2863	V
Twist at Cracking:		V
		deg
Torque Reading at Cracking:		kN
		kN-m
Twist at Post Crack Hold:		V
		deg
Torque Reading Post Crack Hold:		kN
		kN-m
Wall Thickness at Failure:	63	mm
Cover at Failure:	30	mm
Location of Failure from butt:		mm

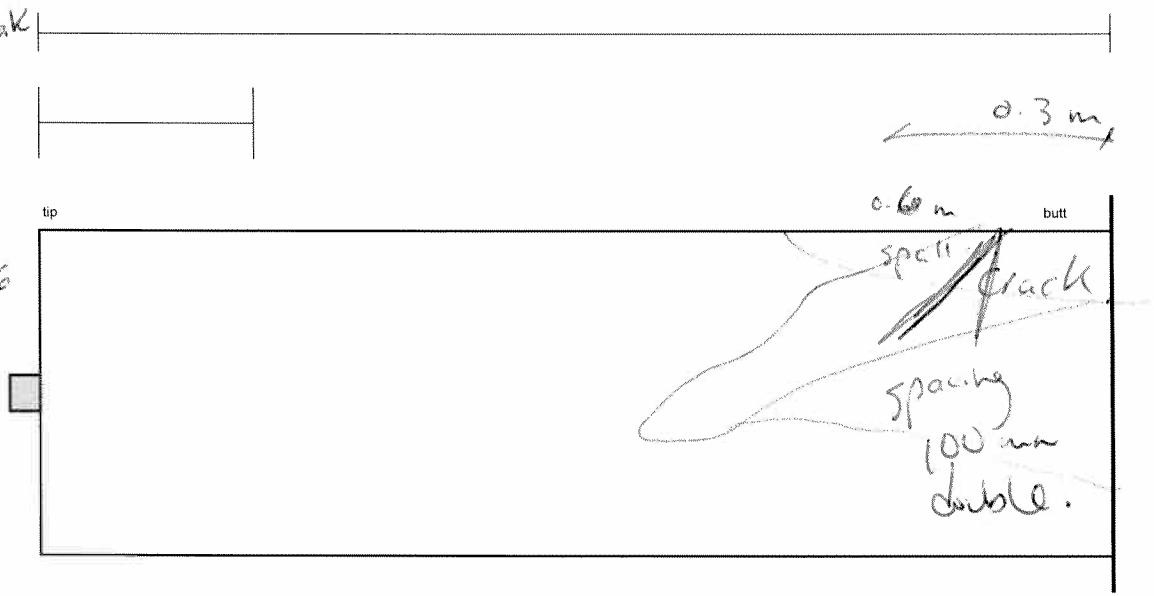

Crack Sketch

Comments:

Post-peak testing for 210-D (using new calibrated voltage divider).
twist voltage from end first test (Oct 30) : 0.285 V (0.427°)
initial zero reading 0.2594 (4.32°) ~ from zero

* marked twist device and reset to previous twist angle. (0.2863 V)

start @ 11:34

~ 26 kN spall big crack → steel yield & rocker failure (helix)
→ lose 5 kN
fluctuates.

zensotec
-0.03

233

TL: 5360

crack

3610 TL: 5360 mm

600

0.3 failure

first heli. failed

200

tip

~150

helical

from top

Crack Sketch

Specimen:	210-CCW-L	
Date Tested:	Nov 6	
Time Tested:	10:55	
Excitation Voltage (load cell)	10:22	V
Calibration (push button) value	21.98	kN
Excitation Voltage (accustar bat)	12.73	V
Zero reading load cell:	0.0006	V
Zero reading twist:	0.4889	V
Twist at Cracking:		V
		deg
Torque Reading at Cracking:		kN
		kN-m
Twist at Post Crack Hold:		V
		deg
Torque Reading Post Crack Hold:		kN
		kN-m
Wall Thickness at Failure:	71	mm
Cover at Failure:	26	mm
Location of Failure from butt:	0.3	m/m
Comments:	Crack @ 12 kN. (first). major move 18.5 + spalling. (popping off). ↳ helical cracking / failure (potentially @ this time). - dropped to wood support. 20 mm paste @ failure point	

-0.02

234

TL = 5357.

Specimen:	210-CW-L	
Date Tested:	Nov 6	
Time Tested:	11:55	
Excitation Voltage (load cell)	10.22	V
Calibration (push button) value	21.95	kN
Excitation Voltage (accustar bat)	12.70	V
Zero reading load cell:	0.0006	V
Zero reading twist:	0.5695	V
Twist at Cracking:		V
		deg
Torque Reading at Cracking:		kN
		kN-m
Twist at Post Crack Hold:		V
		deg
Torque Reading Post Crack Hold:		kN
		kN-m
Wall Thickness at Failure:	(55)	mm
Cover at Failure:	23	mm
Location of Failure from butt:	~0.02	mm

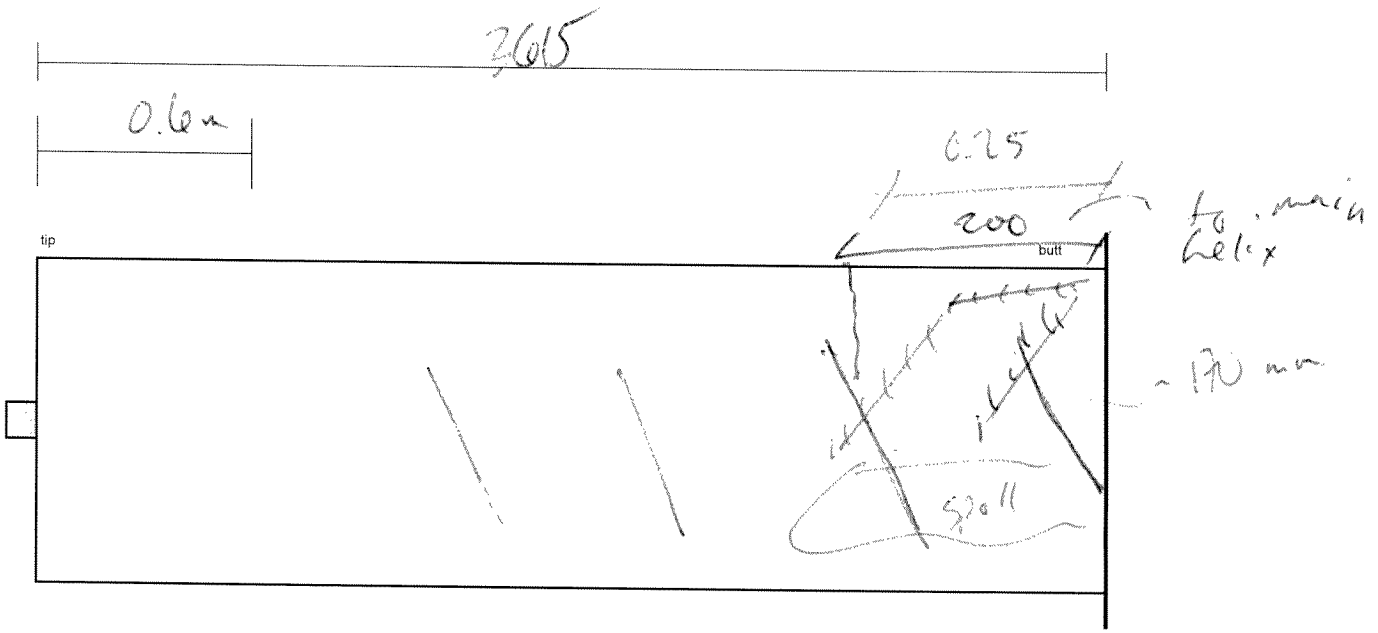

Crack Sketch

Comments:

start @ 11:58 - 11:59.
24.5 kN first crack
then spall drop to 9.2 kN
@ end pile started to bend up (b/c top pile cracked)
20 mm paste.

235

TL: 5350

3622 TL=5350

Specimen:	21=-CCW-N	
Date Tested:	NOV 8	
Time Tested:	10:12	
Excitation Voltage (load cell)	10.22	V
Calibration (push button) value	21.97	kN
Excitation Voltage (accustar bat)	12.74	V
Zero reading load cell:	0.0006	V
Zero reading twist:	0.3316	V
Twist at Cracking:		V
		deg
Torque Reading at Cracking:		kN
		kN-m
Twist at Post Crack Hold:		V
		deg
Torque Reading Post Crack Hold:		kN
		kN-m
Wall Thickness at Failure:	71	mm
Cover at Failure:	24	mm
Location of Failure from butt:	see dwg	mm

0.6

0.6 m

~1/0 Spacing

tip

butt

590

Crack Sketch

xlpm looking 590

Comments:

10:15 0.0553 V restart load cell (movement in cable)

~14 kN (16.64 sensor) first crack @ 3:00

~19 kN (second crack)

~20.5 kN (spall & crack) fracture of helix steel

break & bend downwards to failure

4.5 | 5 kN post

236

TL: 5347 mm

Specimen:	210-CW-N	
Date Tested:	Nov 6	
Time Tested:	1:51	
Excitation Voltage (load cell)	10.22	V
Calibration (push button) value	22.03	kN
Excitation Voltage (accustar bat)	12.69	V
Zero reading load cell:	0.0018	V
Zero reading twist: (0.1080)	0.1068	V
Twist at Cracking:		V
		deg
Torque Reading at Cracking:		kN
		kN-m
Twist at Post Crack Hold:		V
		deg
Torque Reading Post Crack Hold:		kN
		kN-m
Wall Thickness at Failure:	55	mm
Cover at Failure:	27	mm
Location of Failure from butt:	see dwg	mm

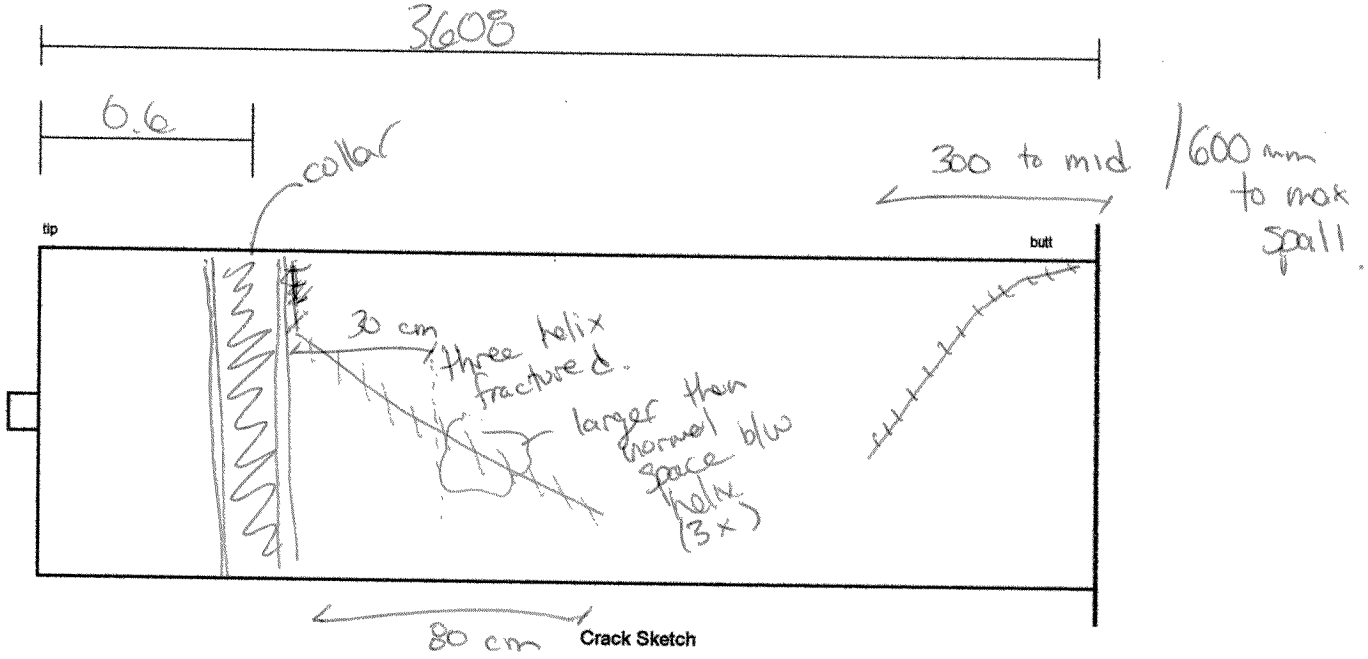

.001

237

Comments:

18.5 kN first crack @ butt.
~23 kN crack and sudden spall.
@ collar (1.2 m down from tip)
- dropped to ~1 kN due to break @ collar

Appendix D

Strut and Tie Model and Code Maximum Spacing Calculations

Strut and Tie Calculation for Transfer Length of Concrete Pole - Point Strand Load

fpu	1860	Mpa	phi p	1	
fpi	1339.2	Mpa	(20 % losses, stressed to 90%)		
Assume					
fci =	25	Mpa	@ transfer		
Ap (one strand)	55.23	mm^2			
	9.52	mm			
tip diameter	210	mm			
wall thickness	55	mm	p - eff	99	perimeter (diameter)
Taper	15	mm/m	w - eff	42	wall thickness
transfer length =	476	mm			
X-section (Ac)	26782.07737	mm^2	phi s	1	
			fy	500	MPa
Pi =	73.96	kN	db	3.5	mm
Pi/L	0.16	kN/mm	As	9.62	mm^2

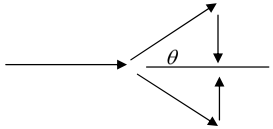

	Assumed s	Diameter at increment load	wall thickness	1/4 centerline perimeter	assumed s - s	p-eff	w-eff	angle of strut (deg)	s	P increment al (kN)	C in strut (kN)	Cr (kN)	T (kN)	Tr (kN)	angle of reinforcem ent	Tr - reduced (kN)	T / Tr reduced # needed
Increment	47.12	210.71	55.00	122.29	-5.95	99	42	25	53.08	8.25	4.55	3.68	1.92	4.81	82.80	4.77	0.40
						99	42	45	24.75	3.85	2.72	1.72	1.92	4.81	86.63	4.80	0.40
						99	42	65	11.54	1.79	2.12	0.80	1.92	4.81	88.43	4.81	0.40
																	#DIV/0!

	1.65	MPa	6.014462 kN
take prestres	2.69801818	MPa	
wt	16.9693254	mm	

Check struts

Compute width of struts AB

Node A is CCC

	alpha	E1	phi c * fcu	max = 0.85*fc	fcu	assume wall thickness	ws
End A	65	0.00287	19.4	21.25	19.4	42	8.6
	45	0.006	13.7	21.25	13.7	42	7.3
	25	0.020396	5.9	21.25	5.9	42	13.3

Node B is CCT

				max = 0.75*fcu			
End B	65	0.00287	19.4	18.75	18.75	42	8.9
	45	0.006	13.7	18.75	13.7362637	42	7.3
	25	0.020396	5.9	18.75	5.858562	42	13.3

SUMMARY

Struts				Ties				
Angle	ws End A	ws End B		# ties	s	OR	Concrete Tie	
25	8.6	8.9	mm	9.0	53		17.0	mm
45	7.3	7.3	mm	19.2	25		17.0	mm
65	13.3	13.3	mm	41	12		17.0	mm

Strut and Tie Calculation for Transfer Length of Concrete Pole - Point Strand Load

fpu	1860	Mpa	phi p	1	
fpi	1339.2	Mpa	(20 % losses, stressed to 90%)		
Assume					
fci =	25	Mpa	@ transfer		
Ap (one strand)	55.23	mm^2			
	9.52	mm			
tip diameter	165	mm			
wall thickness	45	mm	p - eff	75	perimeter (diameter)
Taper	15	mm/m	w - eff	36	wall thickness
transfer length =	476	mm			
X-section (Ac)	16964.60033	mm^2	phi s	1	
			fy	500	MPa
Pi =	73.96	kN	db	3.5	mm
Pi/L	0.16	kN/mm	As	9.62	mm^2

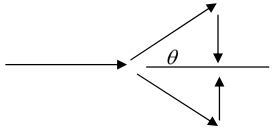

	Assumed s	Diameter at increment load	wall thickness	1/4 centerline perimeter	assumed s - s	p-eff	w-eff	angle of strut (deg)	s	P increment al (kN)	C in strut (kN)	Cr (kN)	T (kN)	Tr (kN)	angle of reinforcem ent	Tr - reduced (kN)	T / Tr reduced # needed
Increment	47.12	165.71	45.00	94.80	6.91	75	36	25	40.21	6.25	3.45	2.39	1.46	4.81	83.05	4.78	0.31
						75	36	45	18.75	2.91	2.06	1.11	1.46	4.81	86.75	4.80	0.30
						75	36	65	8.74	1.36	1.61	0.52	1.46	4.81	88.48	4.81	0.30
																	#DIV/0!
					1.65 MPa			4.558342 kN									
				take prestres	3.14902213 MPa												
				wt	12.8501026 mm												

Check struts

Compute width of struts AB

	alpha	E1	phi c * fcu	Node A is CCC max = 0.85*fc	fcu	assume wall thickness	ws
End A	65	0.00287	19.4	21.25	19.4	36	7.6
	45	0.006	13.7	21.25	13.7	36	6.4
	25	0.020396	5.9	21.25	5.9	36	11.7
				Node B is CCT max = 0.75*fcu			
End B	65	0.00287	19.4	18.75	18.75	36	7.9
	45	0.006	13.7	18.75	13.7362637	36	6.4
	25	0.020396	5.9	18.75	5.858562	36	11.7

SUMMARY

Struts Angle	ws End A	ws End B		Ties # ties	s		OR	Concrete Tie	
25	7.6	7.9	mm	11.8	40			12.9	mm
45	6.4	6.4	mm	25.4	19			12.9	mm
65	11.7	11.7	mm	54	9			12.9	mm

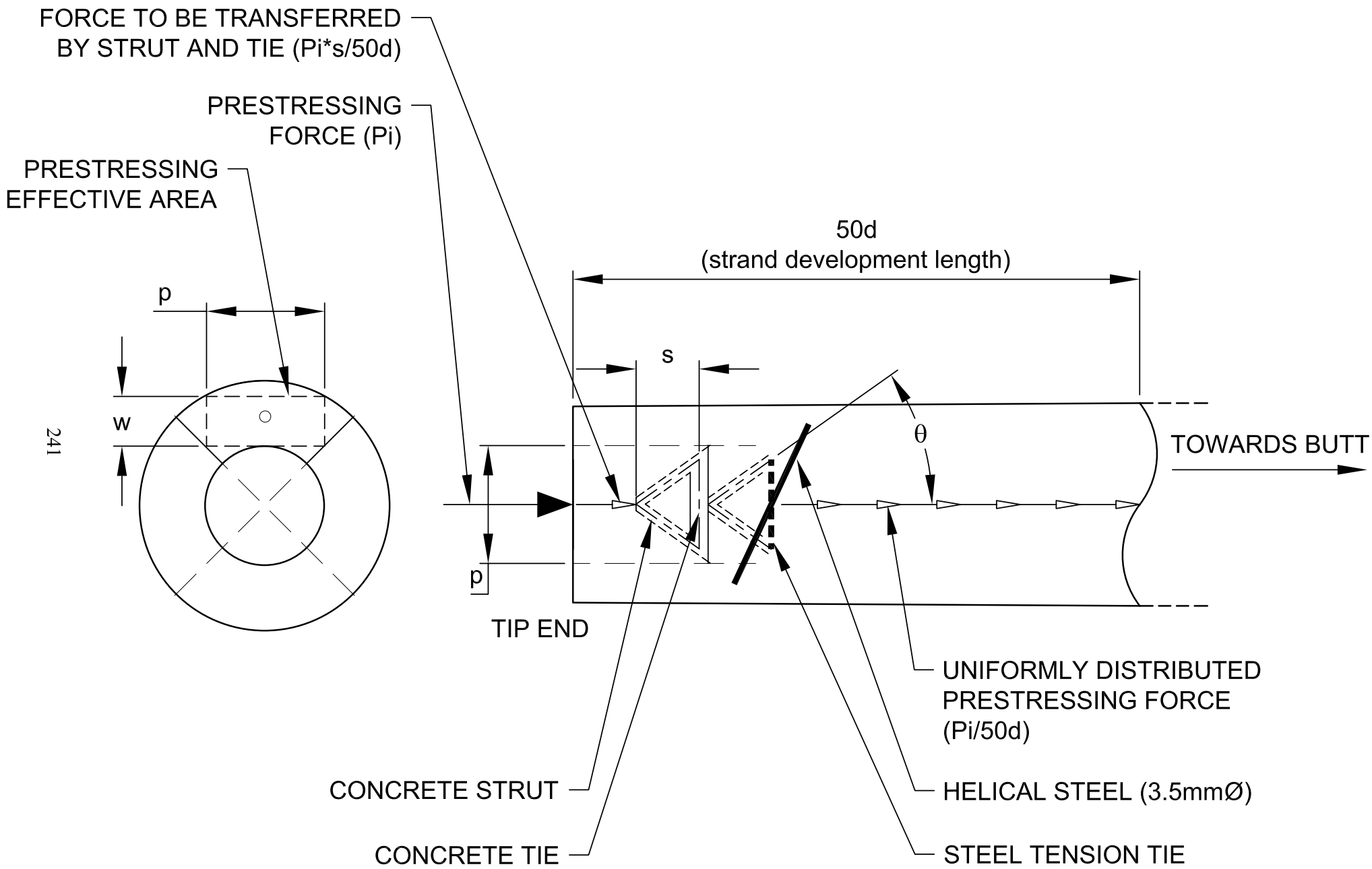
FORCE TO BE TRANSFERRED
BY STRUT AND TIE (Pi*s/50d)
PRESTRESSING
FORCE (Pi)
PRESTRESSING
EFFECTIVE AREA
50d
(strand development length)
p
w
s
θ
TOWARDS BUTT
p
TIP END
UNIFORMLY DISTRIBUTED
PRESTRESSING FORCE
(Pi/50d)
CONCRETE STRUT
HELICAL STEEL (3.5mmØ)
CONCRETE TIE
STEEL TENSION TIE

Maximum Spacing Requirements for Minimum Shear Reinforcement as given by ACI, CSA, EC2

					fpc	12.22916	taken from code tables sheet			
					w	45				
	CSA	ACI		EC-2	f'c	60			Transverse Reinfrocement Requirements	
Av/s	0.15337	0.159761	0.1089	0.204494	fy	500	463 fyl		Tcr = Tr	Ali and White 99 Koutchoukali and Belarbi, 2001
s9.62	62.72407	60.21511	88.33792	47.04306	bw	165	220.9028 Al		36.31394	19.65008393 28.43689
s19.24	125.4481	120.4302	176.6758	94.08611	At	9.62				
max 165	91	123.75		97.5	Ac	21382.46				
	.7d	.75h		.75d	pc	518.3628				
	45.5	61.875			Ao	11309.73				
					ph	417.8318				
165 tip		51.24144			ACI					
					based on uk from EC2 used as ph/8					
165	100.7139	116.6726			CSA Cl. 11.3.8.2					
	50.35695	58.33631			ACI Cl 11.5.5.2 & 11.5.5.3					
165	62.72407	51.24144		47.04306						
if Tf > 0.25Tcr	45.5	51.24144								

					fpc	8.724219	taken from code tables sheet			
					w	55				
	CSA	ACI		EC-2	f'c	60			Transverse Reinfrocement Requirements	
Av/s	0.195198	0.203332	0.1386	0.260264	fy	500	463 fyl		Tcr = Tr	Ali and White 99 Koutchoukali and Belarbi, 2001
s9.62	49.2832	47.31187	69.40837	36.9624	bw	210	220.9028 Al		29.7114	26.29860857 23.0132
s19.24	98.5664	94.62375	138.8167	73.9248	At	9.62				
max 210	126	157.5		135	Ac	34636.06				
	.7d	.75h		.75d	pc	659.7345				
	63	78.75			Ao	18869.19				
					ph	559.2035				
					ACI					
210 tip		65.16603			based on uk from EC2 used as ph/8					
210	128.1813	148.4924			CSA Cl. 11.3.8.2					
	64.09067	74.24621			ACI Cl 11.5.5.2 & 11.5.5.3					
210	49.2832	47.31187		36.9624						
if Tf > 0.25Tcr	49.2832	47.31187								

Appendix E

Typical Fixture Product Sheets and Wind Load Calculations

ORDERING INFORMATION

WOOD POLES

Catalog Number	Figure	Arm Length "A" (Ft.)	Arm Rise "B" (Ft.)	Bracket Net Wt. (Lbs.)	Max. Luminaire Wt. (Lbs.)	Max. Luminaire EPA
WE424	2	4	2'	10	60	3.0
WE636	2	6	2'	12	60	3.0
WEH836	2	8	2'	16	60	3.0
WEHT636	1	6	2'	25	60	3.0
WEHT836	1	8	2'	29	60	3.0
WEHT1036	1	10	2'	33	60	3.0
WEHT1236	1	12	2'	37	60	3.0
WEHT1536	1	15	2'	52	60	3.0
WP218	#	2	1'	7	60	3.0
WP424	#	4	2'	10	60	3.0
WP624	#	6	2'	14	60	3.0

CONCRETE ROUND/SQUARE POLES

Catalog Number	Figure	Arm Length "A" (Ft.)	Arm Rise "B" (Ft.)	Bracket Net Wt. (Lbs.)	Max. Luminaire Wt. (Lbs.)	Max. Luminaire EPA
CE424	2	4	2'	12	60	3.0
CE636	2	6	3'	14	60	3.0
CEH836	2	8	3'	18	60	3.0
CEHT636	3	6	3'	29	60	3.0
CEHT836	3	8	3'	33	60	3.0
CEHT1036	3	10	3'	37	60	3.0
CEHT1236	3	12	3'	41	60	3.0
CEHT1536	3	15	3'	56	60	3.0

WOOD AND/OR CONCRETE POLES

Catalog Number	Figure	Arm Length "A" (Ft.)	Arm Rise "B" (Ft.)	Bracket Net Wt. (Lbs.)	Max. Luminaire Wt. (Lbs.)	Max. Luminaire EPA
WCE424	5	4	2'	10	75	3.0
WCE636	4	6	2'	12	75	3.0
WCE836	4	8	2'	29	75	3.0
WCE1036	4	10	2'	31	75	3.0
WCE1236	4	12	2'	37	75	3.0

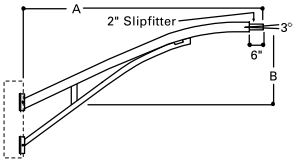

Fig. 1

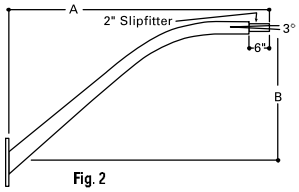

Fig. 2

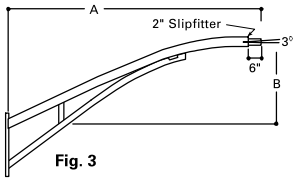

Fig. 3

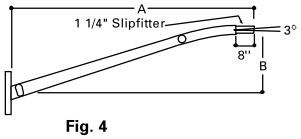

Fig. 4

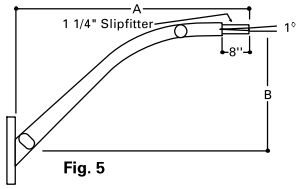

Fig. 5

"W" SERIES GALVANIZED BRACKETS FOR CONCRETE POLES

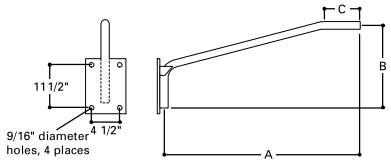

ORDERING INFORMATION

Catalog Number	Pipe Size (In.)	Arm (A) Length (Ft.)	Arm (B) Rise (Ft.)	Bracket Net. Wt. (Lbs.)	Maximum Luminaire Net. Wt. (Lbs.)	Maximum Luminaire EPA
W125C040	1 1/4	4.0	25	16	70	3.1
W200C060	2	6.0	34	29	90	4.0
W200C080	2	8.0	34	48	45	2.4

NOTES: Mounting hardware not included. Available prime painted—Consult your Cooper Lighting Representative.

Centrecon Arm Details

Specify series, shape, material, length, and color.
example: MR-AP-6'-COLOR

- M series
- R-Round Pole
- O-Octagonal Pole
- Aluminum Pipe SP: Steel Pipe
- Length
- Finish

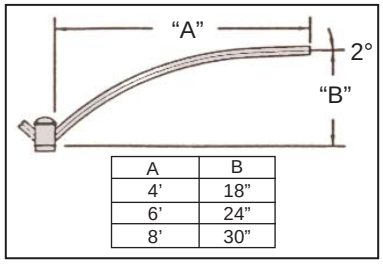

A	B
4'	18"
6'	24"
8'	30"

MR-AP Pipe Arm

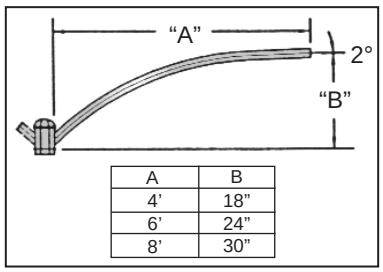

A	B
4'	18"
6'	24"
8'	30"

MO-AP Pipe Arm

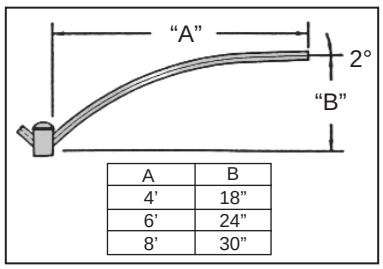

A	B
4'	18"
6'	24"
8'	30"

MR-SP Pipe Arm

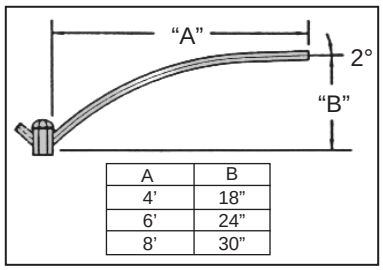

A	B
4'	18"
6'	24"
8'	30"

MO-SP Pipe Arm

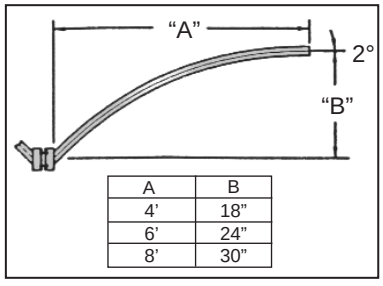

A	B
4'	18"
6'	24"
8'	30"

MR-SC Clamp-on Pipe Arm

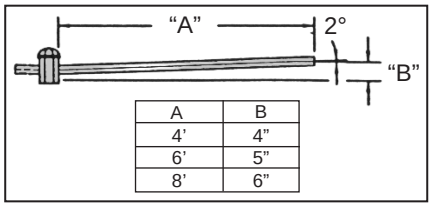

A	B
4'	4"
6'	5"
8'	6"

MO-SS Straight Pipe Arm

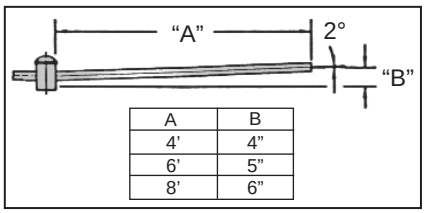

A	B
4'	4"
6'	5"
8'	6"

MR-SS Straight Pipe Arm

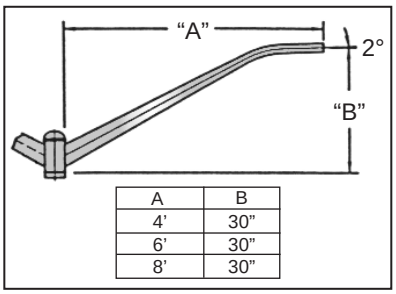

A	B
4'	30"
6'	30"
8'	30"

*MR-AE Elliptical Arm

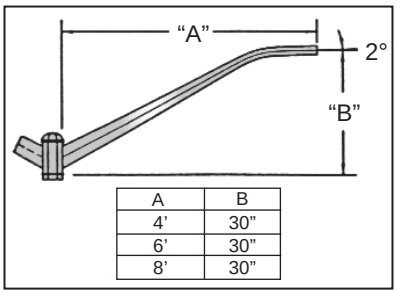

A	B
4'	30"
6'	30"
8'	30"

*MO-AE Elliptical Arm

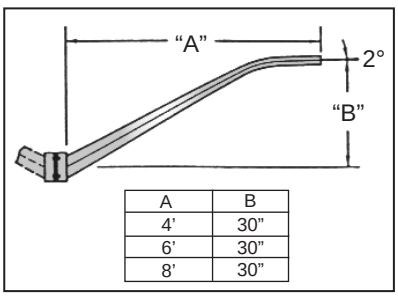

A	B
4'	30"
6'	30"
8'	30"

*MR-AEC Elliptical Clamp-on Arm

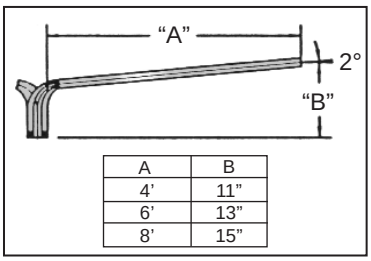

A	B
4'	11"
6'	13"
8'	15"

*MO-ADP Davit Pipe Arm

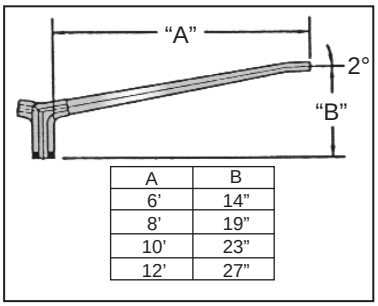

A	B
6'	14"
8'	19"
10'	23"
12'	27"

*MO-AD Davit Arm

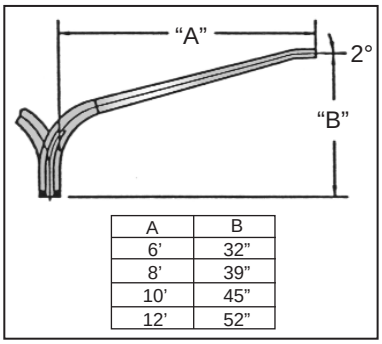

A	B
6'	32"
8'	39"
10'	45"
12'	52"

*MO-ARD Radius Davit Arm

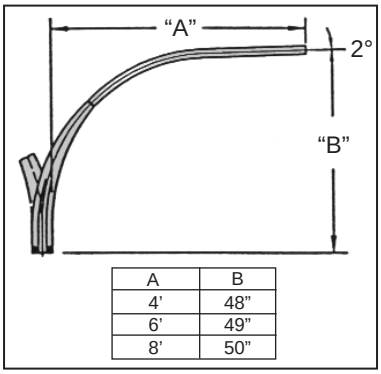

A	B
4'	48"
6'	49"
8'	50"

*MO-AA Davit Hi Rise Arm

*Aluminum only

Contemporary Arm Details

Specify series, shape, material, length, and color.
example: 1-AP-8'-COLOR

- 1-Octagonal
- 2&3-Round
- 5-Square
- Aluminum Pipe Arm (Arm Style)
- Length
- Finish

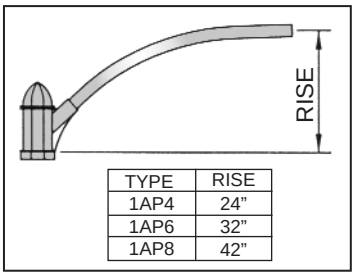

TYPE	RISE
1AP4	24”
1AP6	32”
1AP8	42”

1AP Pipe Arm

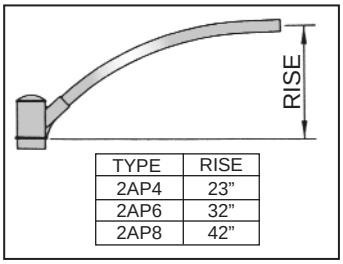

TYPE	RISE
2AP4	23”
2AP6	32”
2AP8	42”

2AP Pipe Arm
3SP (Steel Only)

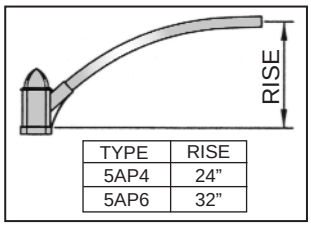

TYPE	RISE
5AP4	24”
5AP6	32”

5AP Pipe Arm

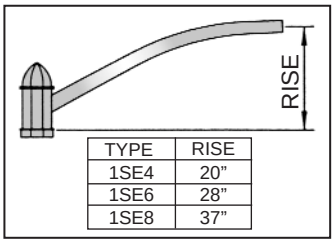

TYPE	RISE
1SE4	20”
1SE6	28”
1SE8	37”

1SE Arm Elliptical Arm

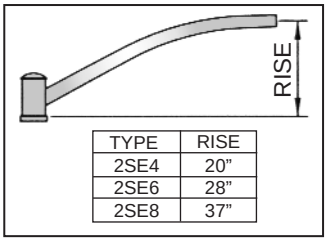

TYPE	RISE
2SE4	20”
2SE6	28”
2SE8	37”

2SE Elliptical Arm
3SE Elliptical Arm

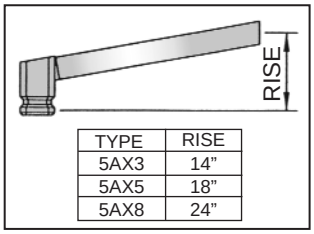

TYPE	RISE
5AX3	14”
5AX5	18”
5AX8	24”

5AX Rectangular Arm

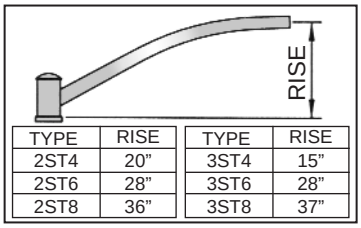

TYPE	RISE	TYPE	RISE
2ST4	20”	3ST4	15”
2ST6	28”	3ST6	28”
2ST8	36”	3ST8	37”

2ST Steel Tapered Arm
3ST Steel Tapered Arm

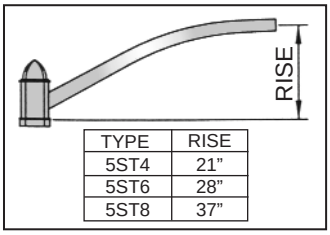

TYPE	RISE
5ST4	21”
5ST6	28”
5ST8	37”

5ST Steel Tapered Arm

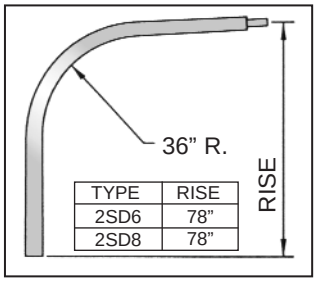

TYPE	RISE
2SD6	78”
2SD8	78”

2SD Davit Tapered Arm

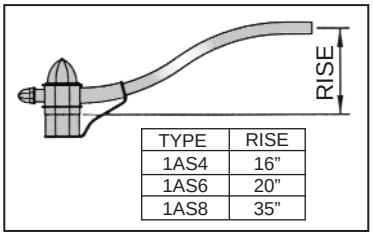

TYPE	RISE
1AS4	16”
1AS6	20”
1AS8	35”

1AS Aladdin Arm

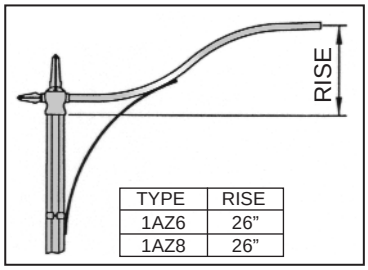

TYPE	RISE
1AZ6	26”
1AZ8	26”

1AZ Aladdin Arm

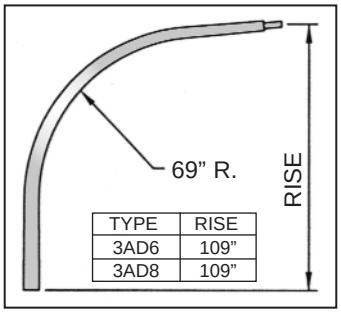

TYPE	RISE
3AD6	109”
3AD8	109”

3AD Davit Tapered Arm

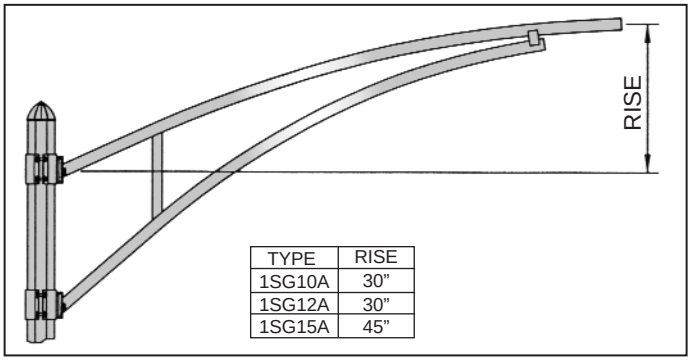

TYPE	RISE
1SG10A	30”
1SG12A	30”
1SG15A	45”

1SG Truss Clamp-On Arm

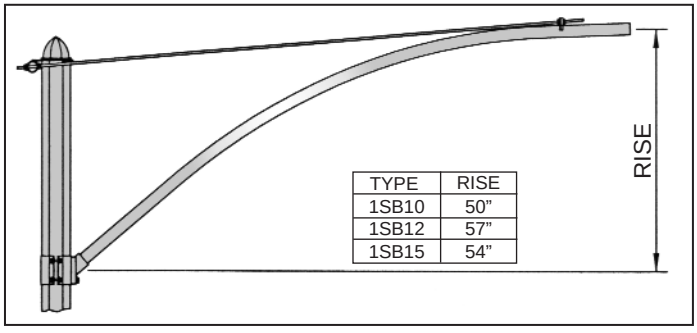

TYPE	RISE
1SB10	50”
1SB12	57”
1SB15	54”

1SB Tie Rod Clamp-On Arm

Decorative caps shown are optional. Standard is a flat cap.

LITHONIA LIGHTING®

Catalog Number	
Notes	Type

FEATURES & SPECIFICATIONS

INTENDED USE

Ideal for lighting roadways, residential streets, storage areas, parking lots campuses and parks.

CONSTRUCTION

Stainless Steel latch enables easy opening with one hand for relamping and servicing. Large surface area "breathing-seal" polyester gasketing protects reflector and lens from contaminants; maintains maximum optical efficiency. Gray polyester powder paint finish is electrostatically applied for superior corrosion resistance. Twist-lock photocontrol receptacle NOT included as standard (To order specify PER option, SEE BELOW)

ELECTRICAL

Reactor, normal power factor ballast standard. High power factor available. (See options.) Two- or three-position (L1, L2, N) tunnel type compression terminal block standard.

OPTICAL SYSTEMS

Ovate refractors in a variety of materials or flat tempered glass full cutoff lens provides a choice of efficient light distributions for every application. Optics are computer designed for maximum performance.

INSTALLATION

Two bolt mast arm mount. Arm compatible for 1.25" - 2.0" (3.2cm - 5.1 cm) mast arm.

LISTING

IP32 rated housing and IP54 rated optical assembly is standard. IP65 rating is available for optical assembly, see options. Standard product is NOT listed by UL, CSA or NOM.

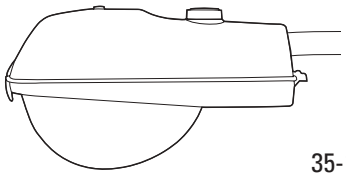

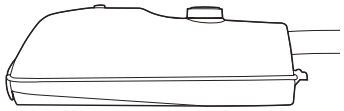

Roadway Lighting

CHE

35-150W HIGH PRESSURE SODIUM

Standard dimensions

(dimensions do not include mounting arm)

Flat Lens EPA:	.61 ft² (.057m²)
Drop Lens EPA:	.77 ft² (.072 m²)
Length:	21" (53.3)
Width:	12-7/8" (32.7)
Flat Lens Depth:	6-7/8" (12.5)
Drop Lens Depth:	10-1/2" (26.7)
Weight:	12 lbs. (5.4 kg)

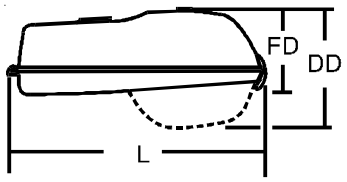

All dimensions are inches (centimeters) unless otherwise noted.

ORDERING INFORMATION

Example: **CHE 100S R2 DLG 120 PER LPI**

Choose the boldface catalog nomenclature that best suits your needs and write it on the appropriate line. Order accessories as separate catalog number.

CHE

Series	Wattage/Lamp Source	Distribution	Lens	Voltage	Ballast Options	Options
CHE	**35S**[1]	**R2**	**DLG** Drop lens glass (standard)	**120**	(blank) Reactor normal power factor (standard)	**Shipped Installed in Fixture**
	50S	**R3**	**DLA** Drop lens acrylic[2]	**L/E**[3]	**RHP** Reactor high power factor	**LPI** Lamp included as standard
	70S		**DLP** Drop lens polycarbonate[2]			**L/LP** Less lamp
	100S		**FL** Flat tempered glass lens, full cutoff			**PER** NEMA twist-lock receptacle only (photocontrol not included).
	150S		**SLG** Sag lens glass			**PEU** NEMA twist-lock PE
						DPL Distribution pattern label
						T2P Terminal block- two position wired L1 L2
						HSS Stainless steel external hardware
						Shipped Separately[4]
						SC Shorting cap for PER option

Notes:
1 Not available with RHP.
2 Available with R2 distribution only.
3 Shipped without ballast/electrical components.
4 May be ordered as an accessory.

DESCRIPTION

The Lumark Hammer's one-piece die-cast housing provides smooth, clean-line aesthetics while ensuring watertight protection of the electrical components. A computer-designed optical assembly delivers repeatable photometrics in four beam patterns for maximum design flexibility. The AIR/AIS mounting option provides contractor friendly, single shipment of fixture with the arm-in-box.

Superior beam utilization and smooth distribution make the Hammer ideal for parking areas, access roadways and other general offstreet area/site lighting applications.

Catalog #		Type
Project		
Comments		Date
Prepared by		

SPECIFICATION FEATURES

A ... Latches
Spring-loaded, die-cast latches provide entry without tools.

B ... Housing
Weather-resistant, one-piece die-cast aluminum housing is finished in dark bronze polyester powder coat as standard. Optional colors available. U.L. listed for wet locations. CSA certified.

C ... Reflector
Hydroformed anodized aluminum reflector delivers repeatable Type I, II, III and Forward Throw distributions.

D ... Gasket
Die-cut, dacron polyester gasket seals out external contaminants. IP65 rated optical assembly.

E ... Door
Removable one-piece die-cast aluminum door with clear flat tempered glass lens.

F ... Socket
Mogul-base porcelain socket for high pressure sodium or above 150W Metal Halide lamps.

G ... Ballast
Removable swing-down ballast assembly standard on arm mount units. Optional hard mount available. Hard mount ballast assembly standard on internal slipfitter option.

HR
HAMMER

70-400W
High Pressure Sodium
Metal Halide

ARM-MOUNTED
AREA/SITE LUMINAIRE

DARK SKY COMPLIANT FCO Full Cutoff

SWING-DOWN BALLAST

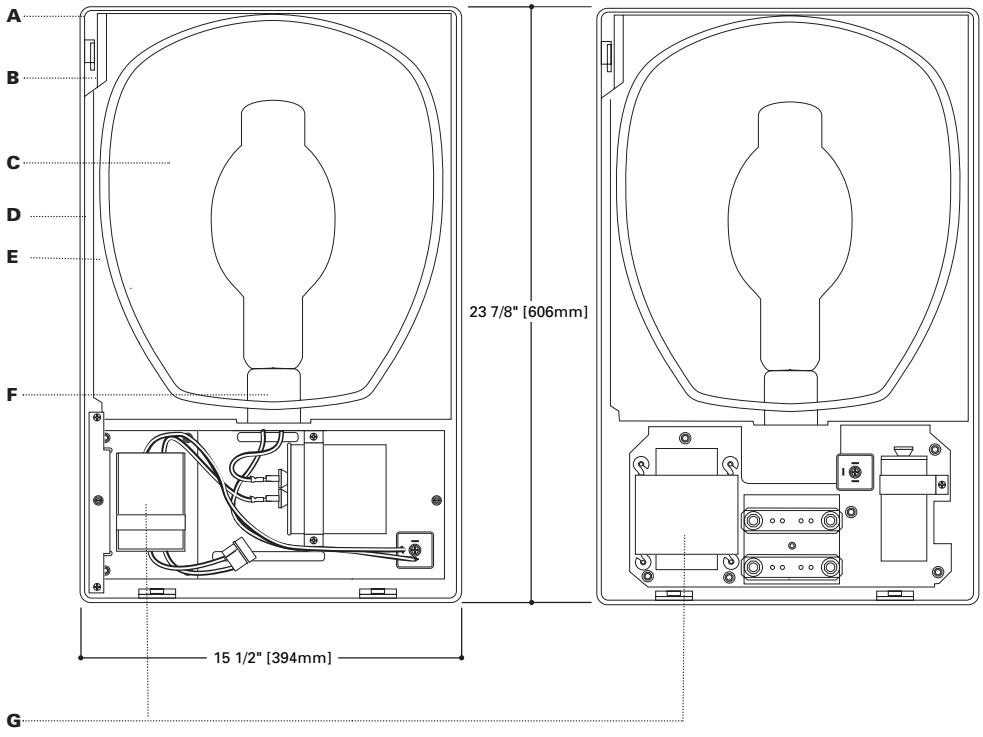

HARD MOUNT BALLAST

ENERGY DATA

Hi-Reactance Ballast Input Watts
70W HPS HPF (95 Watts)
100W HPS HPF (130 Watts)
150W HPS HPF (190 Watts)
150W MH HPF (185 Watts)

CWI Ballast Input Watts
250W HPS HPF (300 Watts)

CWA Ballast Input Watts
175W MH HPF (210 Watts)
200W MP HPF (232 Watts)
200W HPS HPF (250 Watts)
250W MH HPF (295 Watts)
320W MP HPF (365 Watts)
350W MP HPF (395 Watts)
400W MP HPF (448 Watts)
400W MH HPF (455 Watts)
400W HPS HPF (465 Watts)

EPA

Effective Projected Area: (Sq. Ft.)
[Without Arm]
HR: 1.58
[With Arm]
HR: 2.11

SHIPPING DATA

Approximate Net Weight:
31-46 lbs. (14-21 kgs.)

DIMENSIONS

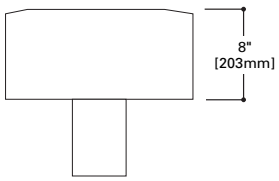

WALL MOUNT DRILLING

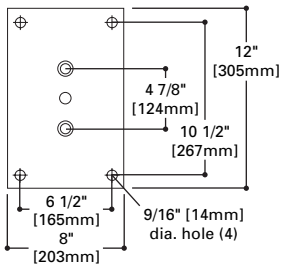

ARM MOUNT DRILLING

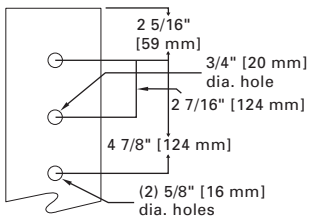

Specifications and Dimensions subject to change without notice.
Consult your representative for additional options and finishes.

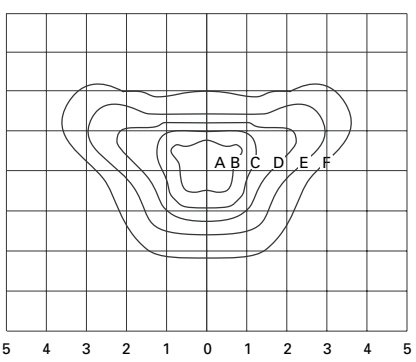

HR-1

HPHR-R3-400-MT

400-Watt HPS, Type III, 50,000-Lumen Clear Lamp

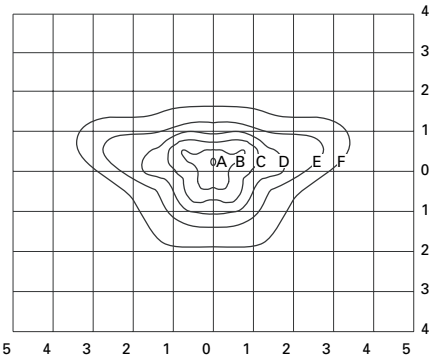

HR-2

MHHR-R2-400-MT

400-Watt MH, Type II, 34,000-Lumen Clear Lamp

Footcandle Table

Select mounting height and read across for footcandle values of each isofootcandle line. Distance in units of mounting height.

Mounting Height HR-1 & 2	Footcandle Values for Isofootcandle Lines				
	A	B	C	D	E
20'	11.25	4.50	2.25	1.13	0.45
25'	7.20	2.88	1.44	0.72	0.29
30'	5.00	2.00	1.00	0.52	0.20

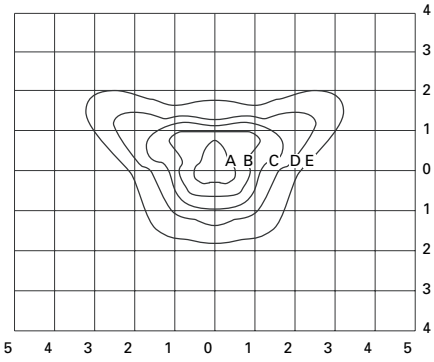

HR-3

MHHR-R3-400-MT

400-Watt MH, Type III, 34,000-Lumen Clear Lamp

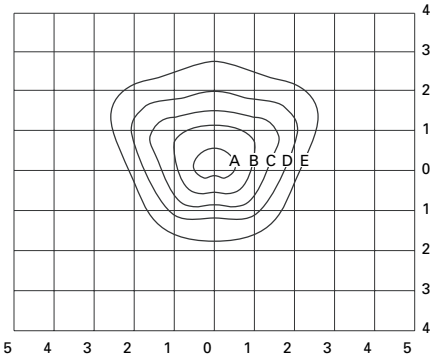

HR-4

MHHR-FT-400-MT

400-Watt MH, Forward Throw, 34,000-Lumen Clear Lamp

Footcandle Table

Select mounting height and read across for footcandle values of each isofootcandle line. Distance in units of mounting height.

Mounting Height HR-3 & 4	Footcandle Values for Isofootcandle Lines				
	A	B	C	D	E
20'	11.25	4.50	2.26	1.13	0.45
25'	7.20	2.88	1.44	0.72	0.28
30'	5.00	2.00	1.00	0.50	0.20

ORDERING INFORMATION

Sample Number: HPHR-R3-400-MT-Q

Lamp Type
HP= High Pressure Sodium
MH= Metal Halide
MP= Pulse Start MH (CWA)[1]

Series
HR= Hammer

Distribution
R1= Type I
R2= Type II
R3= Type III
FT= Forward Throw[2]

Lamp Wattage [3]
70= 70W
100= 100W
150= 150W
175= 175W
200= 200W[4]
250= 250W
320= 320W[4]
400= 400W

Voltage [5]
120V= 120V
208V= 208V
240V= 240V
277V= 277V
347V= 347V
480V= 480V
MT= Multi-Tap, [6] wired 277V
TT= Triple-Tap, [7] wired 347V

Options [8]
AIR= 10" Arm Included for Round Pole
AIS= 10" Arm Included for Square Pole
EM= Emergency Quartz Restrike T4 Lamp w/ Time Delay Relay
F1= Single Fuse (120, 277 or 347V only)
F2= Double Fuse (208, 240 or 480V only)
Q= Quartz Restrike (Hot Strike Only)
LL= Lamp Included[9]
S= 1 1/4" - 2 3/8" Internal Slipfitter (Hard Mount Only)
HS/HR= House Side Cutoff
AF= Four-Stage Air Filter
PER= NEMA Twistlock Photocontrol Receptacle
PC= Button Type Photocontrol
VS/HR= Vandal Shield

Accessories [10]
OA1061XX= Direct Mount Plate for Square Pole
OA1062XX= 10" Arm for Square Pole, .53 EPA
OA1063XX= Direct Mount Plate for Round Pole
OA1064XX= 10" Arm for Round Pole, EPA .53
OA1066XX= Mast Arm Adpater for Existing 2-3/8" OD Horizontal Arm
OA1090XX= Adjustable Slipfitter for 2-3/8" OD vertical tenon
OA1065XX= Wall Mount Bracket
OA/RA1016= Photoelectric Control, 105-285 Volt NEMA Type
OA/RA1027= Photoelectric Control, 480 Volt NEMA Type
OA1028= Field Installed NEMA Twistlock Photocontrol Receptacle (Order Photocontrol Separately)

Notes:
1. 200, 250, 320, 350 and 400W.
2. 400W Forward Throw luminaire must use ED-28 lamp.
3. All lamps are mogul-base except 150W Metal Halide and below are medium-base. Lamp not included.
4. Pulse Start Metal Halide only.
5. Products also available in non-US voltages and 50HZ for international markets.
6. Multi-Tap ballast 120/208/240/277V wired 277V.
7. Triple-Tap ballast 120/277/347V wired 347V.
8. Must be listed in the order shown and separated by a dash.
9. Lamp is shipped separate from luminaire. Lamp is Cooper designated product based on luminaire requirements. Specified lamps must be ordered as a separate line item.
10. Order separately, replace XX with color specification.

STOCK SAMPLE NUMBER (Lamp included)

SAMPLE NUMBER: MHHR340

Lamp Type	Series	Lamp Wattage	Lamp Wattage
HP=High Pressure Sodium **MH**=Metal Halide	**HR**=Hammer	**3**=Type III	**15**=150W **17**=175W **25**=250W **40**=400W

NOTES: Multi-Tap ballast, lamp, arm and round pole adapter are standard for stock products. Options not aviailable with stock products. Refer to standard ordering logic.

DESCRIPTION

Roadway Cobrahead fixtures feature durable die-cast aluminum construction and a computer-designed optical system for sturdiness and optimum photometric control.

Catalog #		Type
Project		
Comments		Date
Prepared by		

SPECIFICATION FEATURES

A ... Housing
Die-cast aluminum housing and integrally cast door hinge are finished in durable grey polyester powder coat.

B ... Reflector
The reflector is precision hydroformed anodized aluminum with a Dacron polyester filter.

C ... Door
Die-cast aluminum door frame has two-position latch to ensure door stays fastened under extreme conditions.

D ... Lens
Removable prismatic refractor for use with high pressure sodium and metal halide lamp sources.

E ... Socket
Adjustable mogul-base porcelain socket.

F ... Ballast Assembly
Hard mounted ballast with encapsulated starter and plastic terminal block for protection from environmental abuse.

G ... Mounting
Two-bolt/one clamp slipfitter for 1 1/4" or 2" mounting arms.

RY
ROADWAY COBRAHEAD

50W-400W
High Pressure Sodium
Metal Halide

SITE/ROADWAY LIGHT

DARK SKY COMPLIANT CO Cutoff

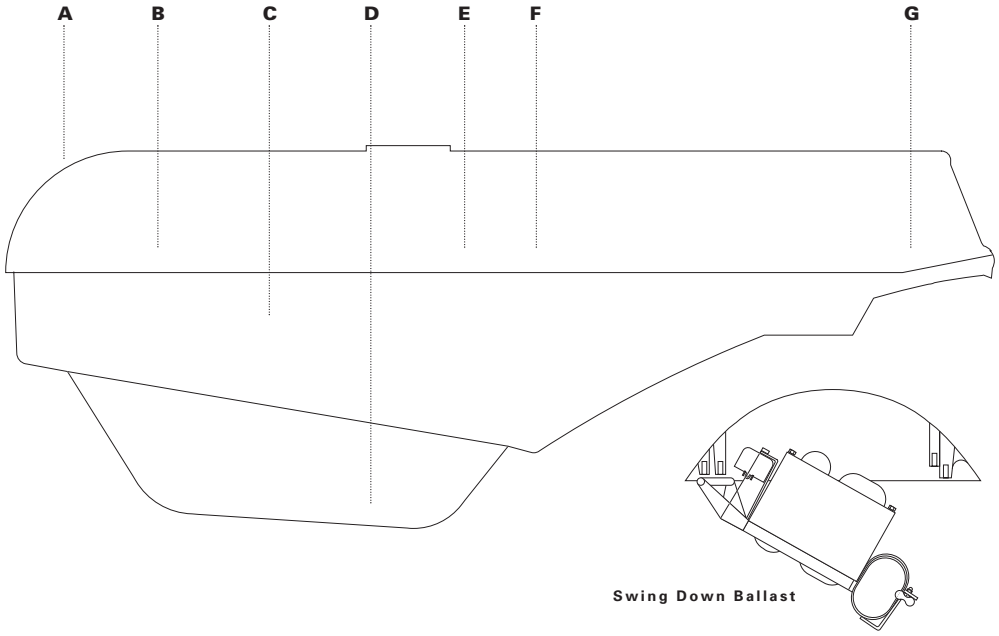

DIMENSIONS

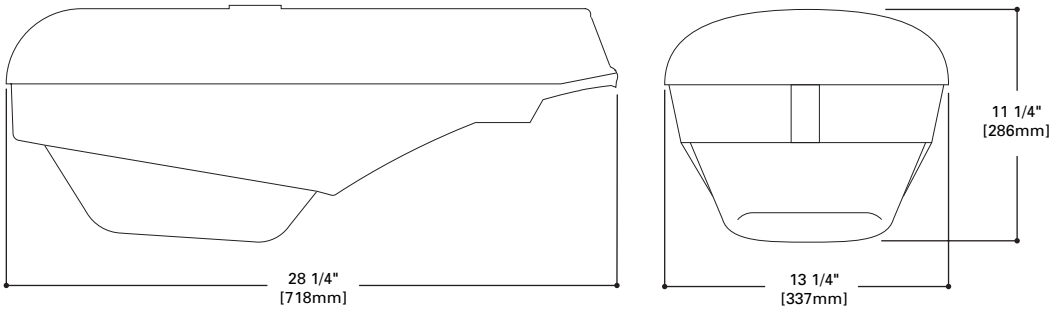

EPA

Effective Projected Area:
.87 Square Feet

SHIPPING DATA

Approximate Net Weight:
49 lbs. (22 kgs.)

Specifications and Dimensions subject to change without notice.
Consult your representative for additional options and finishes.

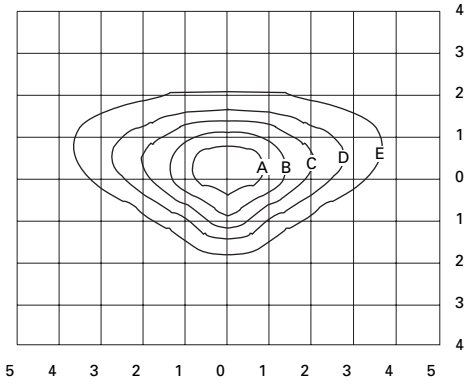

HPRY-GL-2-250-MT-LL
250-Watt HPS
27,500-Lumen Clear Lamp
Type II-Medium Semi-Cutoff

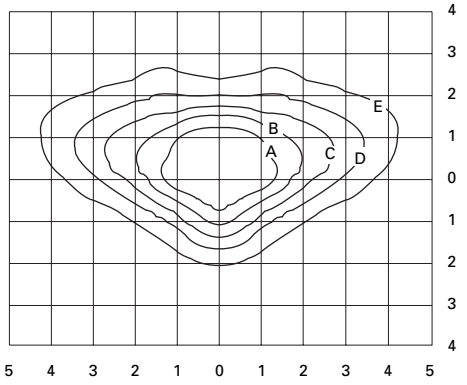

HPRY-GL-3-400-MT-LL
400-Watt HPS
50,000-Lumen Clear Lamp
Type III-Medium Semi-Cutoff

Footcandle Table

Select mounting height and read across for footcandle values of each isofootcandle line. Distance in units of mounting height.

Mounting Height	Footcandle Values for Isofootcandle Lines				
	A	**B**	**C**	**D**	**E**
25'	3.92	1.96	0.98	0.49	0.20
30'	2.72	1.36	0.68	0.34	0.14
35'	2.00	1.00	0.50	0.25	0.10
40'	1.52	0.76	0.38	0.19	0.08

ORDERING INFORMATION

Sample Number: HPRY-GL-3-400-MT-LL

Lamp Type
HP= High Pressure Sodium
MH= Metal Halide

Series
RY= Roadway Cobrahead

Lens Type
AL= Acrylic Refractor[1]
GL= Glass Refractor
PL= Polycarbonate Refractor
FL= Flat Glass Lens[2]

Distribution
2= Type II
3= Type III

Lamp Wattage [3]
50= 50W
70= 70W
100= 100W
150= 150W[4]
175= 175W
250= 250W
400= 400W

Voltage [5]
120V= 120V
208V= 208V
240V= 240V
277V= 277V
347V= 347V
480V= 480V
MT= Multi-Tap, [6] wired 277V
TT= Triple-Tap, [7] wired 347V

Options [8]
EM= Emergency Quartz Restrike T4 Lamp w/ Time Delay Relay
F1= Single Fuse (120, 277 or 347V only)
F2= Double Fuse (208, 240 or 480V only)
LL= Lamp Included[9]
H= Plug-In Starter[4]
K= Leveling Indicator
T= Swing-Down Ballast
PER= NEMA Twistlock Photocontrol Receptacle
PC= Button Type Photocontrol

Accessories [10]
OA/RA1016= Photoelectric Control, 105-285 Volt NEMA Type
OA/RA1027= Photoelectric Control, 480 Volt NEMA Type
OA1028= Field Installed NEMA Twistlock Photocontrol Receptacle (Order Photocontrol Separately)

Notes: **1** Acrylic refractor for 175W maximum.
2 400W Metal Halide requires reduced envelope lamp (ED28) for flat glass.
3 150W and below Metal Halide is medium-base. All other lamps are mogul-base. Lamp not included.
4 High Pressure Sodium only.
5 Products also available in non-US voltages and 50HZ for international markets.
6 Multi-Tap ballast 120/208/240/277V wired 277V.
7 Triple-Tap ballast 120/277/347V wired 347V.
8 Add as suffix in the order shown.
9 Lamp is shipped separate from luminaire. Lamp is Cooper designated product based on luminaire requirements. Specified lamps must be ordered as a separate line item.
10 Order separately.

Pole Classification Based on Wind Load

Date:	
Quote/Job no.:	
Job Name:	
Pole Specification:	
Pole Logic:	

POLE	Height Above Grade	32	(ft)
	Shape	RO	(Pole Logic Code)
	Taper	15	(mm/m)
	Tip Diameter	210	(mm)

FIXTURES	Qty.:	1	(enter 0 if none)
	Height Above Grade (to centre)	9.7	(m)
	EPA (each)	1	(ft^2)

ARMS	Qty.:	1	(enter 0 if none)
	Height Above Grade (to centre)	9.7	(m)
	EPA (each)	0.6	(ft^2)
	Arm Length	8	(ft)

BANNERS	Qty.:	0	(enter 0 if none)
	Height Above Grade (to centre)	0	(m)
	Length	0	(in)
	Width	0	(in)

WIND	Speed (from map)	80	(mph)

Bending Force at 600mm from Tip	**1.55**	(kN)
Tranverse Class	**AA***	(CSA)

Torsion Force	**0.68**	(kN-m)
Torsional Class	**A**	(CSA)

Govering Design Class	**AA***	(CSA)

Checked By Engineering:

New AAHSTO 2001 LOADS

Kz	1.09	
G	1.14	
V	80.57	180 mph
Ir	1	< 10 m
Cd	1	
	4944.859447	Pa

Tf-arm	0.55	kN-m
Tf-fixt	1.75	kN-m
	2.30	kN-m

0.4 kN-m for 80 mph
1.84 kN-m for 160 mph